INTERACTION OF FAST NEUTRONS

WITH LITHIUM AND URANIUM

By

ZAIN AL-DEAN N. AL-RAWI B.Sc., P.G.D., M.Sc.,

A Thesis submitted for the Degree

of

Doctor of Philosophy

Department of Physics

University of Aston in Birmingham

1979

INTERACTION OF FAST NEUTRONS WITH LITHIUM AND URANIUM

A Thesis submitted for the Degree of Doctor of Philosophy, Department of Physics, University of Aston in Birmingham.

by

ZAIN AL-DEAN N. AL-RAWI

SUMMARY

This work is concerned with the investigation of neutron shielding materials that are of possible use in future fusion reactors. Measurements and calculations have been carried out for shield of LiF, U^{238}, a mixture of LiF and U^{238}, and a two region of LiF and U^{238}. The neutron source was a monoenergetic points source of energy 14.1 MeV produced by $D(T,n)^4He$ reaction at the centre of a cylindrical shield.

The measurements were made with a liquid organic scintillator (NE-213), and the gamma-ray background was rejected by pulse shape discrimination using the zero crossing technique.

Calcuations have been carried out in spherical geometry with a multigroup diffusion model where the uncollided flux was calculated by the removal model. The cross-section data used came from the UKNDL-file, and the YOM-20 cross-section set.

Measured and calculated spectra show reasonable agreement, and do not indicate any discrepancies in the cross-section data used.

Removal cross-sections at 14.1 MeV have been experimentally determined for the four shield assemblies and show a good agreement with those used in the calculations which were based on the transport cross-sections.

Key words:

Liquid organic scintillator
Pulse shape discrimination
Neutron interaction with LiF
Neutron interaction with U^{238}
Fast neutron spectra

ACKNOWLEDGEMENTS

I would like to thank Dr. P. N. Cooper for supervising and directing this work, for his continuous guidance and help throughout the period of this work. Thanks are also due to Professor S. E. Hunt for his interest in the work.

I would like to thank Mr. J. Phull, the Laboratory Technician for his help in the maintenance of the accelerator. Thanks are also due to the Physics Workshop staff for their part in the construction of the various facilities.

I am grateful to the Government of the Republic of Iraq for their financial assistance.

Finally, I would like to thank my wife, and my two sons, Omar and Odae for their patience during their absence from their own Country.

TABLE OF CONTENTS

LIST OF FIGURES

CHAPTER 1

INTRODUCTION

1-1 Introduction

The study of the energy distribution of fast neutrons after passing through various thicknesses of different shielding materials which are of interest in nuclear technology is very important not only from the point of view of the theory of neutron penetration through matter but also from the design of nuclear reactors, and their associated equipment.

Much work has already been carried out in developing analytical methods and techniques to handle shielding problems and in obtaining experimental data suitable for design procedures, and the test of theoretical calculations, but there are still differences between results obtained by experiment and those given by calculation.

Attenuation of fast neutrons is affected by degrading the neutron energy by the elastic and inelastic scattering processes, until they are absorbed. The initial degradation of the energy mainly takes place by the inelastic scattering process except for the lightest nuclei, so uncertainties in the inelastic scattering cross-section will seriously affect the accuracy of calculations of neutron energy distribution[1].

The 14.1 MeV neutrons are not directly important for the shielding and blankets of fission reactor, since these neutrons are above the top end of the fission neutron spectrum (about 10 MeV), but they are extremely important for the possible future fusion reactors, since these will most probably use the D,T fusion reactions, thus directly producing 14.1 MeV neutrons.

1-2 The Project Aim

The objectives of the present work are to study the neutron energy distribution spectra of the 14.1 MeV neutron at different depths inside different shielding materials, which are of interest for the future fusion reactors, also to measure the removal cross sections for these materials at 14.1 MeV and see how both the neutron energy distribution spectra and the removal cross-sections measured compared with those calculated.

It is important to carry out experimental studies of the energy distribution of degraded 14.1 MeV neutron inside the shielding materials in order to provide information by which the theoretical calculations could be tested, for suitability of method, and if the measurements are sufficiently accurate for testing cross section data.

14.1 MeV neutrons from the $D(T,n)^4He$ reaction have been used to study neutron energy spectra produced after passing through different thicknesses of LiF, U^{238}, a mixture of LiF and U^{238}, and a two layer shield of LiF and U^{238}. The neutron spectra were measured with a proton recoil scintillation counter using the liquid hydrogenous scintillator NE-213. With this scintillator it was possible to reject gamma radiation induced pulses by pulse shape discrimination. The number of neutrons produced was monitored by counting the associated alpha-particles by using a thin layer of plastic scintillator (NE-102A).

For the theoretical calculations, the removal and multigroup diffusion method was used to calculate the spatial energy distribution of the fast neutrons. The cross section data used for these calculations was taken from the 20-group cross-section

set by Yiftah and Sieger[2] for uranium and aluminium, and the (UKNDL)[3] data set provided microscopic data for ^{6}Li, ^{7}Li and ^{19}F which was converted into multigroup cross-sections matching the Yiftah-Sieger group boundaries. Only the top ten energy groups were used (E_n>0.3 MeV).

1-3 The Application of the Project

The Lithium fluoride and uranium were chosen in the present work due to their potentially useful application in the future fusion reactors for LiF, and in the fusion-fission reactor for both LiF and uranium.

The neutron will be produced in the fusion plasma by the reaction:

$$D + T \longrightarrow {}^{4}_{2}H_{e} + n + 17.6 \text{ MeV}$$

about 80% of the energy released per fusion is given to the neutron, which escapes from the plasma. Thus the plasma can be regarded as an isotropic source of 14.1 MeV neutrons[4]. The main purposes of the blanket surrounding the plasma in a fusion reactor are the conversion of the neutron energy into thermal energy and the breeding of tritium, which is not present in nature due to its short half-life (12 years).

Lithium contains 7.56% ^{6}Li and 92.44% ^{7}Li, and produces tritium by the reactions:

$$^{6}_{3}Li + {}^{1}_{0}n \rightarrow {}^{3}_{1}T + {}^{4}_{2}He + 4.78 \text{ MeV}$$

$$^{7}_{3}Li + {}^{1}_{0}n \rightarrow {}^{3}_{1}T + {}^{4}_{2}He + {}^{1}_{0}n - 2.47 \text{ MeV}$$

^{6}Li has a very high (n,α) cross section at thermal neutron energies, but at 14.1 MeV the (n,nα) reaction cross-section for ^{7}Li isotope is higher than that for the ^{6}Li (n,α) reaction.

Neutrons for these reactions are produced when the deuterium and tritium nuclei burn in the reactor by the $D(T,n)^{4}_{2}He$ reactions. The neutrons produced are captured by a lithium containing blanket surrounding the plasma, which will produce tritium and transform the kinetic energy of the 14.1 MeV neutrons into heat[5].

In several fusion reactor concepts, molten lithium acts as both a breeder material and a heat transfer fluid[6]. Another form of molten lithium of possible use is a molten mixed salt ($LiF - BeF_2$). This is proposed because of the reaction $^{9}Be(n,2n)\ 2^{4}He$, which provides extra neutrons for tritium breeding, and also the molten salt mixture has a lower melting point than pure LiF.

The uranium has a high atomic weight and so is a good fast neutron and gamma ray shielding material. The neutrons from the $D(T,n)^{4}_{2}He$ reaction can be multiplied through fission in a heavy element blanket (U^{238}), surrounding the fusion plasma. The concepts which involve the use of fusion produced neutrons to ultimately produce fission are called the fusion-fission hybrids[7].

The hybrid system Fig. [1-1] is an example of the system, involving the fusion neutron with fissile material (U^{238}) to produce a multiplication of the fusion neutron source strength and also producing more energy from nuclear fission. This effect increases the energy output of the system, possibly increases tritium breeding and also breeds fissile material for use in thermal fission reactors. The thermal fission rate due to breed plutonium in such a blanket would be low due to the high ^{6}Li cross-section at thermal neutron energies.

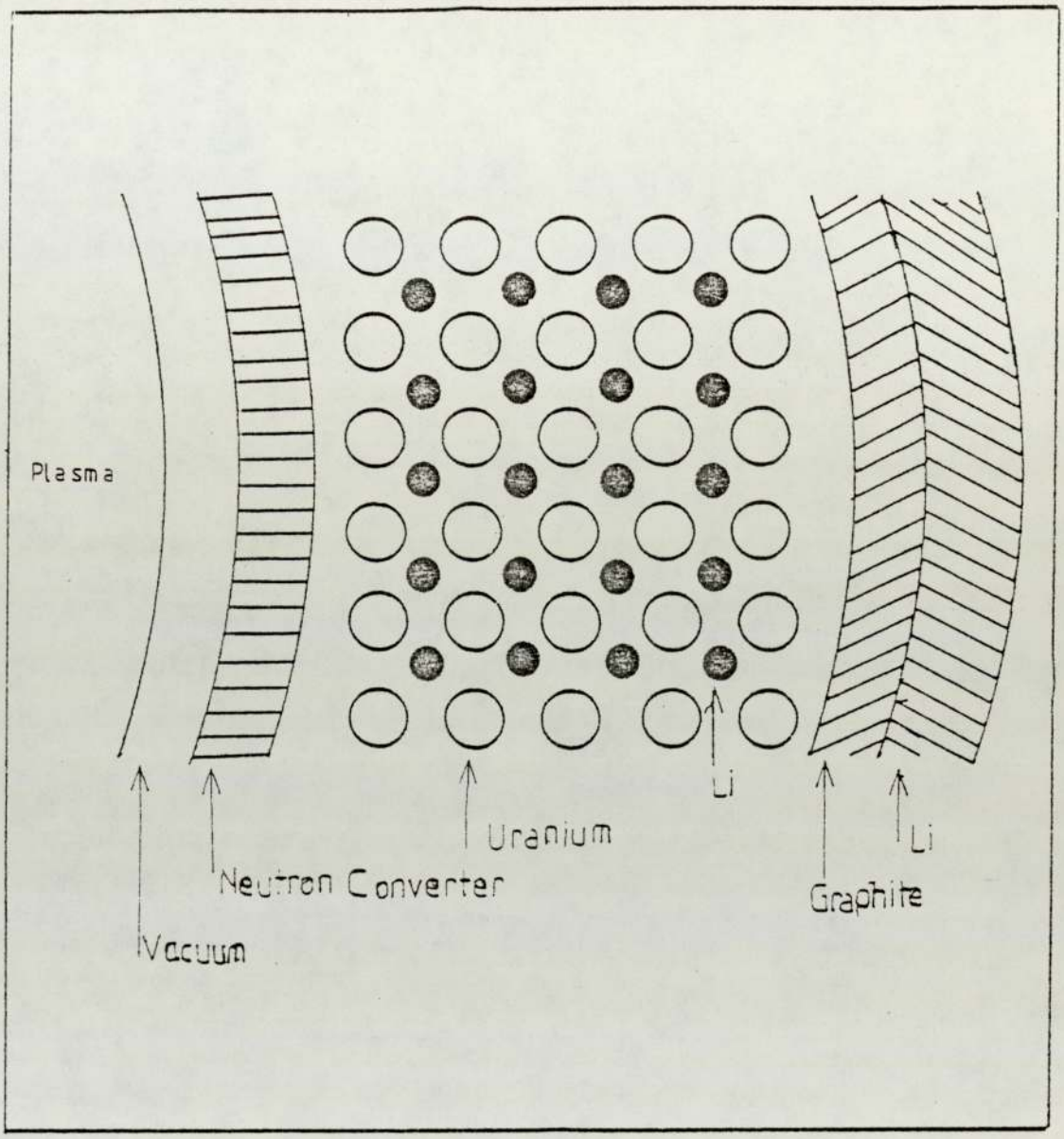

Fig. [1-1] The fusion-fission blanket configuration

CHAPTER 2

NEUTRON INTERACTION WITH MATTER

2-1 Introduction

The interaction of neutrons passing through matter is different from that of either charged particles or gamma-rays.

The neutron carries no charge, so there is no Coulomb repulsion to prevent its interaction with nuclei and so it is able to cross the nuclear boundary even when its velocity is very low. If the nucleus is unchanged in either isotopic composition or internal energy after interacting with the neutron the process is called elastic scattering X(n,n)X; if the nucleus after re-emission the neutron is left in an excited state the process is called inelastic scattering X(n,n')X*. In referring to these processes it is common to say that the incident neutron has been scattered elastically or inelastically, since a neutron reappears after the interaction. However the emerging neutron may not be the same neutron incident on the target nucleus.

The neutron may be absorbed by the nucleus with an emission of gamma photon X(n,γ)Y that is called the radiative capture, the neutron capture may also lead to the emission of charged particles in X(n,p)Y, X(n,α)Y reactions. At higher neutron energies two or more neutrons may be emitted, these are (n,2n), (n,3n) reactions. A detailed description of these processes is given below.

2-2 Elastic Scattering X(n,n)X

The slowing down of fast neutrons is due mainly to the elastic scattering collision between the neutrons and the nuclei of the target. In this type of scattering the kinetic energy is conserved

and the energy level of the target nucleus is the same before and after the collision. By applying the principle of conservation of momentum and energy it is possible to derive a relationship between the scattering angle θ, (where θ is the centre of mass angle) and the energy of the neutron of mass 1 before and after the collision with the nucleus of mass A (where A is almost exactly the mass number), given by [8].

$$E_2 = E_1 \frac{A^2+2A \cos \theta + 1}{(A+1)^2} \qquad \ldots\ldots\ldots 2\text{-}1$$

where

E_1 - is the energy of the neutron before collision

and E_2 - is the neutron energy after collision

If ψ is the angle in the lab.-system then the relationship between the angle in C-M-system and the lab.-system is given by:-

$$\cos \psi = \frac{1+A \cos \theta}{\sqrt{A^2+2A \cos \theta+1}} \qquad \ldots\ldots\ldots 2\text{-}2$$

From equation (2-1) and (2-2) the neutron energy after collision is given by:-

$$E_2 = E_1 \frac{A^2+2\sqrt{A^2-\sin^2\psi}\cdot\cos \psi + \cos 2 \psi}{(A+1)^2} \qquad \ldots\ldots\ldots 2\text{-}3$$

when $\theta = 180°$ then $\psi = 180°$ (unless A = 1 when $\psi = 90°$)

$\theta = 0°$ $\psi = 0$

so from equation (2-3) at $\psi = 0°$, $(E_2)_{max} = E_1$

i.e. no scatter and the minimum value of E_2 occurs when $\psi = 180°$ so

$$(E_2)_{min} = \left(\frac{A-1}{A+1}\right)^2 E_1 \qquad \ldots\ldots\ldots 2\text{-}4$$

The minimum energy of a neutron after a collision depends on the mass of the target nucleus.

Elastic scattering of neutrons can be regarded as being composed of two coherent contributions:-

a - The resonance scattering in which the formation of one of the several decaying states of the compound nucleus (n+X) whose energies lie within about the level width from the energy of the initial (n,X) system followed by decay of the compound nucleus with emission of a neutron having the energy as that of the original incident neutron.

b - The potential scattering in which the neutron does not penetrate the nucleus to form a compound nucleus but without sharing its energy with the target nucleus is scattered as it would be by a potential well. This part may be considered as due to the large number of states of the compound nucleus which are far removed from the incident energy[9].

For lower energy neutrons (< 1 MeV) elastic scattering is nearly isotropic in the centre of mass system[10], as the energy increases the anisotropy also increases. For resonance scattering the angular distribution is characteristic of the spins and parity of the levels of the compound nucleus involved and is more or less isotropic[11].

In potential scattering neutrons are forward peaking and this becomes more pronounced as energy increases. Figure (2-1) shows the

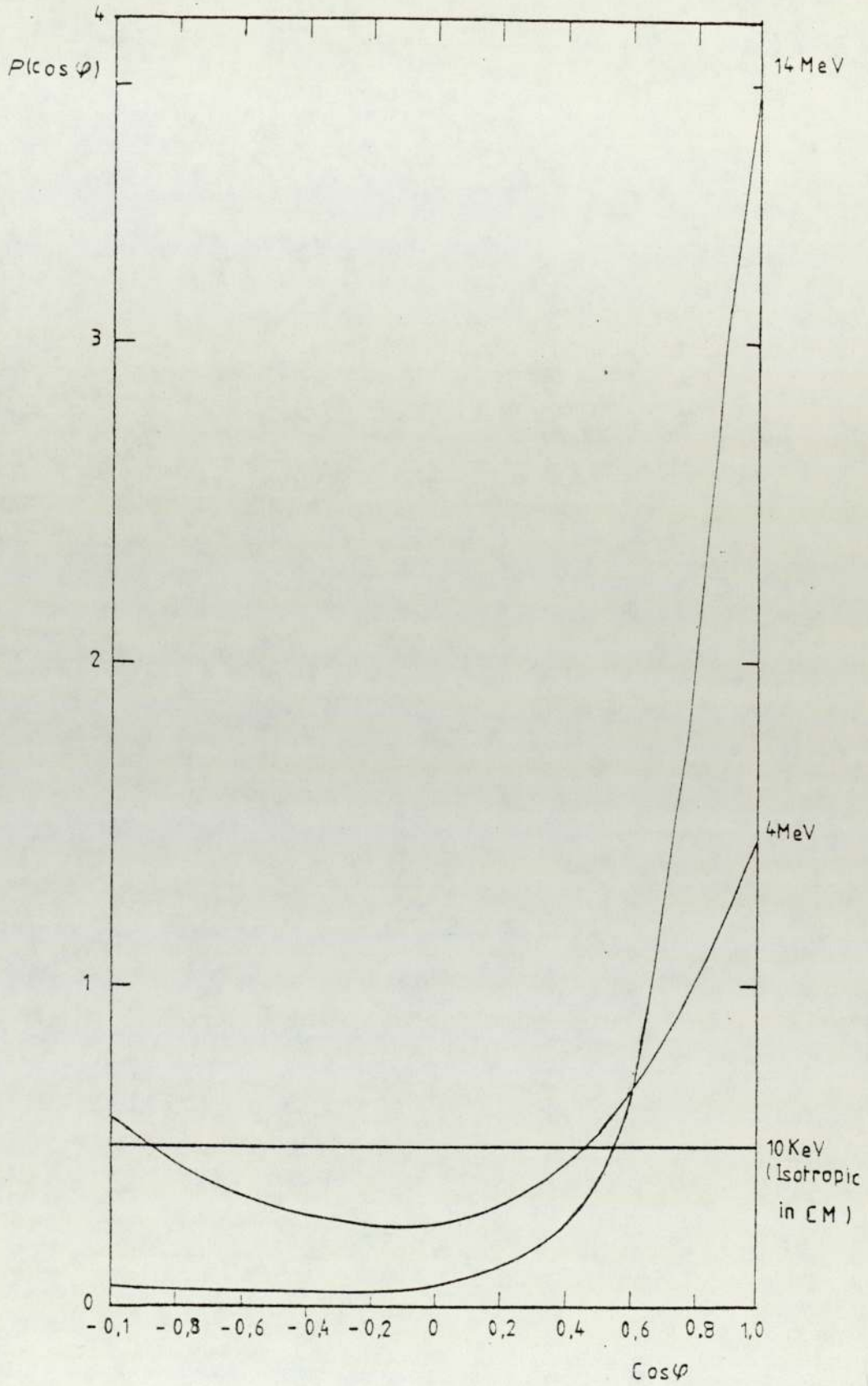

Fig. [2-1] The angular distribution of ^{6}Li elastic scattering [UKNDL]

angular distribution for the ^{6}Li elastic scattering.

2-3 Inelastic Scattering $X(n,n')X^{*}$

The inelastic scattering becomes energetically possible when the neutron energy is great enough to raise the nucleus above its first excited level. The excited nucleus may decay to the ground state by the emission of one or more gamma rays, and the energy of the emitted neutron E is given as the difference between its incident energy E_n and the energy of the first excited level E_1.

$$E = E_n - E_1 \qquad \ldots\ldots\ldots 2\text{-}5$$

The threshold energy which the neutron must have to make the inelastic scattering process energetically possible is given by:-

$$E_{th} = \frac{A+1}{A} E_{ex.} \qquad \ldots\ldots\ldots 2\text{-}6$$

where

E_{th} - inelastic threshold energy

A - mass of the target nucleus

E_{ex} - the energy of an excited state of the target nucleus

In general if a monoenergetic beam of neutrons is incident on a target nucleus a spectrum of neutron energies is emitted consisting of a series of groups corresponding to a transition to different levels. The relative intensities of these groups are determined by the partial widths for the different modes of decay of the compound nucleus, and some of the groups may appear as a continuous spectrum in the region where the levels of target nuclei are very closely spaced.

The inelastic scattering is very important in problems of reactor design and shielding. In the first case it is the main

process by which fast neutrons are slowed down below the inelastic scattering threshold and furthermore inelastic scattering produces gamma rays which have to be considered in shielding problems.

2-4 Radiative Capture X(n,γ)Y

For neutrons below the inelastic scattering threshold the only reactions which occur with appreciable cross-section are elastic scattering and radiative absorption. The radiative capture process is possible at all neutron energies, but is most probable at low energies (less than 1 keV). However at low energies some particle emission reactions with very light nuclei, and fission with very heavy nuclei can take place[9].

When a neutron is captured by the nucleus the resulting compound nucleus is formed in a highly excited state, because the captured neutron adds to the system both its kinetic energy and it binding energy (~ 8 MeV). Since the compound nucleus lies above its ground state it decays either by the re-emission of a neutron or by emitting one or more gamma photons. However the excitation energy of the compound nucleus is shared between its nucleons and the emission of one of these nucleons is not possible until the nucleon gains an energy greater than its binding energy in the nucleus. Therefore one can expect that when the excitation energy is shared among a large number of nucleons, the average time before neutron emission is much more than the average time required for gamma emission, so the compound nucleus may decay by emitting one or more gamma rays[10].

The compound nucleus may release the excitation energy with the emission of a single gamma ray and go to its ground state, or it may emit several gamma rays of lower energy by going from the

excited state level to intermediate levels then finally to the ground state.

The existence of capture gamma rays greatly complicates the shielding problem, since it is no longer sufficient to slow down the neutron and then capture it, and therefore it becomes more significant to use materials as a neutron absorber which do not give gamma rays on capturing the neutron. ^{6}Li is an isotope which has very high capture cross-section at thermal neutron, and on neutron capture gives charged particles which are easily stopped.

2-5 Particle Reactions

Neutrons may also disappear as a result of particle emission reactions, in which the neutron is absorbed by the nucleus which may decay by the emission of other particles, and the nucleus resulting from these interactions may be unstable and decay by further gamma ray or particle emission.

Particle reactions are most prevalent for neutron energies above about 1 MeV. Below that energy the reaction is generally inhibited by the energetics of the process or by the Coulomb barriers which must be penetrated by the reaction products. However in the case of a very light element it may occur at intermediate or thermal energies e.g. $^{10}B(n,\alpha)^{7}Li$, $^{6}Li(n,\alpha)T$.

The most common of the above types of reactions are:-

2-5-1 The (n,2n), and (n,3n) reactions

For an incident neutron with energy greater than the binding energy of the last neutron in the nucleus the emission of two or three neutrons becomes possible.

This reaction could be regarded as a type of inelastic scattering in which the first neutron comes out with an energy less

than the difference between the energy of the primary incident neutron and the threshold energy, in that case the residual nucleus is in a state having enough excitation energy to be able to emit a second neutron. The (n,2n) reaction rapidly becomes more probable than (n,n') reaction as the incident neutron energy increases above the threshold for the (n,2n) reaction, and the bulk of the inelastic scattering is now included as part of the (n,2n) reaction.

The Q-value of the (n,2n) reaction is equal to the binding energy of the most weakly bound neutron in the target nucleus, and the threshold energy in laboratory system is given by:-

$$E_{th} = \frac{A+1}{A} Q \qquad \ldots\ldots\ldots 2\text{-}7$$

where

E_{th} - is the threshold energy

A - is the mass number of the target nucleus

In the case of (n,3n) reaction the relation of the (n,3n) reaction to the (n,2n) reaction is similar to that of the (n,2n) and (n,n') reaction. Thus a third neutron will be emitted if the target nucleus still has sufficient excitation energy after the emission of the second neutron in the (n,2n) reaction to free a further neutron. The (n,3n) cross-section therefore rises from the (n,3n) threshold at the expense of the (n,2n) cross-section. The (n,3n) threshold is so high it ranges from roughly 11 to 30 MeV which makes this reaction unimportant in fission reactor calculations, but it has some significance in fusion reactors.

2-5-2 Charged Particle Reaction (n,p), (n,α)

These reactions are usually endoergic, however in a few light nuclei they are exoergic as $^{10}B(n,\alpha)\ ^{7}Li$, $^{6}Li(n,\alpha)^{3}H$, $^{14}N(n,p)^{14}C$.

These reactions are useful in that they do not give rise to energetic gamma rays.

2-5-3 Fission Reaction (n,f)

In the fission process the nucleus absorbs a neutron and the resulting compound nucleus is so unstable that it immediately breaks up into two lighter nuclei called fission fragments[12]. The probability of neutron induced fission is described by the fission cross-section σ_f and it is a function both of the target nucleus and the energy of the incident neutron.

2-6 Neutron Reaction with LiF

In considering the 14.1 MeV neutron produced from the $D(T,n)^4_2He$ reaction with the LiF, the most important reactions are those that produce tritons. The fast neutrons that react with ^7Li will with fairly high probability produce a triton and neutron by the reaction,

$$^7_3Li + ^1_0n \rightarrow T + ^1_0n + ^4_2He$$

and the resulting neutron may be moderated by elastic scatters with ^6Li and ^7Li nuclei and captured by the ^6_3Li $(n,\alpha)T$ reaction to produce further tritons[13].

The possible reactions of neutrons with lithium fluoride are as shown in table [2-1].

For the thermal region the high cross-section for the $^6Li(n,\alpha)T$ reaction makes it the dominant interaction (in natural lithium 7.56% ^6Li, 92.44% ^7Li 98.59% at 0.025 eV compared with elastic scattering from ^6Li and ^7Li 1.41%). At 1 keV this has changed to 3.5% (n,α) reactions to 65% inelastic scattering in lithium and at 0.5 MeV 2.2% (n,α) reactions to 97.8% elastic

scattering. At 14 MeV the (n,α) reaction only has about 0.13%

TABLE [2-1] The fast neutron reaction with LiF

Interaction	Fig. of the cross-section
^{6}Li (n,α)T	Fig. [2-2]
^{6}Li (n,n)^{6}Li	Fig. [2-3]
^{6}Li (n,n')$^{6}Li^{*}$	Fig. [2-4]
^{6}Li (n,nd)α	Fig. [2-5]
^{6}Li (n,p)^{6}He	Fig. [2-6]
^{7}Li (n,t,n)α	Fig. [2-7]
^{7}Li (n,n)^{7}Li	Fig. [2-8]
^{7}Li (n,n')$^{7}Li^{*}$	Fig. [2-9]
^{19}F (n,n')$^{19}F^{*}$	Fig. [2-10]
^{19}F (n,n)^{19}F	Fig. [2-11]

probability but inelastic reactions are now about 30% of the total, elastic scattering still being the most important reaction[14].

The cross-sections versus energy for the reactions of neutrons with LiF are shown in Figures [2-2] - [2-11].

2-7 Neutron Interaction with U^{238}

U^{238} undergoes fission with fast neutrons: This fission is a threshold reaction and the fission cross-section varies with energy as shown in Figure [2-12].

The second reaction is neutron capture U^{238} (n,γ) U^{239}, which is one of the important reactions in fast reactor calculations, for that reaction there is a need for better cross-section data in the keV energy range since this reaction leads to Pu production,

the uncertainty in the value of this cross-section[15] below 200 keV is ± 15% and between (200-500 keV) is about ± 10%. The cross-section curve is shown[13] in Figure [2-13].

Thirdly the inelastic reactions (n,n) (n,2n) and (n,3n) occur at higher neutron energies if the incident neutron has an energy above the threshold for (n,2n) reaction it is likely that a second neutron will appear, as a result the (n,2n) cross-section rises rapidly above its threshold, and similarly for the (n,3n) reaction as shown in Figure [2-14].

The elastic scatter cross-section for neutrons on U^{238} is shown in Figure [2-15]. At low energy its cross-section has a constant value followed by a very sharp resonance with width usually ~ 1 eV, the cross-section rises to greater heights, as moving to higher energies the resonances can no longer be resolved and then the cross-section becomes a smooth function of the neutron energy[16].

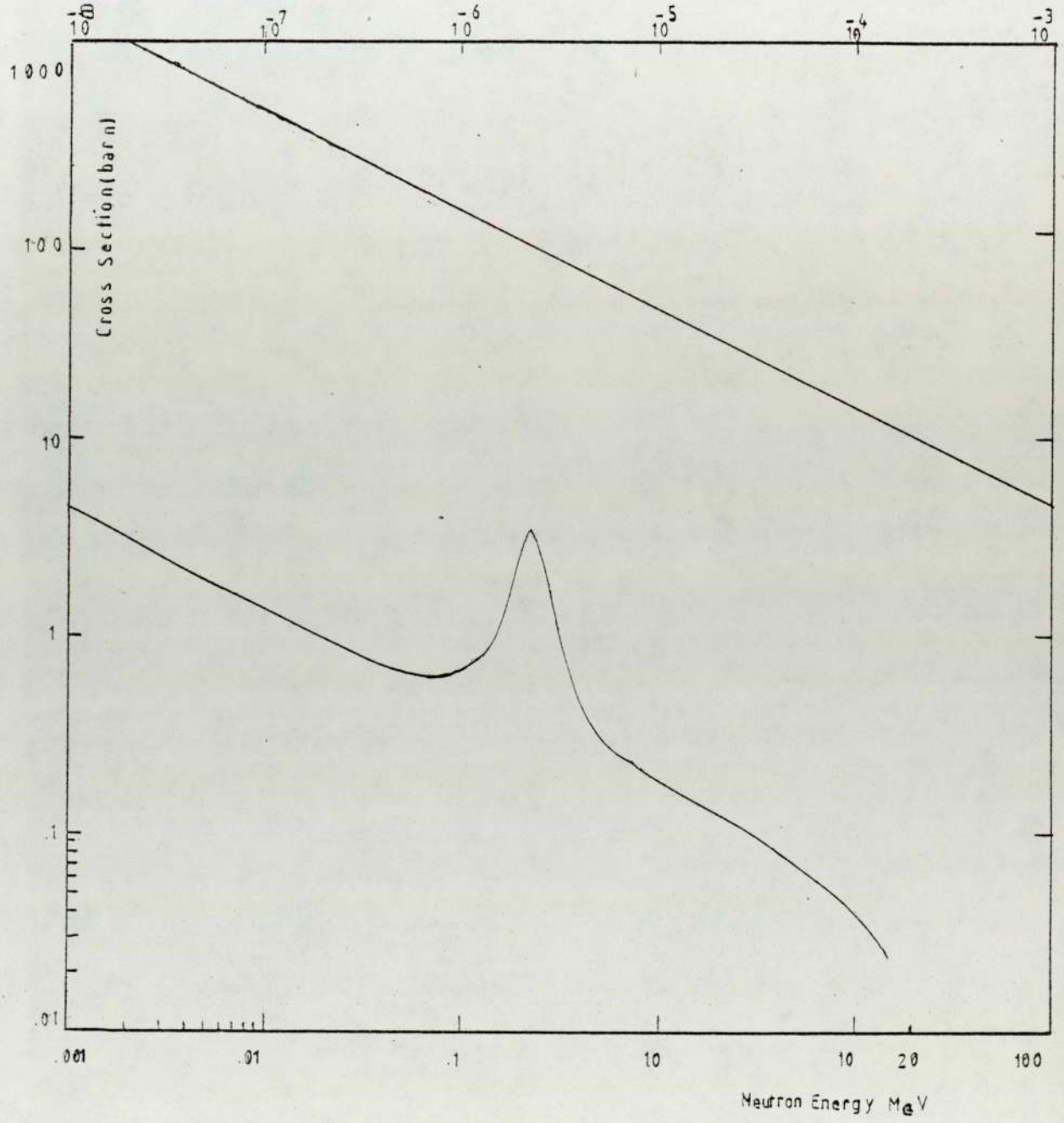

Fig. [2-2] ^{6}Li (n,α)T Reaction Cross-Section [UKNDL]

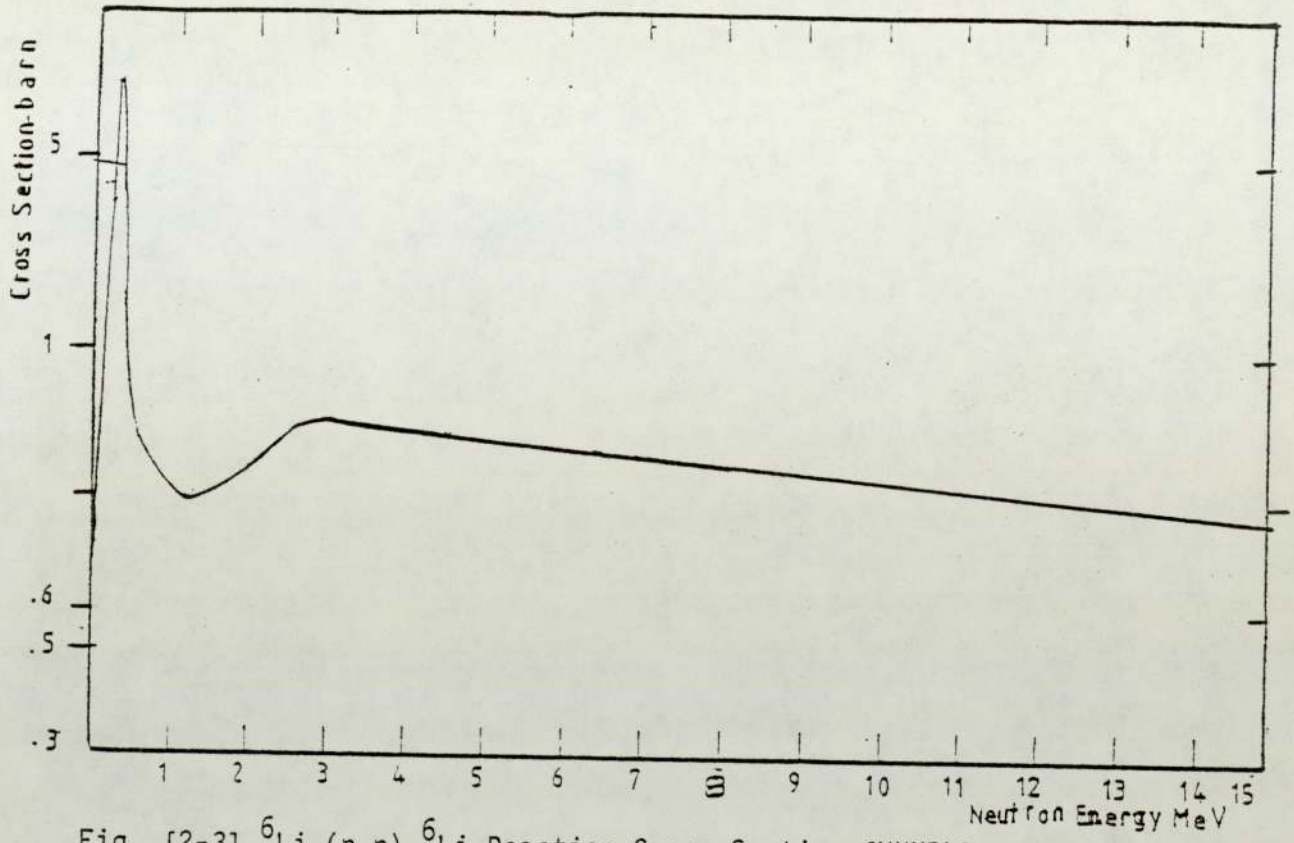

Fig. [2-3] ^{6}Li (n,n) ^{6}Li Reaction Cross-Section [UKNDL]

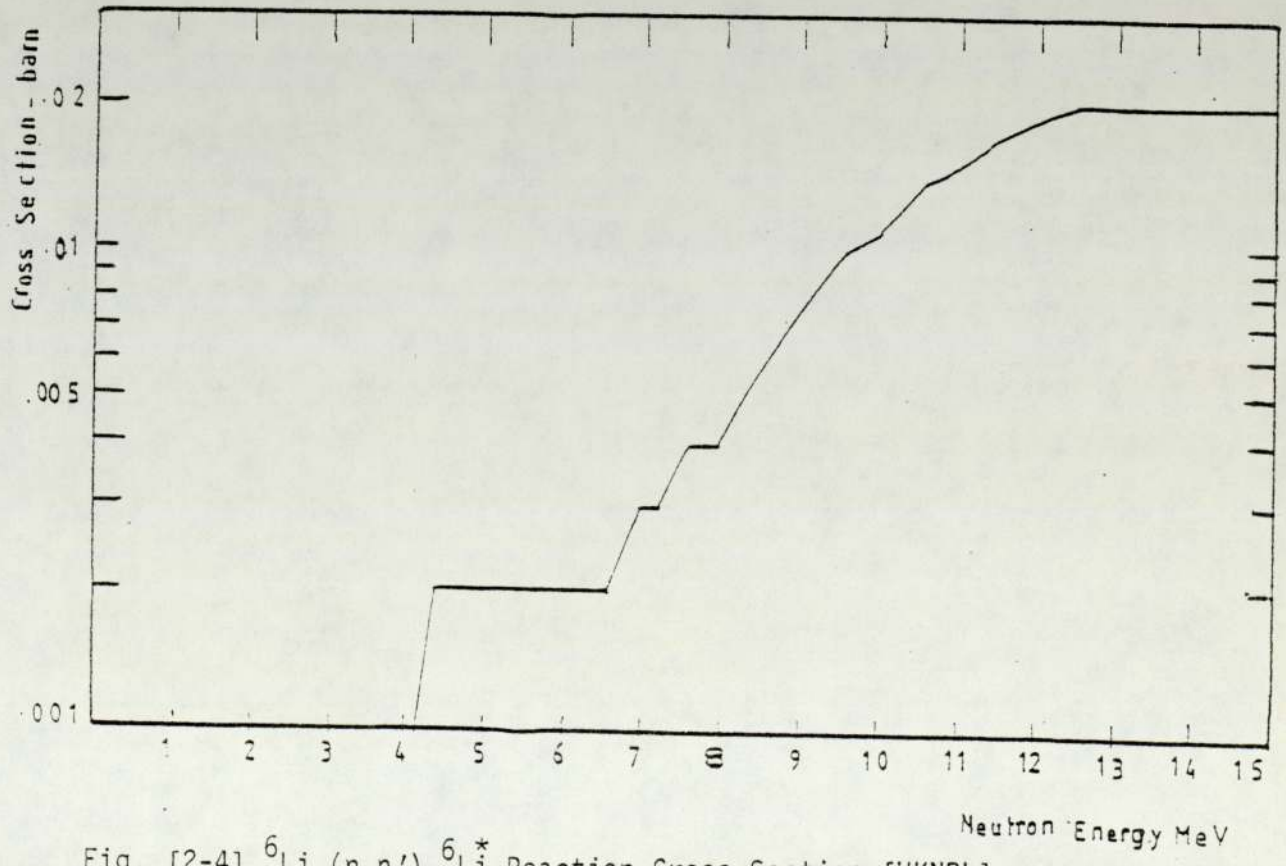

Fig. [2-4] ^{6}Li (n,n') $^{6}Li^{*}$ Reaction Cross-Section [UKNDL]

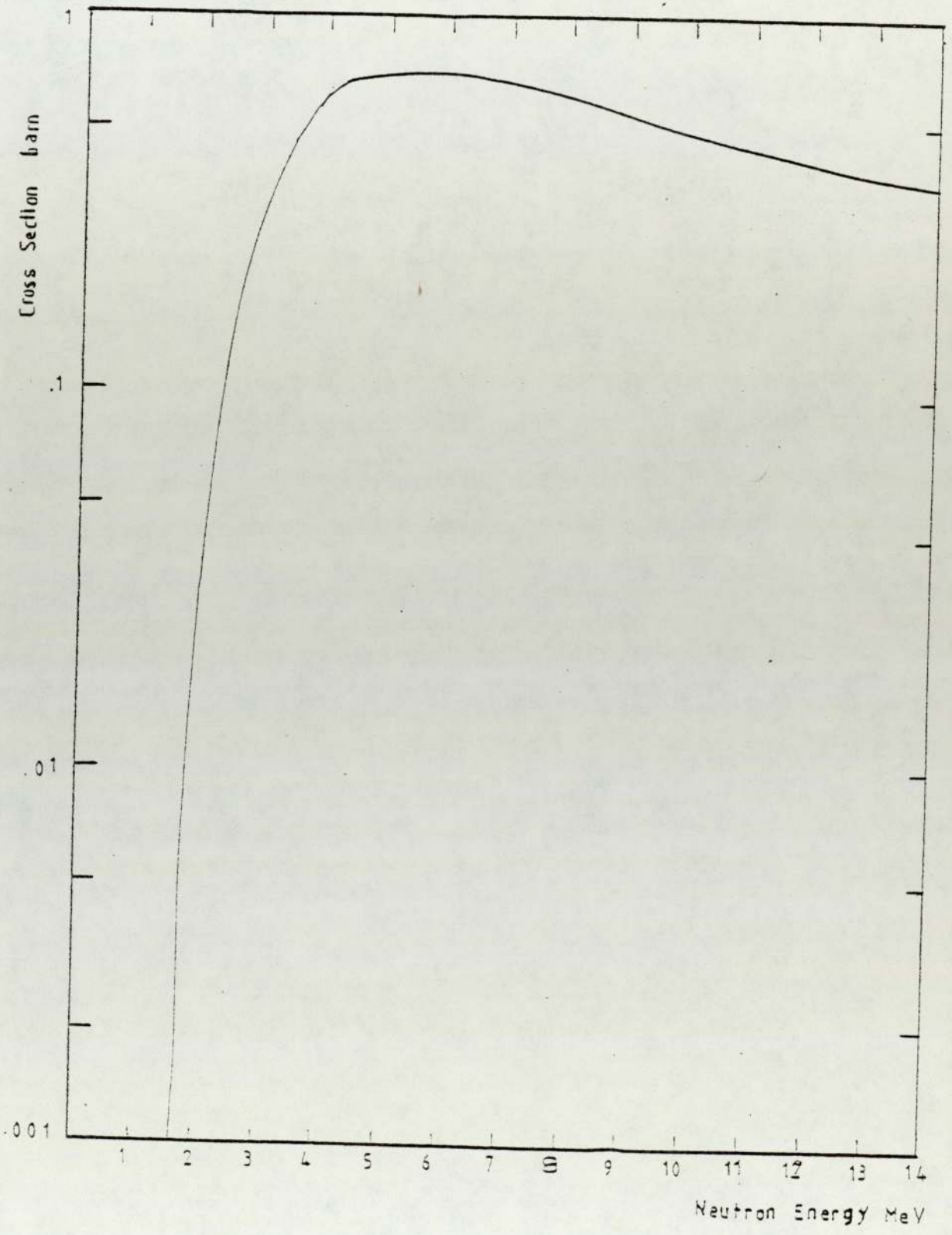

Fig. [2-5] ^{6}Li (n,nd)α Reaction Cross-Section [UKNDL]

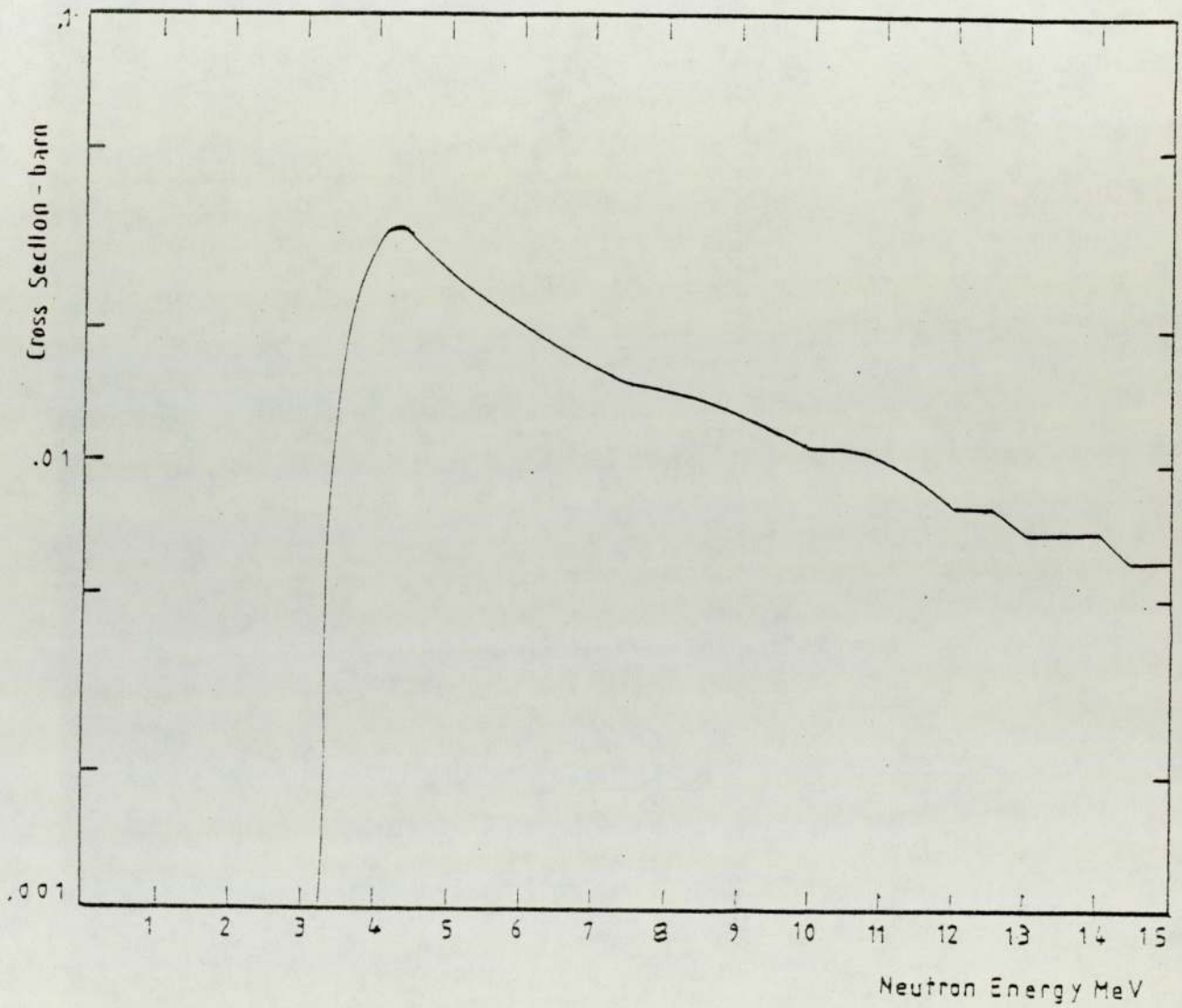

Fig. [2-6] ^{6}Li (n,p) ^{6}He Reaction Cross-Section [UKNDL]

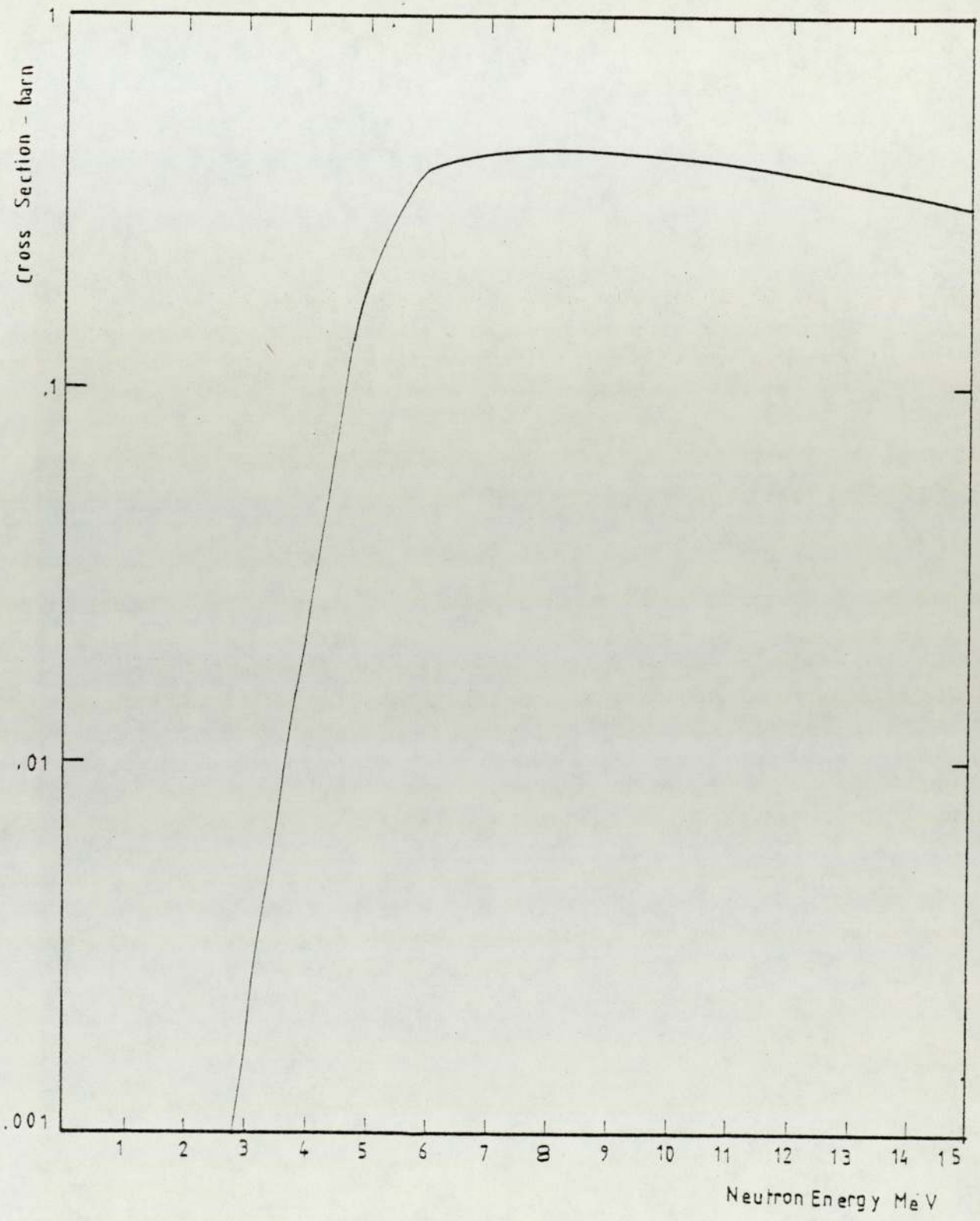

Fig. [2-7] ^{7}Li (n,n,t)α Reaction Cross-Section [UKNDL]

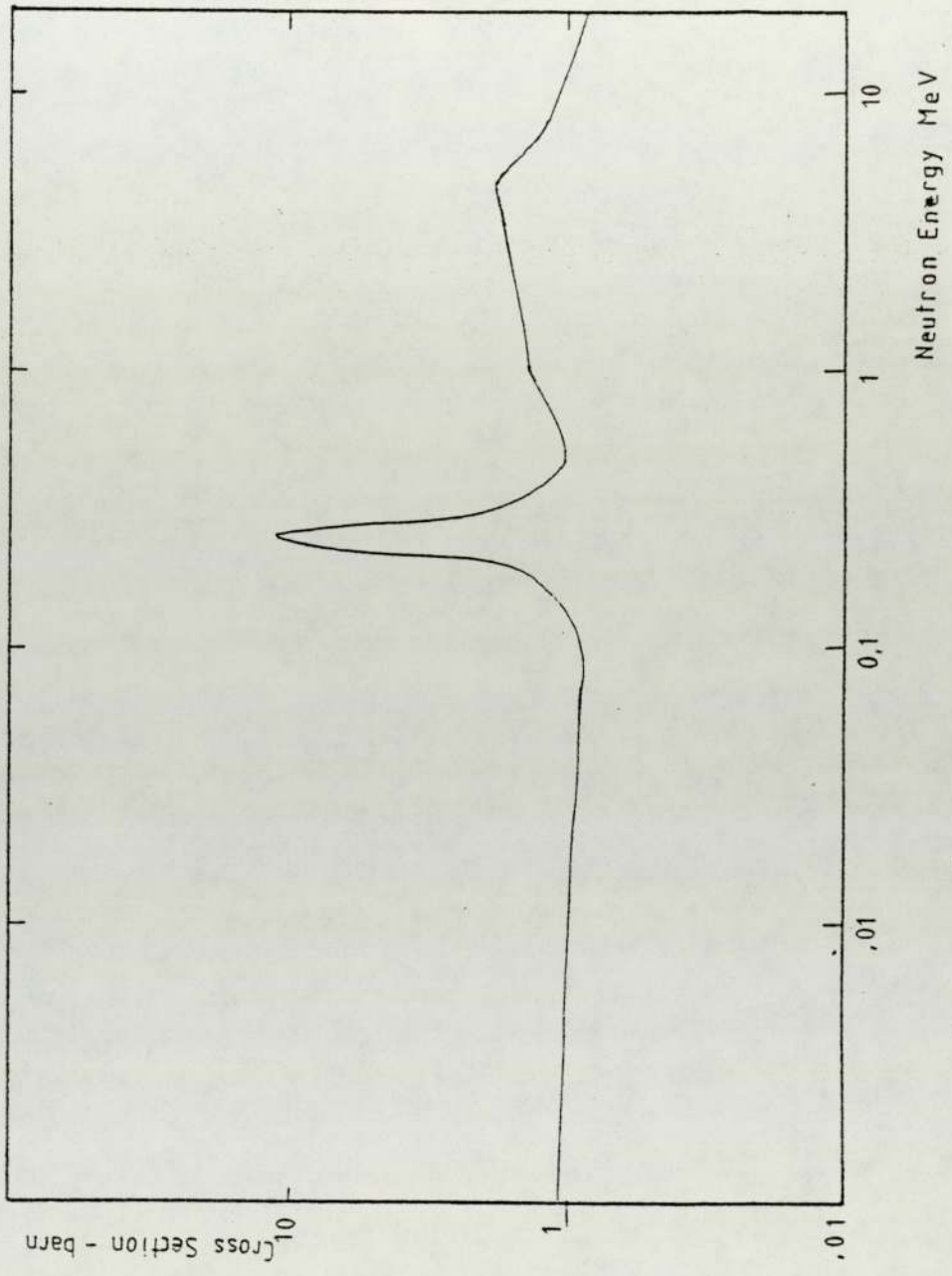

Fig. [2-8] ^{7}Li (n,n) ^{7}Li Reaction Cross-Section [UKNDL]

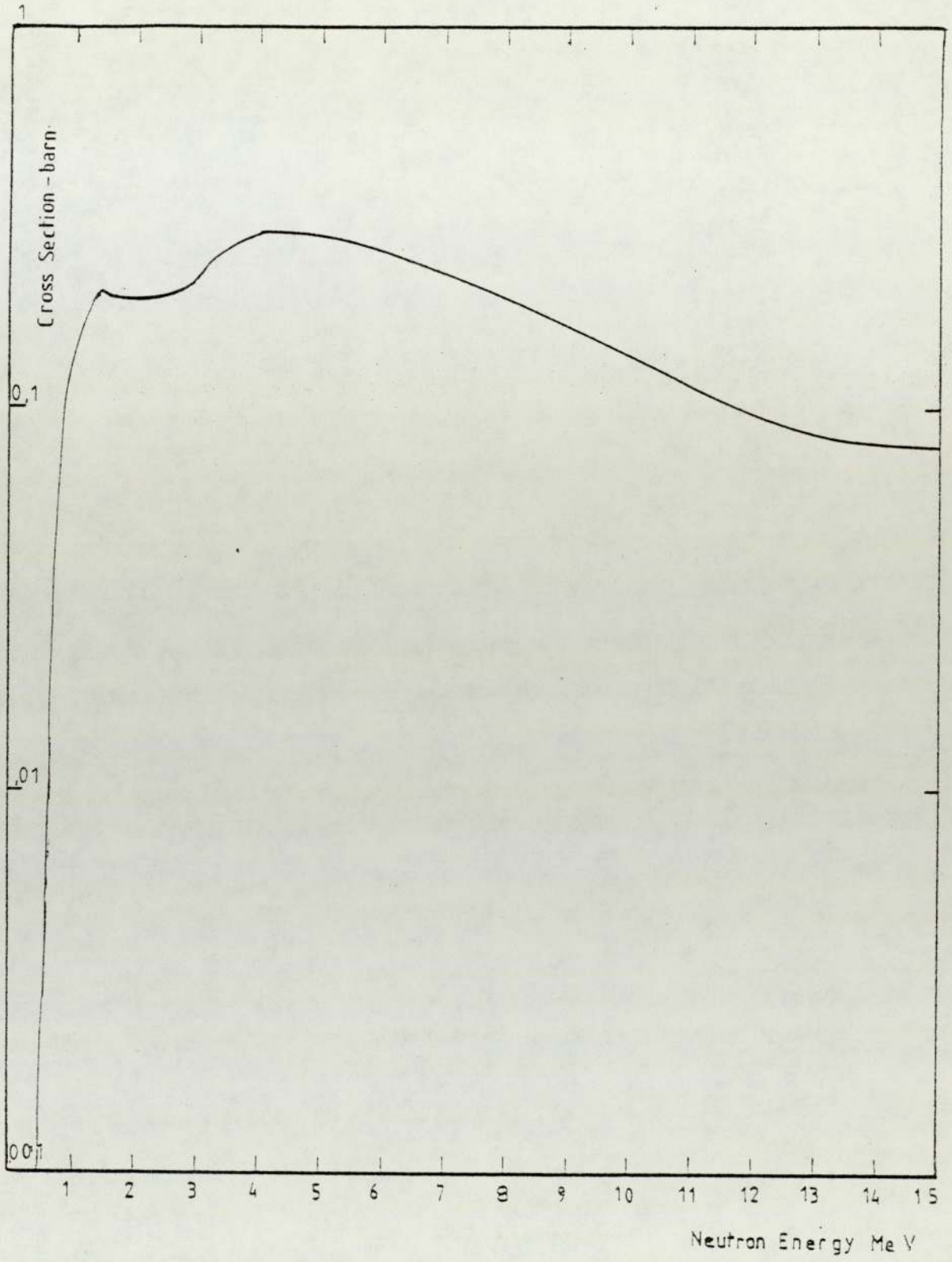

Fig. [2-9] $^{7}Li\ (n,n')\ ^{7}Li^{*}$ Reaction Cross-Section [UKNDL]

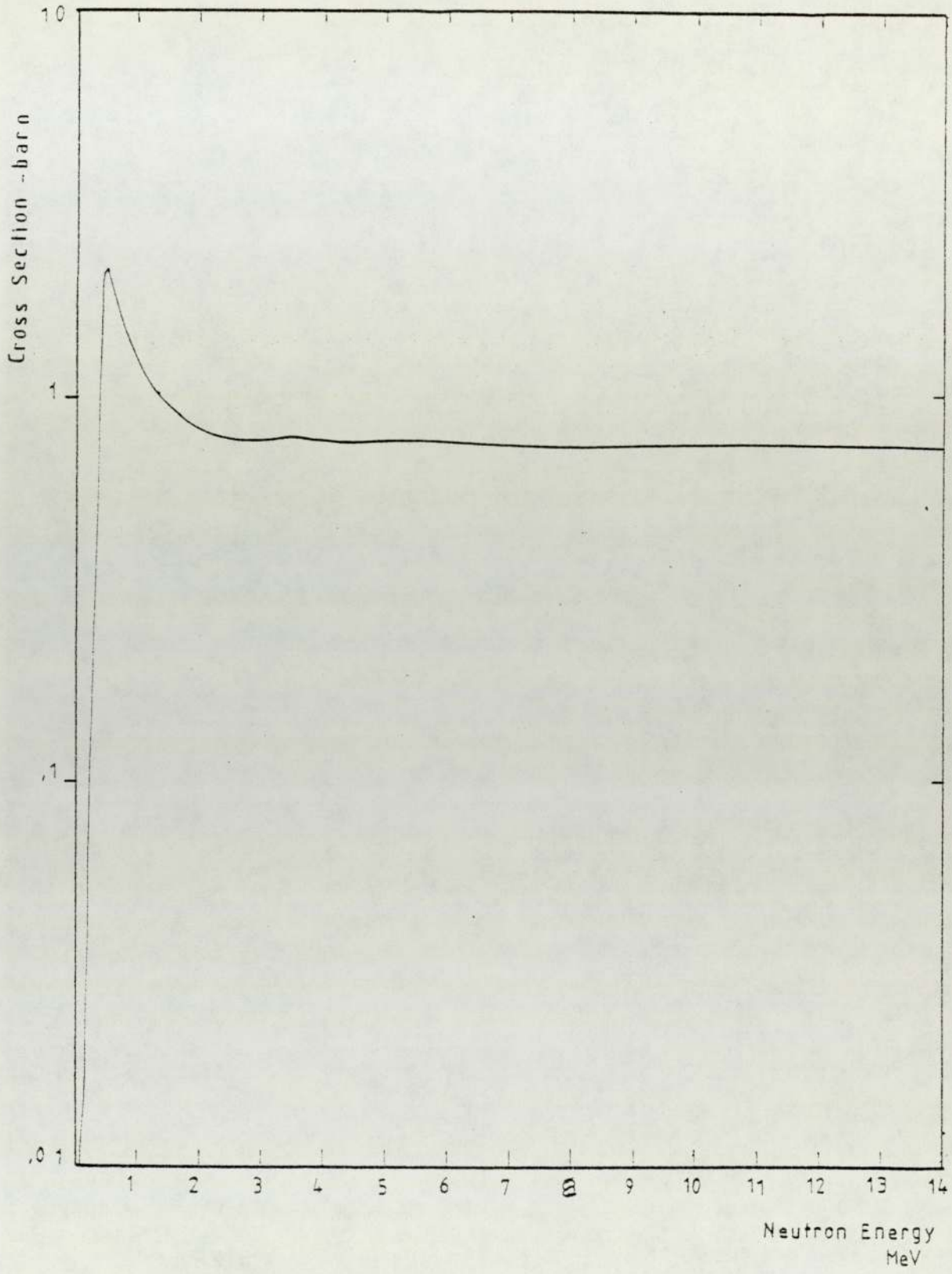

Fig. [2-10] ^{19}F (n,n') $^{19}F^{*}$ Reaction Cross-Section [UKNDL]

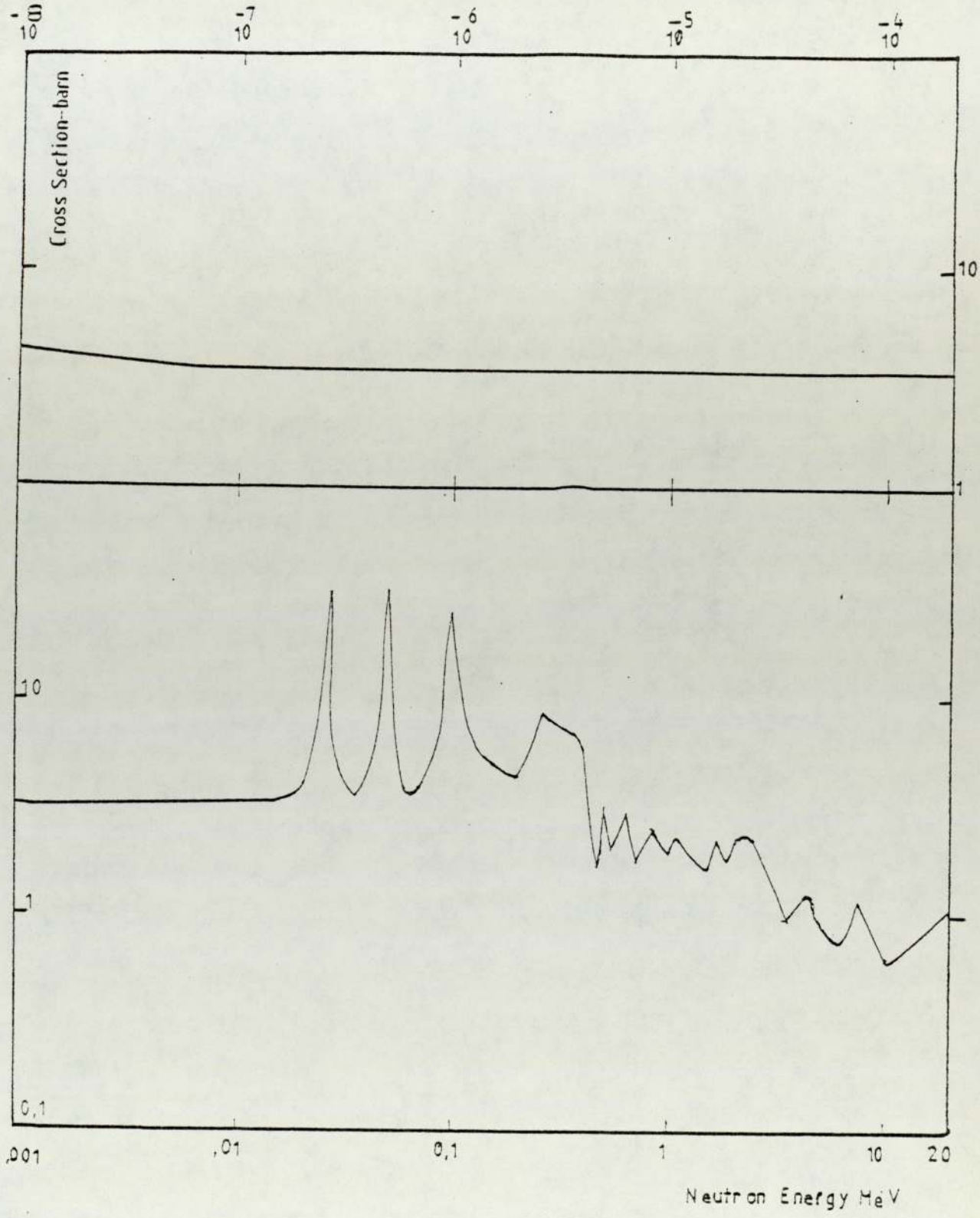

Fig. [2-11] ^{19}F (n,n) ^{19}F Reaction Cross-Section [UKNDL]

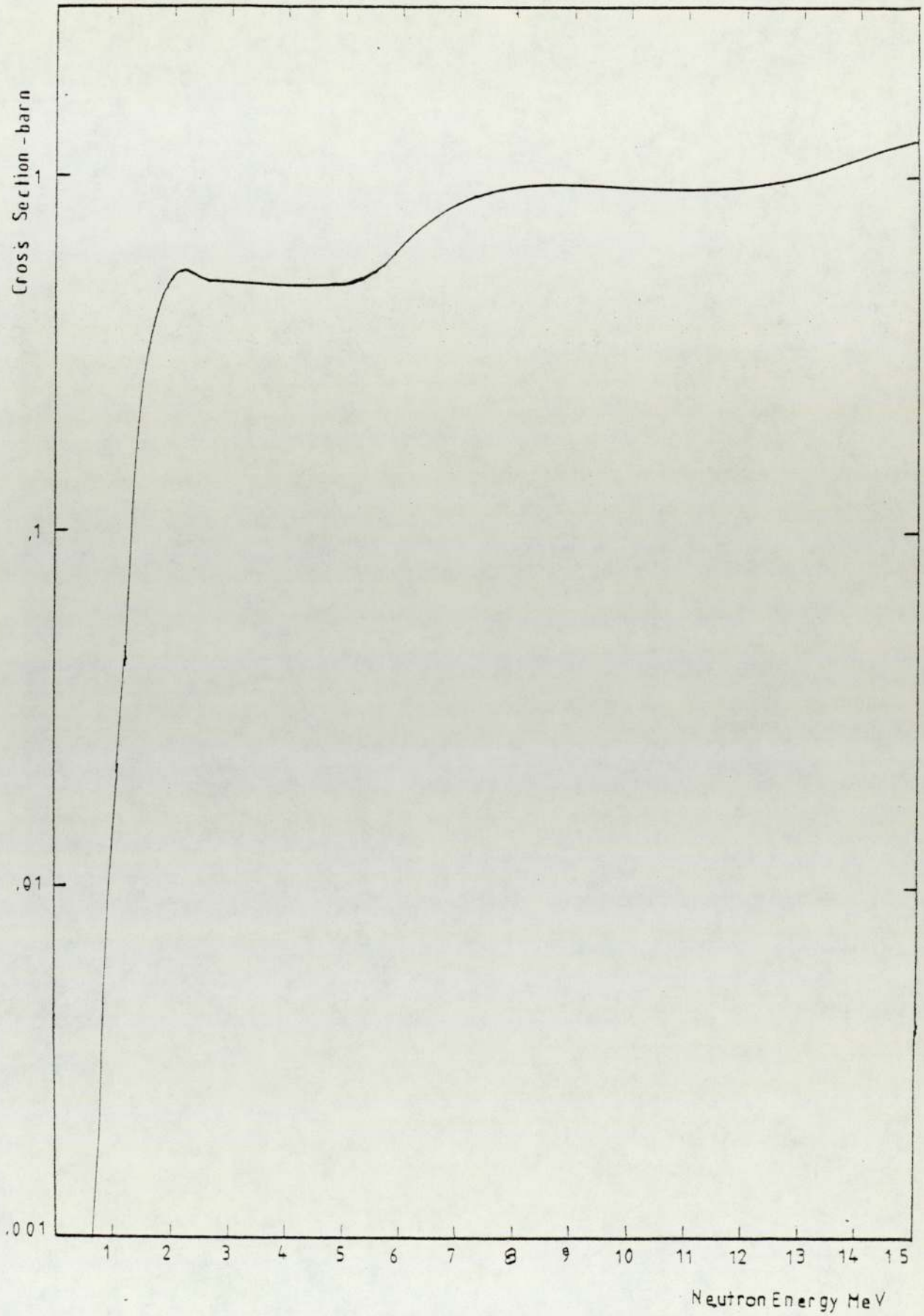

Fig. [2-12] U^{238} Fission-Cross-Section [UKNDL]

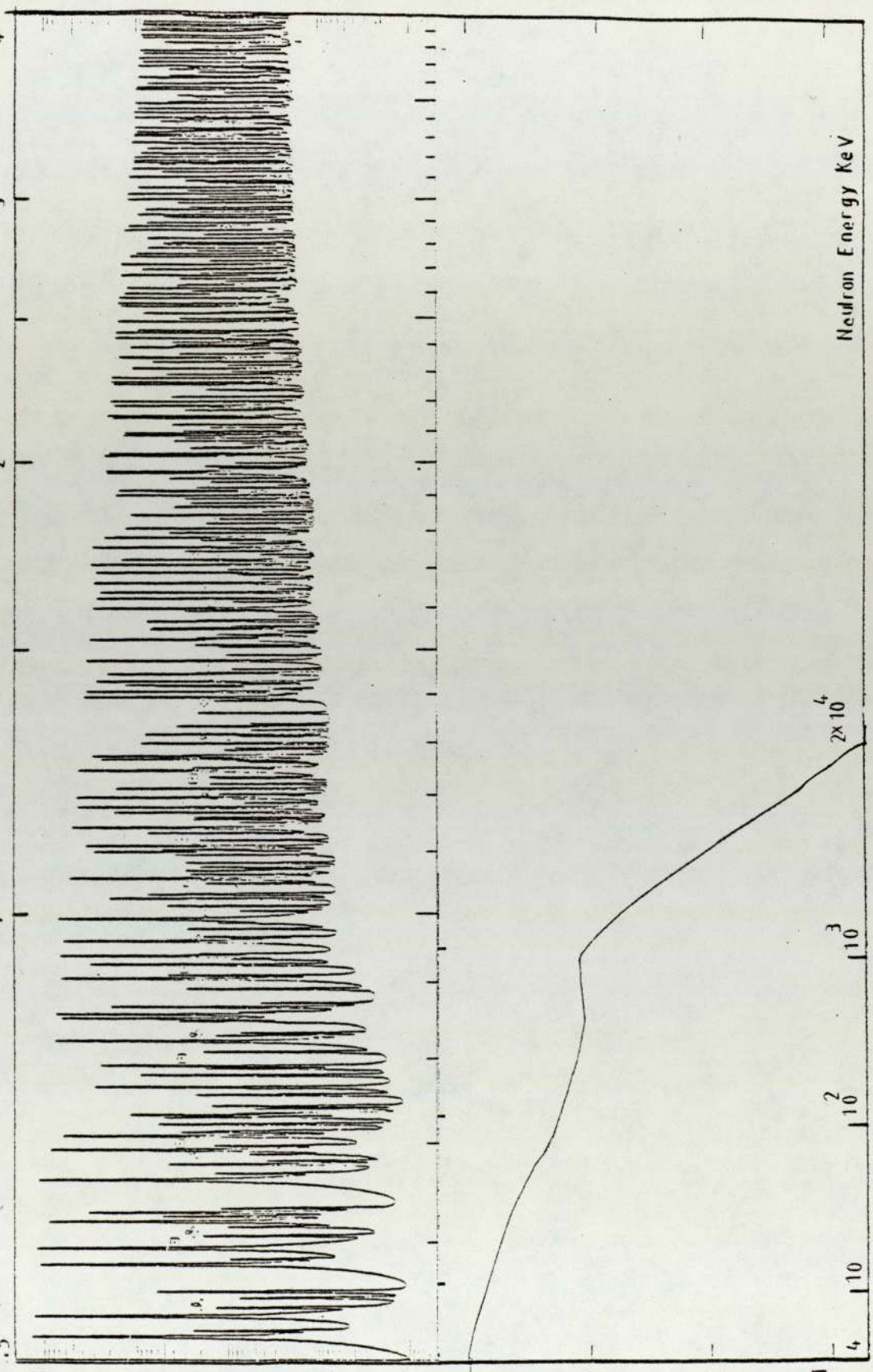

Fig. [2-13] U^{238} (n,γ) Reaction Cross-Section [Ref. 21]

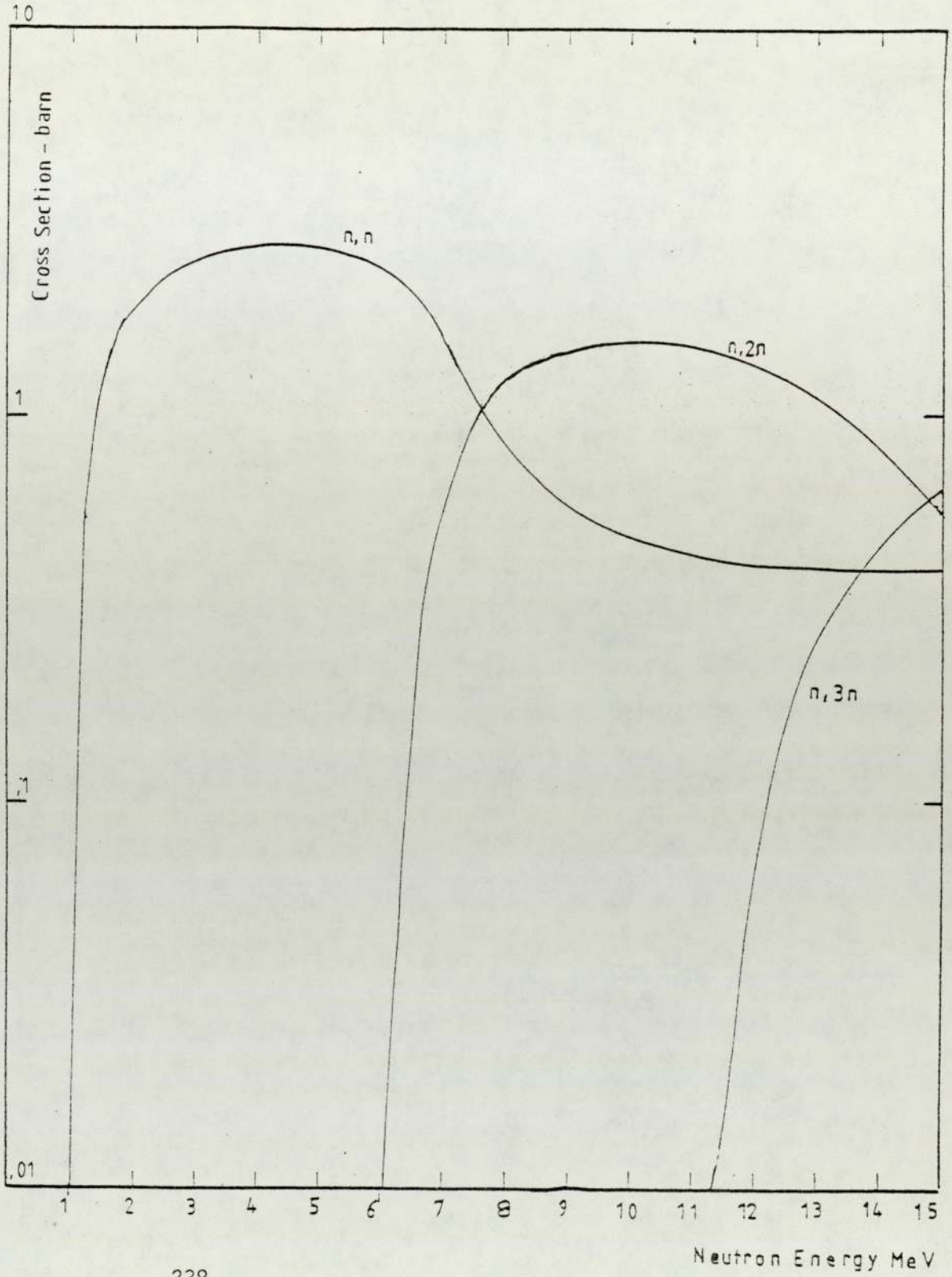

Fig. [2.14] U^{238} (n,n), (n,2n), (n,3n) Reaction Cross-Section [UKNDL]

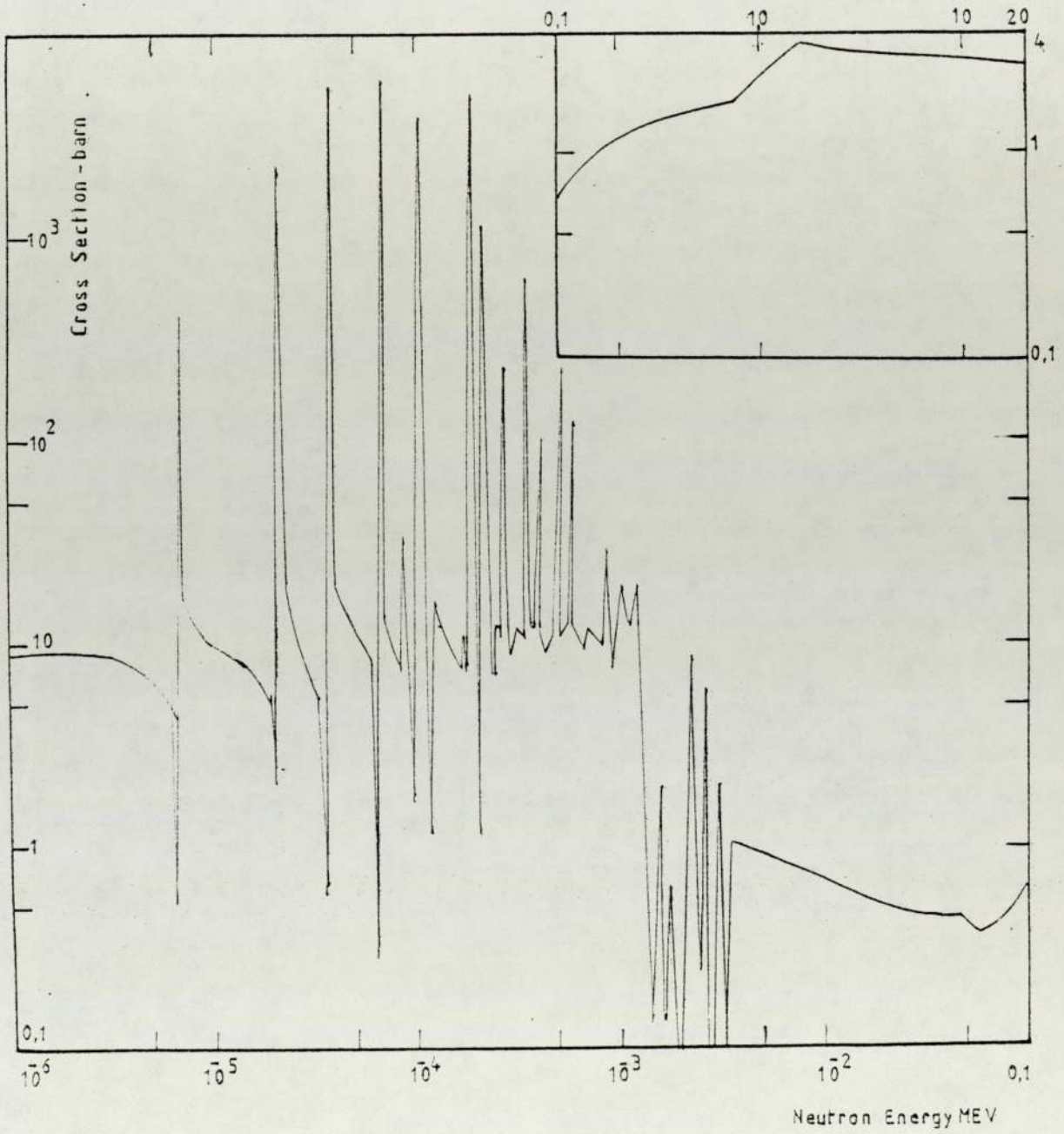

Fig. [2-15] U^{238} (n,n) U^{238} Reaction Cross-Section [UKNDL]

CHAPTER 3

FAST NEUTRON DETECTORS

3-1 Introduction

A detection system usually consists of two parts, a detector for the incident particle and a measuring system to measure the output signals from the detector. The detection of nuclear particles and radiation is based on the detection of ionization produced when passing through matter so the detection of neutrons is in general more complicated than those of charged particle because of their lack of charge and consequent lack of ionizing power, and their very wide range of energies.

Neutron interactions with nuclei are of two types, scattering or absorption. In the scattering interactions the neutron collides with the nucleus and a fraction of the neutron energy is transferred to the recoil nucleus.

In the absorption interaction, the neutron is absorbed by the nucleus and disappears so the neutron must therefore take part in a nuclear reaction which results in the emission of charged particles which in turn interacts with the detector and produce ionization and excitation of the molecules. In such cases the primary energy of the neutron is dissipated through the emission of secondary charged particles which lose their energy on passing through matter. Two media may be involved, one of which is a radiator (scattering material) where the neutron may interact to produce charged particles and another one in which the charged particles may dissipate their energies. These two components of the detection may be physically distinct as in the case when protons are ejected from a hydrogeneous

foil by fast neutrons to expend their energy in ionizing a gas. In this case the energy dissipated in the scattering medium by the charged particles is wasted so if the two components may occupy the same space as when the gas itself is a hydrogen. Therefore it is an advantage in designing a system with a combined reaction and detector medium for the detection of the neutron.

3-2 The Main Parameter Effect Choosing the Neutron Detector

A great variety of methods have been used to measure the energy spectra of fast neutrons[17]. The techniques include nuclear emulsion[18], proton recoil telescope[19], and ^{3}He filled proportional counter[20]. The elastic scattering from hydrogen nuclei which gives rise to detectable recoil protons is the basis for fast neutron detection with the organic scintillators.

For choosing a neutron detector, suitable for certain measurements, the following factors must be considered.

a - The aim of the experiment and the experimental configuration.

b - The energy range of neutrons to be measured.

c - Flux magnitude and its variation.

d - Detector sensitivity and energy resolution.

e - Physical size of the detector.

f - The presence of other ionising radiations.

These parameters are defined by the experimental configuration, that is where the measurement will be performed (outside or inside the medium under investigation) and by the aim of the measurement: To give information about the neutron energy or the flux and in what energy range the measurement will be performed. The flux magnitude and its variation is a critical parameter for choosing a suitable detector of known efficiency and cross-section.

The physical size of the detector is considered as a limiting factor (e.g. when the measurement is performed inside the medium in the shielding investigation) a large size will perturb the flux.

The detector sensitivity to other ionising radiations is a most important factor when choosing a neutron detector. Since a neutron is usually measured in a background of other nuclear radiation (gamma-rays), therefore the detector should either be insentitive to the background radiations (threshold detector) or give output pulses having different amplitudes or different shapes, so it becomes possible to eliminate the unwanted pulses either by applying bias or pulse shape discrimination.

3-3 Reactions used in Neutron Detectors

A neutron may produce a charged particle either by collision or by initiation of a nuclear reaction, therefore most of the neutron detectors are based upon one of the following reactions.

3-3-1 (n-p) Scattering Reaction

The detection efficiency depends on the (n-p) scattering scross-section of hydrogen, which is a smooth function and decreases from 13 barn to 1 barn in the neutron energy range (0.1 - 10 MeV), and to 0.5 barn at 20 MeV[21]. Figure [3-1] shows how the cross-section varies with neutron energy.

The (n-p) reaction is isotropic in the centre of mass system so the distribution in energy of the recoil protons produced by monoenergetic neutrons is constant from zero up to a maximum value of the incident neutron energy and the energy of the recoil proton E_p is given by:

$$E_p = E_n \cos^2\Phi \qquad \ldots\ldots\ldots \quad 3\text{-}1$$

where Φ is the angle which the recoil proton makes with the direction of the incident neutron of energy E_n in the laboratory system.

If the incident neutrons are not monoenergetic and have an energy spectrum $\phi_o(E_n)$, recoil protons of energy E will be generated by neutrons of energy $E_n \geq E$.

The number of recoil protons N(E) in a unit energy interval is given by:

$$N(E) = A \int_{E}^{\infty} \frac{\phi_o(E_n)(1-e^{-\Sigma d})}{E_n} dE_n \qquad \ldots\ldots\ldots \text{3-2}$$

where

Σ - the macroscopic scattering cross-section of hydrogen assuming a pure hydrogen detector

d - the detector thickness

A - detector area

By differentiating the recoil proton spectrum given by equation (3-2), we obtain the neutron energy spectrum in the following equation.

$$\phi_o(E) = \frac{E}{A(1-e^{-\Sigma d})} \frac{d\,N(E)}{dE} \qquad \ldots\ldots\ldots \text{3-3}$$

The (NE - 213) liquid scintillator detector which will be discussed hereafter is an example of proton recoil detectors.

3-3-2 Neutron Induced Reactions

The neutron interacts with the nucleus to form a compound nucleus which has an excess energy due to the binding and kinetic energy of the neutron. This energy may be released by the ejection of an energetic charged particle or by the emission of a gamma ray.

For the purpose of the neutron detection the following classification for the induced reaction are useful.

a - Exoergic reactions

In this type of reaction energy is released after the interaction of the neutron with some specific nucleus.

The reaction

$$^{3}He + n \rightarrow T + p + 765 \text{ keV}$$

is important for the neutron detection because there is a high cross-section for slow neutrons, and the product nucleus has no excited state so that for each neutron energy there is a single reaction, i.e. a monoenergetic neutron source will be represented by a line spectrum. The cross-section variation with neutron energy is shown in Figure [3-2].

For thermal neutrons the energy release is 0.765 MeV, therefore the total available energy from the capture of for example a 1 MeV neutron is 1.765 MeV which is low enough so that the emitted proton (energy 1.324 MeV) and the triton (energy 0.441 MeV) can easily be stopped in the detector, while at the same time the energy expended by the electrons from gamma ray interactions in a moderate size of ^{3}He filled chamber is considerably less than 0.765 MeV, so that their pulses will not distort the spectrum and can be eliminated with a suitable discriminator. However there are some disadvantages of this detector for the neutron energy above 1.02 MeV that the recoil ^{3}He nucleus from elastic scatters will have energy greater than 0.765 MeV so ^{3}He recoiled nucleus will appear above this peak due to the capture of thermal neutrons, and in addition that ^{3}He is relatively rare and expensive. Another useful reaction is

$$^{6}Li + n \rightarrow \alpha + T + 4.78 \text{ MeV}$$

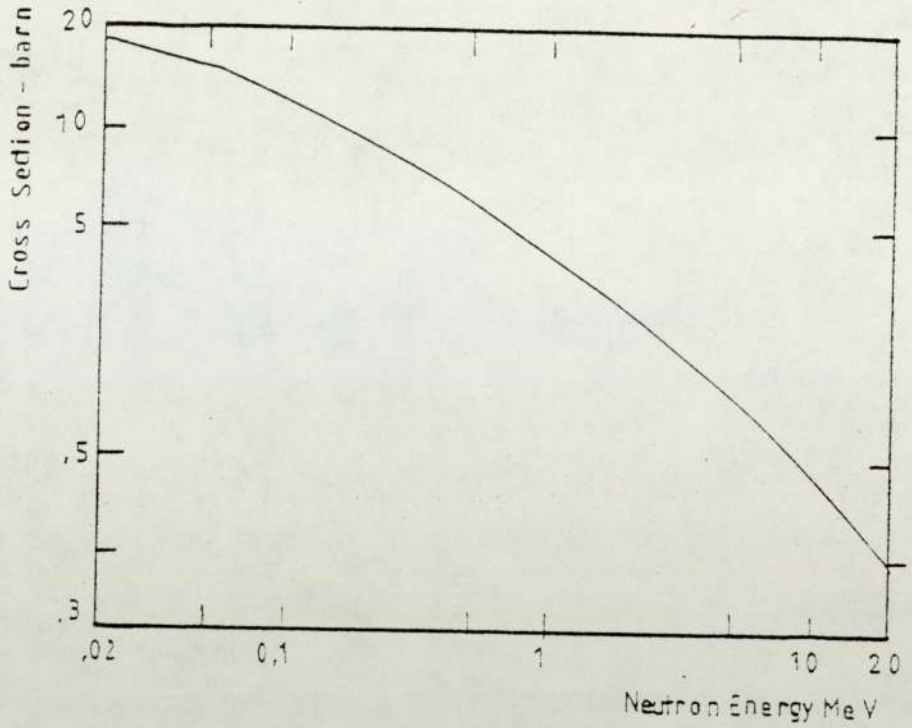

Fig. [3-1] $^{1}_{1}H$ Total Cross-Section [ref. 21]

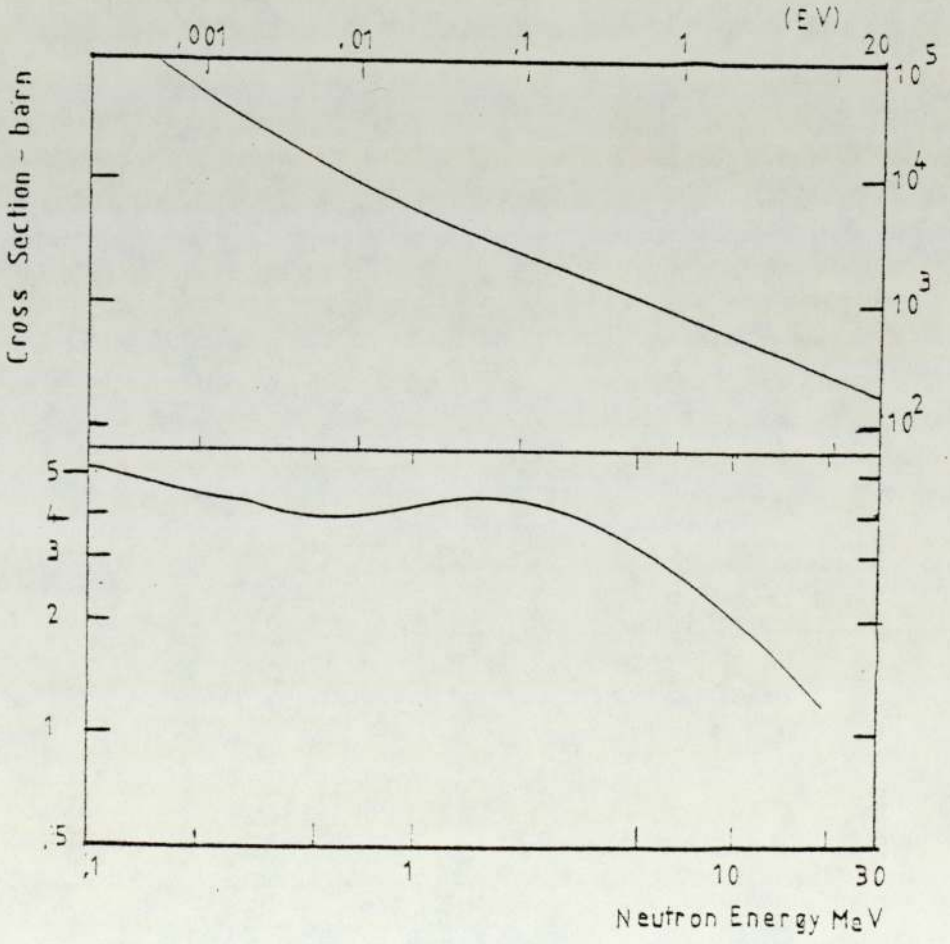

Fig. [3-2] ^{3}He Total Cross-Section [ref. 21]

That reaction has a very high cross-section for thermal neutrons (946 barn at 0.025 eV) the cross-section varies as $\frac{1}{v}$ in the thermal region, and has a peak of 3.4 barn at 0.235 MeV, and then drops down as shown in Figure [2-2]. The main advantage of this reaction is the high Q-value, so that pulses from electrons induced by high energy gamma rays will deposit energy in the detector much less than that value.

Lithium is used in scintillation counters as LiI or ^{6}LiI crystals as well as in photographic plates as a Li-loaded emulsion for the thermal, slow and fast neutron spectrum measurements[22,23,24,25]. But fast neutron measurement becomes difficult even with very low thermal neutron fluxes present, due to the very high thermal cross-section.

b - Endoergic reactions

For the threshold reaction, the kinetic energy of the reaction products is less than the kinetic energy of the initial particles by an amount equal to the reaction energy, i.e. energy is absorbed rather than liberated (however this is not true for fast fission). A direct detection of an endoergic reaction is difficult and one normally measures the activity of the radioactive products, therefore the radioactive product must have a suitable half-life so that the activity after irradiation can be followed for at least two half lives. This is important because other sources of activity may be present in the sample as a result of irradiation.

The (n,p) and (n,α) reactions are of interest in neutron detection as threshold detectors[26]. These reactions usually take place with light elements, since for the heavy elements the high coulomb barrier prevents this emission. The main threshold detectors of these types are shown in Table [3-1].

Table 3-1 Some of the threshold reactions for the fast neutron detector

Reaction	Half-life	Threshold energy MeV
$^{31}P(n,p)^{31}S_i$	2.7 hours	1.4
$^{32}S(n,p)^{32}P$	14 days	2
$^{27}Al(n,p)^{27}M_g$	9.6 min	3
$^{56}Fe(n,p)^{56}M_n$	2.6 hour	5
$^{27}Al(n,\alpha)^{24}N$	15 hours	6

Another threshold reaction (n,2n) is used as threshold detector. In this reaction a second neutron is ejected from the nucleus, so that the threshold energy is the binding energy multiplied by a correction factor $(\frac{A+1}{A})$ allowing for centre of mass motion[27]. Above the threshold energy the cross-section generally rises to a fairly flat peak around (3-5)MeV above the threshold. A typical detector is $^{63}Cu(n,2n)^{62}Cu$ with half-life of 10 minutes, and threshold about 11 MeV.

c - Thermal fission

Thermal fissile materials such as U^{233}, U^{235} and Pu^{239} are usually used for measuring thermal neutron fluxes for many purposes. They have considerable advantage over other neutron detectors where there is a gamma-ray background, since the energy release per fission

is relatively high giving fission fragments with energy about 80 MeV compared with the energy of gamma rays. Thermal cross-section is about (500-1000) barns which varies rapidly with resonances in the eV region.

For the fast fission reaction detector the fissionable elements U^{234}, U^{236}, Np^{237}, U^{238} and Th^{232} are commonly used. This fission process takes place above a certain threshold energy and these nuclides are usually used for measuring fast neutron spectra, since the cross-section above the threshold energies is relatively flat and the threshold energies cover a wide range (0.26 MeV in U^{234}, 0.32 MeV in Np^{237}, 0.70 MeV in U^{236}, 1.3 MeV in U^{238} and 1.5 MeV in Th^{232}) of considerable interest in fast reactor spectra[28].

3-4 Neutron Detector used in Present Work

The organic scintillators are used widely for measuring the energy spectrum of different radiation particles. They are available either as a pure crystal (stilbene) or in various combinations as liquid or solid solutions. The most important advantages of organic scintillations are their high speed response ($\sim 10^{-9}$ sec), high efficiency of detection for fast neutrons, and providing exact information on the number, time of arrival, and energy of nuclear particle. They can give information on the type of detected particles from the differences in the decay of the light output which is very important if the measurements are to be carried out in mixed fields of radiation.

Therefore the scintillator chosen for the present work was a small (25 mm x 25 mm) cylinder of (NE-213) liquid scintillator because it offers a good compromise between efficiency and resolution, and is small enough to fit in the shielding assembly without grossly

perturbing the system.

The (NE-213) scintillator is made with Xylene activators and POPOP as a wave shifter. Naphthalene is added to enhance the slow component of light emission. The scintillator was glass-encapsulated and bubbled with pure hydrogen (or nitrogen) to remove the undesirable oxygen which selectively quenches the slow component of light emission[29].

A plastic light pipe 25 mm in length and tapering from 25 mm to 19 mm couples the scintillator to the P.M. tube.

The NE-213 scintillator has the following characteristics:

a - Enhanced emission of delayed light which gives it good pulse shape discrimination between high and low linear energy transfer particles[30].

b - It has greater hydrogen content than stilbene[31].

c - NE-213 is a liquid so its response to the neutron is isotropic.

d - Its response to alpha-particles and carbon recoils from 14 MeV neutrons is only about half the pulse height that is produced with stilbene scintillator[29,32].

The scintillator and the P.M. tube are shown in Figure [3-3].

3-5 The Scintillator-Photomultiplier Tube Coupling

The photomultiplier tube chosen in the present work was an EMI-9826B tube 19 mm in diameter, having an electron transit time of 25 ns, and rise time of 2.2 ns. This tube has 12 stages of amplification which in spite of their small size are capable of high gain (1×10^7) without loss of stability, and it has a low dark current.

The voltage divider network Figure [3-4] is for fast pulse application, the values of the resistances were chosen to provide a series current in the network much greater than the mean anode current[33]. The voltage between cathode and focus electrode is fixed at 150 v by the Zener diode. Capacitors are required to provide peak pulse currents and to avoid pulse distortion.

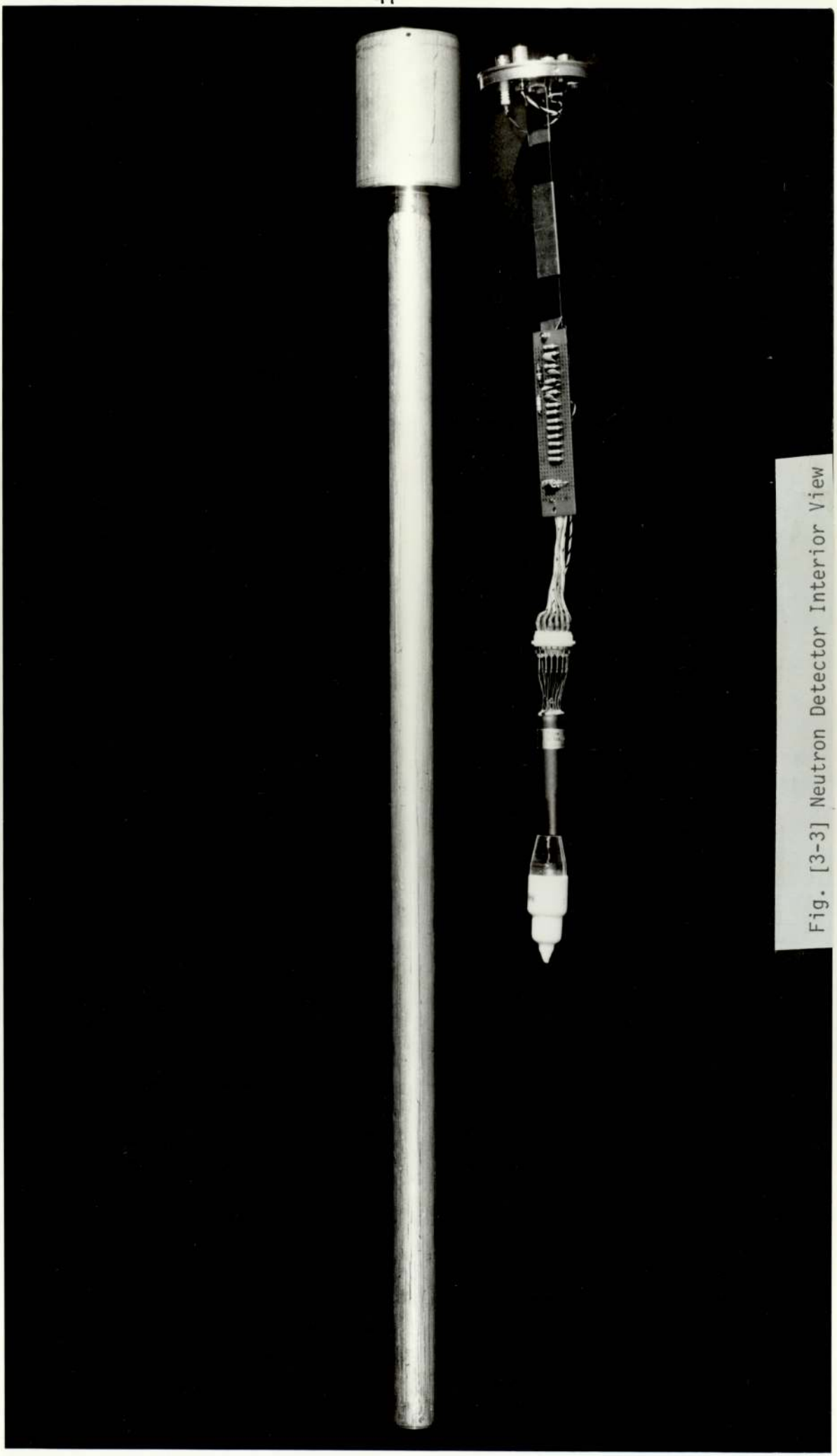

Fig. [3-3] Neutron Detector Interior View

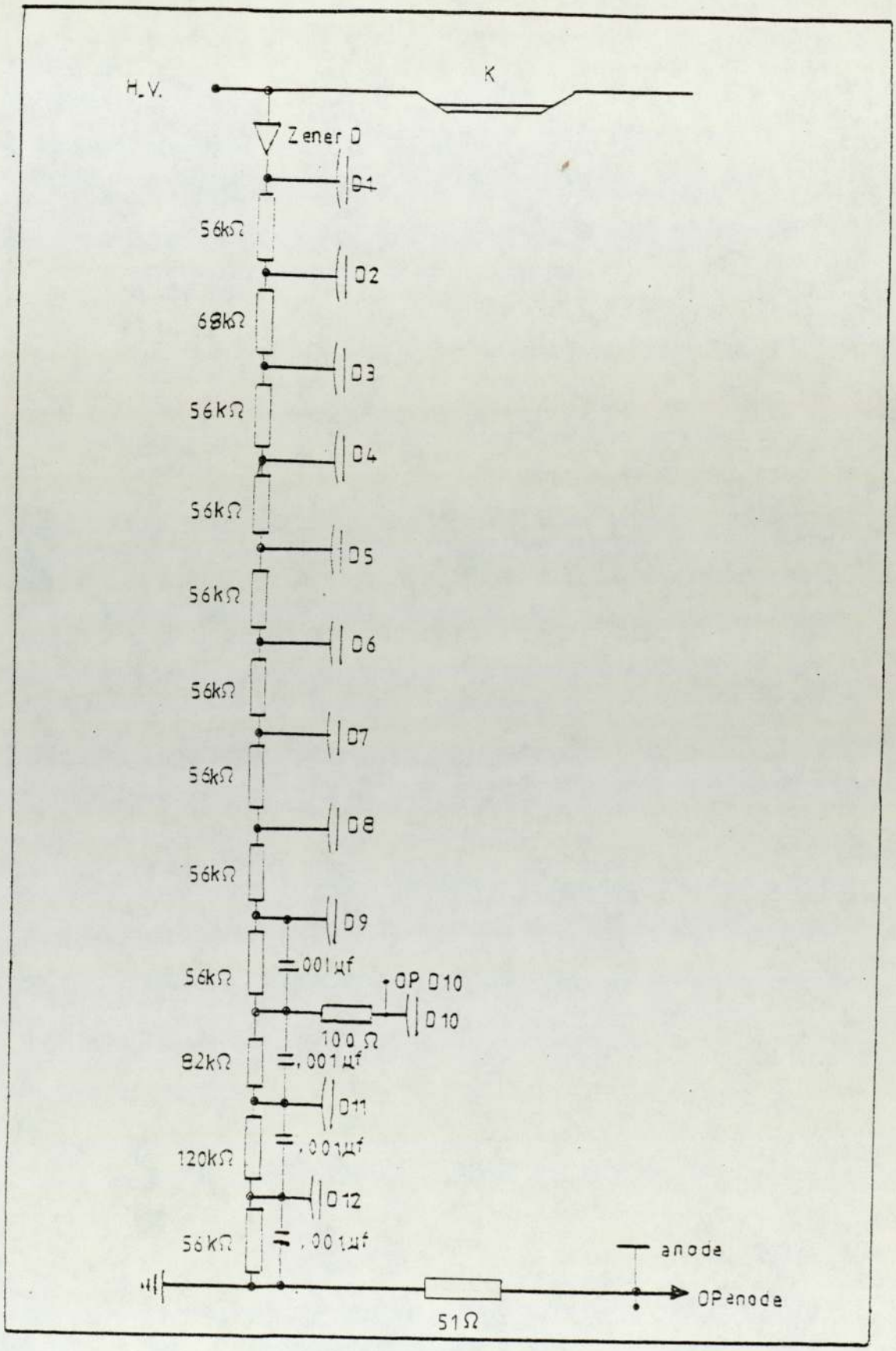

Fig. [3-4] The EMI - 98263 Photomultiply Tube Dynode Resistant Chain

CHAPTER 4

NEUTRON SPECTROSCOPY AND PULSE SHAPE DISCRIMINATION

4-1 Introduction

In the scintillation detector the mode of decay and the decay time of the light emission from the scintillator is important when the timing resolution of the instrument is estimated or when the physical processes in the scintillator are the subject of study[34]. These characteristics achieved new prominence following the report by Wright[35], that scintillations produced by alpha-particles and electrons in anthracene crystals showed decay times of 53 mμ sec and 31 mμ sec respectively. It was subsequently reported[36,37,38], that some organic scintillators have been used for measuring the number, time of arrival, energy, and particle identification of nuclear radiations.

The stilbene crystals and the liquid organic scintillators (NE-213) are used in nuclear spectroscopy because they possess desirable physical characteristics, good detection efficiency[39], large size, high speed and a good discrimination capability[40,41,42,43,44]. The pulse shape discrimination of (NE-213) is independent of the temperature for the separation and width of the peak[45].

The disadvantages include non linear light output for heavy particles and the consequent difficulty of relating the pulse spectrum resulting from proton recoils to the neutron energy spectrum.

4-2 Discrimination between Neutron and Gamma Radiation

The technique of pulse shape discrimination in liquid scintillation detectors has been widely used to detect and single out neutrons when a large background of gamma radiation is present[46]. The discrimination between the recoil electron and proton pulses during the present work was performed using the method of zero crossing technique which has been used by Alexander[47], and many other workers[48,49,50,51,52]. The zero crossing technique makes use of information contained in the time dependence of the current pulse from the photomultiplier tube.

In these scintillators the pulse consists of a component with a short decay time plus a component with a long decay time. The energy contained in the long time decay component is quite different for the recoil electron (from gamma ray) and the recoil proton (from neutron), assuming equal recoil energies. When the pulses are integrated and double differentiated the zero cross-over point is different for the neutron and the gamma ray as shown in Figure [4-1]. The timing of the cross-over with respect to the start of the pulse is sensitive to decay components in the scintillation but insensitive to pulse amplitude.

The time relationship between neutron and gamma ray pulse shapes at various points in the pulse shape discrimination system is shown in Figure [4-2]. Neutrons and gamma rays interacting with the scintillator produce at the pick-off dynode of the photomultiplier current pulses having different decay times. After integration and subsequent double differentiation, bipolar voltage pulses are produced from the dynode current pulses. These bipolar pulses cross the base line at different times corresponding to the pulse shapes independent of amplitude. Measuring of the zero crossing times of

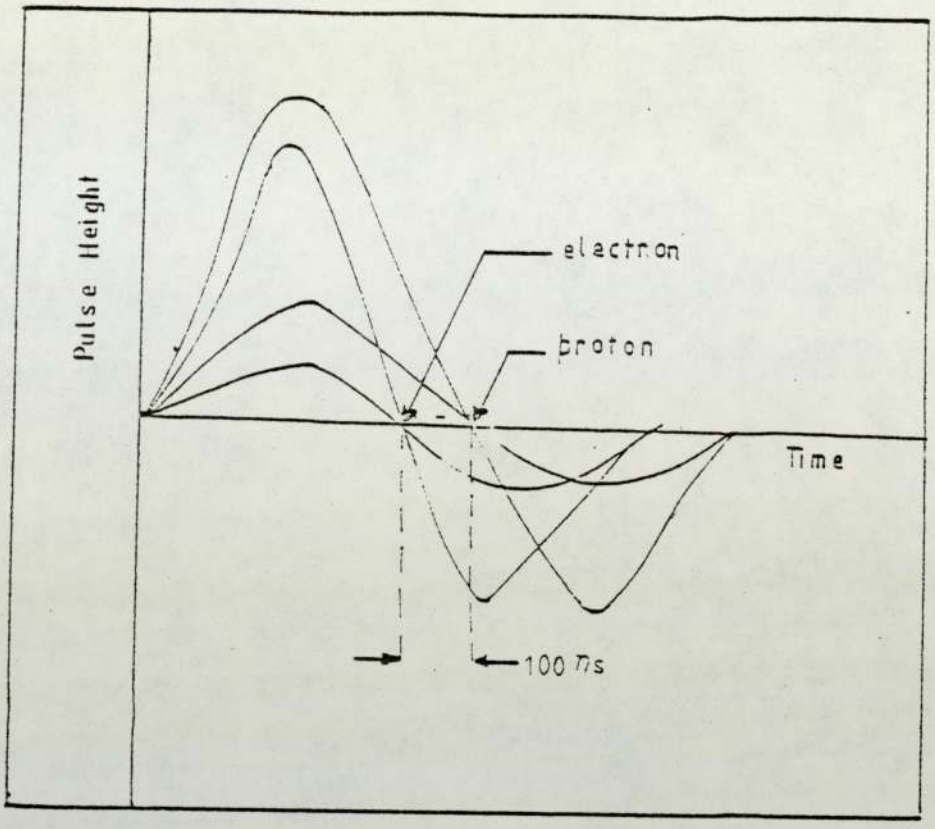

Fig. [4-1] Double Differential Dynode Pulses

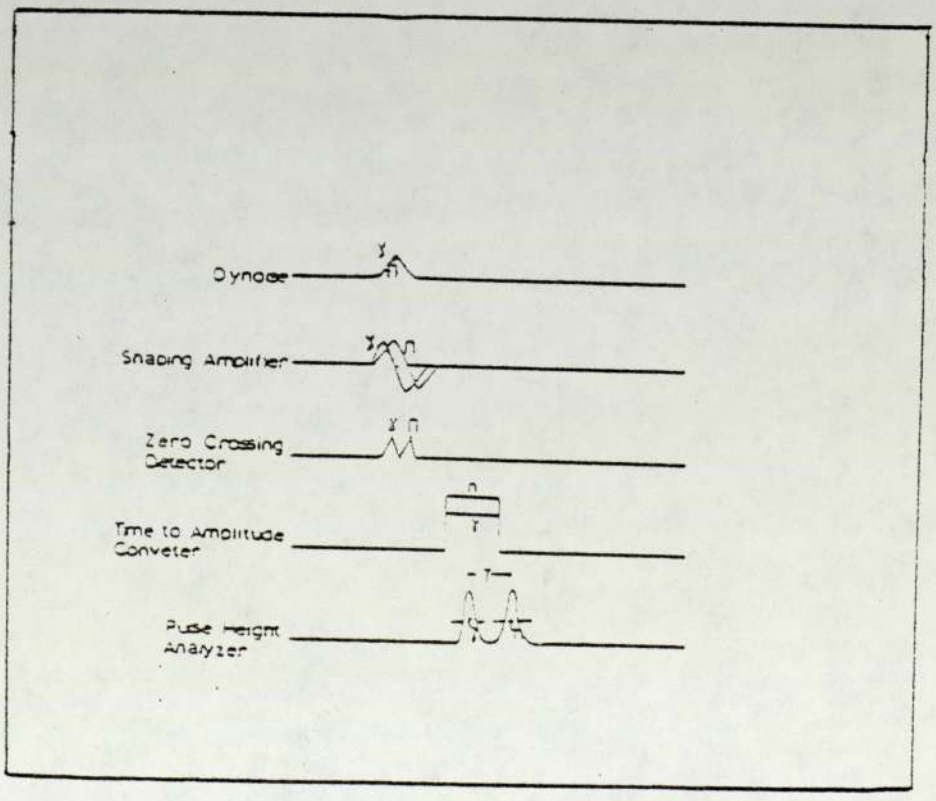

Fig. [4-2] The Time Relationship between Neutron and Gamma Ray

the bipolar pulse relative to the start then uniquely determines the nature of the interacting particle[53].

In neutron gamma ray discrimination, the nature of the neutron source, dynamic range of pulse amplitude and the counting rate are important considerations, since they will ultimately determine the degree of discrimination that is achieved. In particular measurements at high count rates will result in pile-up which may affect the pulse shape, also the measurement performed over a large dynamic range may be affected by electronic limitations such as photomultiplier tube and amplifier noise rather than by intrinsic P.S.D. properties of the scintillator.

A figure of merit for pulse shape discimination may be defined as:

$$M = \frac{T}{t_n + t_\gamma} \qquad \ldots\ldots\ldots 4\text{-}1$$

where T - The separation between neutron peak and gamma ray peak

t_n, t_γ - F.W.H.M. for the neutron peak and gamma peak respectively.

An adaptation of the method used by G.W. McBeth et al[49] is used for discrimination between the electron and proton pulses. This system operates by measuring the time difference between a fast anode current pulse and the zero crossing of a doubly differentiated voltage pulse obtained from dynode 10. A detailed description of that method follows.

4-3 Pulse Shape Discrimination System

The NE-213 scintillator was coupled to EMI-9826B tube as discussed in [3-5] and shown in Figure [3-4]. The linear output signal is taken from dynode number 10, the current pulses are integrated by the input capacitor of the preamplifier. This gives

a voltage step of rise time determined by the scintillator decay time and the time constant of the amplifier input network which produces a decaying pulse with a 50 μs decay constant.

Double differention is accomplished in the main amplifier by means of resistance and capacitor network. The main amplifier and the zero crossing discrimination must have a small cross-over walk in order that the recoil proton and recoil electron pulses at the output of the zero crossing discriminator occur at nearly constant times measured with respect to the anode pulse as a zero time reference for a wide range of pulse amplitudes. The difference in zero crossing times is typically ~ 100 ns.

Small time difference ($\leq$ 1 μs) are commonly measured by time to pulse amplitude converters which produce output signals of amplitude proportional to the time difference between the input signals.

The anode pulse after being suitably delayed is used as the start signal for the time to amplitude convertor. The stop signal is obtained from the zero crossing, the output of the time to amplitude convertor gives the neutron-gamma time spectrum. Figure [4-3] shows the time relation between neutron and gamma ray pulse shapes at various points in the P.S.D. system.

In the present work the P.S.D. is set up by measuring the counting rate at the output of the fast coincidence as a function of the delay in the delay and gate generator. The delay and gate generator is adjusted to produce a coincidence pulse with a leading edge occurring within $\pm \tau$ of the leading of the electron zero crossing signals (where 2τ is the resolving time of the coincidence unit). Any zero crossing signals that occur outside this time interval are then blocked by the coincidence unit. Figure [4-4] is the block diagram

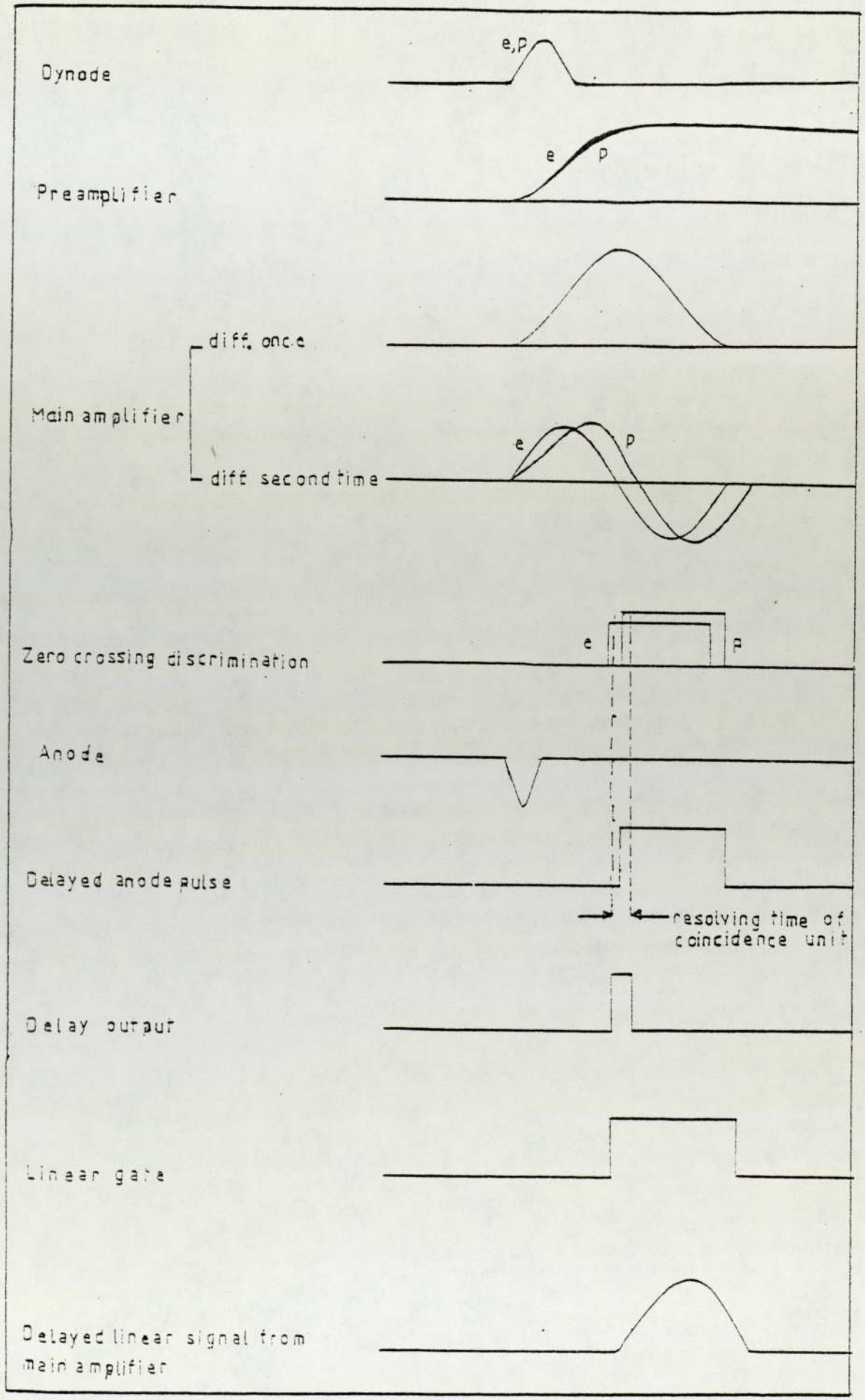

Fig. [4-3] The Time Selection output pulses at various Point in the P.S.D. System.

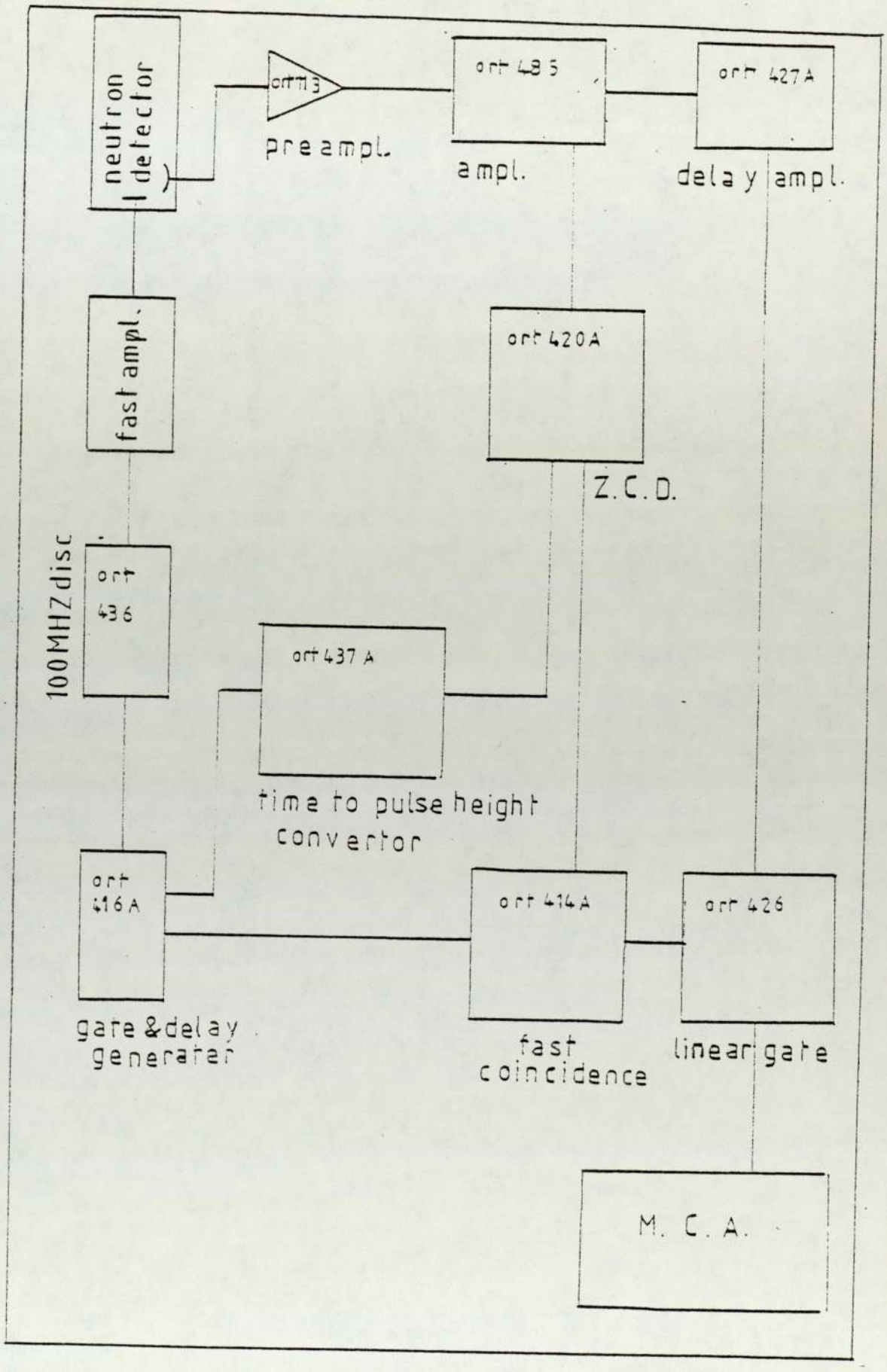

Fig. [4-4] The Block Diagram of the P.S.D. System.

of the P.S.D. system. This compares with the system used by McBeth et al[49] which uses anticoincidence between the falling edge of the delayed anode pulse and the electron pulse. He appeared to have a much wider time separation between neutron and gamma pulses (although without improving the relative separation of the neutron and gamma ray time peaks) and this time separation was too great for the resolving time of the coincidence unit. It was found possible by a simple modification to increase the resolving time to 150 ns instead of the standard 100 ns which enabled all the appropriate pulses to be measured. Coincidence was used because the leading edges of the pulses were sharper than the trailing edges.

The recoil proton output pulses from the coincidence unit are then applied to the linear gate which controls the passage of the linear delayed pulses coming from the main amplifier through the linear delay amplifier, and the sorted proton pulses from the linear gate are passed to the input of the multichannel analyzer (INOTECH Type 5200, used as a 512 channel system). Figure [4-5] shows the measuring system used.

4-4 Calibration of the Spectrometer

The spectrometric measurement is concerned with the analysis of pulse amplitude distribution, which is proportional to the number of photons in a light pulse arriving at the photocathode of the photomultiplier, and so it is related (non-linearly) to the amount of energy absorbed in the scintillator, so the pulse amplitude distribution is given by:-

$$V(E) = K\, P(E) \qquad \ldots\ldots\ldots \quad 4\text{-}2$$

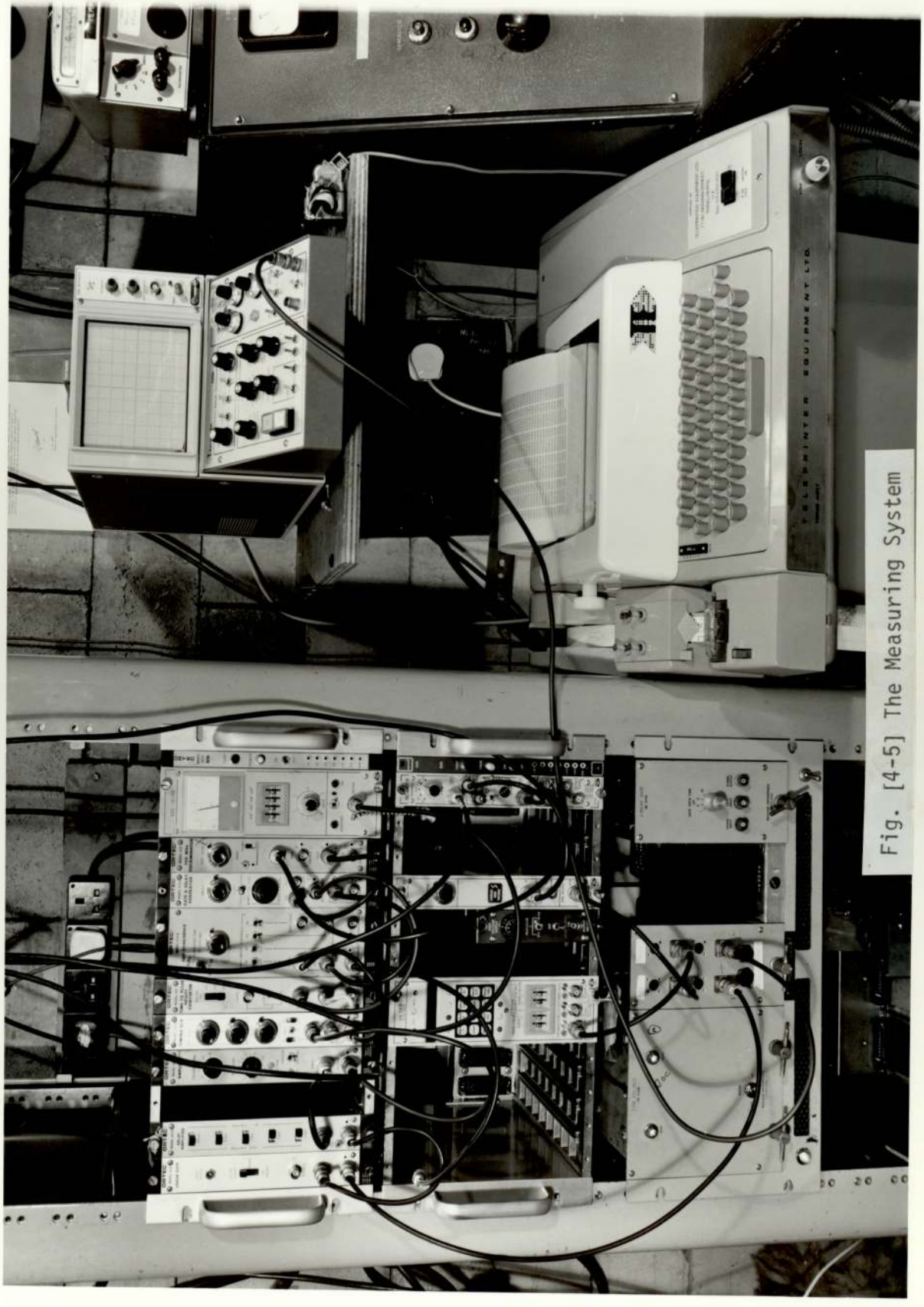

Fig. [4-5] The Measuring System

where

K - is a constant which is the energy relation between the pulse height and the light output

P(E) - is the pulse height of the light yield

The above relation is sometimes distorted due to the characteristics of electronic devices used in the spectrometer, such distortion can be taken over by a factor D(E) which depends on energy and therefore equation (4-2) will become:

$$V(E) = K.P(E).D(E) \qquad \ldots\ldots\ldots 4\text{-}3$$

Therefore for each practical case, especially when adjusting a new spectrometer a certain series of measurements should be performed to test the linearity of the spectrum. If the calibration result is that D(E) = 1, this means the absence of non linear distortion.

The set of measurements and tests which were carried out for the spectrometer are described below.

4-4-1 Spectrometric Linearity

The spectrometer linearity was tested by means of gamma-ray sources ^{137}Cs, ^{22}Na, the channel number is plotted against the maximum energy of the Compton electron (E_{max}) which is generated as a result of the Compton scattering process with the scintillator, the value of the maximum energy for gamma quanta of energy E_o is given by:

$$E_{max} = \frac{E_o}{1+0.5\frac{1}{2E_o}} \qquad \ldots\ldots\ldots 4\text{-}4$$

The value of the maximum energy E_{max} is taken at the half-height of the Compton edge [54].

Figure [4-6] shows the linearity of the spectroscopy up to about first $\frac{1}{8}$ of the scale.

To check the linearity of the full scale used during the present work, the gain of the main amplifier was fixed and the channel number of the Compton edge of ^{22}Na was found, together with the half-height channel number of the 14.1 MeV neutron spectrum edge. Then the gain of the main amplifer was doubled and the H.V. on the detector was reduced until the Compton edge of the ^{22}Na was restored to its original position. By checking that the 14.1 MeV neutron edge was at the same position the system linearity was established over the whole range.

4-4-2 The relation between Recoil Proton and Electron

The relation between the pulse height and energy of the recoil proton can be expressed by giving the pulse height in terms of equivalent electron energy as follows[55].

For

$$E_e < 1.85 \text{ MeV}$$

$$Ep = 3.48\, E_e^{\frac{2}{3}} \qquad \ldots\ldots\ldots 4\text{-}5$$

and for

$$E_e > 1.85 \text{ MeV}$$

$$Ep = 1.78\,(E_e + 1.1) \qquad \ldots\ldots\ldots 4\text{-}6$$

for $E_e = 1.85$ MeV, the $Ep = 5.25$ MeV

E_e - is the equivalent electron energy corresponding to the same pulse size and is proportional to pulse size.

The shape of this relation should hold for individual NE - 213 scintillators but the scale may vary slightly.

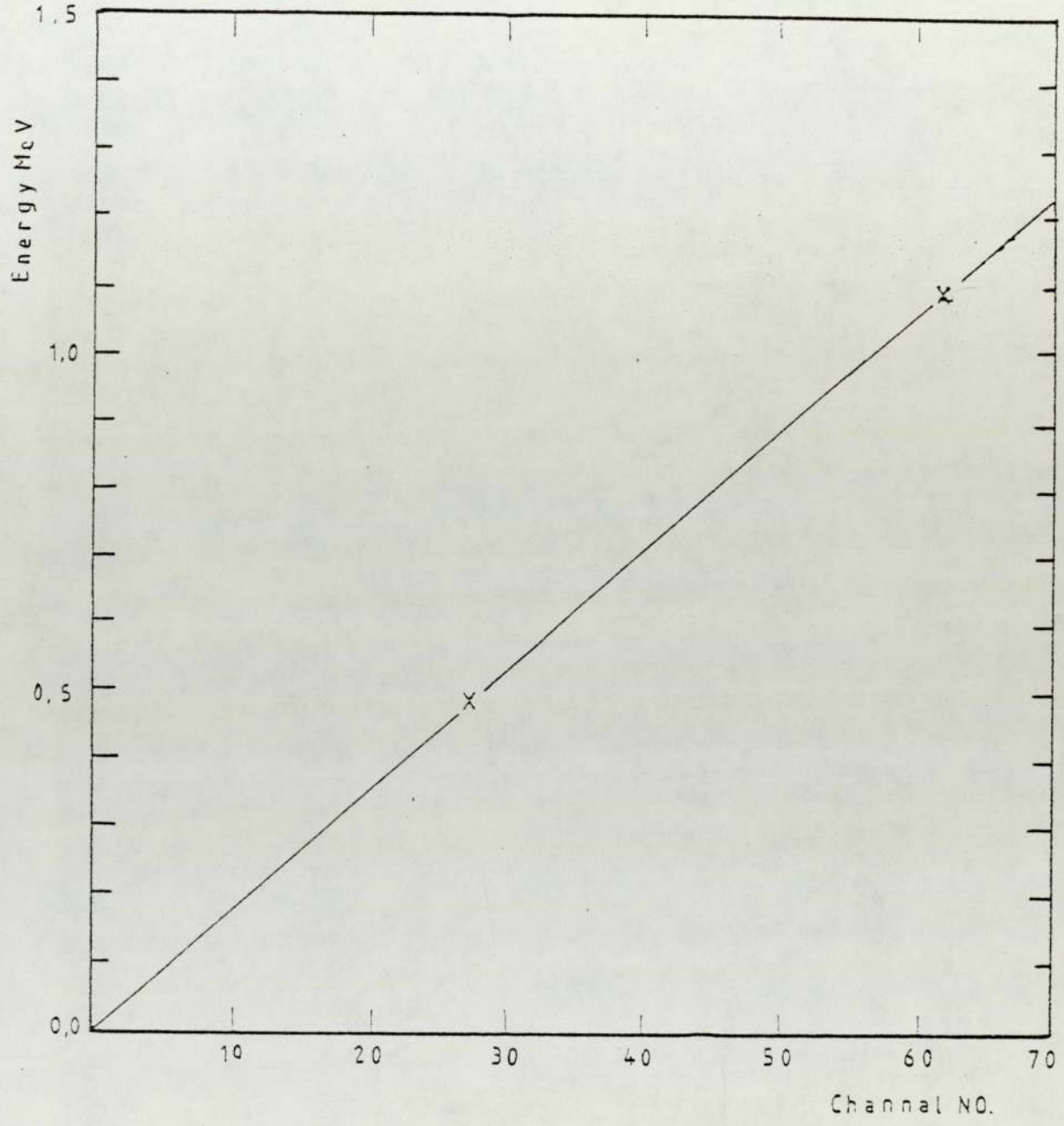

Fig. [4-6] The Linearity of the Spectroscopy.

Consequently it is convenient to relate the proton pulse size (P) to the recoil proton energy (E_p) from equations (4-5) and (4-6), since except for very low energies the light output from an electron is proportional to energy.

For $E_p > 5.25$ MeV

$$P = \frac{E_p}{12.14} - 0.161 \qquad \ldots\ldots\ldots 4\text{-}7$$

and for $E_p < 5.25$ MeV $\qquad \ldots\ldots\ldots 4\text{-}8$

where $$P = \frac{E_p^{\frac{3}{2}}}{44.3}$$

P - is normalized to 1.00 at 14.1 MeV

The relation between pulse height and energy for recoil protons normalized to 1.00 at 14.1 MeV is shown in Figure [4-7].

4-4-3 The Standardization of the Gain and the Energy Scale

The gain standardization has been found to be one of the most troublesome problems in the experimental measurements. This was ensured by measuring the ^{22}Na pulse height spectrum at the time of the neutron experiment when the LiF shielding was in use, and adjusting gain to keep the Compton edge in the same position. In the case when the uranium shielding was in use (which gave considerable gamma-ray background) the check was for the position of 14.1 MeV neutron edge, corresponding to an electron energy of 6.82 MeV. Figure [4-8] shows the pulse height spectrum for the 14.1 MeV as obtained on the P.H.A.

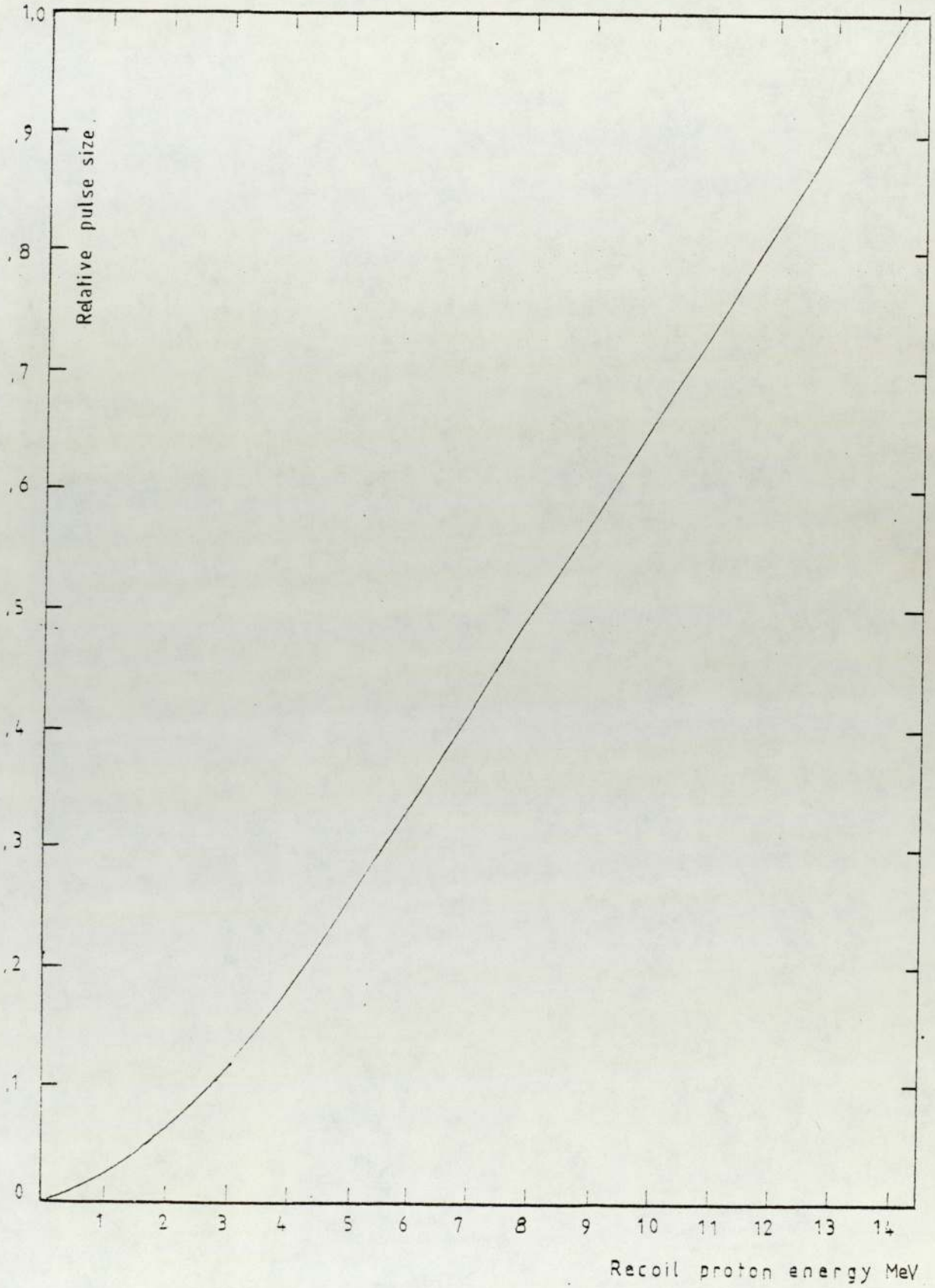

Fig. [4-7] The Relation between Pulse Height and the Recoil Proton Normalize to 1.0 at 14.1 MeV.

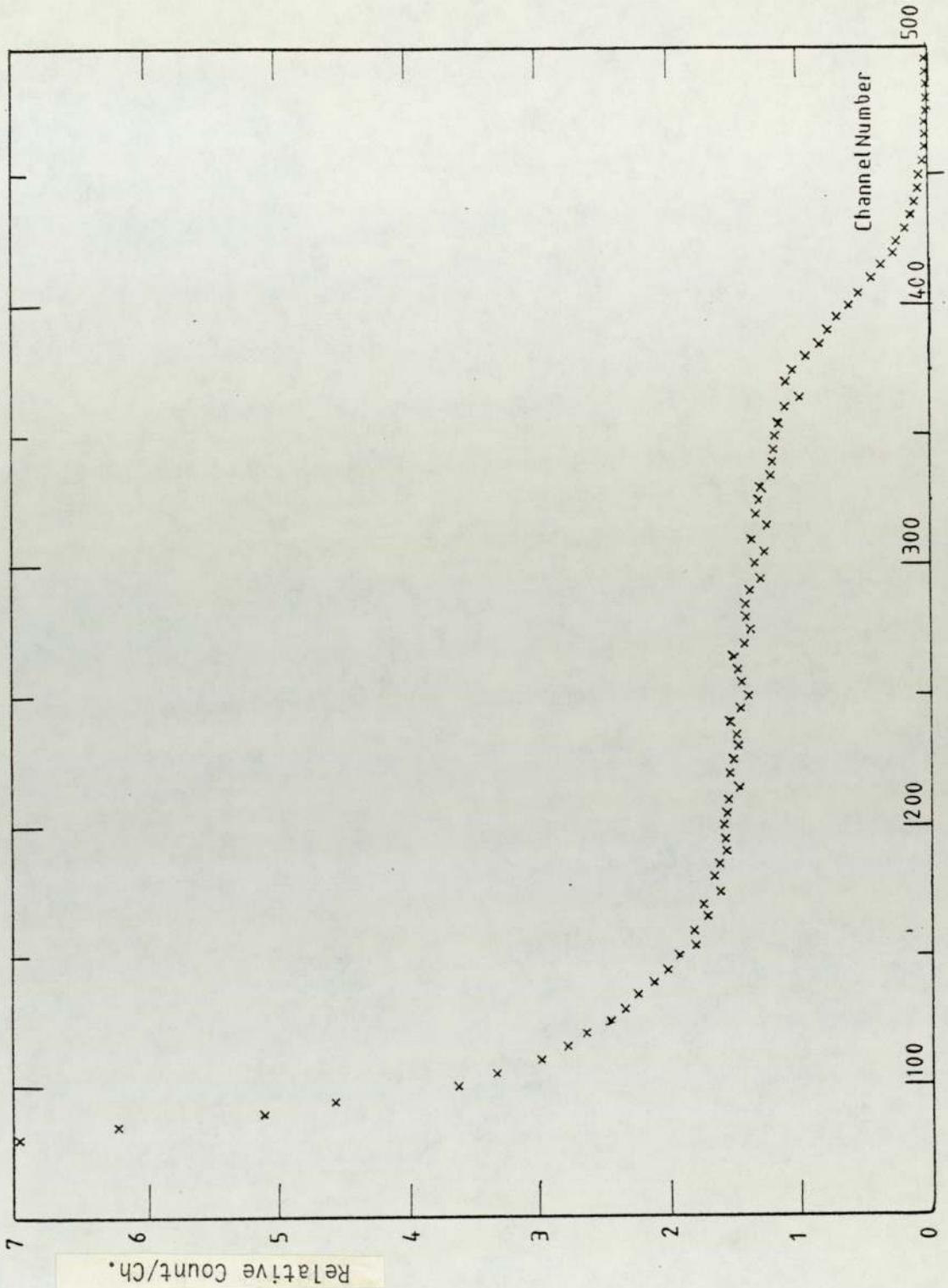

Fig. [4-8] The Pulse Height Spectrum for the 14.1 MeV Neutron as obtained from the P.H.A.

4-5 Detector Efficiency

For a cylindrical scintillator length d and area πR_c^2 with a parallel neutron beam ϕ_o incident normally on the plane face, the reaction rate for the first collision proton recoil is:

$$\phi_o \frac{N_H\sigma_H}{N_H\sigma_H+N_C\sigma_C} (\pi R_c^2)(1-e^{-a})$$

where

$$a = (N_H\sigma_H - H_C\sigma_C)d$$

The efficiency = $\frac{\text{reaction rate}}{\text{flux}}$

Therefore

$$\varepsilon = \frac{N_H\sigma_H}{N_H\sigma_H+N_C\sigma_C} \pi R_c^2 (1-e^{-a}) \qquad \text{..... 4-9}$$

In a shielding assembly the flux is more nearly isotropic and so the efficiency was calculated from the fraction of incident neutrons in a parallel beam interacting in a spherical scintillator of the same volume ($\frac{4}{3}\pi R^3 = \pi R_c^2 d$). This efficiency is independent of neutron direction and so is more closely applicable to the experimental arrangement used. No simple function such as the exponential exists for this case, but sufficient accuracy is obtained by the following power series which was derived by expressing the exponential as a power series in the integration over the sphere volume.

$$= \frac{N_H\sigma_H}{N_H\sigma_H+N_C\sigma_C} [\pi R^2] \left[\frac{2}{3}(a+ \frac{1}{10} a^3 + \frac{1}{560} a^5 + \frac{1}{30240} a^7 + \frac{1}{2661120} a^9) - \frac{1}{4} (a^2 + \frac{1}{18} a^4 + \frac{1}{720} a^6 + \frac{1}{50400} a^8 + \frac{1}{5443200} a^{10})\right] \qquad \text{..... 4-10}$$

where

R - radius of the sphere, and

$a = 2(N_H \sigma_H + N_C \sigma_C)R$

The NE-213 scintillator used in the present work has the parameters:

Chemical formula = $CH_{1.213}$

density = 0.874 gm cm^{-3}

N_H = 0.048342×10^{24} atom cm^{-3}, the number of hydrogen nuclei

N_C = 0.03985×10^{24} atom cm^{-3} the number of carbon nuclei

The data of scattering cross-section for hydrogen $\sigma_{(n,H)}$ was obtained from the relation[28].

$$\sigma_{(n,H)} = \pi[5.603/(1 + 7.415E + 0.1105 E^2) + 0.8652/(1 + 0.2427E + 0.0028E^2)] \text{ barns/atom} \quad \ldots\ldots\ldots 4\text{-}11$$

and the cross-sections for carbon σ_C were taken from cross-section data[21] Figure [4-9].

In the above discussion only single scattering events were considered. Recoil protons can be produced by neutrons which have been already scattered one or more times by carbon or hydrogen, double scattering from hydrogen results in the production of two recoil protons at practically the same instant of time. Such events are registered as one proton by the photomultiplier tube and thus the number of recoil protons registered is not affected. However, double scattering from hydrogen does result in a distortion of the output pulse height spectrum of the scintillator. Recoil protons may also be produced by neutrons which have a first collision with carbon

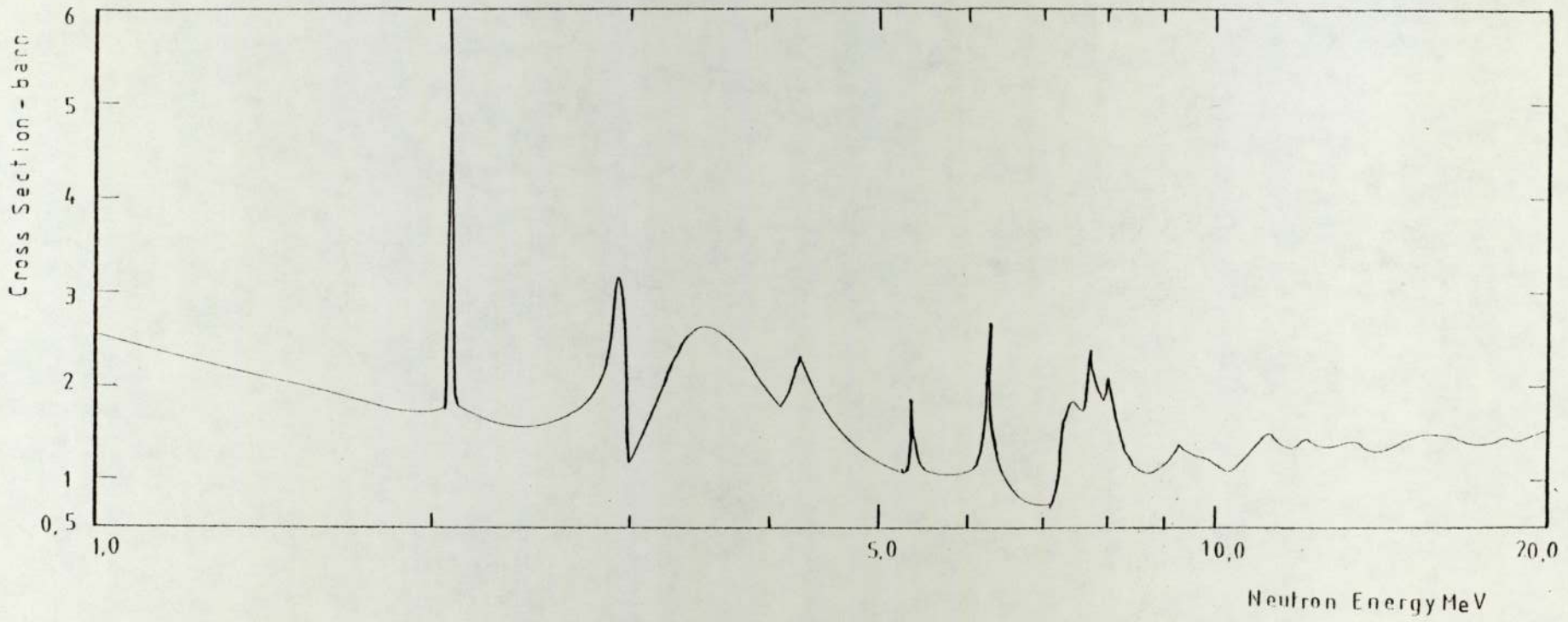

Fig. [4-9] Carbon Cross-Section [ref. 21]

and second collision with hydrogen, this results in an increase in the number of protons produced.

The value of ε_n the detector efficiency was calculated using formula (4-10) for neutron energies between (0.1 - 15) MeV and is plotted in Figure [4-10].

4-6 Correction for the Scintillator Size (Shape Correction)

The relation between the observed pulse height spectrum and the neutron spectrum contain a correction factor which depends on the scintillator size and is a function of the neutron energy. The second scattering and wall effects must be treated together since they both depend upon scintillator size. As the scintillator size increases second scattering becomes more important while wall effect becomes less important. Both these corrections are given by[31]:

$$B = (1 - 0.78 R_{max}/L') + 0.09\, N_H L\, \sigma_{n,H} + 0.077\, N_H \sigma'_{n,H} r \quad \ldots\ldots\ldots 4\text{-}12$$

where

R_{max} - The range of proton which receives the full neutron energy mg/cm^2.

L' - The scintillation thickness in mg/cm^2

L - The scintillation thickness in cm

r - The scintillation radius in cm

N_H - The number of hydrogen atom, atom cm^{-3}

$\sigma_{n,H}$ - Hydrogen cross-section at energy E

$\sigma'_{n,H}$ - Hydrogen cross-section at energy 0.68E

The correction was calculated over a range of neutron energies (0.1 - 15) MeV for the NE-213 scintillator and is shown in Figure [4-11]. This correction was derived for monoenergetic neutrons but is thought to be applicable to a broad neutron spectrum. The corrections

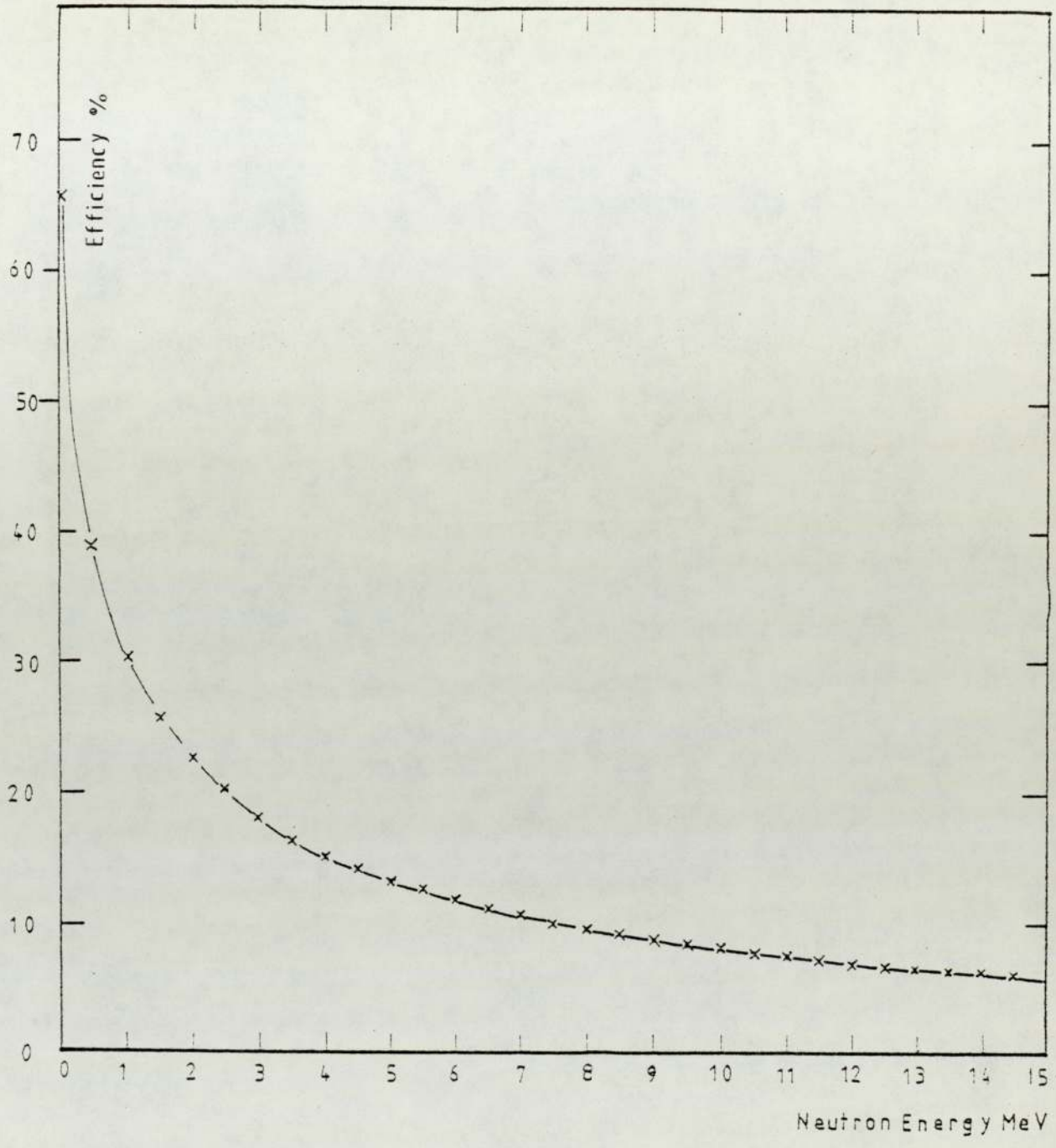

Fig. [4-10] Neutron Detector Efficiencies for NE-213 of 2.54cm Length.

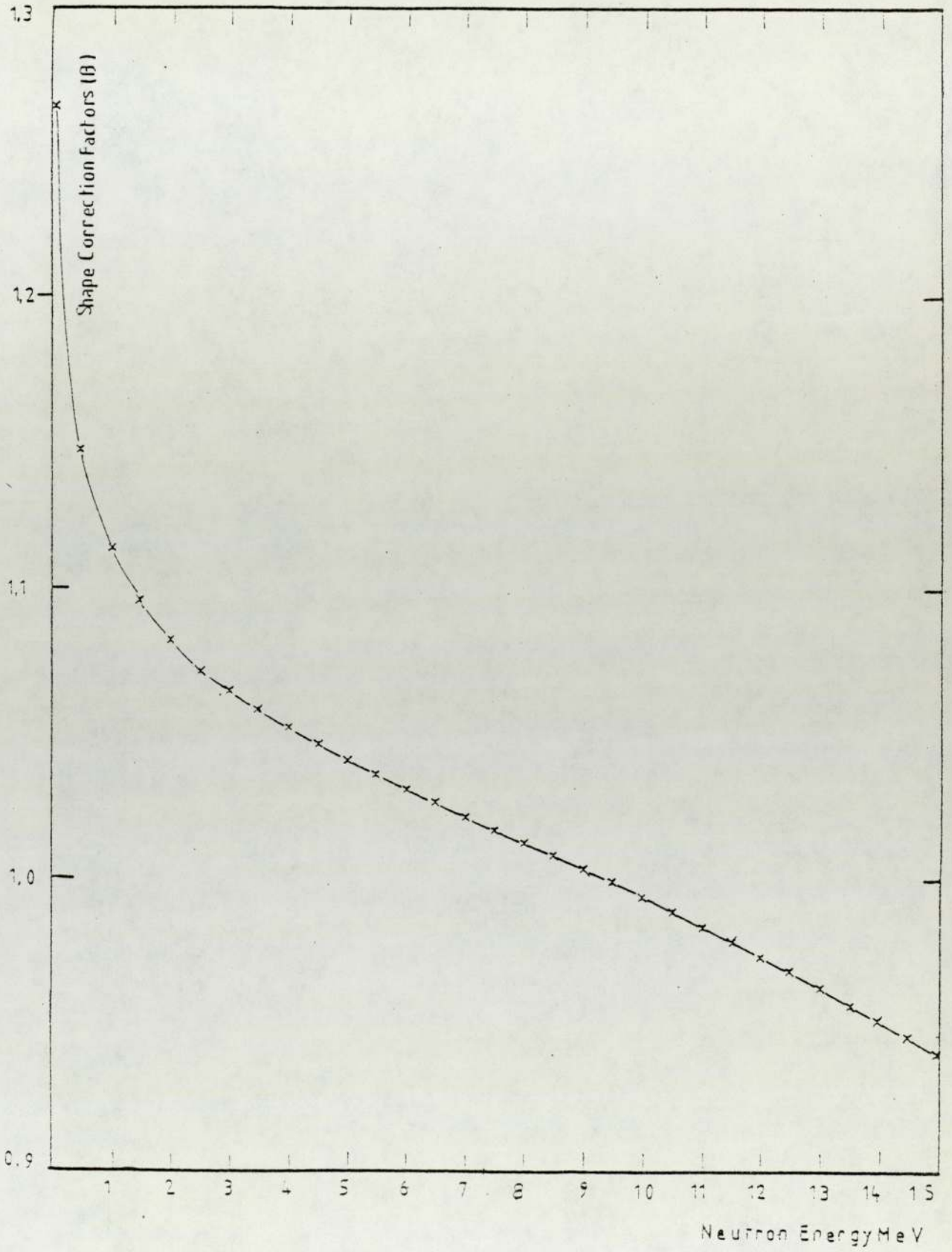

Fig. [4-11] Shape Correction Factors for the NE-213 Scintillator (2.54 x 2.54)cm.

calculated were applied to the unfolded neutron spectrum to eliminate the size effect.

The scattering of neutrons from carbon nuclei produces only small light pulses due to the low energy ($\leq 0.284\ E_n$), and short range of the recoil carbon nuclei. Pulses from carbon recoils are less in size than from protons energy $\simeq \frac{1}{20} E_n$. Neutron induced reaction in carbon which lead to charged particles can be ignored as the reaction thresholds are high and the cross-sections are much smaller than the (n-p) scattering cross-sections.

4-7 Smoothing of the Experimental Data

The measured pulse amplitude data contain statistical fluctuations. Because it is necessary to differentiate the measured data these fluctuations, if ignored, will give fluctuations in the neutron energy spectrum which may have a larger amplitude than the structure of the actual neutron spectrum, so the measured spectrum has to be smoothed before applying the unfolding method.

In the present work the smoothing is done by a least squares fit of a quadratic to a limited number of points which may be explained as follows[56].

To fit a series of equally spaced points Y_i, to a curve

$$Y = a_o + a_1 X + a_2 X^2$$

There must be always an odd number of points (seven in the present work, ranging from -3 to + 3 in step of one). The least squares condition is that the sum of the squares of the difference between the computed number Y_i and the observed numbers is a minimum so

$$\sum_{-3}^{+3} [a_o + a_1 X + a_2 X^2 - Y_i]^2 = \text{minimum} \quad \ldots\ldots\ldots \quad 4\text{-}13$$

by putting the partial derivatives of equation (4-13) with respect to a_0, a_1 and a_2 equal to zero we get:

$$a_o = \frac{-2y_{-3} + 3y_{-2} + 6y_{-1} + 7y_0 + 6y_1 + 3y_2 + 2y_3}{21} \quad \ldots\ldots\ldots 4\text{-}14$$

$$a_1 = \frac{-3y_{-3} + 2y_{-2} - y_{-1} + y_1 + 2y_2 + 3y_3}{28} \quad \ldots\ldots\ldots 4\text{-}15$$

$$a_2 = \frac{5y_{-3} - 3y_{-1} - 4y_0 - 3y_1 + 5y_3}{84} \quad \ldots\ldots\ldots 4\text{-}16$$

From (4-14, 4-15, 4-16) in equation (4-13) and putting X = -3, -2, -1, 0, 1, 2, 3 respectively we get:

$$Y_{-3} = \frac{64y_{-3} + 30y_{-2} + 6y_{-1} - 8y_0 - 12y_1 - 6y_2 + 10y_3}{84} \quad \ldots\ldots\ldots 4\text{-}17$$

$$Y_{-2} = \frac{30y_{-3} + 24y_{-2} + 18y_{-1} + 12y_0 + 6y_1 - 6y_3}{84} \quad \ldots\ldots\ldots 4\text{-}18$$

$$Y_{-1} = \frac{6y_{-3} + 18y_{-2} + 24y_{-1} + 24y_0 + 18y_1 + 6y_2 - 12y_3}{84} \quad \ldots\ldots\ldots 4\text{-}19$$

$$Y_o = \frac{-2y_{-3} + 3y_{-2} + 6y_{-1} + 7y_0 + 6y_1 + 3y_2 - 2y_3}{21} \quad \ldots\ldots\ldots 4\text{-}20$$

$$Y_1 = \frac{-12y_{-3} + 6y_{-2} + 18y_{-1} + 24y_0 + 24y_1 + 18y_2 + 6y_3}{84} \quad \ldots\ldots\ldots 4\text{-}21$$

$$Y_2 = \frac{-6y_{-3} + 6y_{-1} + 12y_0 + 18y_1 + 24y_2 + 30y_3}{84} \quad \ldots\ldots\ldots 4\text{-}22$$

$$Y_3 = \frac{10y_{-3} - 6y_{-2} - 12y_{-1} - 8y_0 + 6y_1 + 30y_2 + 64y_3}{84} \quad \ldots\ldots\ldots 4\text{-}23$$

In the present work the computer program NEUTRON, Appendix 1, used equations, 4-17, 4-18, 4-19, 4-20, 4-21, 4-22 and 4-23 for smoothing the data, the forms y_{-3}, y_{-2}, y_{-1} were used for the first 3 points and y_1, y_2, y_3 for the last 3 points, all the other points were smoothed using the form y_0. Smoothing was carried out four times first on the raw data and then a further three times on the successive sets of smoothed data.

4-8 The Unfolding Method

The experimental data given by the spectrometer measurements do not produce directly the desired information on the energy distribution of the recorded particles. To obtain such information the raw data must be interpreted and unscrambled before an evaluation of the quantities which the experiment was designed to measure can be obtained.

In the measurement of the energy spectrum of neutrons whenever the detection system is based on the proton recoil technique, the experimental pulse amplitude distribution is related to the energy spectrum of the recoil protons. An appropriate analysis or unfolding method must therefore be performed on the measured pulse amplitude distribution to evaluate the neutron energy spectrum.

In the present work the method of differentiation was used which is considered as the simplest (and most accurate) for measuring real neutron spectra[57]. Assuming that a scintillator of thickness d, received in a unit time a number of neutron $\phi_o (E_n)$. The number of recoil protons in the unit time due to a single scattering is given by

$$Np = \frac{\Sigma H}{\Sigma} \phi_o [1-\exp(-\Sigma d)] \quad \ldots\ldots\ldots 4\text{-}24$$

see paragraph (4-5)

where

Σ - is the macroscopic total cross-section for neutrons by the nuclei in the scintillator

Σ_H - is the macroscopic scattering cross-section for hydrogen atoms

The energy spectrum of the recoil protons due to a single scattering is calculated assuming that the n-p scattering is isotropic in the centre of mass system leads to $P(E_p) = \frac{1}{E_n}$, which is a good approximation up to 14 MeV[28]. So the number of recoil protons with energy E in the unit energy interval is:

$$N(E) = \phi_o[1 - \exp(-\Sigma d)]/E_{max} \quad \ldots\ldots\ldots 4\text{-}25$$

The maximum value of energy which the recoil protons can gain from the scattering neutron by the hydrogen nuclei is equal to the neutron energy E_n, and therefore equation (4-25) will be for a cylindrical scintillator

$$N(E) = A\phi \frac{\Sigma_H}{\Sigma} [1 - \exp(-\Sigma d)]/E_n \quad \ldots\ldots\ldots 4\text{-}26$$

If the scintillator received neutrons of complicated energy spectrum $\phi(E_n)$, the recoil proton of energy E will be generated by neutrons of different energy starting from $E_n = E$, so the number of recoil protons in a unit energy interval is (see equation 3-2)

$$N(E) = A \int_E^\infty \frac{\Sigma_H}{\Sigma} \frac{\phi(E_n)\,[1-\exp(1-\Sigma d)]}{} dE_n \quad \ldots\ldots\ldots 4\text{-}27$$

By differentiating equation (4-27) with respect to E_n and dropping the subscription we get,

$$\phi(E) = \frac{E}{A \frac{\Sigma_H}{\Sigma} [1-\exp(-\Sigma d)]} \quad \frac{dN(E)}{dE}$$

from equation 4-9

$$\varepsilon = A \frac{\Sigma_H}{\Sigma} [1-\exp(-\Sigma d)]$$

therefore

$$\phi(E) = \frac{E}{\varepsilon} \quad \frac{dN(E)}{dE} \qquad \ldots\ldots\ldots 4\text{-}28$$

This means that the neutron spectrum can be calculated from the energy distribution of the recoil protons by differentiation.

From the experiment the measured data are the pulse amplitude distribution N(V) and not the recoil proton energy distribution, so by assuming that the protons of energy E produce pulses of amplitude V, the number of the protons in the interval dE should be equal to the number of pulses with amplitude V within interval dV i.e.

$$N(E)\, dE = N(V)\, dV.$$

By differentiating with respect to E we get

$$\frac{dN(E)}{dE} = \frac{d}{dV} \left[N(V) \frac{dV}{dE} \right] \frac{dV}{dE} \qquad \ldots\ldots\ldots 4\text{-}29$$

From equation (4-29) on (4-28) we get

$$\phi(E) = \frac{E}{\varepsilon} \cdot \frac{dV}{dE} \cdot \frac{d}{dV} \left[N(V) \frac{dV}{dE} \right] \qquad \ldots\ldots\ldots 4\text{-}30$$

Thus the analysis of the results was reduced to a multiplication of the measured pulse height distribution N(V) by $\frac{dV}{dE}$ for (each channel), differentiation with respect to the pulse height scale, followed by multiplication by $\frac{dV}{dE}$ [58]

From equation (4-2) we get

$$\frac{dV(E)}{dE} = K \frac{dP(E)}{E}$$

so equation (4-27) will be, including the shape correction factor (equation 4-11) as follows:

$$\phi = \frac{EK^2}{\varepsilon B} \cdot \frac{dP}{dE} \cdot \frac{d}{dV} \left[N(V) \frac{dP}{dE} \right] \quad \ldots\ldots\ldots 4\text{-}31$$

In order to minimize the oscillations in the differentiation of the experimentally amplitude distribution, Kazanzkii et al[57] suggested the method of least squares for determination of the derivative. In that method the spectrum is expressed over seven adjacent points with a pitch ΔV in the form of a second order parabola (generally similar to the smoothing method), then

$$\frac{d}{dV} \left[N(V) \frac{dP}{dE} \right] = \frac{d}{dV} f(V_i)$$

For the central point

$$\frac{d}{dV} f(V_i) = \frac{3f_{i-3} + 2f_{i-2} + f_{i-1} + f_{i+1} - 2f_{i+1} - 3f_{i+3}}{28 \Delta V} \quad \ldots\ldots\ldots 4\text{-}32$$

generally similar expressions were derived for the first and last 3 points of the data which could not be central in a group of 7 points.

Thus the analysis of the results was reduced to a multiplication of the measured pulse height N(V) by $\frac{dP}{dE}$ for each channel, then differentiating with respect to pulse height followed by multiplication by a normalising factor which is given by:

$$F = Q/G \times C_{\alpha} \quad \ldots\ldots\ldots 4\text{-}33$$

where

Q - is the normalised neutron source strength

G - the geometry factor for the alpha-particle detector

$C\alpha$ - is the number of counts recorded by the associated alpha-particle monitor

4-9 Testing the Spectroscopy and the Unfolding Method

A check on the spectroscopy and the unfolding method technique is done by measuring the continuous spectrum from a standard neutron source, by analysing the position of the peaks and comparing these with known spectrum.

In the present work a 0.3 Ci ^{241}Am-Be source was used. The source is supplied by Radio-Chemical Centre, Amersham, U.K., the yield of the source 2.5×10^6 n/sec the source was covered by a 3 mm lead sheet to cut off the 60 KeV gamma rays from Am^{241}.

Comparing the measured spectra Figure [4-12] with these reported by Radio-Chemical Centre[59] which obtain a spectrum for Am-Be shows peaks at 3.3, 4.3, 4.9, 6.8 and 7.7 MeV and a shoulder at 9.5 MeV. However in the present work for the 0.3 Ci Am-Be source there are peaks at 4.75, 5.75, 7.25 and 8.5 MeV and a shoulder at 9.0 MeV. A point which must be made is that (Lock[59]) experiments are only a comparison between a certain source produced at Amersham Centre at a given time.

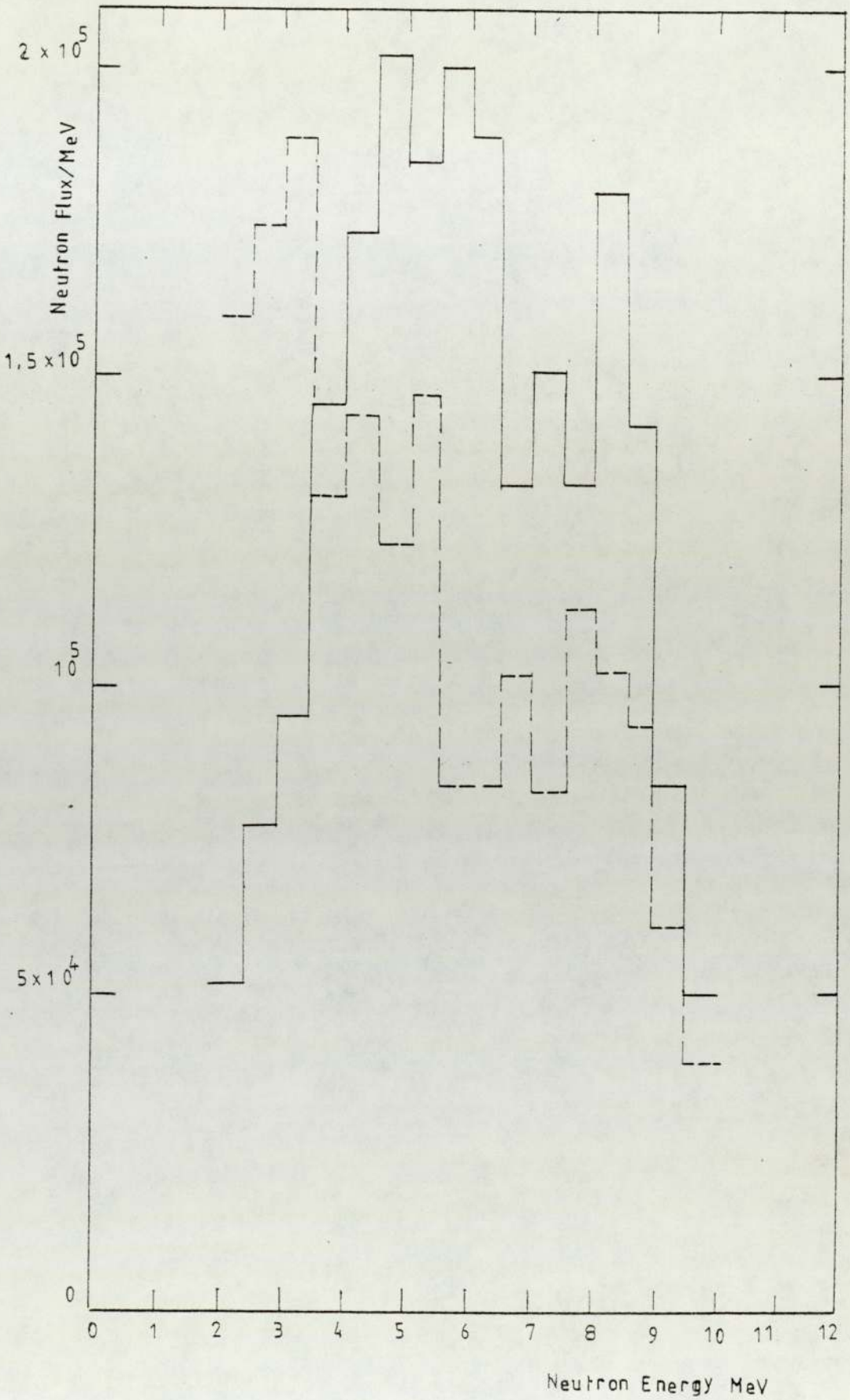

Fig. [4-12] Neutron Spectra from 0.3 Ci Am-Be Neutron Source.
- measured
- - - measured by E.A. Lorch (ref. 59)

CHAPTER 5

NEUTRON PRODUCTION AND THE SHIELDING ASSEMBLY

5-1 Introduction

Neutrons were produced from the $D(T,n)^4He$ reaction, with deuterium ions of energy about 120 keV (obtained by using a S.A.M.E.S. type J accelerator) incident on the tritium target, a neutron of 14.1 MeV being obtained at 90^o to the beam direction.

The spectra of fast neutrons passing through the shielding of LiF and U^{238} have been measured for a short cylindrical assembly with a point source of 14.1 MeV neutrons at the centre. This was the nearest approximation possible to the sphere used for calculation purposes. The measurement was made with the NE-213 detector at different distances from the centre of the assembly. The intensity of the neutron source was monitored by the alpha particle associated with the neutron by a plastic (NE-102A) scintillator.

5-2 S.A.M.E.S. Accelerators and the Target

The deuteron beam was accelerated by the S.A.M.E.S. type J accelerator shown in Figure [5-1]. The accelerating voltage is produced by an electrostatic generator which is housed in a hermetically sealed unit in a hydrogen atmosphere. The generator can deliver 2mA at + 150 kV with a stability of $\pm$ 1%[60].

The target and shielding assembly are situated at the far end of the laboratory (6.5 meter) away from the accelerator. Due to the length of the beam tube an auxilliary pumping stage at the target end was necessary to maintain a pressure of less than 10^{-5} mm.Hg, and also

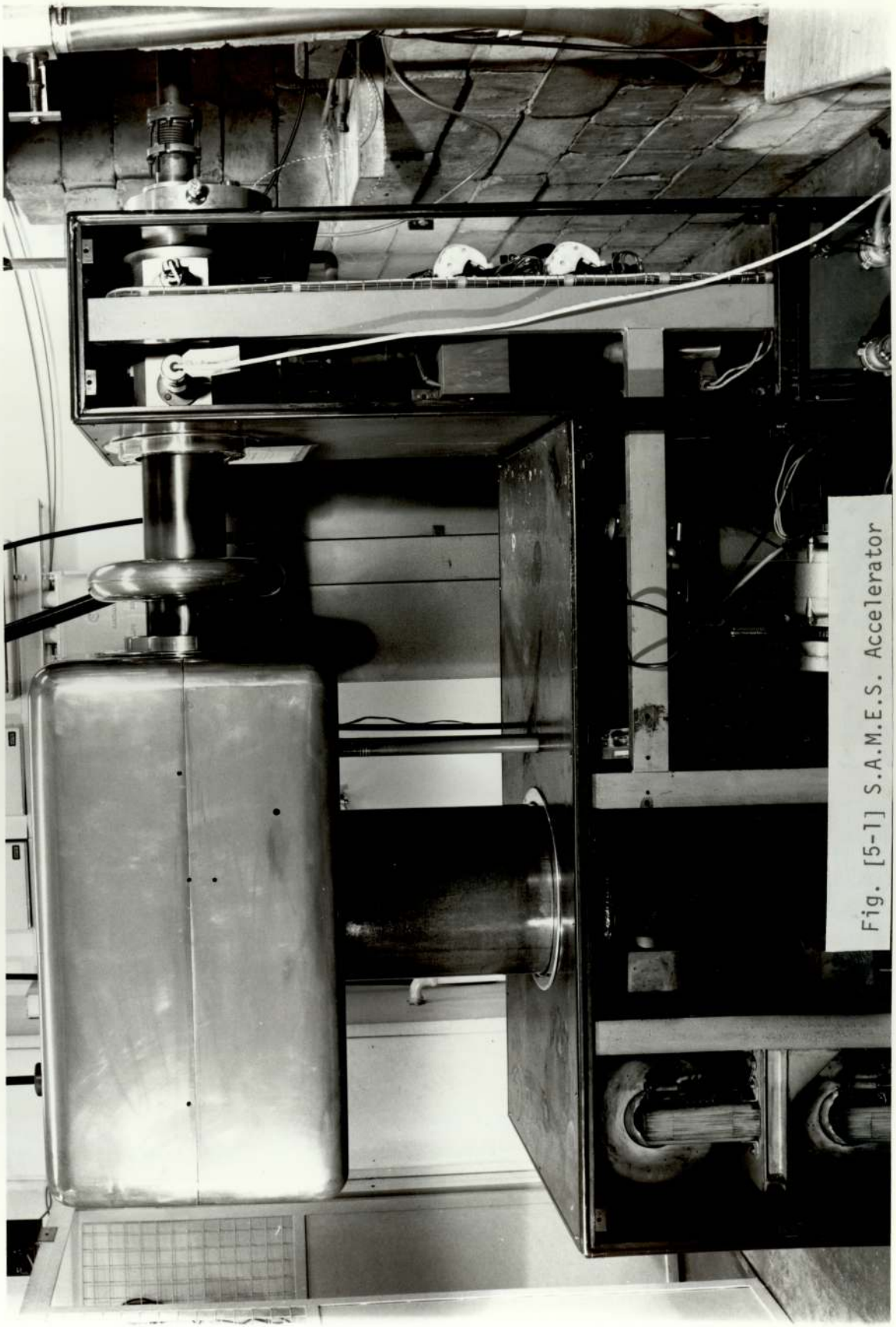

Fig. [5-1] S.A.M.E.S. Accelerator

extra beam focusing was required. This was achieved by two electrostatic quadruple lenses[61].

The targets used were of the type TRT-51 supplied by the Amersham Radio Chemical Centre. The target has a copper backing disc of 2.82 cm diameter and 0.25 mm thickness, a very thin layer of titanium of 2.5 cm diameter and 0.257 mg cm^{-2} is deposited by vacuum evaporation[62]. This is then exposed to tritium gas which is absorbed to give a tritium content of about one tritium atom for each titanium atom. There is some uncertainty about the tritium distribution in these targets, but these depend on the manufacturing technique and condition. However the possible distribution of tritium and the average energy and yield are relatively unimportant at low bombarding energies from its effects on the emitted neutron spectrum[63,64] although the absolute yield may be strongly affected.

5-3 The D(T,n) ^{4}He Reaction

The nuclear reaction:

$$^3_1H + ^2_1H \rightarrow ^4_2He + n + 17.596 \text{ MeV}$$

has been used as a source for the production of neutrons of high energy.

Because of the high Q-value the variation of neutron energy with the incident deuteron beam energy is relatively small.

The products of that reaction will show the energy of 17.596 MeV plus the bombarding energy, nearly as the inverse ratio of their masses depending on the angle of emission which gives the neutron[65],

$17.596 \times \frac{4}{4+1} = 14.1$ MeV, and the alpha particle

$17.596 \times \frac{1}{4+1} = 3.51$ MeV, at zero bombarding energy.

The energy of neutrons emitted at very low bombarding energies,

at 90^{o} to the incident beam is 14.1 MeV with small variations due to bombarding energy.

The cross-section for this reaction rises to a peak of 5.1 barn[66,67,68,69] at a deuteron energy of 110 keV as shown in Figure [5-2].

5-3-1 Kinematics of $D(T,n)^{4}He$ Reaction

In the $D(T,n)^{4}He$ reaction it is possible to compare the energy and the angle of emitted particles by using the laws of conservation of energy and momentum. The reactions produce two particles, neutron of mass m_3 and alpha particles of mass m_4, the mathematical expression for the energy of neutron E_3 as a function of angle is given by the following expression[70,71].

$$E_3 = (\mu E_1 + Q)\frac{m_4}{m_3+m_4} + E_1\left(\frac{m_1}{m_1+m_2}\right)^2 \frac{m_3}{m_1}\cos\phi$$

$$\mp 2\cos\phi\frac{m_1 m_3}{m_1+m_2}\sqrt{\frac{E_1(\mu E_1+Q)m_4}{m_3+m_4} - \frac{E_1 2\sin^2\phi}{(m_3+m_2)}\cdot\left(\frac{m_1 m_2}{m_1+m_2}\right)} \quad \ldots\ldots\ldots 5\text{-}1$$

where

m_1, E_1 - is the mass and energy of the deuteron, and

m_2 - the mass of the triton at rest

m_3 - neutron mass

m_4 - alpha-particle mass

ϕ - the angle with respect to incident beam in the hole system

$$\mu = \frac{m_2}{m_1+m_2}$$

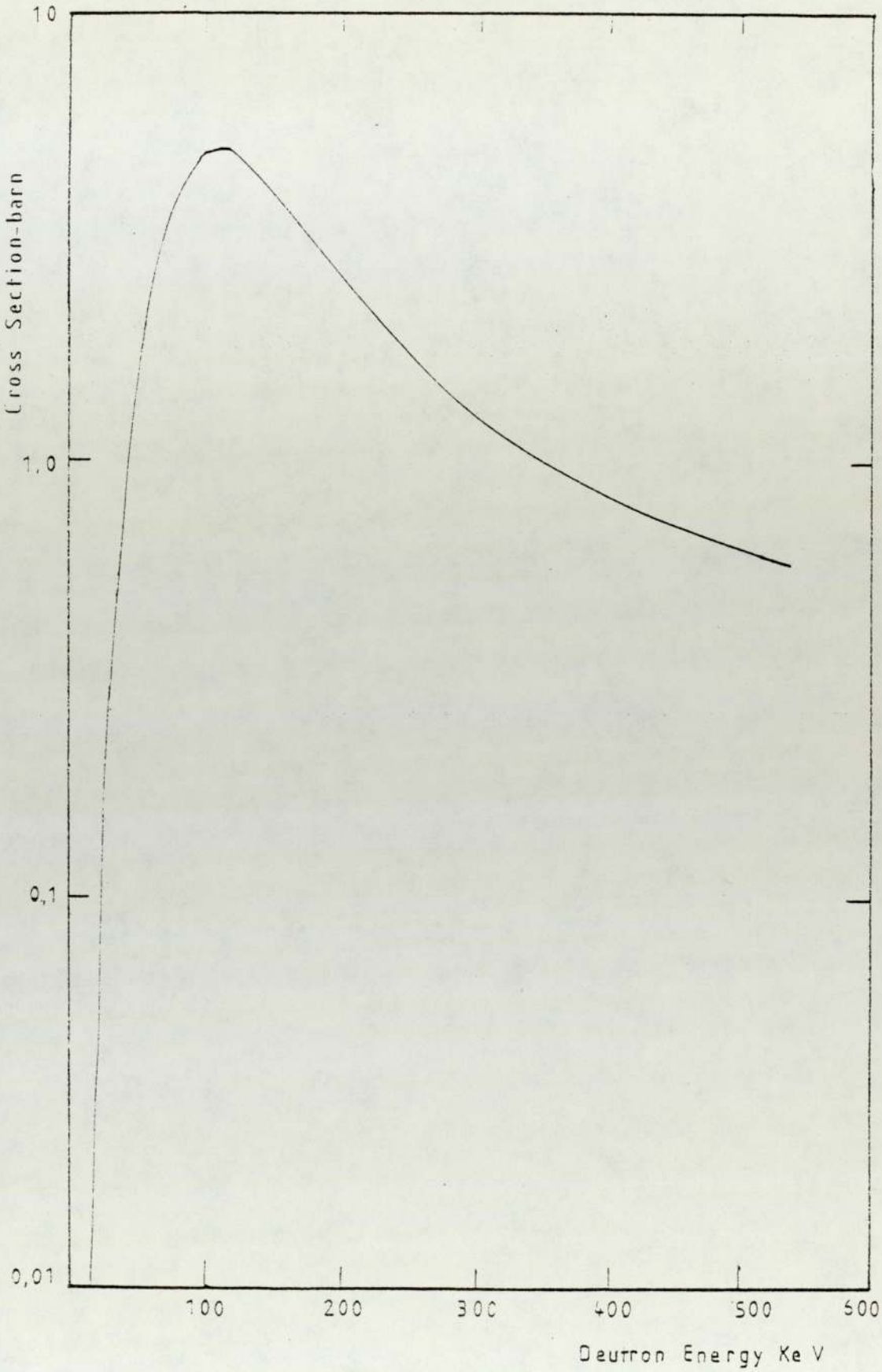

Fig. [5-2] Total Cross-Section for $D(T,n)^4He$ Reaction

In deriving equation 5-1, it is easier first to work out the mathematical equation for the conservation of energy and momentum in the C.M-system and then transfer to the lab-system.

The variation of the neutron energy emitted from the $D(T,n)^4He$ reaction for various deuteron energies as a function of the laboratory angle is shown in Figure [5-3].

5-4 Measurement of Neutron Yield by Associated Alpha-Particle

The expression for the total neutron yield per detected alpha particle is[63]

$$N = \frac{\int_0^E \sigma c.M(E) \frac{dX}{dE} dE}{\frac{\Delta\Omega_\alpha}{4\pi} \int_0^E \sigma c.M(\theta,E) \frac{dX}{dE} \left(\frac{d\omega_{c.M}}{d\omega_{Lab.}}\right)_\alpha dE} \quad \ldots\ldots\ldots 5\text{-}2$$

where

$\Delta\Omega_\alpha$ - is the solid angle subtended by the alpha detector.

$\sigma c.M(E)$, $\sigma_{C.M.}(\theta.E)$ - The cross-section and the differential cross-section for the (D,T) reaction in the c.M. system.

$\frac{dX}{dE}$ - the inverse of the rate of energy loss of deuteron in the target.

θ - the angle of emitted alpha-particle in c.M. - system.

$\frac{d\omega_{c.M}}{d\omega_{lab}}$ - the solid angle conversion factor from the c.M. to the lab-system for the detected alpha-particle.

E - is the incident deuteron energy.

Implicit in the derivation of equation (5-2) the following assumptions must be considered:

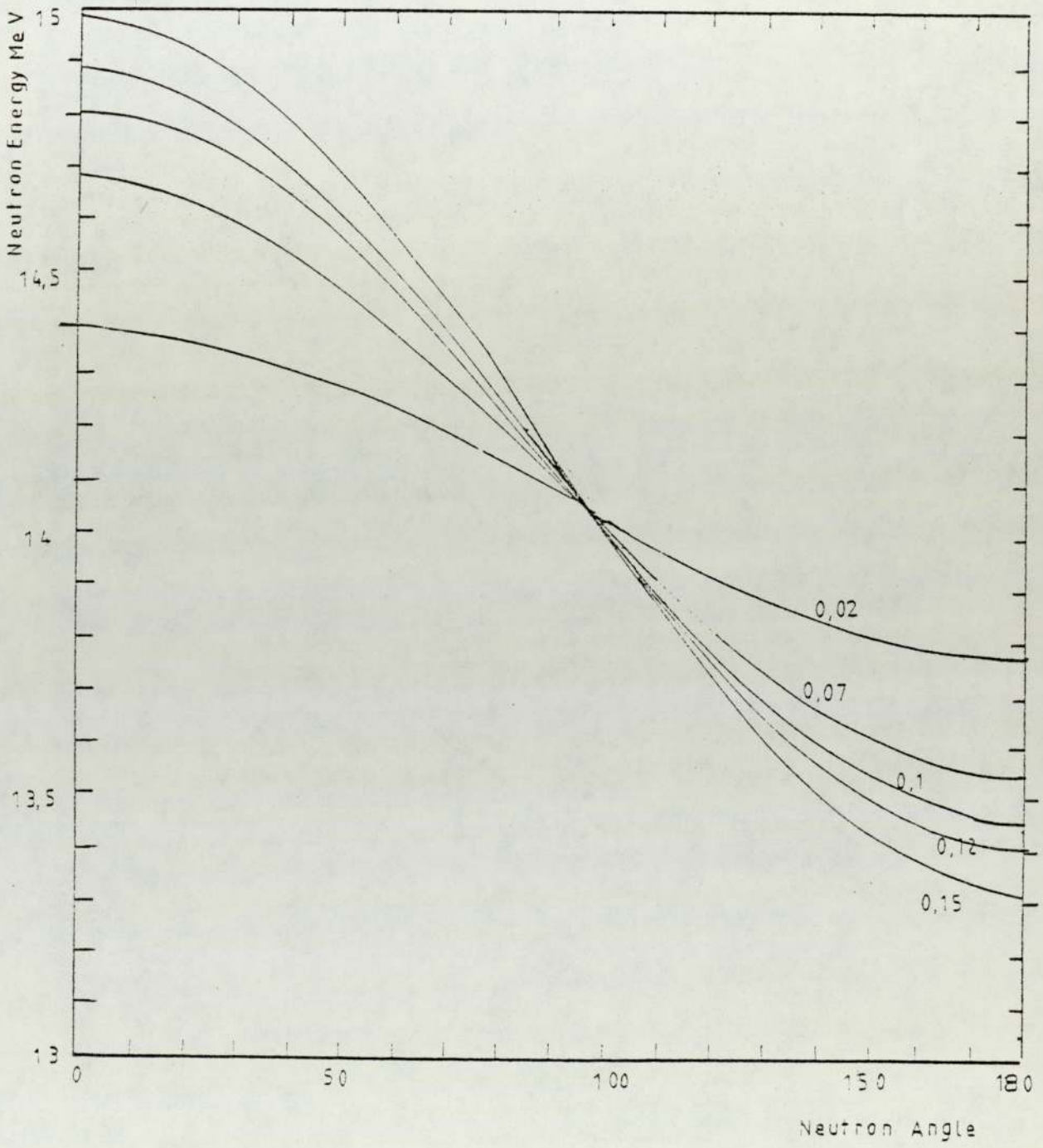

Fig. [5-3] The Variation of Neutron Energy with the Angle of Emission from D,T Reaction at Different Deuteron Energy.

a - the reaction products are isotropically distributed in the centre of mass system for the incident deuteron energies.

b - $\frac{dX}{dE}$ is fairly well known in the region from (0-E).

c - no scattering of the incident deuteron

In measuring of the neutron yield by the detection of the alpha-particles, it is important to know the angular distribution of alpha-particle so we can transform the number of counts to the total yield. For deuteron beams of energy used at the present work (120 keV) the angular distribution of both the neutron and alpha-particle are isotropic in the centre of mass system, so in the laboratory system the degree of anisotropy at 90^{o} is equal to 0.9946 for 3.5 MeV alpha-particle and is equal to 0.9997 for the 14.1 MeV neutron at a deuteron energy of 120 keV. The alpha-particle anistropy which varies with deuteron energy and angle can effectively be eliminated by detecting the alpha-particle at an angle of 90^{o} to the incident deuteron beam[72], since the angular distribution in the laboratory system and the centre of mass system is almost the same at 90^{o}.

The associated alpha-particle emitted from the $D(T,n)^{4}He$ reaction which has an energy of 3.5 MeV was initially detected by the (NE-102A) plastic scintillator placed inside the beam tube at a distance 55 cm from the target in the backward direction at an angle of 175^{o} to the deuteron beam, the scintillator was coupled to an external photomultiplier tube with a light pipe. This was done in order to simplify construction of the shield. It was noticed however that the detector gave very high counting rates following a high voltage trip. This could not be tolerated as it meant that the recorded alpha-particle counts were unreliable. No satisfactory

explanation of this effect has been found, tests showed that light leakage or earth loops were not responsible. It may possibly be due to the badly defocussed beam which occurs as the voltage collapses causing strong production of D-D neutrons by the drive in target effect very close to the (NE-102A) alpha-particle detector. However this was mostly overcome after trial and error by using a flight tube at an angle of 90^{o} to the beam tube. In this arrangement the target was inclined at 45^{o} to the direction of both the incident deuteron beam and the axis of the flight tube, in order to give minimum absorption to the alpha-particle energies from the target as shown in Figure [5-4] and Figure [5-5].

In addition a relay system was arranged to break the inputs to the alpha-particle scaler and the pulse height analyser at the occurrence of a high voltage trip. This was also arranged to give simultaneous start and stop to the two detector inputs.

5-5 The Alpha-particle Detector

The alpha-particle is a doubly charged particle so it does not easily penetrate to the nucleus and its primary interaction is with the electrons and the Coulomb field surrounding the nucleus. The alpha-particle loses energy to the surrounding medium primarily through ionization and because of the intense ionization produced it can be detected with 100% efficiency.

In the present work the NE-102A plastic scintillator was chosen because it is readily available in thin sheets, has a high light output, fast decay time, a low neutron detection efficiency for thin sheets and being an organic material with low Z number it has a low detection efficiency for gamma-rays, and a most important 100% detection efficiency for the 3.5 MeV alpha-particles. The range of alpha-particle in NE-102A scintillator is shown in Figure [5-6][73]

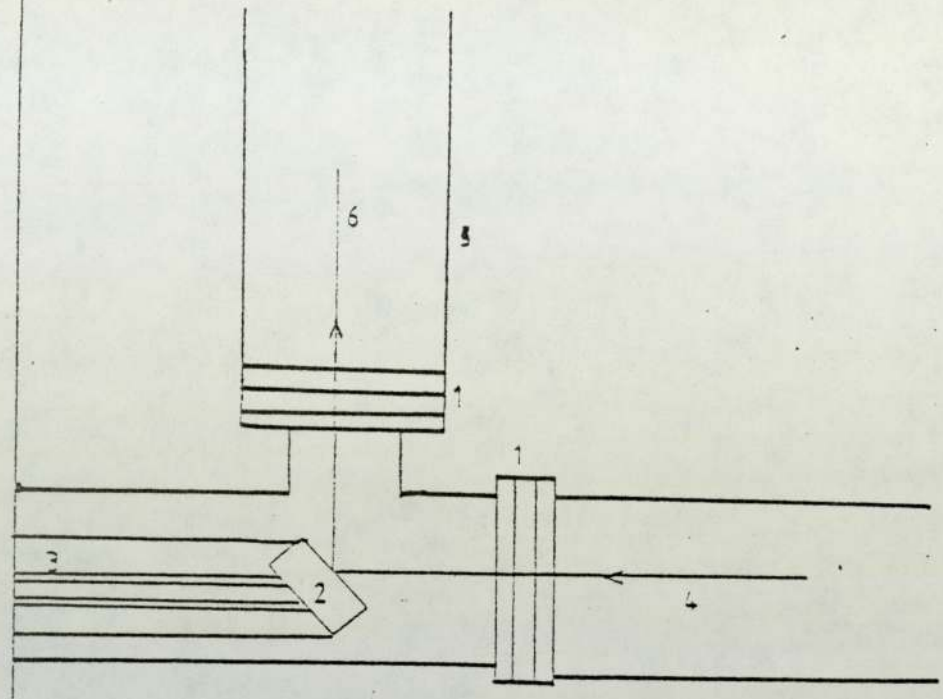

1 Flange

2 Tritium target

3 Coaling tube

4 Deuteron beam

5 Alpha-particle flight tube

6 Alpha-particle direction

Fig. [5-4] The Target Assembly and the Alpha Flight Tube.

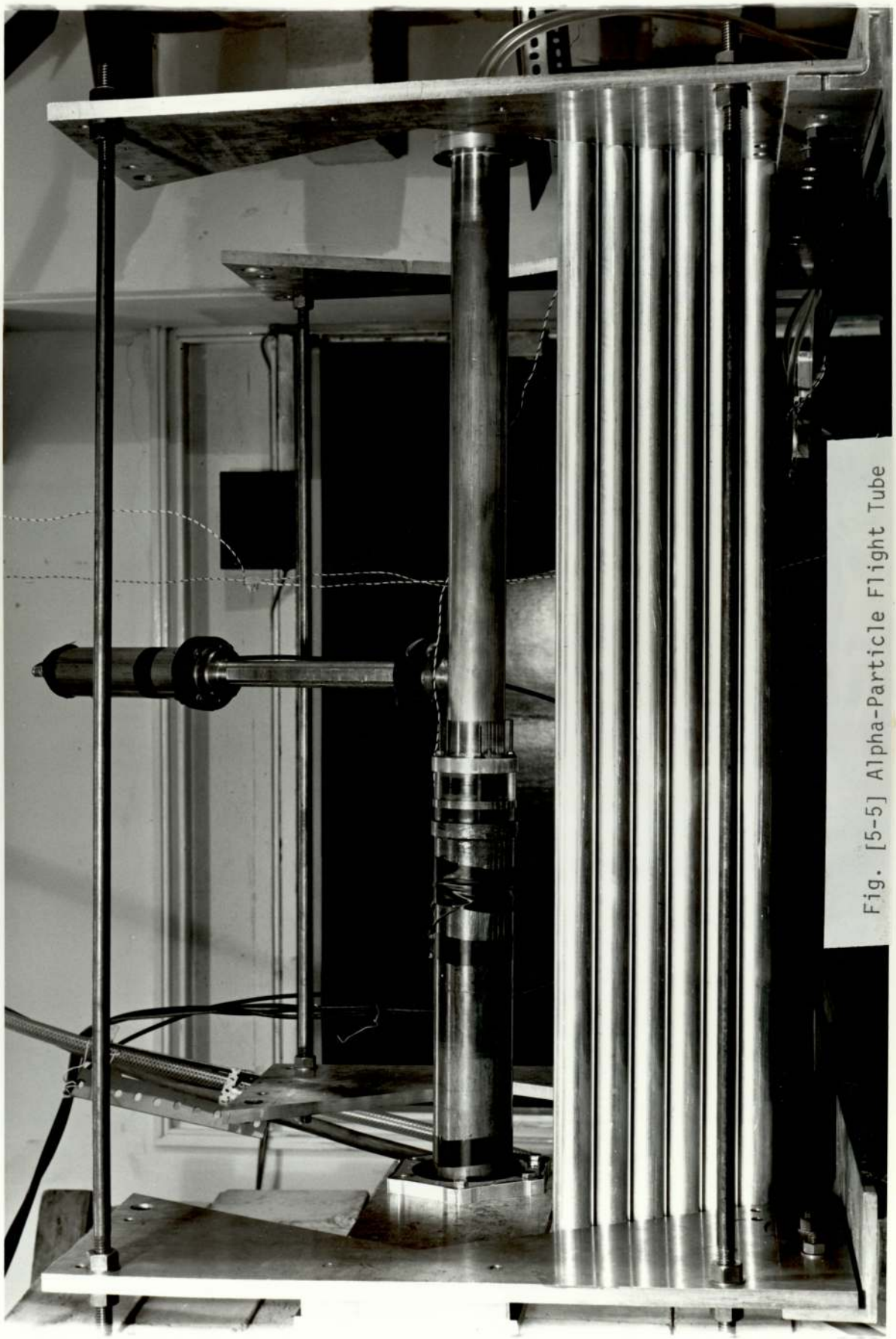

Fig. [5-5] Alpha-Particle Flight Tube

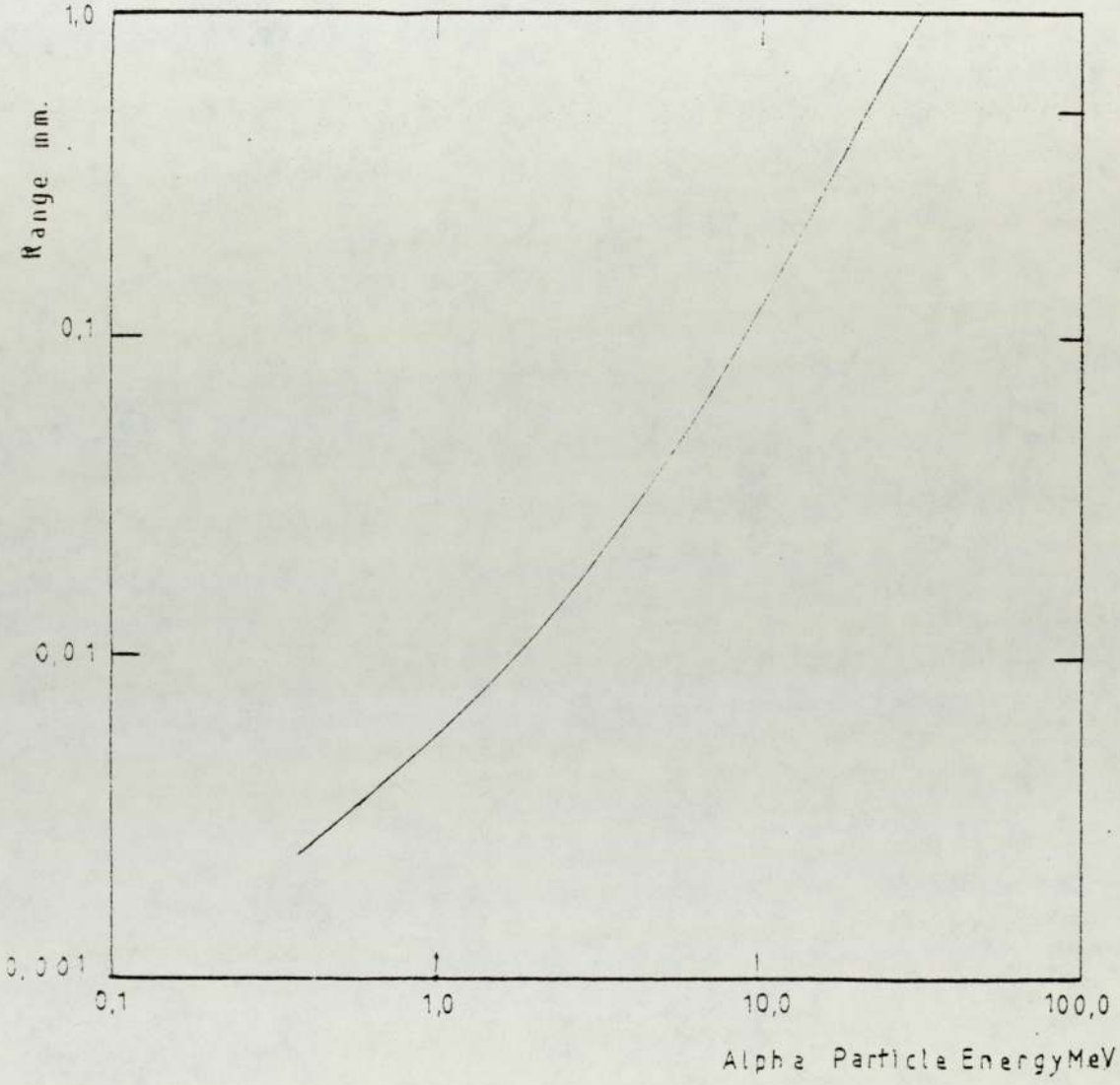

Fig. [5-6] The Alpha-particle Range in the NE-102A Scintillator

which gives a range of 0.025 mm for 3.5 MeV alpha-particles.

The scintillator used was 0.5 mm thick and was coupled to an EMI-9524B photomultiplier tube. The scintillator was placed inside the flight tube at a distance 33 ± 0.1 cm from the target, the interior view of the scintillator and the photomultiplier tube is shown in Figure [5-7]. A very thin foil of Aliminium (0.0015 mm) was used to cut out light and to prevent scattered deuterons from reaching the scintillator. The output pulses from the photomultiplier tube were fed to a charge sensitive amplifier and then to a scaler.

In order to determine the real number of alpha-particles and in turn the absolute number of neutrons, the number of alpha counts recorded by the detector have to be multiplied by a factor G (the geometry factor), which depends on the solid angle that the alpha detector subtends at the source.

Assuming C_α is the alpha-particle count recorded by the detector at a distance R, so the source strength S_o is given by:

$$S_o = \frac{C_\alpha}{(\Delta\Omega/4\pi)} \qquad \ldots\ldots\ldots \text{5-4}$$

where

S_o - is the source strength of an isotropic alpha-particle source in the laboratory system, and

$\Delta\Omega$ - is the solid angle subtended by the detector of a diameter D at a distance R from the source, and given by

$$\Delta\Omega = \frac{\text{area}}{(\text{distance})^2}$$

$$\Delta\Omega = \frac{\pi D^2}{4R^2} \text{ (provided that } D \ll R)$$

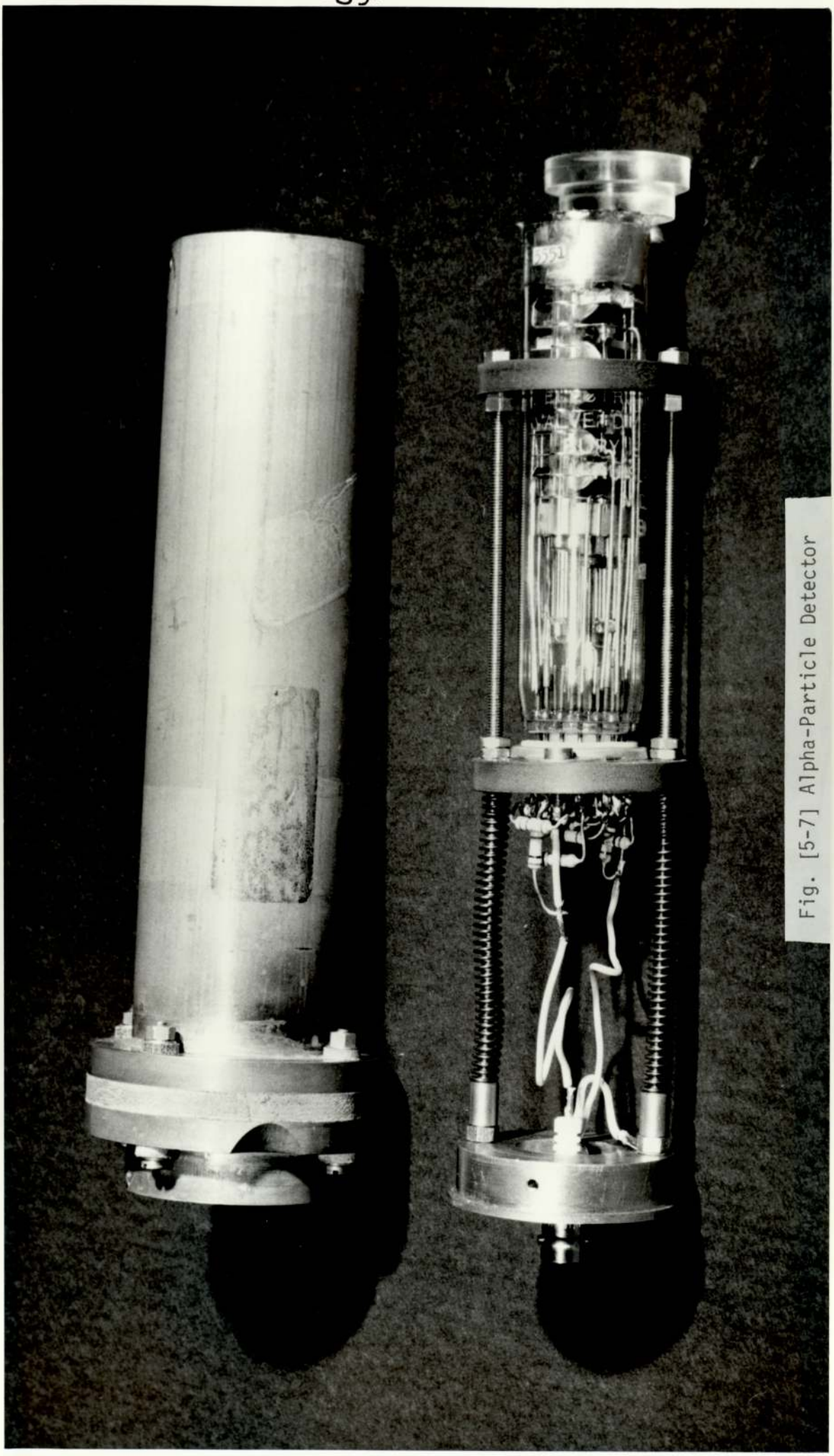

Fig. [5-7] Alpha-Particle Detector

Assuming that R is large and the target area is small enough so it is effectively a point source, therefore

$$S_o = C_\alpha \frac{16R^2}{D^2}$$

and

$$S_o = C_\alpha G \qquad \ldots\ldots\ldots 5\text{-}5$$

where $$G = \frac{16R^2}{D^2}$$

The value of the geometry factor was calculated to be equal to 1.13×10^5. This value was used in the computer program (Appendix 1) written for analysis of the data to normalise all the measurements to the same source strength. The 14.1 MeV neutron spectrum from the $D(T,n)^4He$ reaction is shown in Figure [5-8] and was derived by using the computer program neutron (Appendix 1).

5-6 Neutrons Produce in the Experimental Assembly

a - Neutrons from the (D,D) reaction

This reaction is described by the equation:

$$^2D + {}^2D \rightarrow {}^3He + {}^1n + 3.28 \text{ MeV}$$

The angular distribution of the neutron from such reaction is not isotropic and the degree of anisotropy, which is forward peaked, varies with deuteron energy. Using lower deuteron energies, the spectrum of neutron at 90^o is approximately monenergetic with an energy of about 2.5 MeV if a thick target is used[69].

Because of the target assembly used for the tritium and the beam tube material used in the present work the (D,D) reaction can occur due to the drive in target effect and the spectrum measured

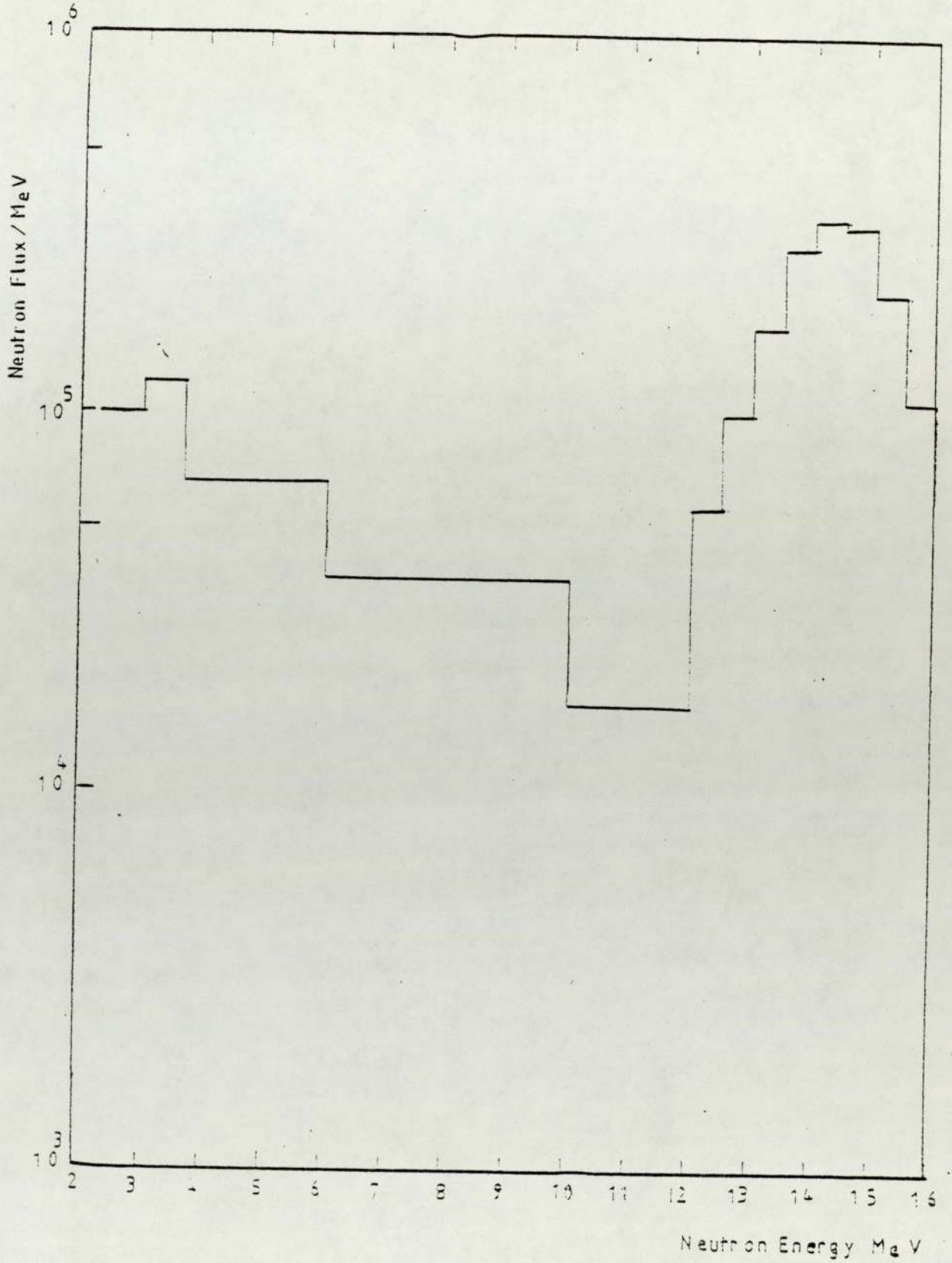

Fig. [5-8] 14.1 MeV Neutron Spectrum from the D,T Reaction

using a plain copper target instead of the tritium target is shown in Figure [5-9]. (There is no direct correlation between the vertical scale of Figure [5-8] and Figure [5-9] since currents were low and difficult to measure accurately).

b - The Spontaneous Fission Neutron

In the uranium shielding spontaneous fission neutrons are produced. About 23 nuclei per gram suffer spontaneous fission per hour on the average [74]. For a full load of uranium this is about 3.2×10^4 fast neutrons per second from fission. Figure [5-10] shows the spectrum of spontaneous fission neutrons and Figure [5-11] shows the fission neutron spectrum measured by the (NE-213) detector and unfolded by the use of computer program neutron (Appendix 1).

5-7 The Shielding Assemblies

The assembly is 86 cm overall length 82 cm effective length and made in a hexagonal shape of 7.725 cm centre to corner for the inner hole so the beam tube can go through and a maximum 29.35 cm centre to corner outer boundary, seven layers of the shielding material being possible with LiF and uranium. The assembly supporting frame is of aluminium. It supports the ends of the tubes to minimize disturbance of measurements and itself supported on rails so it is very easy to move the whole shielding assembly to allow for other experimental uses.

The hexagonal shape was chosen to be close to cylindrical geometry and is easy to build from rods. A cross-section of the assembly is shown in Figure [5-12].

The design was governed by the shape and size of the uranium rod available (81 cm in length and 3.09 cm in diameter) so the same

shape and size of aluminium tubes was chosen for the LiF which filled the tubes up to 82 cm length, the remainder being aluminium end caps. The average density of the LiF inside the tube was about 0.87 gm cm^{-3} which is much lower than the density of a LiF crystal, but the powdered form would not pack more densly.

The assembly was designed with the tubes touching rather than having a supporting lattice plate in order to minimize the air voids in the system. Figure [5-13] shows a view of one of the experimental shielding assemblies.

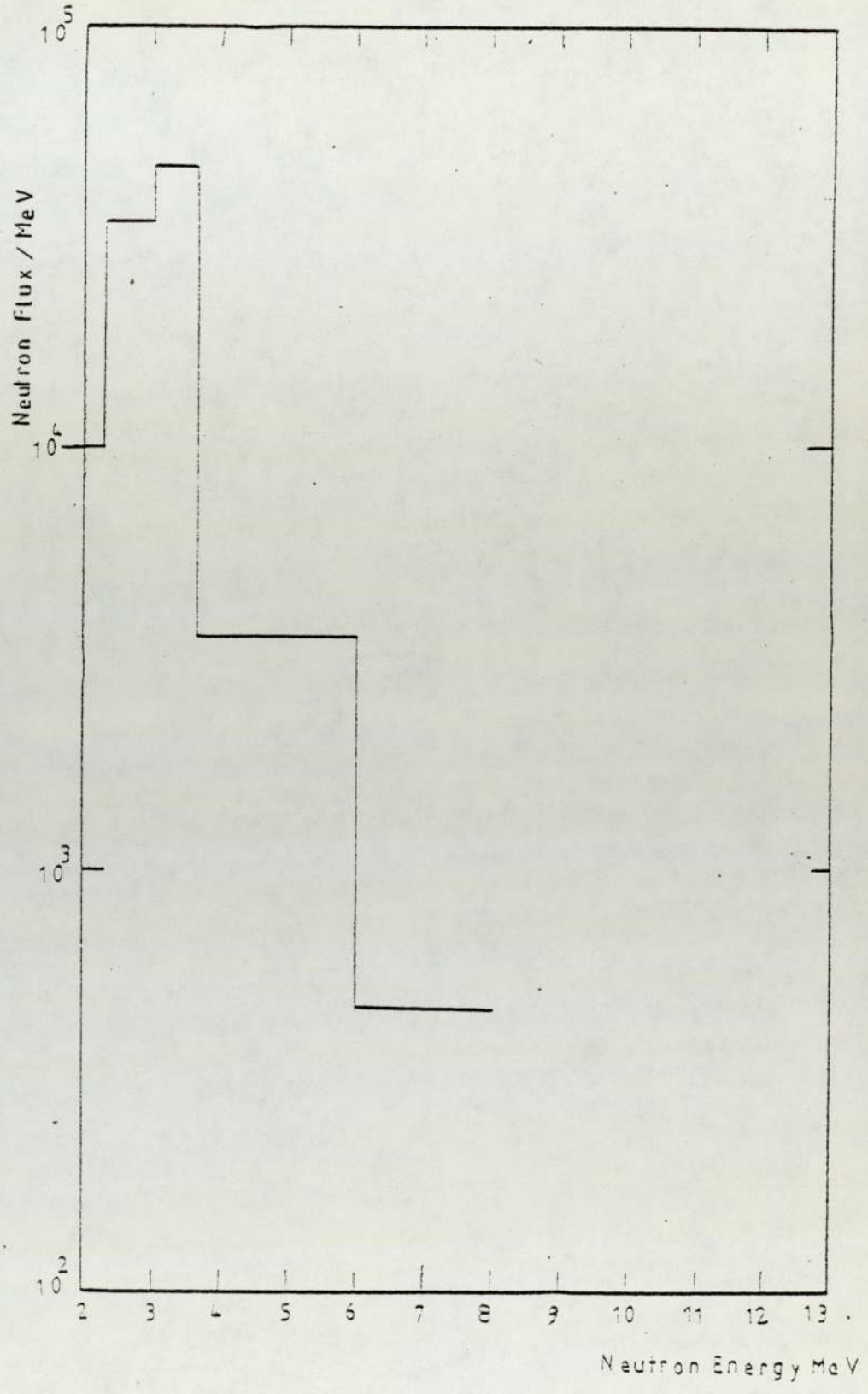

Fig. [5-9] The D-D Reaction Spectrum

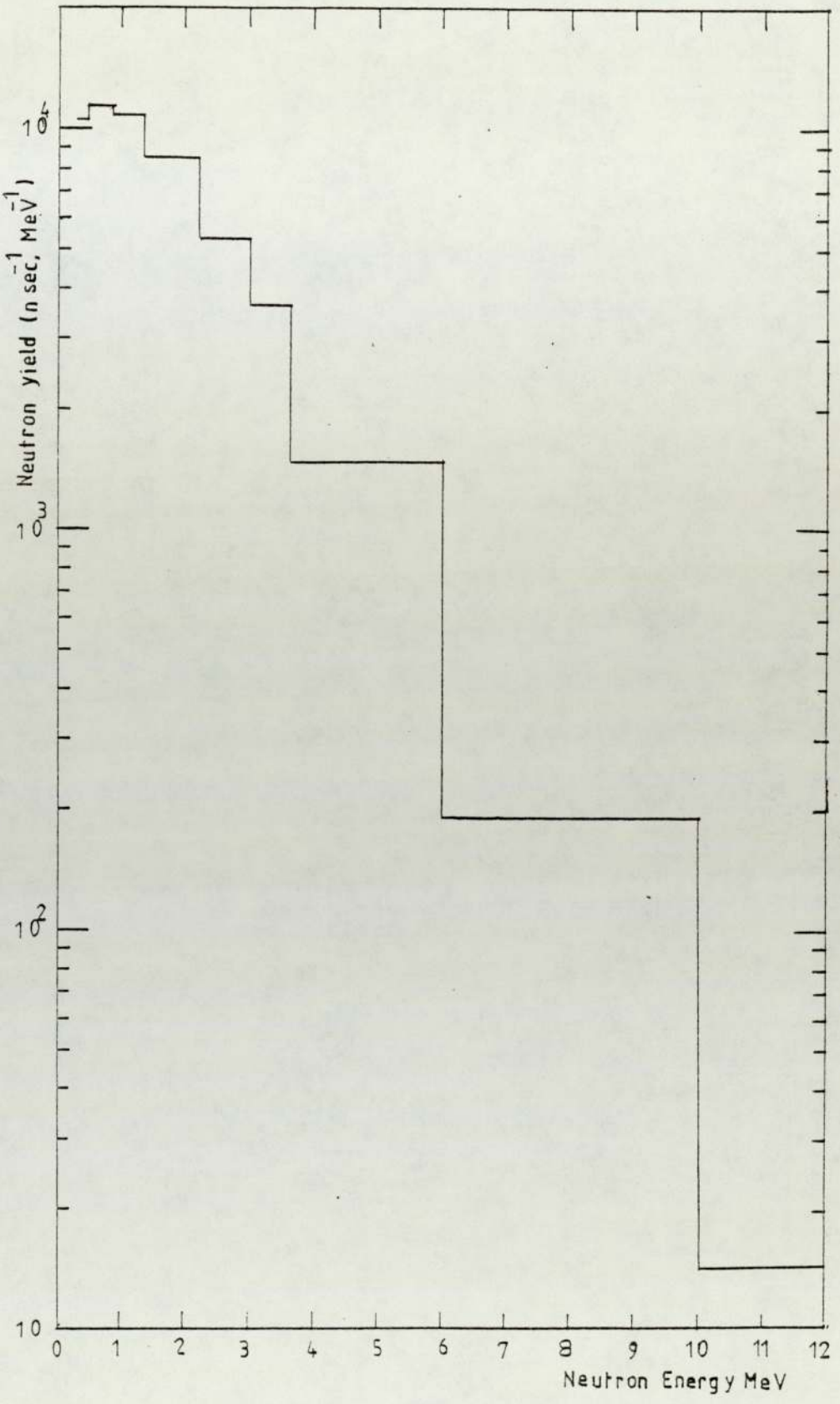

Fig. [5-10] Spontaneous Fission Neutron Yield from two ton of Uranium

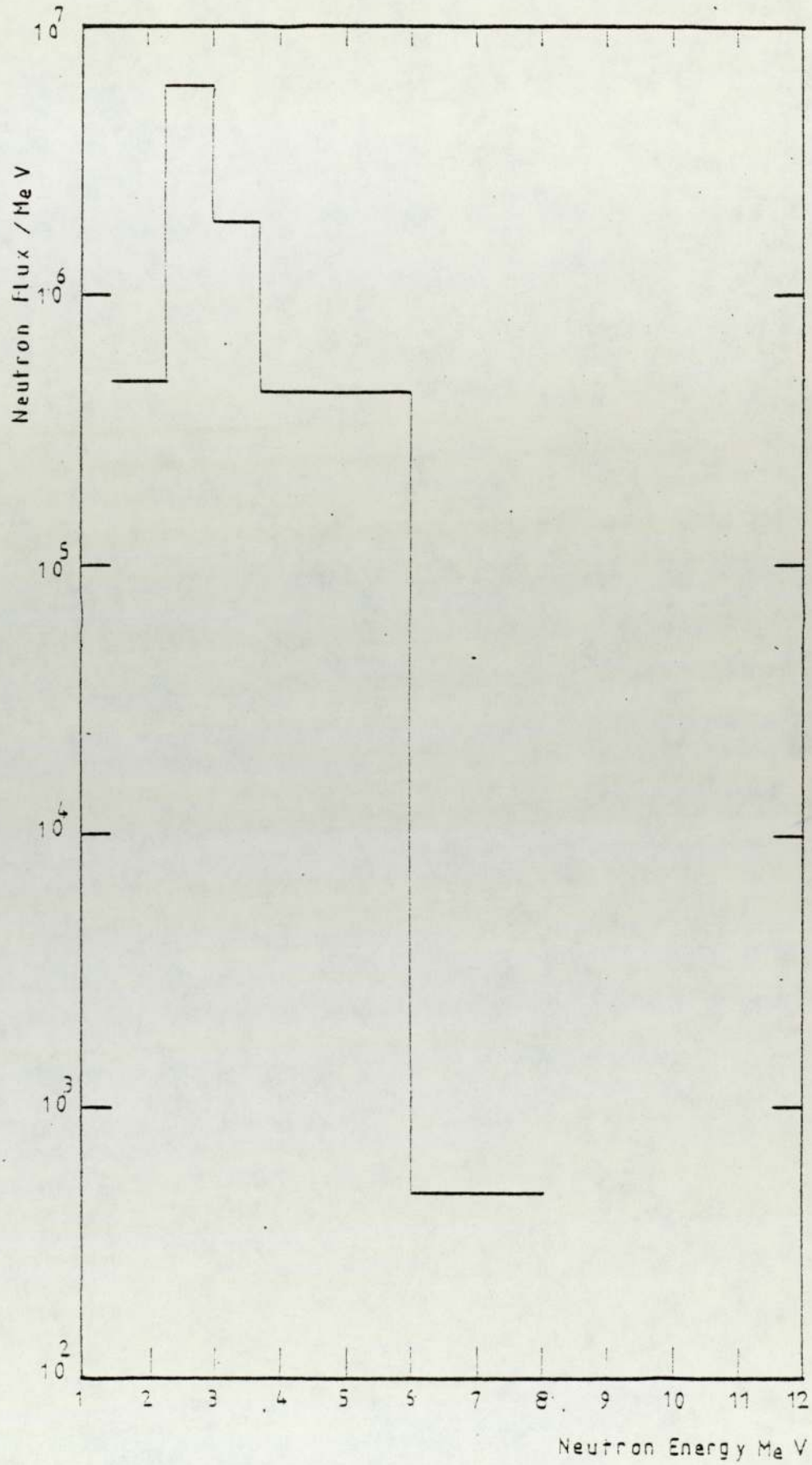

Fig. [5-11] Neutron Flux due to Spontaneous Fission

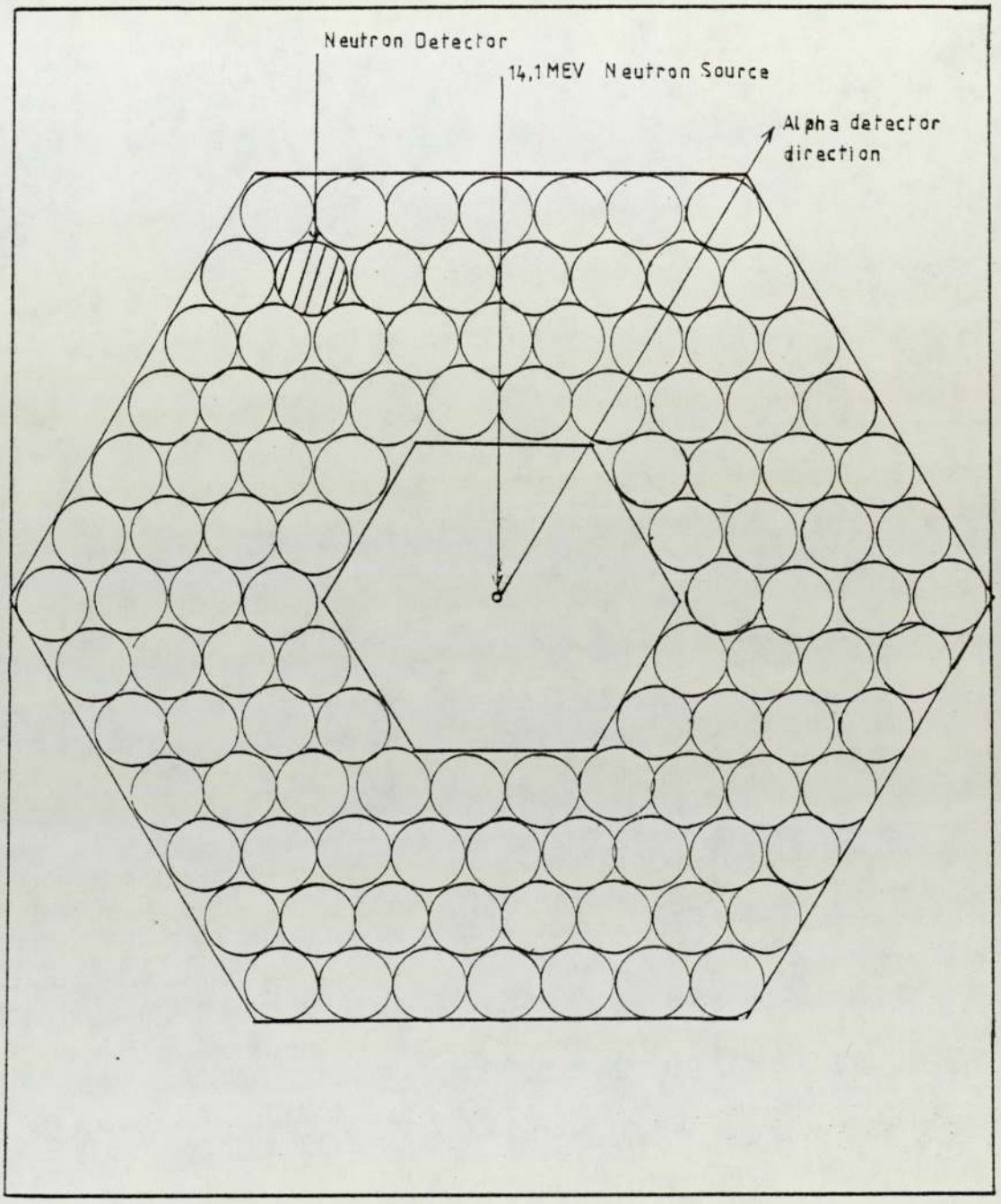

Fig. [5-12] Cross-Section Through the Shielding Assembly

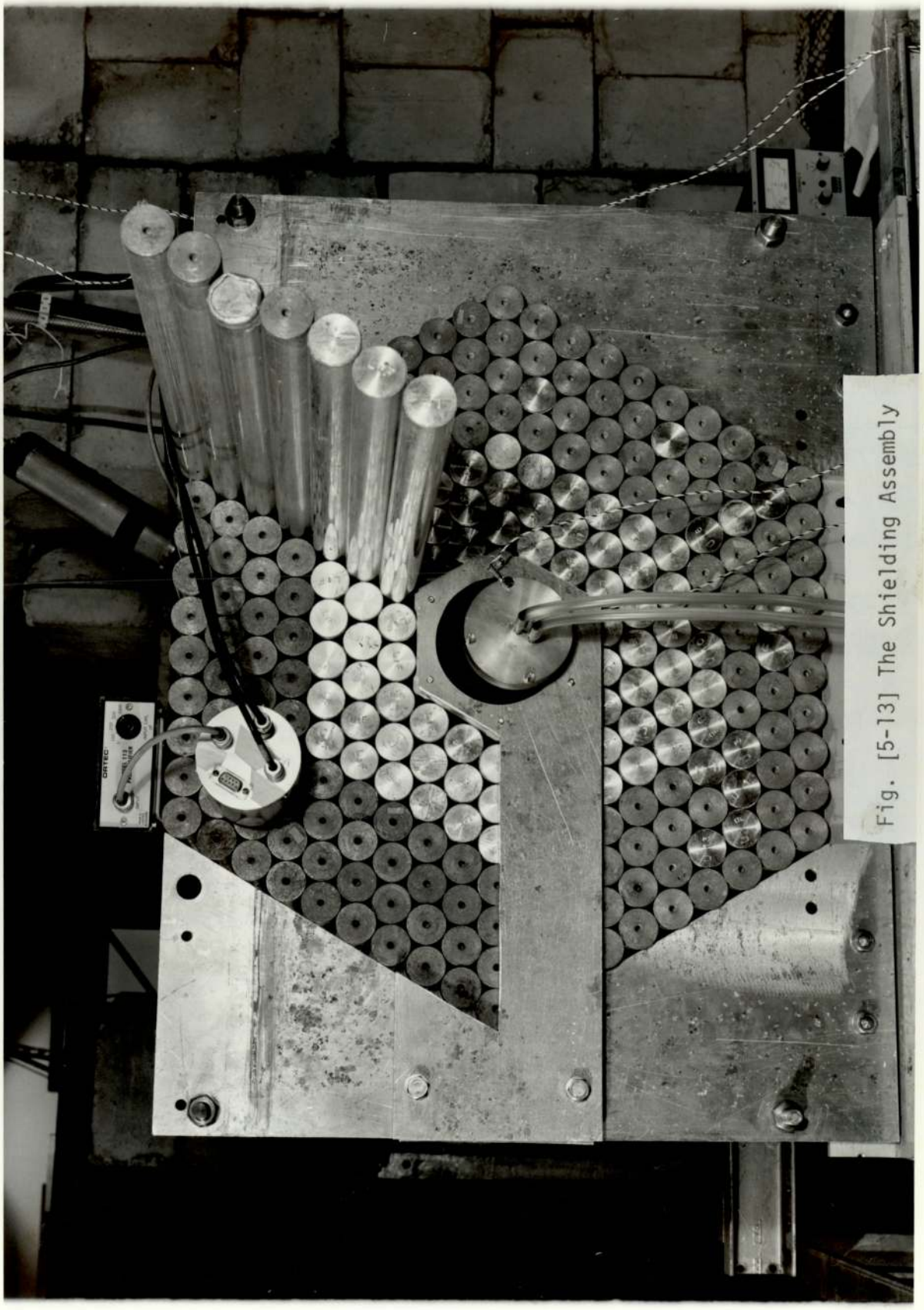

Fig. [5-13] The Shielding Assembly

CHAPTER 6

THEORETICAL CONSIDERATIONS

6-1 Introduction

The neutrons move about in the shielding material in a complicated zigzag path due to repeated collisions with the nuclei. This motion is similar in some aspects to gaseous diffusion or the diffusion of the heat. The fundamental difference between the theory of the diffusion of gases and that of neutrons is that the molecules of a gas collide with each other whereas neutrons collide with the nuclei of the medium in which they diffuse and not with themselves because the density of neutrons is extremely small even in high power nuclear reactions[75,76].

The treatment of these collisions can be described by the transport method formulated by Maxwell and Boltzmann in which one can predict the neutron flux distribution throughout the medium.

The transport method has been widely used for several years for the study of attenuation of monoenergetic neutrons, therefore the study of a wide energy range must be represented by a group structure. The inaccuracy in the average group cross-section can lead to unacceptable error in the estimation of the neutron flux behind the shielding, even if the effective group cross-sections are known with a good accuracy, since the value of the effective group cross-section of an interaction can be changed with the shielding thickness if the groups are too wide in energy, due to changing neutron spectrum.

The application of the Boltzmann transport theory to practical design calculation was made by empirical methods. These methods

are mainly based on the results of experimental studies of the transport equation to the study of neutron slowing down problems by L.S. Ornstein-Ohlenbek[77] and E. Fermi[78].

In the past 30 years, the technical development of high speed computers with large storage capacities has led to a wider application of numerical methods for solving the transport equation. This has resulted in several hundred different reactor codes which were written for many types of digital computers[79]. Unfortunately where the computational techniques of these codes are discussed in the published papers usually the name of the code is mentioned only, so the choice of a method which is suitable for a certain application is difficult.

6-2 The Transport Theory

Three view points of different degrees of complexity can be used in establishing the basic equation of transport or diffusion theory.

In the first (kernal method), the probability that a neutron appears at a given point with a given set of properties after appearing at some other point with other properties is weighted with a general transfer function (kernal) usually determined experimentally.

The second view is the integral transport theory which seeks to relate the collision density after n collision to the collision density after n-1 collisions.

Thirdly is called the general transport theory (Boltzmann) it seeks to compute the distribution of the neutrons from a general integro differential equation into which only macroscopic cross-sections and no other experimental information enter[75].

The Boltzmann transport equation is given by[80]:

$$\Omega.\nabla\Phi(r,U,\Omega) + \Sigma_t(r,U).\Phi(r,\Omega,U)$$

$$= \int_{U-\varepsilon_i}^{U} dU' \int d\Omega\Sigma_e(r,U)\Phi(r,\Omega',U') \cdot g_e(\Omega',U':\Omega,U)$$

$$+ \int_{U-\varepsilon_i}^{U} dU' \int d\Omega'\Sigma_i(r,U')\ \Phi\ (r,\Omega',U') \cdot g_i(\Omega',U':\Omega,U)$$

$$+ g_f\ (U) \int_{o}^{\infty} dU' \int d\Omega'\upsilon(U')\ \Sigma_f(r,U) \cdot \Phi(r,\Omega',U')$$

$$+ S_o\ (t,U,\Omega) \qquad \text{..... 6-1}$$

where

$\Sigma_t,\Sigma_e,\Sigma_i,\Sigma_f$ -are the macroscopic, total, elastic, inelastic and fission cross-section respectively

$\Phi(r,U,\Omega)$ -is the angular neutron flux

$U-\varepsilon_i$ -represents the lowest lethargy from which neutrons may be elastically or relatively scattered into U

S_o -is the external neutron source

υ -the number of neutrons produced per fission

6-3 Method Used for Solution of the Boltzmann Transport Equation

Methods of solution of the transport equation are inherently complex due to the integro-differential form of the equation. An exact solution of the equation is limited to a few highly specialized problems, and the most practical techniques are approximate methods.

In recent years considerable progress has been made in the solution of one speed neutron transport equations. K.M. Case[81] in 1960 found a complete set of eigen functions for one-speed neutron transport equation for the case of isotropic scattering. This has been extended by J. Mika[82] to include anisotropic scattering and has been used by J. H. Ferziger et al[83] to solve some thermalization problems. J.J. Melnerey[84] found a solution of the space-energy angle dependent neutron slowing down problem by a method parallel to those developed by Case.

In general the methods and techniques used to solve the transport equation are described hereafter.

6-3-1 The Spherical Harmonic Method

The spherical harmonics method theory for approximation to the Boltzmann transport equation has been developed in various reports, in a tensor form by C. Mark[85], and its simplified form for spherical and plane symmetry[86]. Avery's much simplified method is given by Davison[87], for use with complicated geometeries.

The spherical harmonics method approximation consisting of a series of differential equations which are independent of the angular direction. This is done by expanding the function Φ, g_e, g_i and g_f in equation (6-1) in terms of spherical harmonics by a - Assuming that these functions can be written as an infinite power series in the variable μ with coefficients that depend on Z.

$$\mu = \text{Cos } \theta$$

where

θ - is the angle between the Z-axis and Ω.

b - Assuming that the medium is isotropic and homogeneous so that the cross-section is independent of Z, and the scattering is azimuthally symmetric about the initial direction of motion of the neutron

$$g_e(\mu', U' : \mu, U) = g_e(U', U, \mu_o)$$

$$= \sum_{L=o}^{\infty} \frac{2L+1}{4\pi} g_{e,L}(U',U) P_L(\mu_o) \quad \ldots\ldots\ldots 6\text{-}2$$

and

$$g_i(\mu', U' : \mu, U) = \sum_{L=o}^{\infty} \frac{2L+1}{4\pi} \cdot g_{i,L}(U':U) P_L(\mu_o) \quad \ldots\ldots\ldots 6\text{-}3$$

where

P_L - the Legendre polynomial of degree L, and

$\mu_o = \Omega \cdot \Omega' = \text{Cos } \theta_o$

The angular neutron flux is expressed as follows:

$$\Phi(Z,\mu,U) = \sum_{L=o}^{\infty} \frac{2L+1}{4\pi} \cdot \Phi_L(Z,U) \cdot P_L(\mu) \quad \ldots\ldots\ldots 6\text{-}4$$

and

$$S_o(Z,\mu,U) = \sum_{L=o}^{\infty} \frac{2L+1}{4\pi} \cdot S_{o_L}(Z,U) P_L(\mu) \quad \ldots\ldots\ldots 6\text{-}5$$

we have for the Legendre polynomials

$$\int_{-1}^{1} P_L(\mu)P_n(\mu)d\mu = \frac{2}{2L+1} \quad \text{if } n = l$$

$$= o \quad \text{if } n = -l \qquad \ldots\ldots\ldots 6\text{-}6$$

Substituting equation (6-2 - 6-5) into the transport equation and using the relation in equation (6-6), we get the spherical harmonic form of the Boltzmann transport equation.

6-3-2 The Discrete Ordinates S_N Method

In 1953 Carlson[88] improved the S_N method and used it to solve the transport equation. To compute the numerical solution of the discrete ordinates equation efficiently these methods must fulfil two essential requirements[89].

a - The equation relating to the central flux and the two end points fluxes should provide a good approximation of the true variation of the flux in the neighbourhood of the cell.

b - An additional equation combined with the discrete ordinate equations must produce a final set of equations that can be solved easily and quickly on the computer.

The S_N method was originally developed for the case of isotropic scattering and has been extended to take account of anisotropic scattering by using the transport cross-section given by[90].

$$\sigma_t = \sigma_s \left[1 - \int_{-1}^{+1} \mu f_e(\mu)\, d\mu \right] \qquad \ldots\ldots\ldots 6\text{-}7$$

where

σ_t, σ_s - The transport and scatter cross-section respectively

$f_e(\mu)$ - The angular distribution of scattered neutrons

In this method the integral in the transport equation is approximated by a discrete ordinate quadrature, the solid angle is divided into N segments and discrete direction and weights. For a plane and spherical geometry the range of $\mu = -1$ to $\mu = +1$ is divided into equal intervals, and $\Phi(\mu)$ is taken to vary linearly with μ in each intervals, then the range of integration over μ is divided into equal sub-intervals N. Let the points which define these sub-intervals be,

μ_n (n = 0, 1, 2, ... N), so that

$\mu_o = -1$ and $\mu_N = +1$

The number of intervals N define the order of approximation, so the angular flux for a certain energy group i is given by

$$\Phi_i(r,\mu) = \frac{(\mu-\mu_{n-1})}{(\mu_n-\mu_{n-1})} \cdot \Phi_i(r,\mu_n) + \frac{(\mu_n-\mu)}{(\mu_n-\mu_{n-1})} \cdot \Phi_i(r,\mu_{n-1}) \quad \text{..... 6-8}$$

This approximation is then used to reduce the one velocity transport equation to a set of N equation in N + 1 variables $\Phi(r,\mu_n)$. The additional equation to be combined with it is obtained by setting $\mu = -1$ directly in the one velocity Boltzmann transport equation, the resulting set is then solved numerically for the fluxes.

The method is now one of the most important analytical tools in the reactor shielding calculation, it has the advantage of being

more suited to large digital computers[91].

6-3-3 The Slowing Down Theory

The description of the Fermi age theory is available in the published literature[92,93,94]. The conditions for this theory to be fulfilled are firstly, inelastic scattering is assumed absent, the elastic scattering is spherically symmetric in the centre of mass system and, thirdly the effect of chemical bonding is neglected.

The theory treats the succession of discrete energy losses in individual collision by which neutrons are actually slowed down as equivalent to a continuous slowing down process which results in the same average rate of energy loss. In the Fermi theory it is assumed that diffusion theory is valid at all energies[94].

The arrival and departure of neutrons with lethorgies between U and U+dU in the volume element at a position r, may be expressed in terms of slowing down density q(r,U) which is defined as the number of neutrons crossing a lethargy level U per cubic centimeter per second. The number entering dU is q(r,U) and the number leaving dU is q(U+dU,r).

Thus,

$$S(U)\,dU = q(r,U) - q(r,U+dU) \qquad \ldots\ldots\ldots \text{6-9}$$

or

$$S(U)\,dU = -\frac{d_q(U,r)}{dU}\,dU \qquad \ldots\ldots\ldots \text{6-10}$$

Combining equation (6-9, 6-10) with the diffusion equation $D\nabla^2\phi+S = 0$, we get

$$D(U)\nabla^2\phi(r,U) = \frac{d_q(r,U)}{dU} \qquad \ldots\ldots\ldots \text{6-11}$$

The relation between the neutron flux and slowing down density is given by:

$$\Phi = \frac{q}{\xi\Sigma_s} \qquad \text{so}$$

$$D\nabla^2 q = \xi\Sigma_s \frac{dq}{dU} \qquad \text{..... 6-12}$$

From the above discussion, the Fermi theory applies to a medium in which there is no absorption of neutrons, but it is found that for a weakly absorbing medium a sufficient approximation is:

$$q^*(U) = p(U) \cdot q(U)$$

where

$p(U)$ = The resonance escape probability for a neutron of energy U.

6-3-4 The Moments Methods

This method was proposed by Spicer et al[95], and used by Goldstein and Wilkin[96], for extensive computer calculations to obtain build-up factors and differential energy spectra for infinite homogeneous media as a function of the penetrations.

The polynomial method in a semi-numerical technique which has been used to give quite accurate solutions to the Boltzmann equation. In this method the angular flux is expanded in a series of Legendre polynomials, and assuming that the scattering is spherically symmetric in the centre of mass system. By this it reduces the original equation containing three variables (Ω,r,U) to a sequence of coupled integro-differential equation of two variables (r,U), then these equations are multiplied by $p_L(\omega,\Omega)$ and integrated over all solid angles. In this way one obtains a double sequence of linear integral equations for the spatial moments

of the Legendre coefficients.

The solution of Boltzmann equation by using this method has been carried out for both neutrons and gamma rays in an infinite homogeneous media with a simple source[75]. However the solution for neutrons is more complicated than that for gamma rays and that is because of the rapid change in neutron cross-section with energy and because neutrons undergo many collisions before absorption.

The main advantage of the method is the determination of the fast neutron space energy distribution after considering the anisotropy of elastic scattering.

6-3-5 Monte Carlo Method

The Monte Carlo method is a technique for solving physical and mathematical problems by using random of sampling of an analog nature[97]. The most extensive and successful applications have been to physical problems that are inherently statistical.

The problem of neutron transport is basically concerned with random events such as the behaviour of neutrons when interacting with matter. In this problem the histories of a large number of neutrons are followed from collision to collision. In going from one collision to another the problem is to determine the distance travelled before the next collision takes place, the type of collision and the energy, and direction of the neutron after the collision.

The Monte Carlo result however is exact only when an infinite number of independent estimates of a given result have been obtained. Any answer that derives from a finite number of tries has a statistical uncertainty.

The Monte Carlo method has the major advantage of allowing even complex transport problems to be formulated rather easily, and can obtain an exact solution to the Boltzmann transport equation[98]. The main disadvantage of the method is that its results are statistically uncertain.

A survey for the application of the method for shielding and reactor calculation is given by Goertzel et al[94], and the application to the transport problem by Kalos et al[97] and Arnecke et al[99].

6-3-6 The Diffusion Theory Method

The diffusion method is a simplified method for solving the Boltzmann transport equation by assuming that all neutrons have the same lethargy (U) and under the conditions that, the scattering processes with nuclei do not involve any change in the neutron energy. The basic assumption of the elementary diffusion theory is the validity of Fick's law.

The relationship between the flux and the current are identical in form with Fick's law, which has been used for many years to describe diffusion phenomena in gases and liquids. For this reason the use of that law in reactor theory leads to a diffusion approximation[16].

Fick's law states that the current density vector is proportional to the negative gradient of the flux.

$$J(r) = - D \text{ grad } \Phi(r) \qquad \ldots\ldots\ldots 6\text{-}13$$

where

D - The diffusion coefficient having the dimension of length.

The above relation is valid only for the diffusion of neutrons in regions which are not closer to boundaries than two or three mean free paths, the absorption cross-section is very small, and the neutrons are scattered without loss in energy.

From the continuity equation, the diffusion equation in the steady state $\frac{dn}{dt} = \frac{1}{v}\frac{d\Phi}{dt} = 0$, is given by

$$D\nabla^2\Phi - \Sigma_a \Phi + S = 0 \qquad \text{..... 6-14}$$

where

∇^2 - the Laplacien operator, and

Σ_a - the absorption cross-section

The absorption cross-section can be determined from the macroscopic scattering and capture cross-section and the average cosine of the scattering $\overline{\mu}_o$ which is given by:

$$\overline{\mu}_o = \frac{2}{3A} \qquad \text{..... 6-15}$$

where

A - the atomic weight of the element of the diffusion medium

In case of mixture of elements in which the ith element has an atomic scattering cross-section σ_i

$$\overline{\mu}_o = \frac{\sum_i \left[N_i\sigma_i\left(\frac{2}{3A_i}\right)\right]}{\sum_i [N_i\sigma_i]} \qquad \text{..... 6-16}$$

where

N_i - The number density of the ith type of atoms in the mixture.

The most important type of boundaries occurring in reactor problems are between comparatively dense media and essentially vacuum, and to

handle such problems a boundary condition at the surface of the medium is assumed of the form:

$$\frac{1}{\Phi}\frac{d\Phi}{dn} = -\frac{1}{d} \qquad \text{..... 6-17}$$

where

d - the extrapolation length

The value of d is chosen such that the solution to the diffusion equation satisfying equation (6-17) matches as nearly as possible the rigorous solution given by transport theory in the interior of the medium[16], d is given by

$$d = 0.71\ \lambda_{tr} \qquad \text{..... 6-18}$$

where

λ_{tr} - the transport mean free path of the medium and is given by

$$\lambda_{tr} = \frac{1}{\Sigma_s(1-\mu_o)}$$

For the treatment of a continuous energy spectrum the energy range is divided into discrete groups and each group is treated separately with its appropriate parameter.

6-4 The Removal Diffusion Method

Albert and Welton[100] introduced the concept of removal cross-section to describe the attenuation of neutrons by the removal collision. The removal diffusion method is a process in which the neutrons slow down by firstly removal collision and secondly a diffusion process, so the penetration of the forward neutrons is described by a removal process which consists of an exponential and a geometrical attenuation factor and the diffusion theory then predicts their migration following such collisions.

The neutron flux can be obtained from the knowledge of the removal cross-section and in cases where it is not available one can use the transport cross-section[101], which is given by:

$$\sigma_t = \sigma_{tot.} - \int_{4\pi} \sigma_{el}(\theta) \text{ Cos } \theta \text{ d } \Omega \qquad \ldots\ldots\ldots \text{ 6-19}$$

where

$\sigma_{tot.}$ - the total cross-section, and

$\sigma_{el}(\theta)$ - the elastic scattering cross-section for scattering in a solid angle $d\Omega$ in the direction of θ.

In this method the energy range of the neutrons is divided into a number of energy intervals and it is assumed that the monoenergetic diffusion theory is applied to the neutrons within each interval. The removal method can be applied with the age theory to predict the subsequent slowing down after a removal collision.

The removal cross-section for the material used in the shielding must be determined, and it has been shown they are roughly $\frac{2}{3}$ of the total cross-section[102]. It has been suggested that the removal cross-section is effectively the same as the transport cross-section i.e.:

$$\Sigma_r = \Sigma_{tr} = \Sigma_t - \bar{\mu}\Sigma_s \qquad \ldots\ldots\ldots \text{ 6-20}$$

where

$\bar{\mu}$ - is the mean cosine of the scattering angle and is given by[16].

$$\bar{\mu} = \frac{2\pi}{\sigma_s} \int_0^{\pi} \sigma_s(\theta) \text{ Cos } \theta \text{ Sin } \theta d\theta \qquad \ldots\ldots\ldots \text{ 6-21}$$

where

θ - is the angle of scatter in lab. system

The distribution of monoenergetic source neutrons above a certain threshold for most shielding materials may be conveniently described by the following expression[103].

$$\Phi(r,E_o) = \frac{Q}{4\pi r^2} e^{-\Sigma_r d} \qquad \ldots\ldots\ldots 6\text{-}22$$

where

Q - the strength of the source

d - the shield thickness

r - the distance between the source and detector

Σ_r - the macroscopic removal cross-section

Avery et al[104], used the removal calculation in conjunction with the multigroup diffusion theory to describe the penetration of the forward directed neutron and the diffusion theory to predict where their angular distribution is nearly isotropic.

6-5 Choice and Comparison of the Calculation Method

The spherical harmonics P_n approximation method and the polynomial S_N method are widely used for multilayered shields[104]. The application of the spherical harmonics technique to the transport equation is difficult and becomes formidable for multigroup energy cases. The method has been extended to cover the anisotropic scattering and the approaches have been applied in the P_3 and P_5 approximations[105, 106]. In general the P_n approximation seems to offer no particular advantage over the S_N method, however it is more suited to modern high speed computers.

The S_N-method produces good neutron penetrating results in simple geometries with less computer time than the other accurate method. But the geometry of the problems to be solved was not sufficiently simple and the suitable computer is not available for use so this method had to be rejected.

The Monte Carlo method is considered as the most developed for practical design calculation. In principle that method can incorporate any arbitrary geometry, source anisotropy, and scattering properties. In addition it is able to handle three dimensional geometries for the multigroup cross-section[107, 108]. However the Monte Carlo method has some limitation due to the time needed to build up accuracy and the large amount of computer store needed.

In the present work the available codes developed for the method could not be used because they were unsuitable for running on the available computer due to the large amount of storage space needed and length of calculation as well as incompatibility of certain sub-routines with the available computer. Consequently a method had to be used which was compatible with the restrictions of the computing facilities.

The removal diffusion theory is a good method for reactor shielding design, some reasons for using the multigroup theory are[104, 109],

a - The neutron flux spectrum may change rather rapidly in the vicinity of interfaces between materials with differing shielding properties, the multigroup method can to some extent take account of this.

b - Because of scattering resonances in the cross-section of certain materials, neutrons can stream through large thicknesses without much attenuation. A suitable choice of the energy groups in the multigroup model can allow for this behaviour.

c - The multigroup diffusion equations are easily adaptable for solution by the computer.

The main disadvantage is that the neutron flux has to be assumed to be isotropic in each group except the highest energy group, which is treated by the removal method. This may not be a good approximation for small shields or for boundaries involving large changes in material constants and the main justification will be how closely theory and experiment agree.

In the present work the removal diffusion method was chosen and the description of the method follows.

6-6 The Multigroup Method

In the multigroup method of calculation, the energy range is divided into a number of intervals, the higher the number of groups, the higher accuracy is acheived providing that the data are accurately known.

A comparison of methods in general use show that these rely largely on numerical solutions of the relevant multigroup equation[110]. Recommendations for the optimum use of diffusion theory vary from choosing an empirically obtained multigroup neutron cross-section data set (Avery et al)[111], to choosing a correct diffusion constant for each energy group[112, 113].

For the solution of the multigroup equation assuming G neutron energy groups, there are G roots to the solution of the equations:

$$D_J \nabla^2 \Phi_J - \Sigma_{rJ} \Phi_J + S_J = 0 \qquad \text{..... 6-23}$$

where

J - indicates the energy group and ranges from 1 - G

Σ_{rJ} - the removal cross-section given by

$$\Sigma_{rJ} = \Sigma_a + \sum_{k=J+1}^{G} \Sigma_{el\ j\to k} + \Sigma_{in}$$

Σ_a - the macroscopic absorption cross-section

$\Sigma_{el}{}_{J\to K}$ - the macroscopic elastic scattering cross-section from group j to group k

Σ_{in} - the macroscopic inelastic scatter = $\sum_{k=J+1}^{G} \Sigma_{in\ j\to k}$

S_J - the neutron source given by

$$S_J = \chi_J \sum_{k=1}^{G} (\upsilon\Sigma_f)_K \Phi_K + \sum_{k=1}^{j-1} \Sigma_{el\ k\to j} \Phi_k + \sum_{k=1}^{J-1} \Sigma_{in}{}_{K\to J} \Phi_K$$

To solve equation 6-23, one of the following methods can be used.

6-6-1 Fundamental Mode Method

This method only applies to an unreflected system of uniform composition, by using either an eigenvalue or final source option[114]. Because of the unreflected system of a uniform composition one can assume that all the group fluxes have the same eigen function so:

$$\nabla^2 \Phi = -\mu^2 \Phi$$

assume a value of S_f (unity is usually chosen), then uncouple the

dependence of one group on all the others and therefore for

$S_f = 1$

$$-\mu^2 D_J + \Phi_J - \Sigma_{rJ}\Phi_J + \Sigma_{el}{}_{J-1}\Phi_{J-1} + \sum_{k-1}^{J-1} \Sigma_{in}{}_{K\to J}\Phi_K + \chi_J = 0$$

..... 6-25

The General solution of (6-25) is given by:

$$\Phi_J = \frac{\chi_J + \Sigma_{el}{}_{J-1}\Phi_{J-1} + \sum_{k=1}^{J-1} \Sigma_{in}{}_{k\to j}\Phi_K}{\mu^2 D_J + \Sigma_{r_J}} \qquad \text{..... 6-26}$$

A value for μ^2 is first made and using the equation (6-26) to evaluate Φ_1 to Φ_G in turn, since the fission source is assumed equal to one.

The fission source S_f is then calculated from

$$S_f = \sum_{k=1}^{G} (\upsilon\Sigma_f)\Phi_K$$

So if the value of μ^2 is correct then the value S_f will be one, and if not successive values of μ^2 are tried until the value that makes $S_f = 1$ is found. Such a calculation can be used for fast reactors to compute a histogram of the Multigroup neutron energy spectrum.

6-6-2 The Finite Difference Method

For the purpose of the present work the finite difference method was used. By choosing sufficiently small intervals it is possible to obtain a solution to the multigroup diffusion equation which is sufficiently accurate such that any errors can be attributed to the diffusion theory approximation, rather than to the numerical approximation procedure[115].

The solution of a second order differential equation of the form[116] is as follows:

$$-D\nabla^2 \Phi_n + \Sigma\Phi_n = S_n \qquad \ldots\ldots\ldots 6\text{-}27$$

For the spherical geometry:

$$\nabla^2\Phi_n = \frac{d^2\Phi}{dr^2} + \frac{2}{r}\frac{d\Phi}{dr} \qquad \ldots\ldots\ldots 6\text{-}28$$

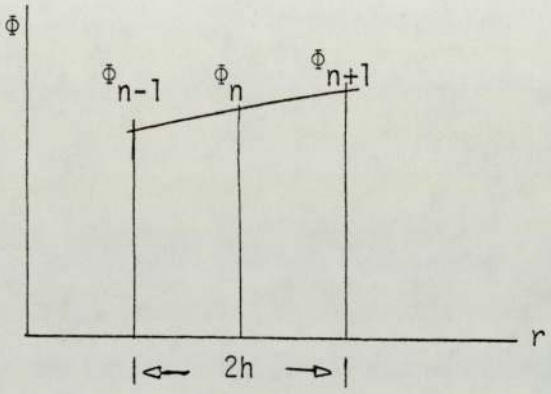

$$\frac{d\Phi}{dr} = \frac{\Phi_{n+1} - \Phi_{n-1}}{2h}$$

$$\frac{d^2\Phi}{dr^2} = \frac{\Phi_{n+1} + \Phi_{n-1} - 2\Phi_n}{h^2}$$

$r = nh$, so equation 6-27, will be

$$-\frac{D}{h^2}\left[1 - \frac{1}{n}\right]\Phi_{n-1} + \left[\frac{2D}{h^2} + \Sigma\right]\Phi_n - \frac{D}{h^2}\left[1 + \frac{1}{n}\right]\Phi_{n+1}$$

$$= S_n \qquad \ldots\ldots\ldots 6\text{-}29$$

or

$$a_{1n}\Phi_{n-1} + a_{2n}\Phi_n + a_{3n}\Phi_{n+1} = S_n \qquad \ldots\ldots\ldots 6\text{-}30$$

where

$$a_{1n} = -\frac{D}{h^2}\left[1 - \frac{1}{n}\right] \qquad \ldots\ldots\ldots 6\text{-}31$$

$$a_{2n} = \left[\frac{2D}{h^2} + \Sigma\right] \qquad \ldots\ldots\ldots 6\text{-}32$$

$$a_{3n} = -\frac{D}{h^2}\left[1 + \frac{1}{n}\right] \qquad \ldots\ldots\ldots 6\text{-}33$$

Consequently a set of such equations exist for each mesh point.

The method of solution, together with the treatment of inner and outer boundaries as well as internal boundaries is given in Appendix 2.

The spectra of fast neutrons which have passed through LiF and U^{238} shielding at various thicknesses inside the shielding have been calculated by using the combination of the multigroup diffusion theory and the removal diffusion equation using the method described above.

6-7 The Multigroup Constants

To obtain the average values of the group constants in a particular group, it is necessary to know the neutron spectrum within the group. That spectrum may be known in thermal system being Maxwellian for thermal neutron and have a $\frac{1}{E}$ variation for slowing down neutron, when $\Phi(U)$ is taken as a constant. In the fast system there is no such well defined spectrum and several groups are needed for correct representation.

In a multigroup calculation the entire range of neutron lethargy is divided into G groups which may or may not be of equal size.

The flux $\Phi_g(r)$ of the neutron in the gth group is defined by:

$$\Phi_g(r) = \int_{Ug-1}^{Ug} \Phi(r,U)\, dU \qquad \ldots\ldots\ldots 6\text{-}34$$

Ug and U_{g-1} are the upper and lower lethargies of the group respectively, and

$\Phi(r,U)$ - is the lethargy dependent flux at the point r.

6-7-1 Cross-Section

The neutrons may disappear from a group either in an absorption interaction or as the result of elastic or inelastic scattering which increases their lethargy to that of another group, the average cross-section in general is defined by:

$$\overline{\Sigma}_g = \frac{1}{\Phi_g} \int_{Ug-1}^{Ug} \Sigma(U)\, \Phi(U)\, dU \qquad \ldots\ldots\ldots 6\text{-}35$$

6-7-2 Diffusion Coefficient

The diffusion of neutrons within each group is described by an average diffusion coefficient given by:

$$D_g = \frac{\int_{Ug-1}^{Ug} D(U)\, \nabla^2 \Phi(r,U)\, dU}{\int_{Ug-1}^{Ug} \nabla^2 \Phi(r,U)\, dU} \qquad \ldots\ldots\ldots 6\text{-}37$$

∇^2 - the Laplace operator

The value of Dg is usually a function of r, unless the Φ (r,U) can be written as a function of r and U

$$\Phi (r,U) = F (r) \cdot \Phi (U)$$

where Φ (U) - is the lethargy dependent part of the flux.

This approximation must be made in order to carry out the group calcuation, and that Dg will be given by:

$$Dg = \frac{1}{\Phi g} \int_{Ug-1}^{Ug} D(U)\ \Phi(U)\ dU \qquad \ldots\ldots\ldots\ 6\text{-}37$$

In the case of isotropic scattering in the lab. system which is true only at low energy the value of Dg can be calculated from the method of transport and is given[16].

$$D = \frac{\lambda tr}{3} \qquad \ldots\ldots\ldots\ 6\text{-}38$$

But for anisotropic scattering this quantity is decomposed into many terms by the number of collisions which the neutron suffers in the course of it is flight from a region i to a region J[117]. So for the anisotropic scattering and for strong absorption, Dg should be determined from the following equation[16].

$$\frac{\Sigma_s}{2}\left(\frac{D}{\Sigma_a}\right)^{\frac{1}{2}} \cdot \ln \frac{\left|\Sigma_t + \left(\frac{\Sigma_a}{D}\right)^{\frac{1}{2}}\right|}{\left|\Sigma_t - \left(\frac{\Sigma_a}{D}\right)^{\frac{1}{2}}\right|} = \frac{1+3D\Sigma_s\bar{\mu}}{1+3D\Sigma_t\bar{\mu}} \qquad \ldots\ldots\ldots\ 6\text{-}39$$

where

Σ_t, Σ_s, Σ_a - are the macroscopic total, scattering and absorption cross-section respectively.

$\bar{\mu}$ - the average value of the cosine of the scattering angle in the lab. system.

6-7-3 Group Cross-Section

The transfer neutron from gth group to the (g+i) group (i=1,2,3 ..) as a result of elastic or inelastic scatter can be described by the group transfer cross-section which is given by:

$$\Sigma_{g\to g+i} = \Sigma_{s_{g\to g+i}} + \Sigma_{in_{g\to g+i}} \qquad \ldots\ldots\ldots 6\text{-}40$$

The average elastic scattering cross-section for the gth group is defined by:

$$\Sigma_{sg} = \frac{1}{\Phi_g} \int_{Ug-1}^{Ug} \Sigma_s (U)\, \Phi (U)\, dU \qquad \ldots\ldots\ldots 6\text{-}41$$

Σ_s - is constant in the group, and

Σ_{sg} - is the actual macroscopic scattering cross-section at any lethargy within the group

The neutron transfer by scattering from one group to another described by $\Sigma_{g\to g+i}$, these are defined so that $\Sigma_{g\to g+i}.\Phi_g(r)$ is equal to the number of neutrons which are transferred from the gth group to the (g+i) group per cm^3 sec^{-1} at the point r.

The value of the elastic scattering cross-section depends on both the nuclear properties of the materials in the system, and the number and width of groups used in the calculation. If the maximum increase in lethargy of a neutron undergoing an elastic collision is less than the width of energy group, the neutron can only be elastically scattered into the adjacent group, and the groups are said to be directly coupled. The constant $\Sigma_{sg\to g+1}$, can be computed from 6-40 assuming that $\Sigma_{sg}.\Phi_g$ is the total number of scattering collision per $cm^3.sec^{-1}$ in the gth group.

If $\bar{\xi}_g$ is the average lethargy increase in an elastic collision in the gth group, the neutrons require $Ug/\bar{\xi}_g$ collisions on the average in order to traverse that group. If there are $\Sigma_{sg}.\Phi_g$ collision cm^{-3} sec^{-1} in the gth group therefore the number of neutrons scattered out of that group will be equal to $\bar{\xi}\Sigma_{sg}.\Phi_g/U_g$ cm^{-3} sec^{-1}. Since these neutrons must enter the (g+1) th group in the directly coupled case the cross-section is given by

$$\Sigma_{sg\rightarrow g+1} = \frac{\bar{\xi}_g \Sigma_{sg}}{U_g} \qquad \ldots\ldots\ldots \text{6-42}$$

The group transfer cross-section for inelastic scattering is straightforward. Consider the lethargy interval dU' in the (g+1) th group. Since neutrons can be scattered into dU' as the result of collisions at any lethargy in the gth group, the number arriving per cm^{-3} sec^{-1} in du' from this group is the number

$$\text{scattered into dU} = dU' \int_{Ug-1}^{Ug} \Sigma_s\,(U)\ \Phi\ (U)\ p(U\rightarrow U')\ dU.$$

It follows that the total number of neutrons transferred from the gth group to the (g+1) th group is

$$= \int_{Ug}^{Ug+1} \int_{Ug-1}^{Ug} \Sigma_s(U)\ \Phi\ (U)\ p(U\rightarrow U')\ dU\ dU'$$

and this number is equal to $\Sigma_{in_{g\rightarrow g+1}}.\Phi$, so

$$\Sigma_{in\ g\rightarrow n} = \frac{1}{\Phi_g} \int_{Ug}^{Ug+1} \left[\Sigma_s\ (U)\ \Phi\ (U) \int_{U_n}^{U_{n+1}} P(U\rightarrow U')\ dU \right] dU$$

$\ldots\ldots\ldots$ 6-43

where

$P(U \rightarrow U')$ - the probability distribution fraction for inelastic scattered neutrons

The source of the cross-section data, and the inelastic scattering probability for the multigroup calculation was the Yiftah Sieger et al[2] and the UKNDL file[3] which covered 11 groups of neutron energy ranging from 0.3 MeV up to 14.1 MeV.

For the (n,2n) and (n,3n) reactions in the uranium the group constants were calculated from UKNDL and added to the upper energy group of the Yiftah Sieger et al[2], since these were originally absent.

For the ^{6}Li, ^{7}Li and ^{19}F the group constants derived from the UKNDL[3] on the assumption that the neutron lethargy flux is constant ($\Phi(E) \propto \frac{1}{E}$) because the form of the flux is not known. Since the lethargy intervals are small (≤ 0.5) the constant is not very sensitive to the flux form used.

A computer program DATA was written for the macroscopic data preparation (Appendix 3), and two computer programmes were used in the present work based on the method explained in Appendix 2, one for one material region (Appendix 4), and the other for two regions (Appendix 5).

6-7-4 Fission

If fissile materials are present in the system it becomes necessary to define the average fission cross-section for each group as in 6-35.

The prompt fission neutrons are emitted with a continuous energy spectrum, and so

$$\chi_g = \int_{U_{g-1}}^{U_g} \chi(U)\, dU \qquad \ldots\ldots\ldots 6\text{-}44$$

$\chi(U)$ - is the fission spectrum normalized to one emitted neutron

The average number of neutrons emitted for fission depends upon the energy of the incident neutron, and for fission induced by neutrons of the gth group is given by:

$$\upsilon_g = \frac{1}{\Phi g} \int_{U_{g-1}}^{U_g} \upsilon(U)\, \Phi(U)\, dU \qquad \ldots\ldots\ldots 6\text{-}45$$

CHAPTER 7

EXPERIMENTAL AND CALCULATED RESULTS

7-1 Introduction

Fast neutron spectra have been measured at different radii from the 14.1 neutron source situated at the centre of the shield, which was constructed of LiF and uranium. An NE-213 scintillation counter using P.S.D. to reject the gamma ray background was used for the measurements.

ALL the measurements and calculated results were normalized to a neutron source strength of 1×10^9 neutron per second for comparison purposes.

In addition to 14 MeV source strength, degraded neutrons from the target assembly and from the D-D reaction were considered and fed into the spectrum calculation for each energy group[118], using experimentally obtained values. The spontaneous fission neutron source was also included when uranium shielding material was used.

The removal cross-section for the first energy group (14.0 - 14.1) MeV, for LiF, Uranium, a mixture of LiF and Uranium, and a two region system (inner region LiF and the outer uranium) have been determined experimentally and compared with the values used in the removal calculation.

7-2 Fast Neutron Spectra in a LiF Shielding Material

The neutron spectra were measured for neutron energies between 1.35 and 14.1 MeV inside a LiF shield at distances of 9.3, 12.4, 17.8, 18.6, 21.7 and 24.8 cm from the point source in the centre.

The measured and calculated spectra are plotted as neutron flux MeV^{-1} versus neutron energy in MeV and are shown in Figure [7-1 to 7-6].

The figures show that the neutron spectral shape does not change very much with shield thickness. It is seen that there is generally good agreement between the measured spectra and those calculated by the removal diffusion method above the (2.225 - 3.0) MeV neutron energy group, and as the shielding thickness increases there is some difference at the neutron energy group (10 - 12) MeV.

For the first energy group (14.0 - 14.1) MeV, there is good agreement between measured and calculated total neutron flux compared at different thickness inside the shielding material. The comparison was made by finding the area under the calculated first energy group and also the area of the rather broad measured peaks centred on 14.1 MeV.

Table [7-1] represents the total calculated and measured flux for the (14.0 - 14.1) MeV energy group at different thicknesses inside the LiF shielding assembly.

Table [7-1] The Total Flux for the First Energy Group at Different thicknesses inside the LiF Shielding

Thickness in cm	Total neutron flux (n cm^{-2} sec^{-1}) for a source strength of 1 x 10^9 n sec^{-1}.	
	Calculated	Measured
9.3	8.314 x 10^5	7.76 x 10^5
12.4	3.83 x 10^5	3.58 x 10^5
17.8	1.308 x 10^5	1.2886 x 10^5
18.6	1.148 x 10^5	1.1063 x 10^5
21.7	6.879 x 10^4	7.1516 x 10^4
24.8	4.315 x 10^4	4.466 x 10^4

The difference between the measured and calculated spectra may be due to the difference in the experimental and theoretical geometries (cylindrical and spherical respectively), the use of diffusion theory and the uncertainties in the group constants. This comment applies to all the systems investigated.

7-3 Fast Neutron Spectra in Uranium Shielding Materials

Figure [7-7 to 7-16] shows the measured and calculated neutron spectra inside uranium shielding material of thicknesses of 9.3, 10.1, 12.4, 15.5, 17.8, 18.6, 20.2, 21.7, 24.8 and 27.9 cm, from the central source.

The form of the spectrum for neutron energies below 6 MeV does not change as the thickness of the shielding increases. From the figures it can be seen that in that energy region the number of neutrons is higher compared with that measured in a LiF shield. This is because for the lighter element elastic slowing down is important, whereas for heavy elements such as uranium the slowing down of the neutron by inelastic scattering is the main interaction which produces directly more low energy neutrons.

As shown in the figures the calculated and measured spectra at all the measured points are in reasonable agreement.

For the first group there is a good agreement between the calculated and measured total neutron flux at a different thickness inside the shielding material as shown in Table [4-2].

Table [7-2] The Total Flux for the First Energy Group at Different Thicknesses inside the U^{238} Shielding

Thickness in cm	Total neutron flux (n cm^{-2} sec^{-1}) for a source strength of 1 x 10^9 n sec^{-1}	
	Calculated	Measured
9.3	7.693×10^5	7.29×10^5
10.1	5.999×10^5	5.63×10^5
12.4	3.036×10^5	3.45×10^5
15.5	1.363×10^5	1.91×10^5
17.8	7.901×10^4	7.42×10^4
18.6	6.64×10^4	6.94×10^4
20.2	4.739×10^4	5.66×10^4
21.7	3.423×10^4	3.35×10^4
24.8	1.838×10^4	1.95×10^4
27.9	1.019×10^4	1.04×10^4

7-4 Fast Neutron Spectra in a Mixture of a LiF and U^{238}

The shielding was built up from 88 LiF tubes and 88 uranium tubes (1:1 in volume). The spectra for the fast neutron inside the shielding were measured at radii of 9.3, 10.1, 12.4, 15.5, 17.8, 18.6, 20.2, 21.7, 24.8 and 27.9 cm from centre of the shielding assembly, and with the calculated spectra are represented in Figures [7-17 - 7-26].

From the figures it can be seen that the general shape of the spectrum does not change with thickness and there is an agreement between the measured and calculated spectra for all the energy group

down to 2.225 MeV. Below this there is a difference as in the previous measurements because the P.S.D. system fails to fully distinguish between gamma ray and neutron pulses, which move into the gamma ray region at lower energies.

For the first energy group there is a good agreement between the calculated and measured spectrum as shown in Table [7-3].

Table [7-3] The Total Neutron Flux for the First Energy Group at a Different thicknesses inside a Mixture of LiF and U^{238} Shielding

Thickness in cm	Total neutron flux (n cm^{-2} sec^{-1}) for a source strength of 1 x 10^9 n sec^{-1}	
	Calculated	Measured
9.3	7.998×10^5	7.87×10^5
10.1	6.359×10^5	5.94×10^5
12.4	3.411×10^5	3.240×10^5
15.5	1.655×10^5	1.81×10^5
17.8	1.014×10^5	1.03×10^5
18.6	8.712×10^4	8.86×10^4
20.2	6.463×10^4	6.44×10^4
21.7	4.852×10^4	5.03×10^4
24.8	2.816×10^4	2.98×10^4
27.9	1.687×10^4	1.73×10^4

7-5 Fast Neutron Spectra in a Two Region of LiF and U^{238} Shielding Material

A two region of the shielding built from LiF inner region 72 tubes in a three inner layer and 150 U^{238} tubes the outer region four layer

(1:2 in volume).

The measurements were carried out at radii of 9.3, 10.1, 12.4, 15.5, 17.8, 18.6, 20.2, 21.7, 24.8 and 27.9 cm inside the shielding. The measured and calculated spectra represented in Figure [7-27 - 7-36], shows reasonable agreement between the measured and calculated spectra, the slope and the shape of the spectra does not change with the increase of the shielding thickness.

For the first energy group there is a good agreement between the measured and calculated spectra and the total neutron flux at different thickness inside the shielding assemblies represented in Table [7-4].

Table [7-4] The Total Neutron Flux for the First Energy Group at a Different Thicknesses inside a two layer of LiF and U^{238} Shielding

Thickness in cm	Total neutron flux (n cm^{-2} sec^{-1}) for a source strength of 1 x 10^9 n sec^{-1}	
	Calculated	Measured
9.3	8.314 x 10^5	7.9 x 10^5
10.1	6.74 x 10^5	6.57 x 10^5
12.4	3.83 x 10^5	3.44 x 10^5
15.5	2.009 x 10^5	1.94 x 10^5
17.8	1.258 x 10^5	1.21 x 10^5
18.6	1.058 x 10^5	1.09 x 10^5
20.2	7.548 x 10^4	7.37 x 10^4
21.7	5.45 x 10^4	5.46 x 10^4
24.8	2.928 x 10^4	2.88 x 10^4
27.9	1.623 x 10^4	1.48 x 10^4

In the inner region the spectrum is very close to that measured and calculated in the LiF shielding assembly which in the outer region is more like that measured and calculated in the uranium shielding material.

7-6 The Removal Cross-Section Calculation

The removal cross-section is used to determine the number of neutrons which are removed from the first energy group (14.0 - 14.1) MeV by the removal collision, we have that:

$$\Phi\,(r,E_o) = \frac{Q}{4\pi r^2}\ \exp\,[-\,\Sigma_{rem}t] \qquad \ldots\ldots\ldots\ 7\text{-}1$$

The value of the removal cross-section can be determined if the flux values at two or more different radial positions are known. From equation (7-1)

$$\Sigma_{rem}t = \log_e \frac{Q}{4\pi} - \log_e\,(\Phi.r^2)$$

$$t = r - r_o$$

$$\log_e\,(\Phi r^2) = -\,\Sigma_{rem}.r + \Sigma_{rem}.r_o + \log_e\left(\frac{Q}{4\pi}\right) \qquad \ldots\ldots\ldots\ 7\text{-}2$$

From equation (7-2) it is clear that the determination of the removal cross-section does not need the knowledge of the absolute source strength of the neutrons, and so the uncertainty in the absolute efficiency of the detector does not enter in the evaluation of the removal cross-section.

In the calculation and measured result the value of the inner radius which is the distance from the neutron source to the inner layer of the shielding material which is equal to 7.6 cm was added to the shielding material thickness.

Figure [7-37 - 7-40] represent the total flux for the four shielding assemblies at different shielding thickness and shows how for the first energy group (14.0 - 14.1) the neutron flux varies with distance in the shielding.

The values of the measured neutron fluxes inside the shielding materials for the first energy group multiply by R^2, with the value of the shielding thickness (R) was fitted by the method of the least square fit from which the slope gives the removal cross-section. A computer program (Appendix 6) written for that purpose.

Figures [7-41 - 7-44] represent the fitting curves for the measured and compared with that calculated.

The removal cross-section for the different materials is represented in Table [7-5].

Table [7-5] The Removal Cross-Section for the Different Material

	Shielding Material	Removal cross-section cm^{-1}	
		Calculated	Measured
One-region	LiF	0.0640	0.054 ± 0.003
One-region	U^{238}	0.1100	0.1068 ± 0.0042
One-region	Mixture LiF, U^{238}	0.0894	0.0834 ± 0.0027
Two-region	LiF	0.0640	0.0624 ± .0093
	U^{238}	0.1100	0.116 ± .0059

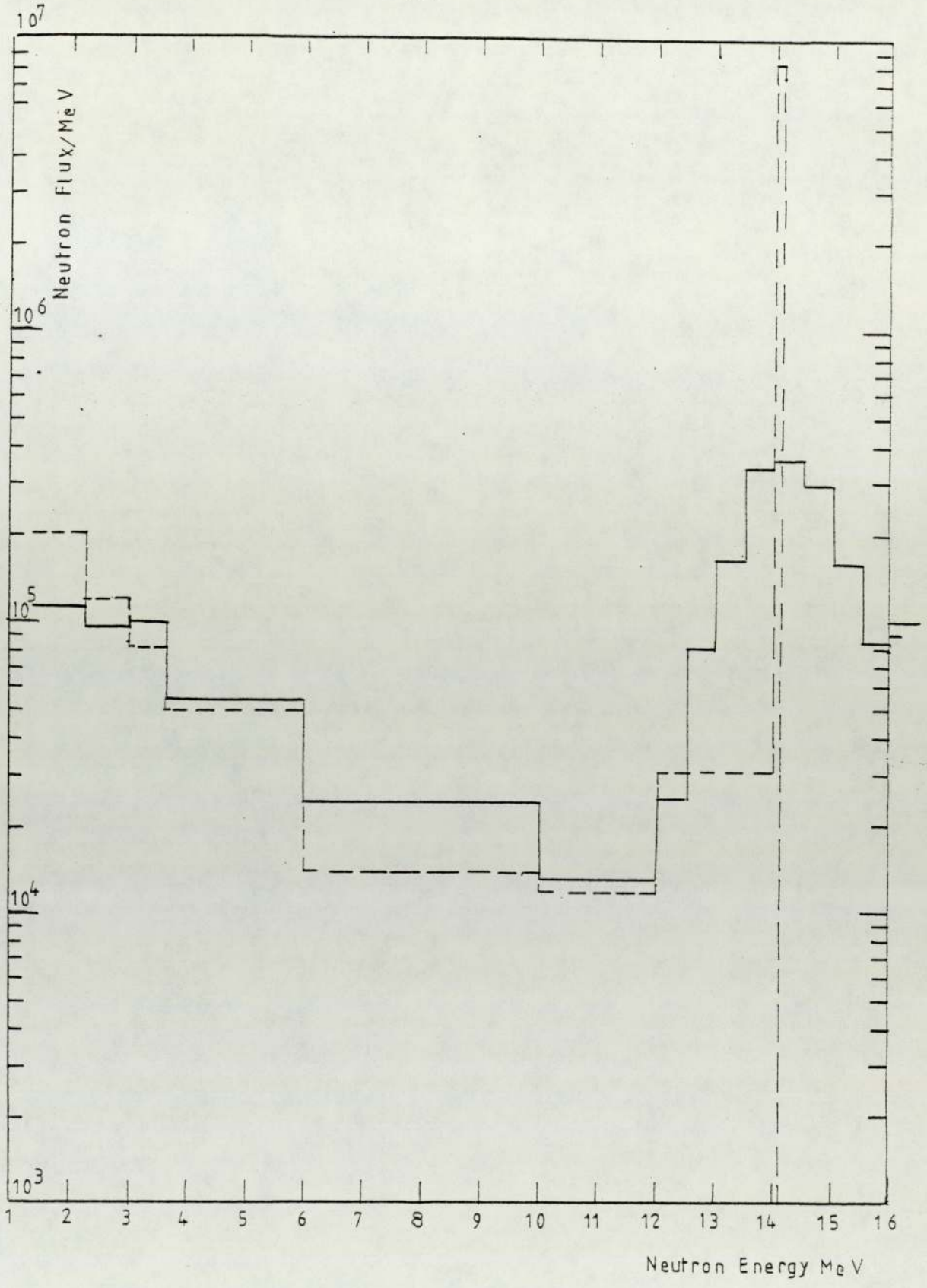

Fig(7-1) Fast Neutron Spectra inside LiF Shielding at 9.3 cm from the Centre.

-------- Calculated

_____ Measured

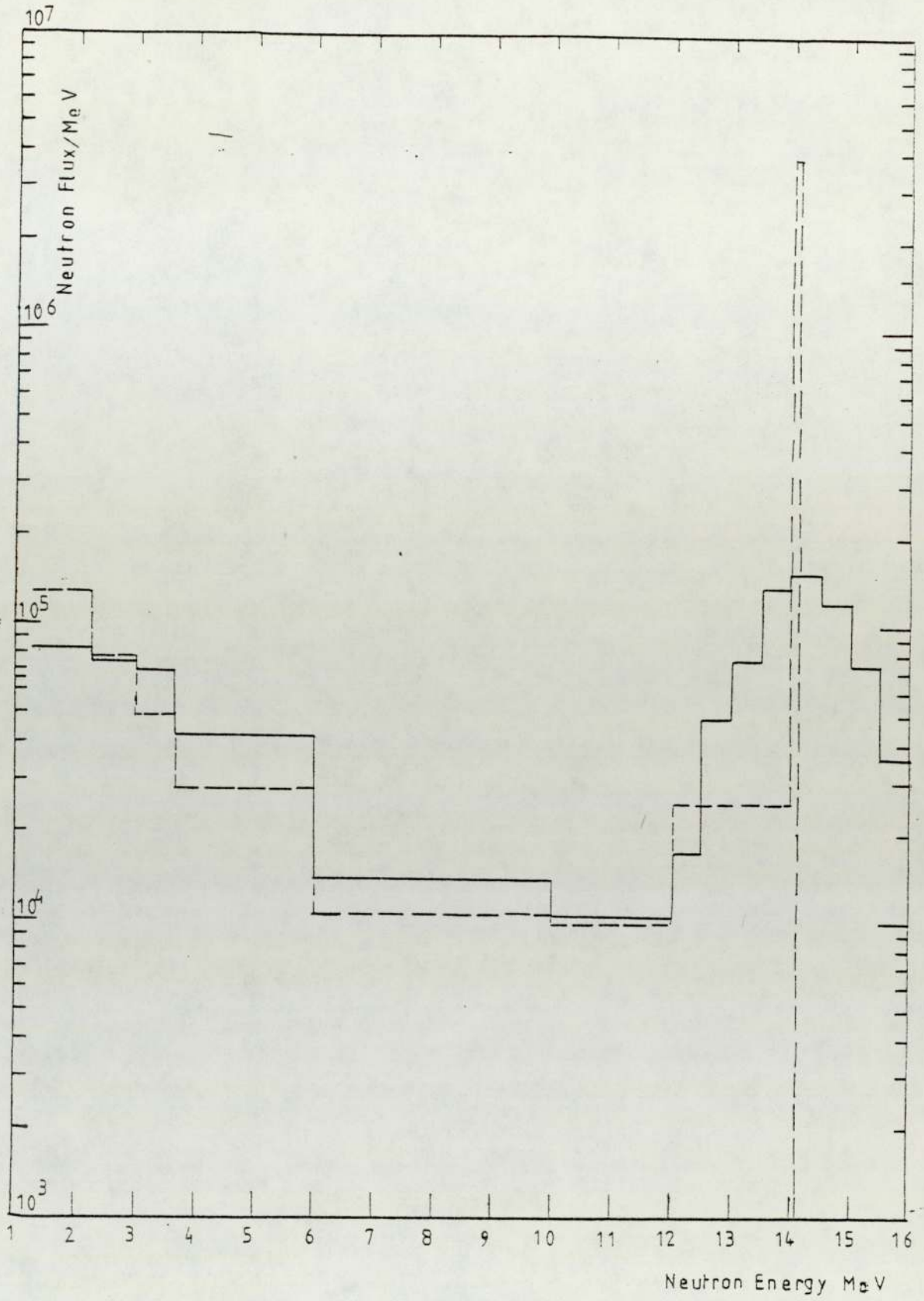

Fig [7-2] Fast Neutron Spectra inside LiF Shielding at 12.4 cm from the Centre.

-------- Calculated

_____ Measured

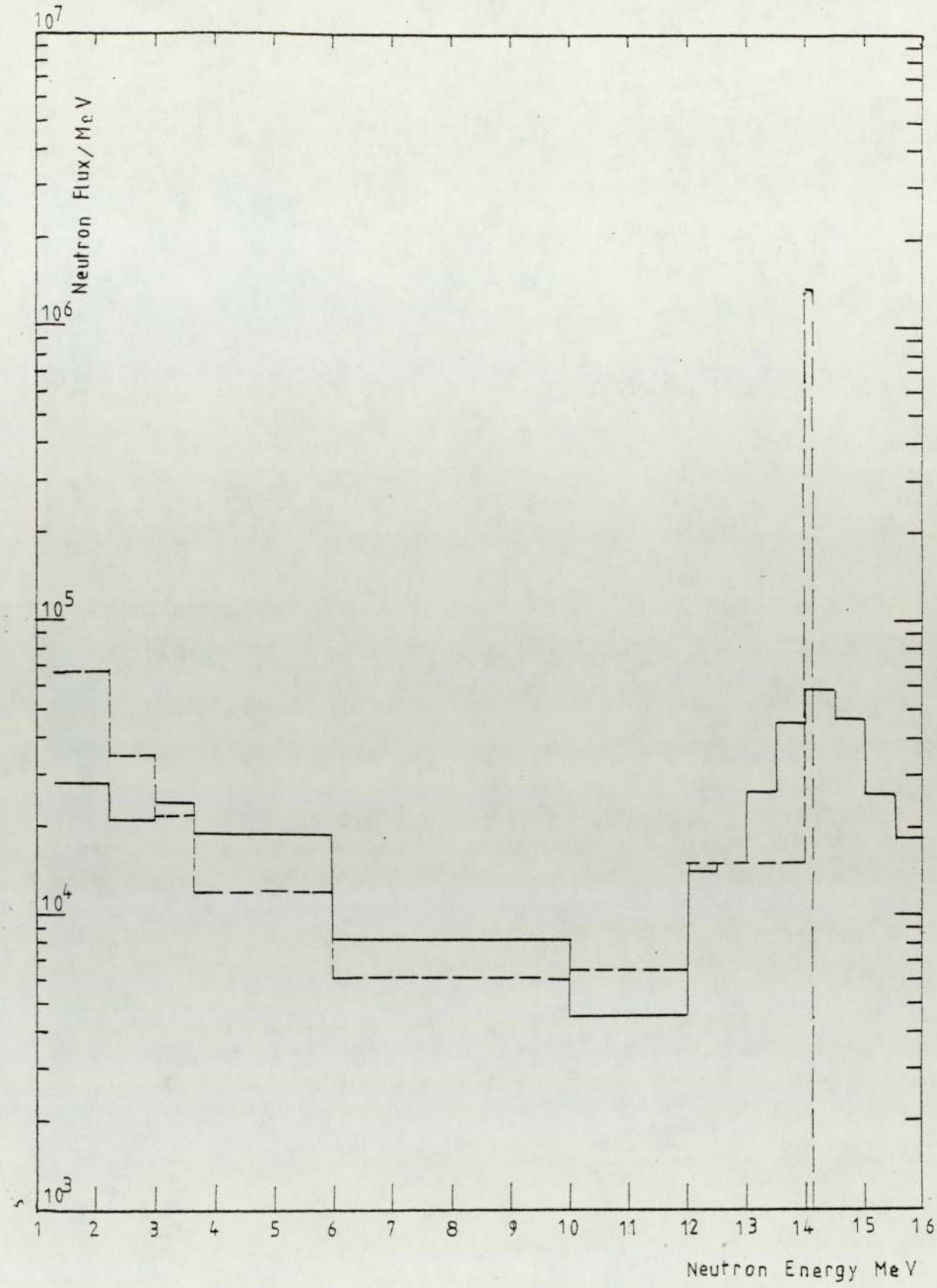

Fig[7-3] Fast Neutron Spectra inside LiF Shielding at 17.8 cm from the Centre.

-------- Calculated

_____ Measured

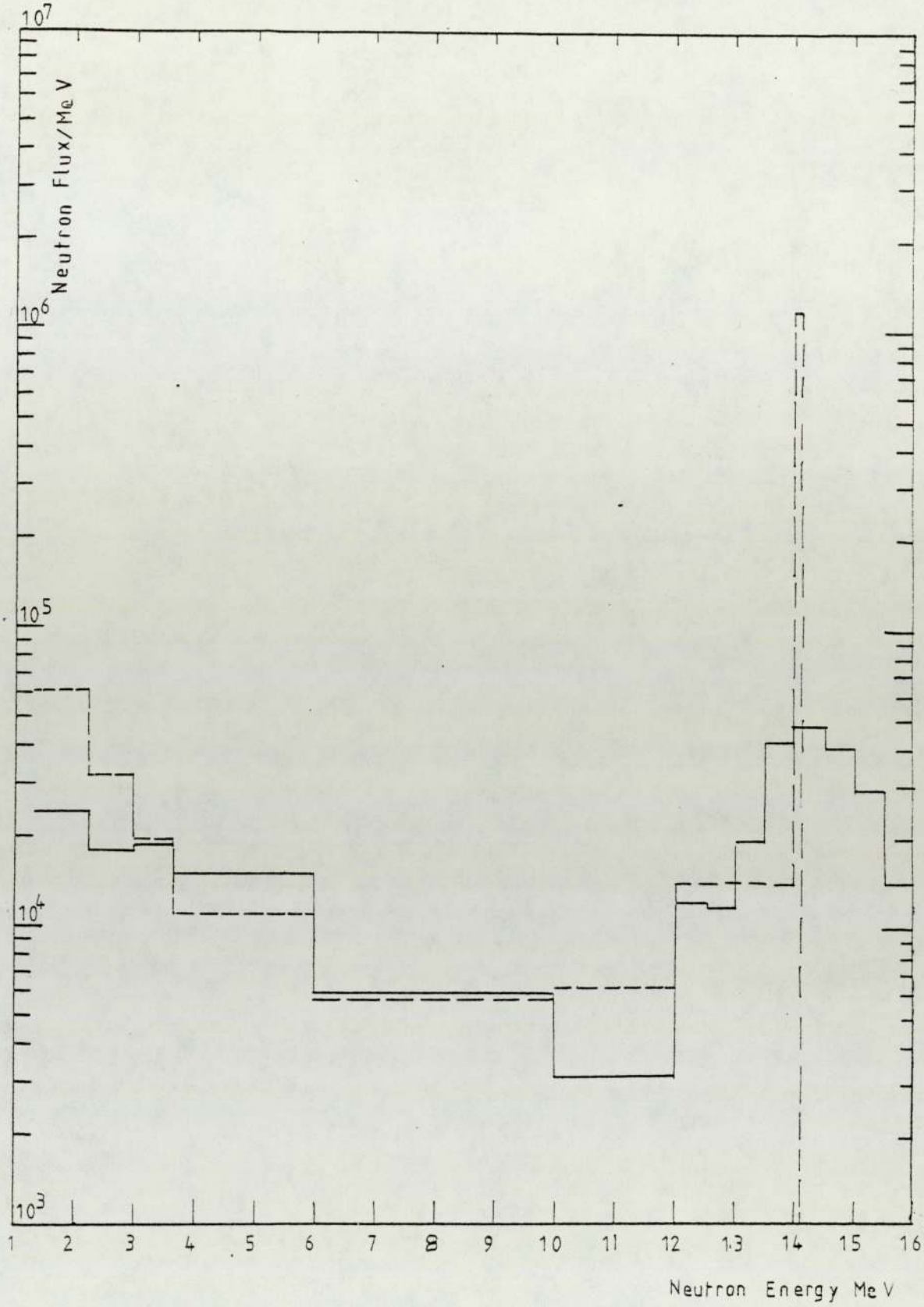

Fig[7-4] Fast Neutron Spectra inside LiF Shielding at 18.6 cm from the Centre.

-------- Calculated

_____ Measured

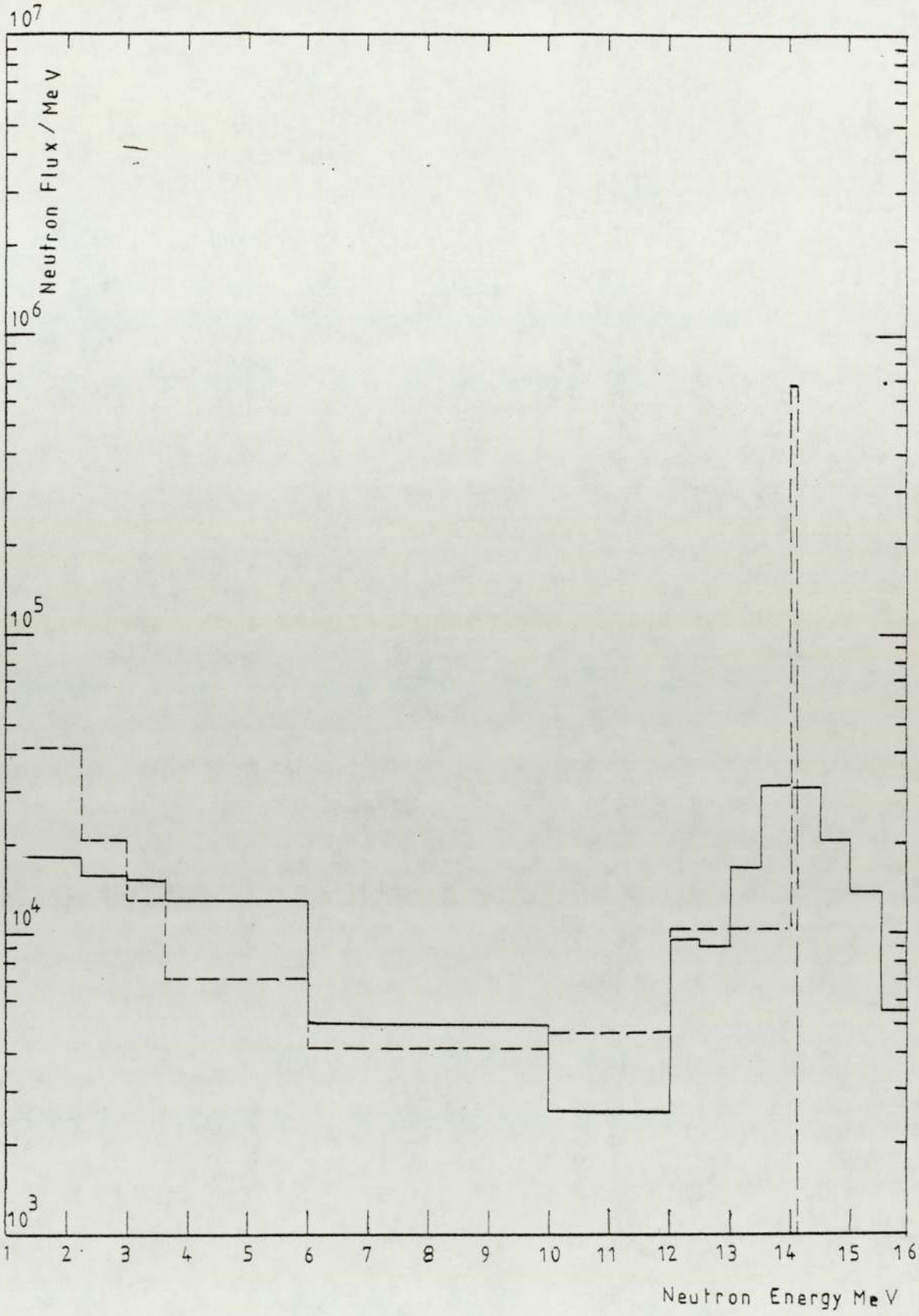

Fig[7-5] Fast Neutron Spectra inside LiF Shielding at 21.7 cm from the Centre.

-------- Calculated

_____ Measured

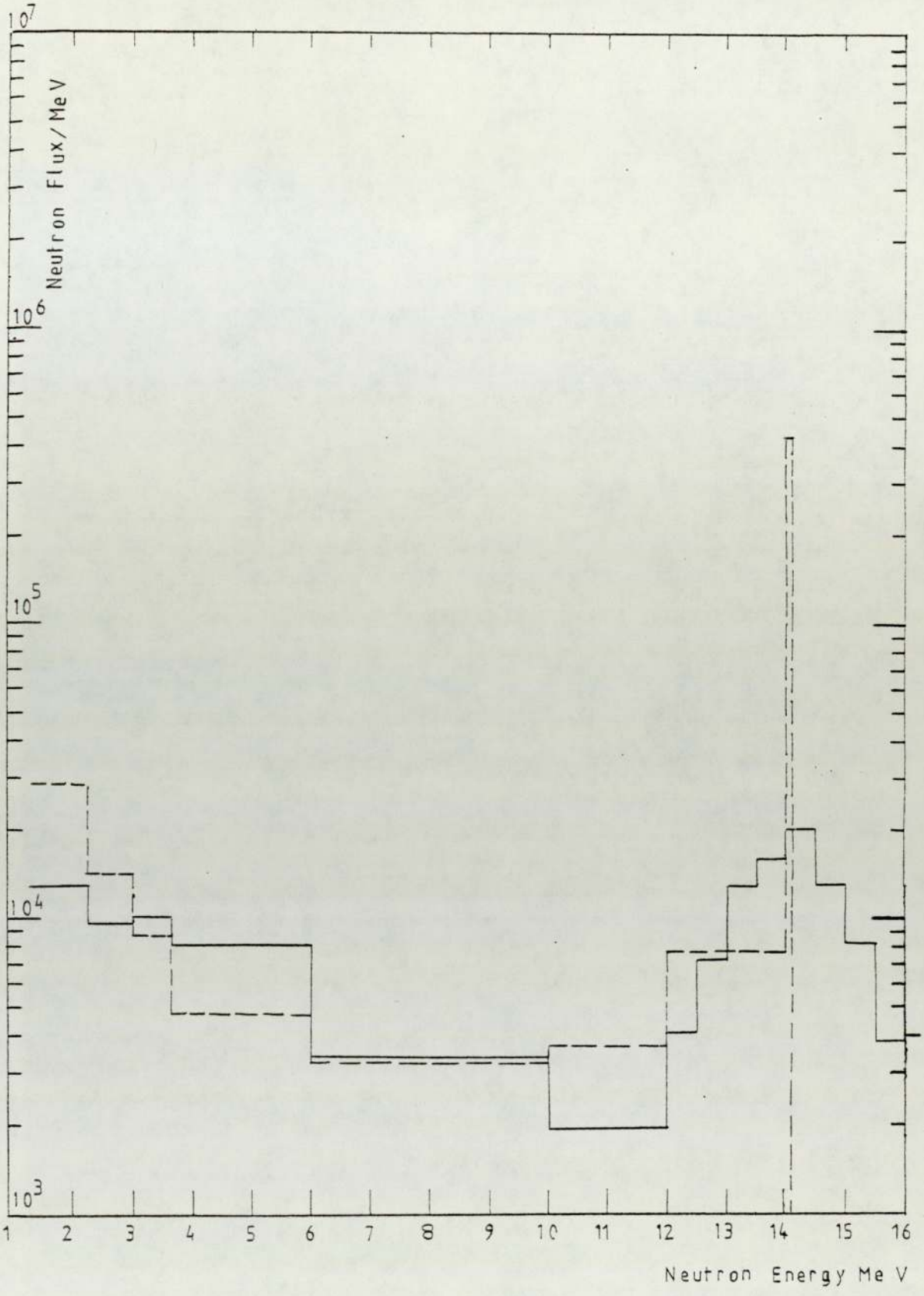

Fig[7-6] Fast Neutron Spectra inside LiF Shielding at 24.8 cm from the Centre.

-------- Calculated

_____ Measured

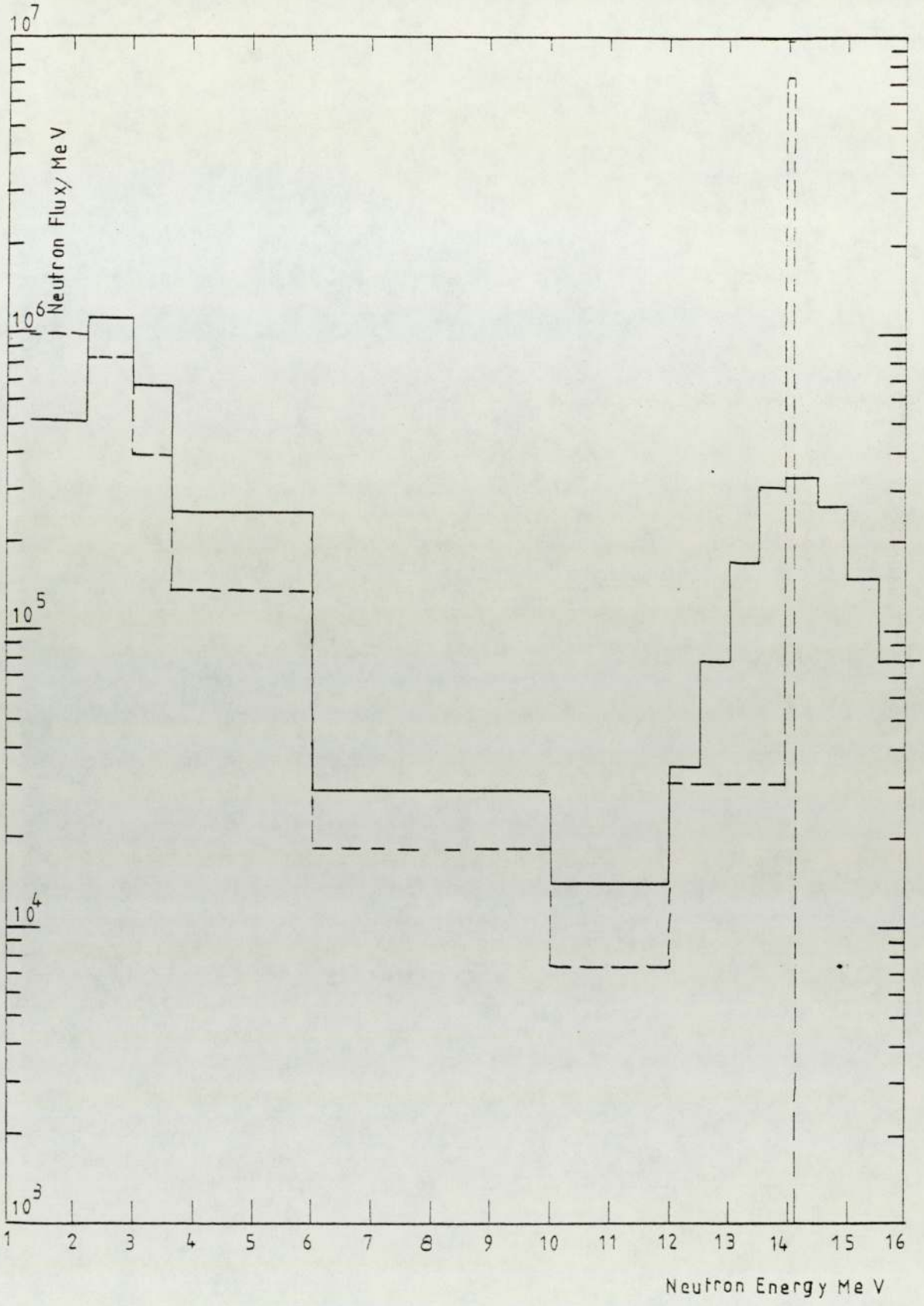

Fig[7-7] Fast Neutron Spectra inside U^{238} Shielding at 9.3 cm from the Centre.

-------- Calculated

_____ Measured

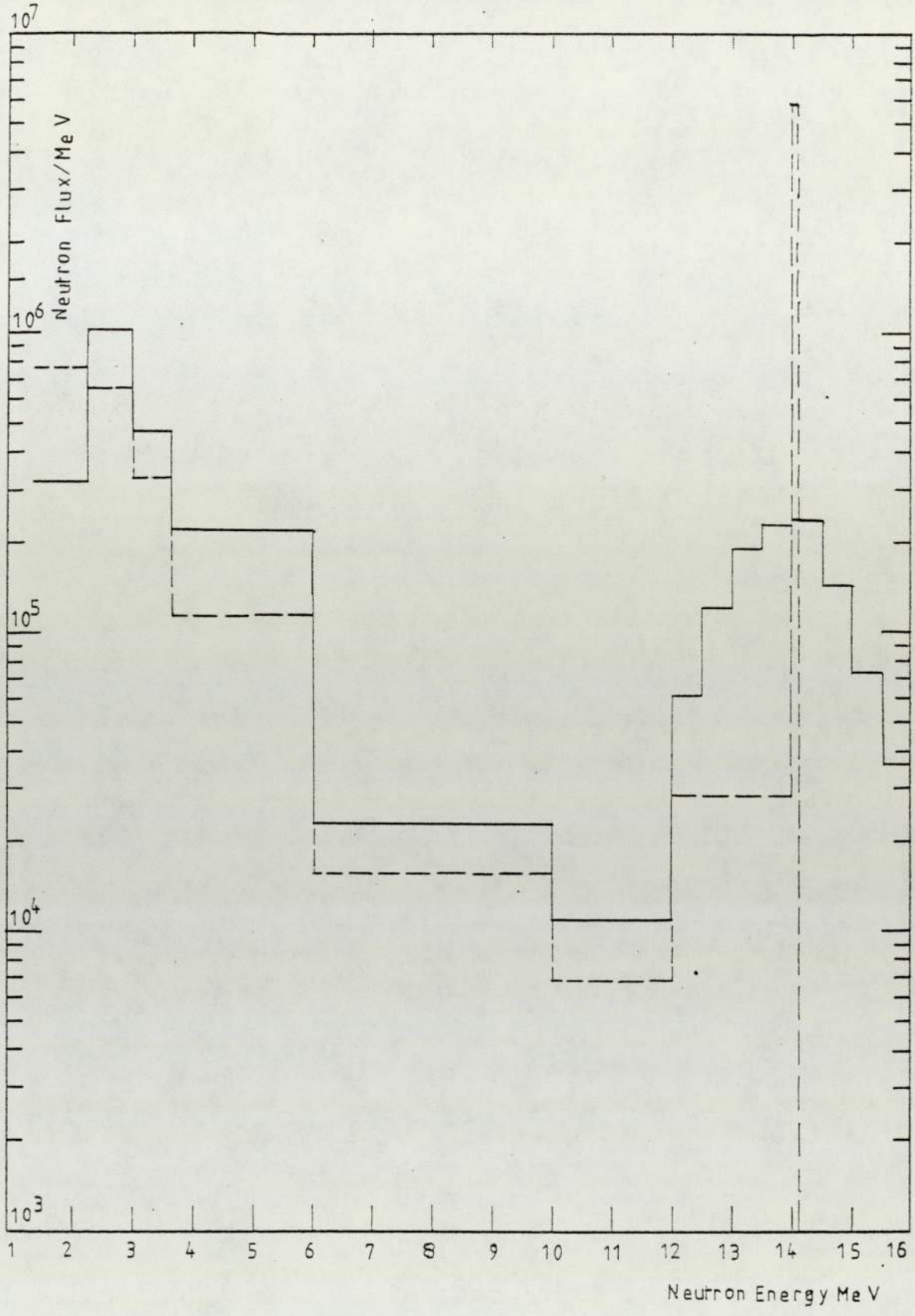

Fig[7-8] Fast Neutron Spectra inside U^{238} Shielding at 10.1 cm from the Centre.

-------- Calculated

_____ Measured

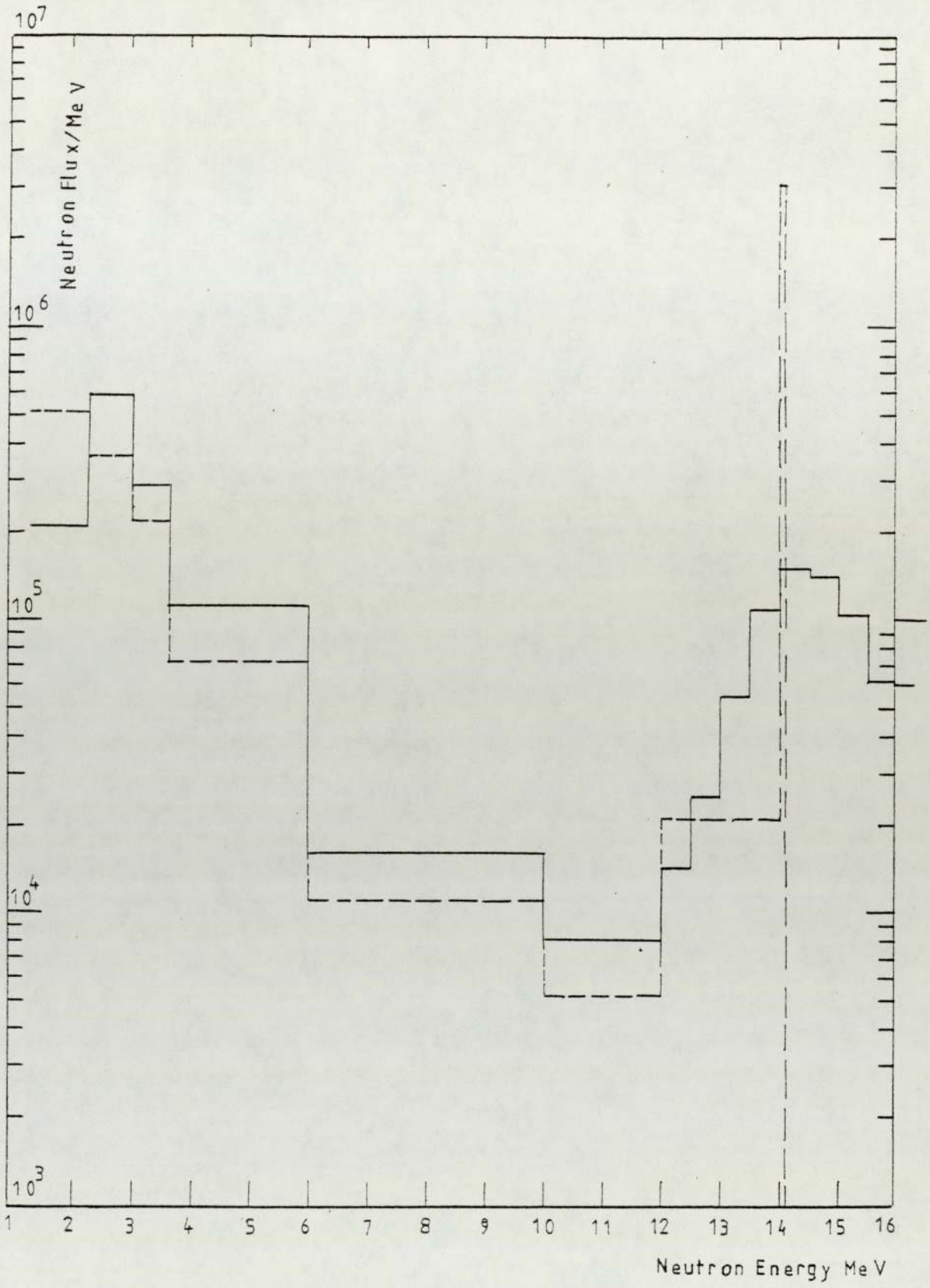

Fig[7-9] Fast Neutron Spectra inside U^{238} Shielding at 12.4 cm from the Centre.

-------- Calculated

_____ Measured

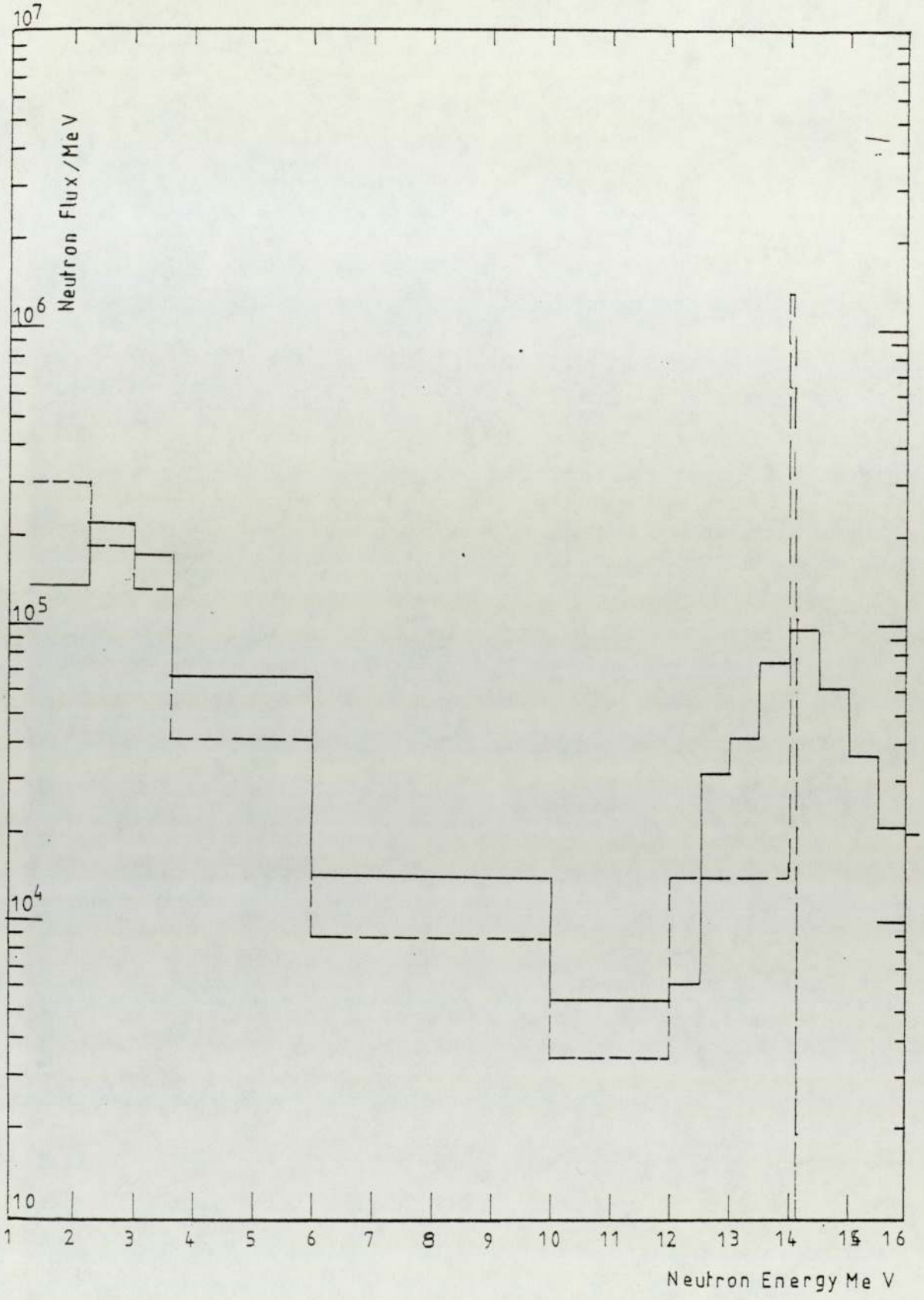

Fig[7-10] Fast Neutron Spectra inside U^{238} Shielding at 15.5 cm from the Centre.

-------- Calculated

_____ Measured

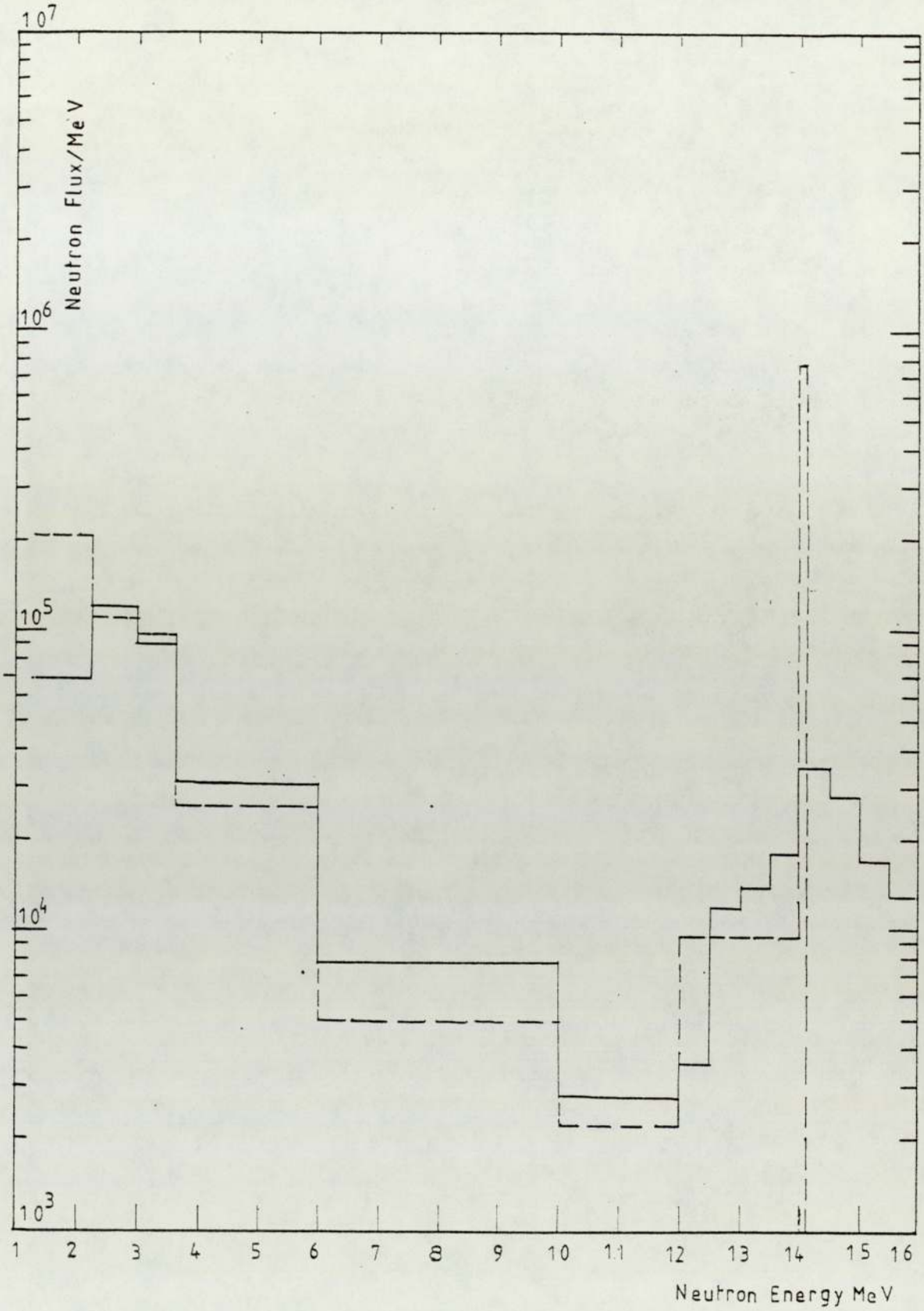

Fig[7-11] Fast Neutron Spectra inside U^{238} Shielding at 17.8 cm from the Centre.

-------- Calculated

_____ Measured

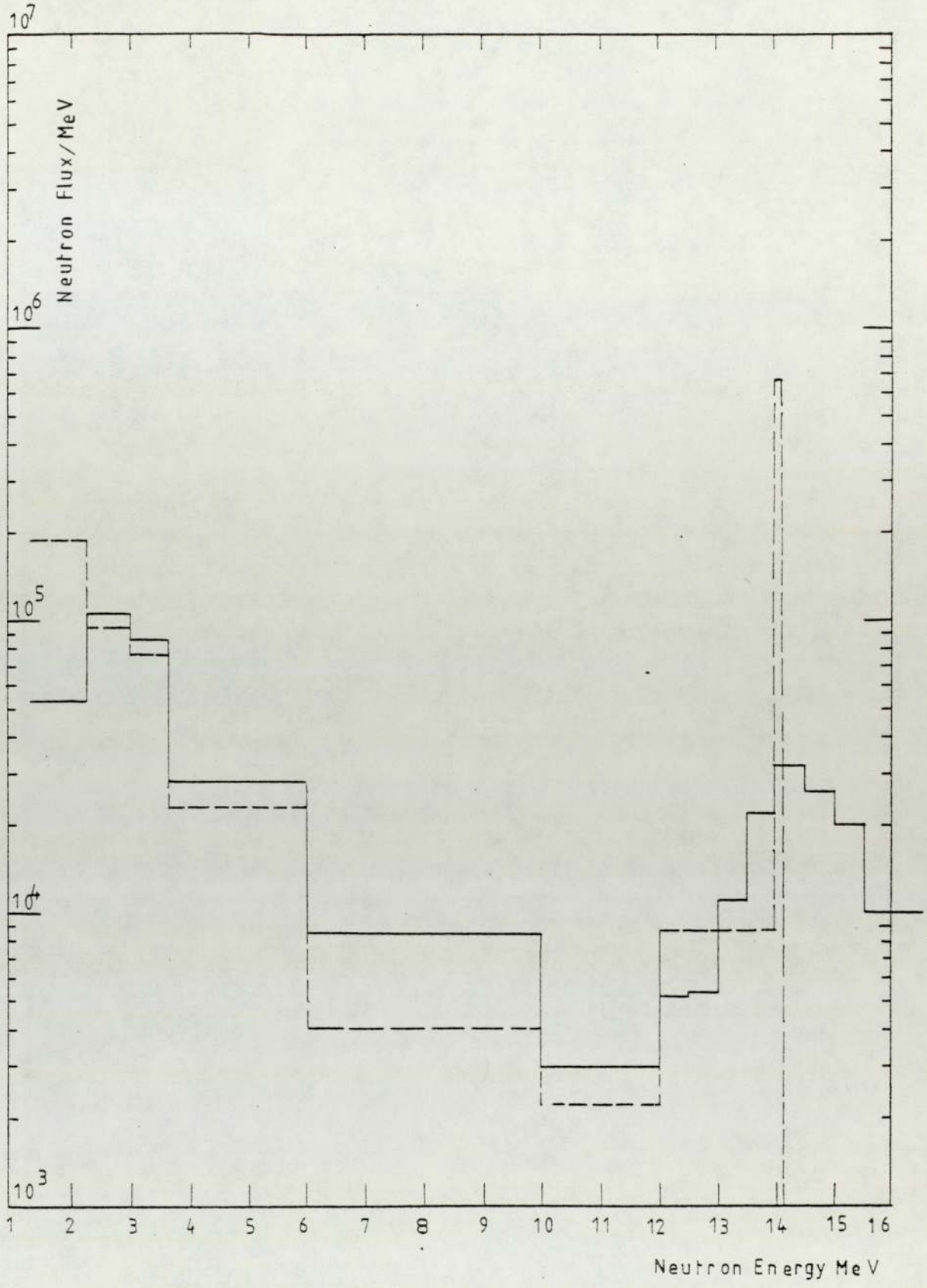

Fig[7-12] Fast Neutron Spectra inside U^{238} Shielding at 18.6 cm from the Centre.

-------- Calculated

_____ Measured

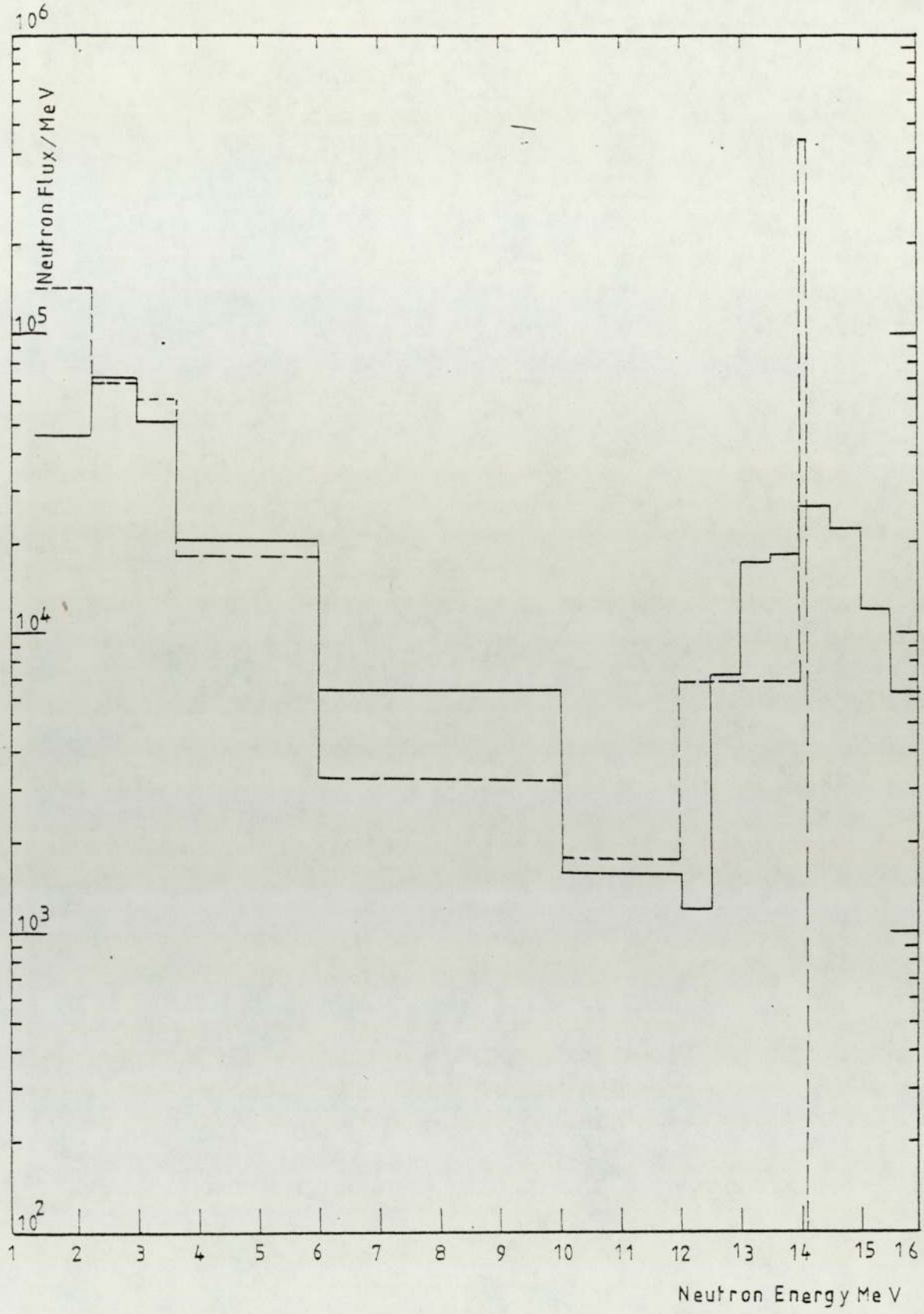

Fig.[7-13] Fast Neutron Spectra inside a U^{238} Shielding at 20.2 cm from the Centre.

-------- Calculated

_____ Measured

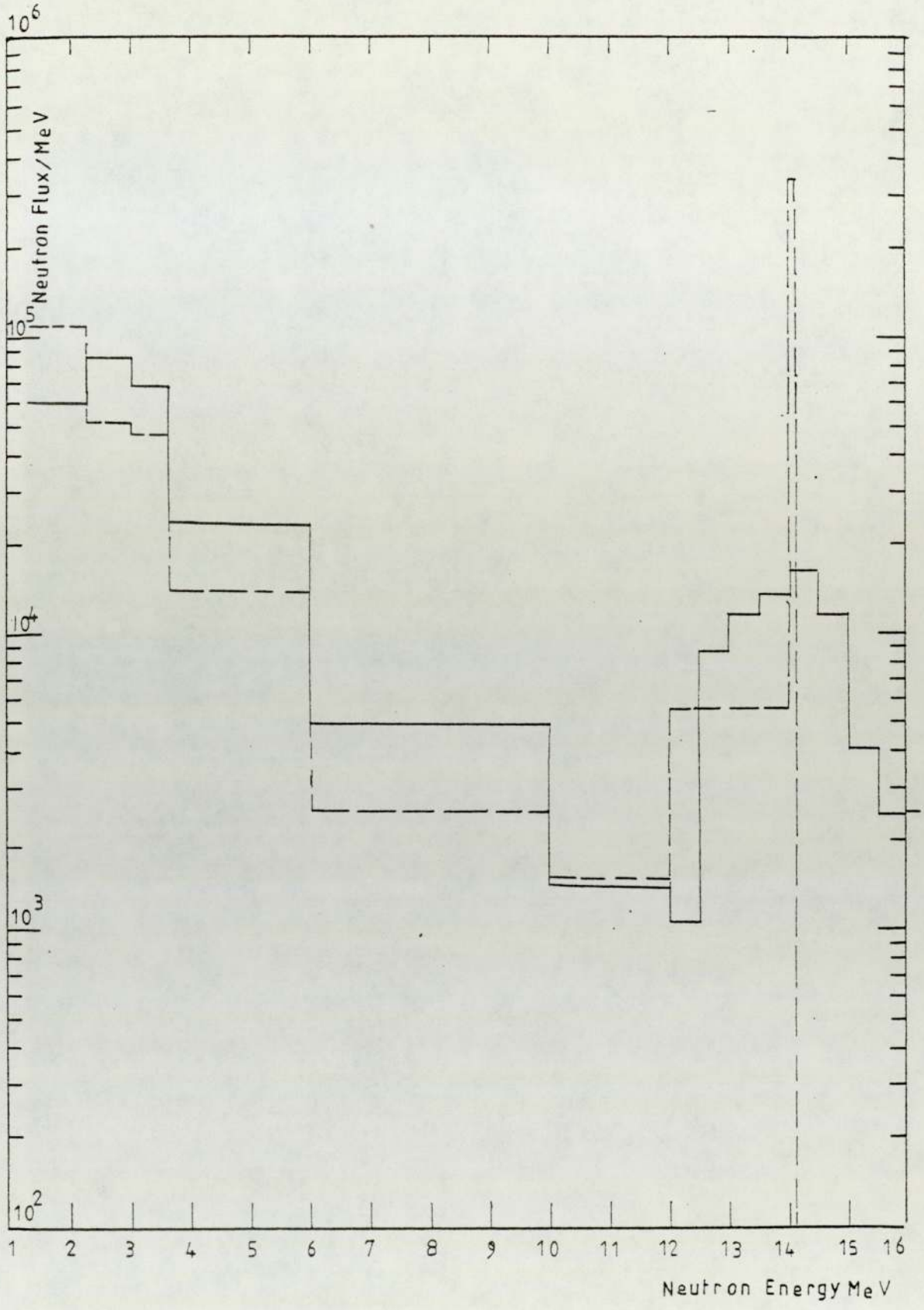

Fig[7-14] Fast Neutron Spectra inside U^{238} Shielding at 21.7 cm from the Centre.

-------- Calculated

_____ Measured

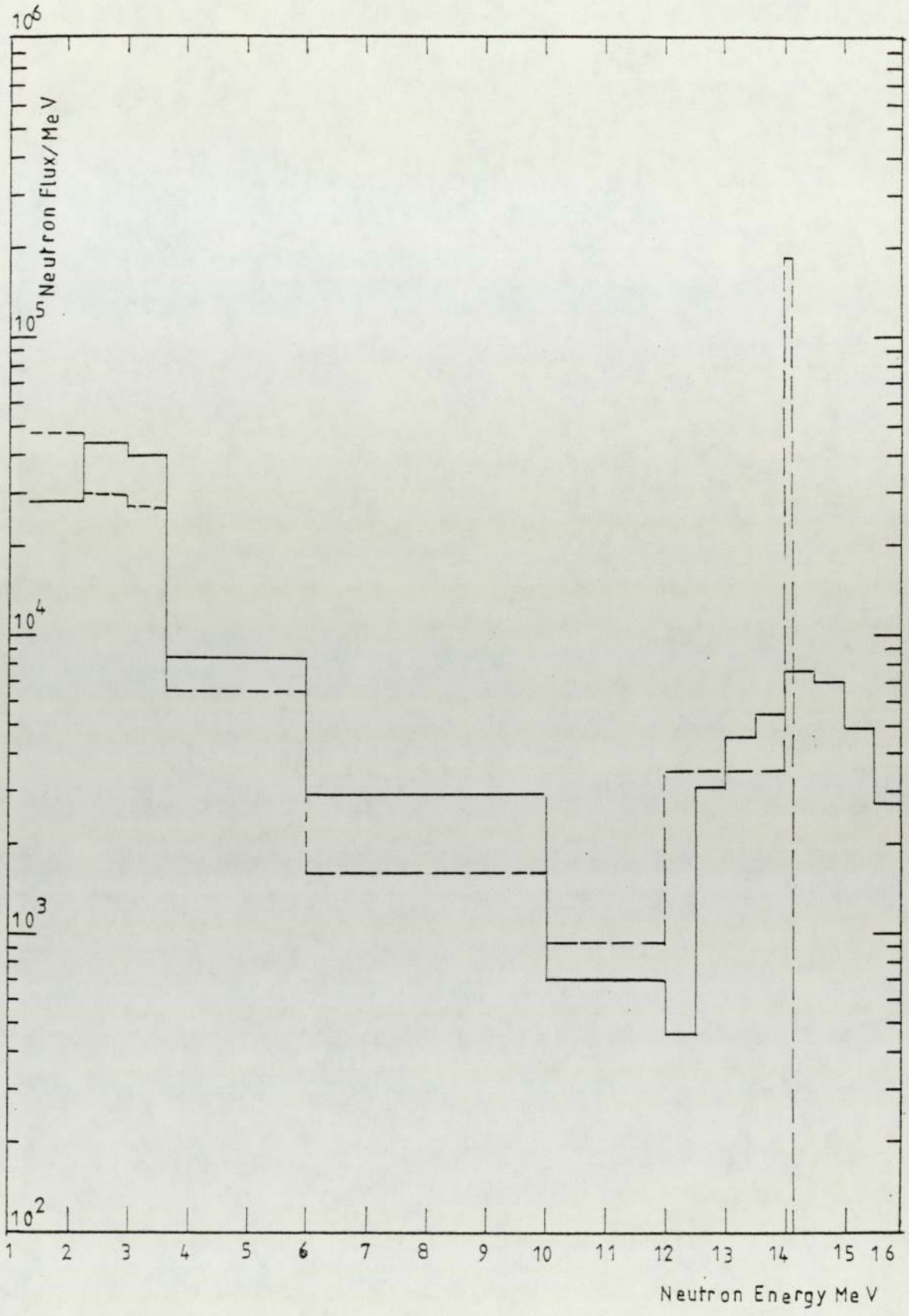

Fig[7-15] Fast Neutron Spectra inside a U^{238} Shielding at 24.8 cm from the Centre.

-------- Calculated

_____ Measured

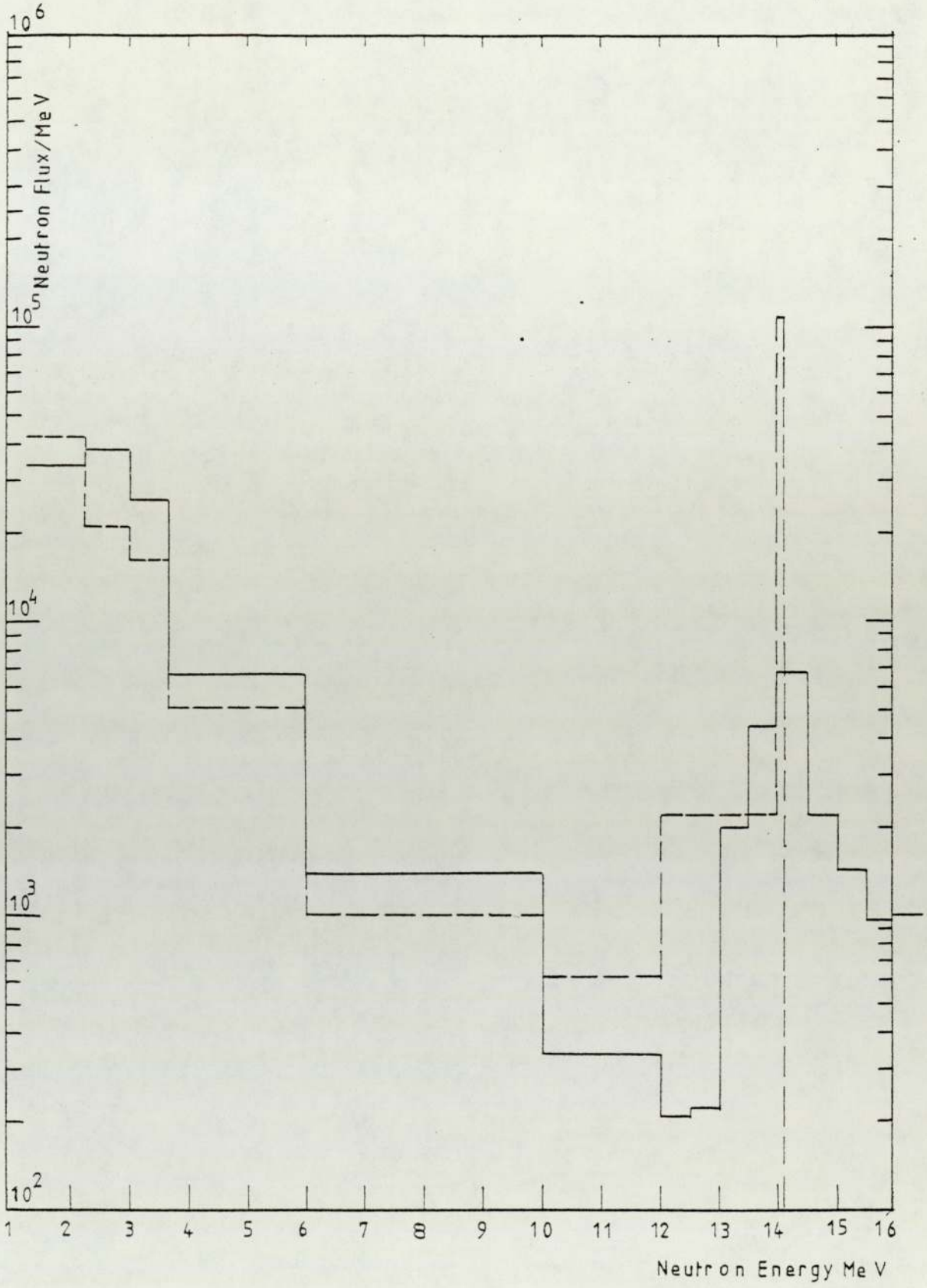

Fig[7-16] Fast Neutron Spectra inside a U^{238} Shielding at 27.9 cm from the Centre.

-------- Calculated

_____ Measured

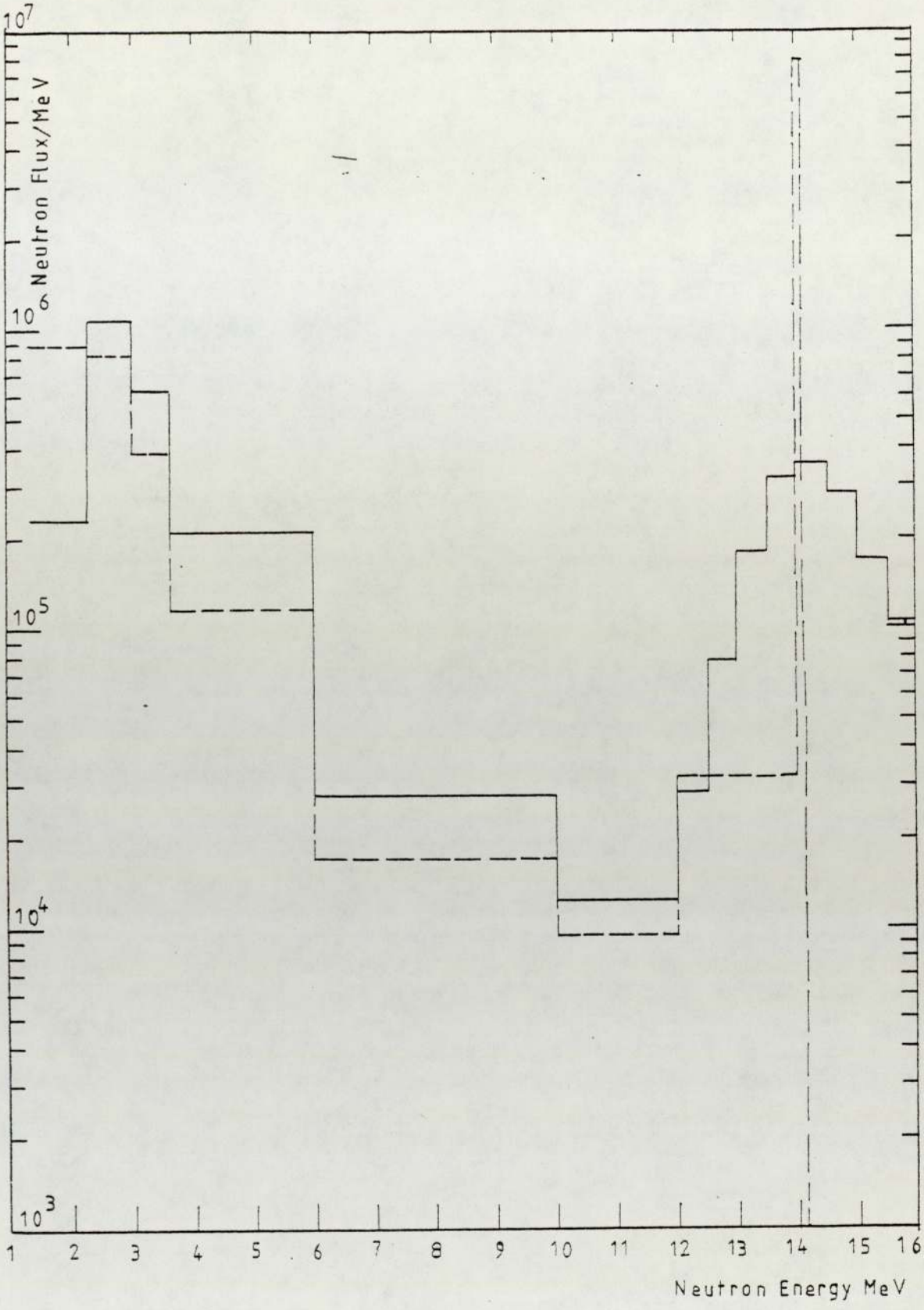

Fig[7-17] Fast Neutron Spectra inside a Mixture Shielding of LiF and U^{238} at 9.3 cm from the Centre.

-------- Calculated

_____ Measured

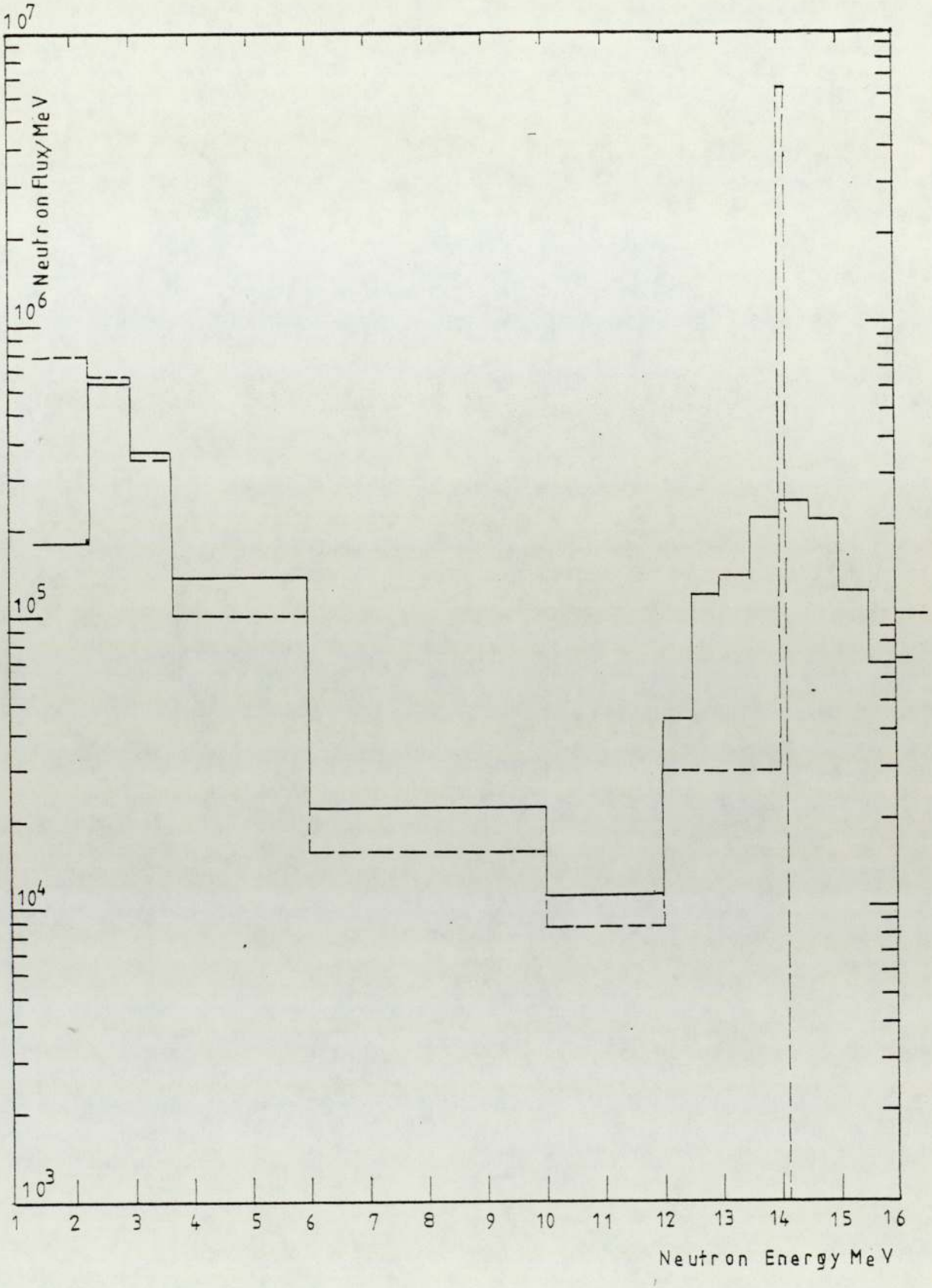

Fig[7-18] Fast Neutron Spectra inside a Mixture Shielding of LiF and U^{238} at 10.1 cm from the Centre.

-------- Calculated

_____ Measured

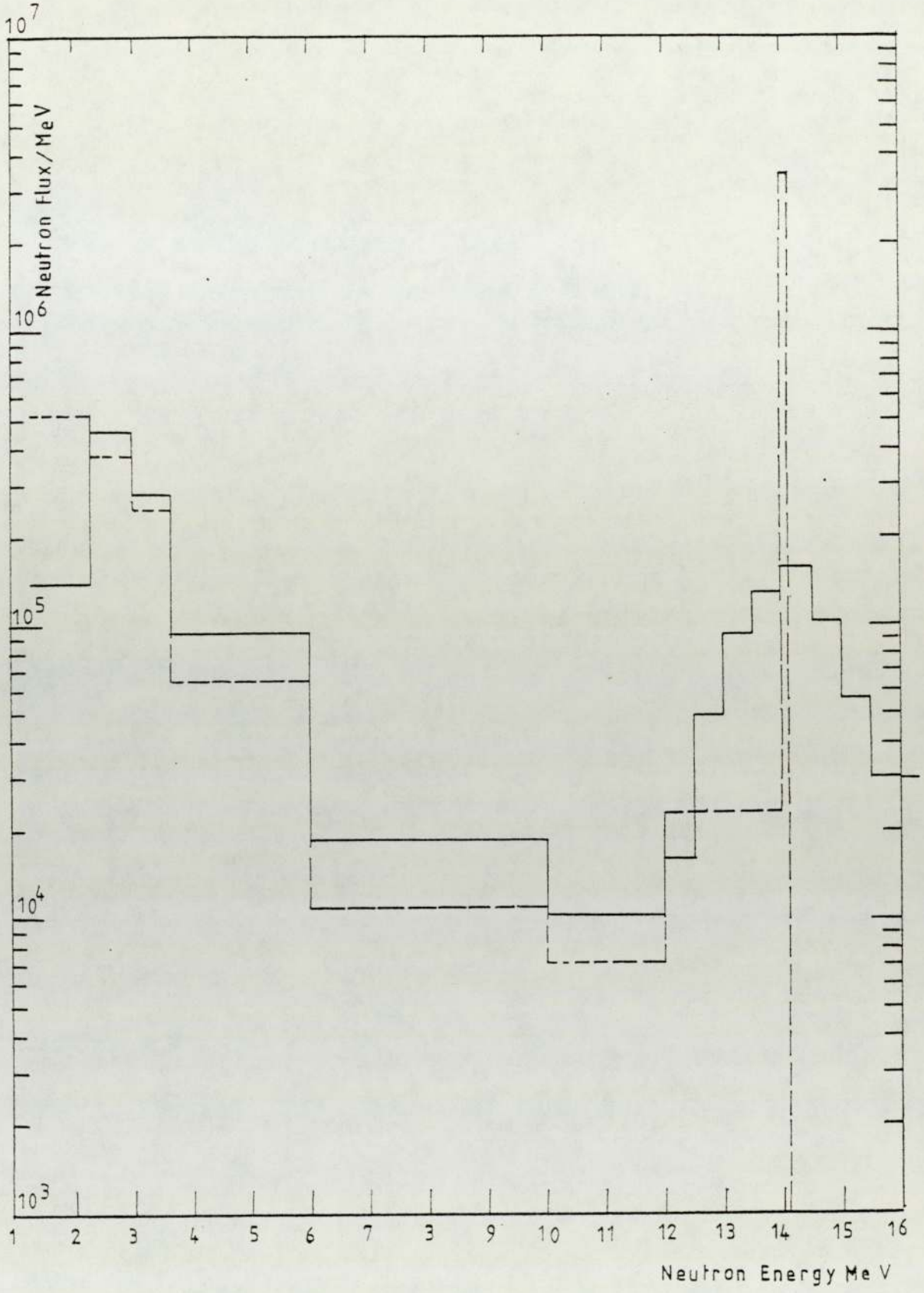

Fig[7-19] Fast Neutron Spectra inside a Mixture Shielding of LiF and U^{238} at 12.4 cm from the Centre.

-------- Calculated

_____ Measured

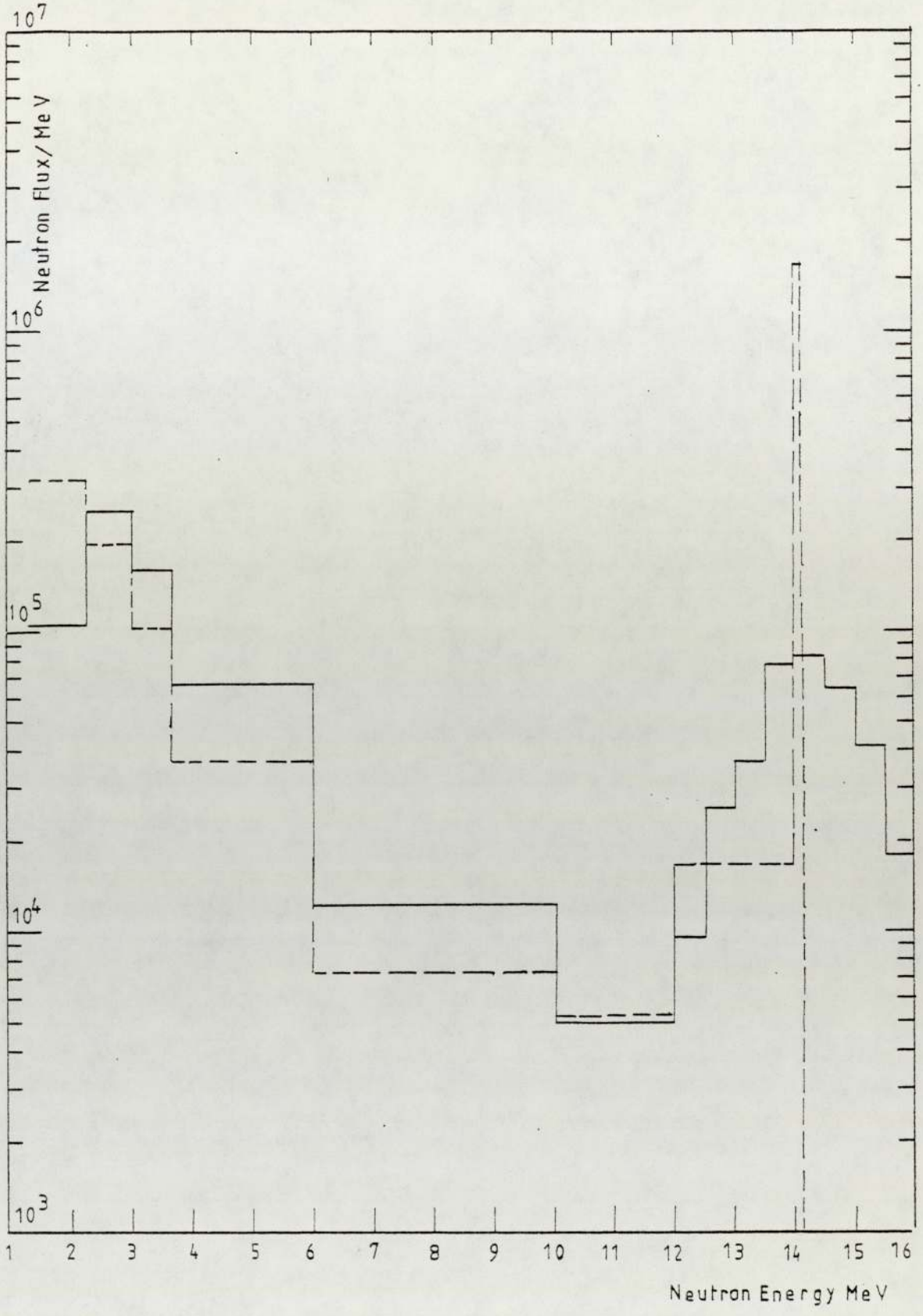

Fig[7-20] Fast Neutron Spectra inside a Mixture Shielding of LiF and U^{238} at 15.5 cm from the Centre.

-------- Calculated

_____ Measured

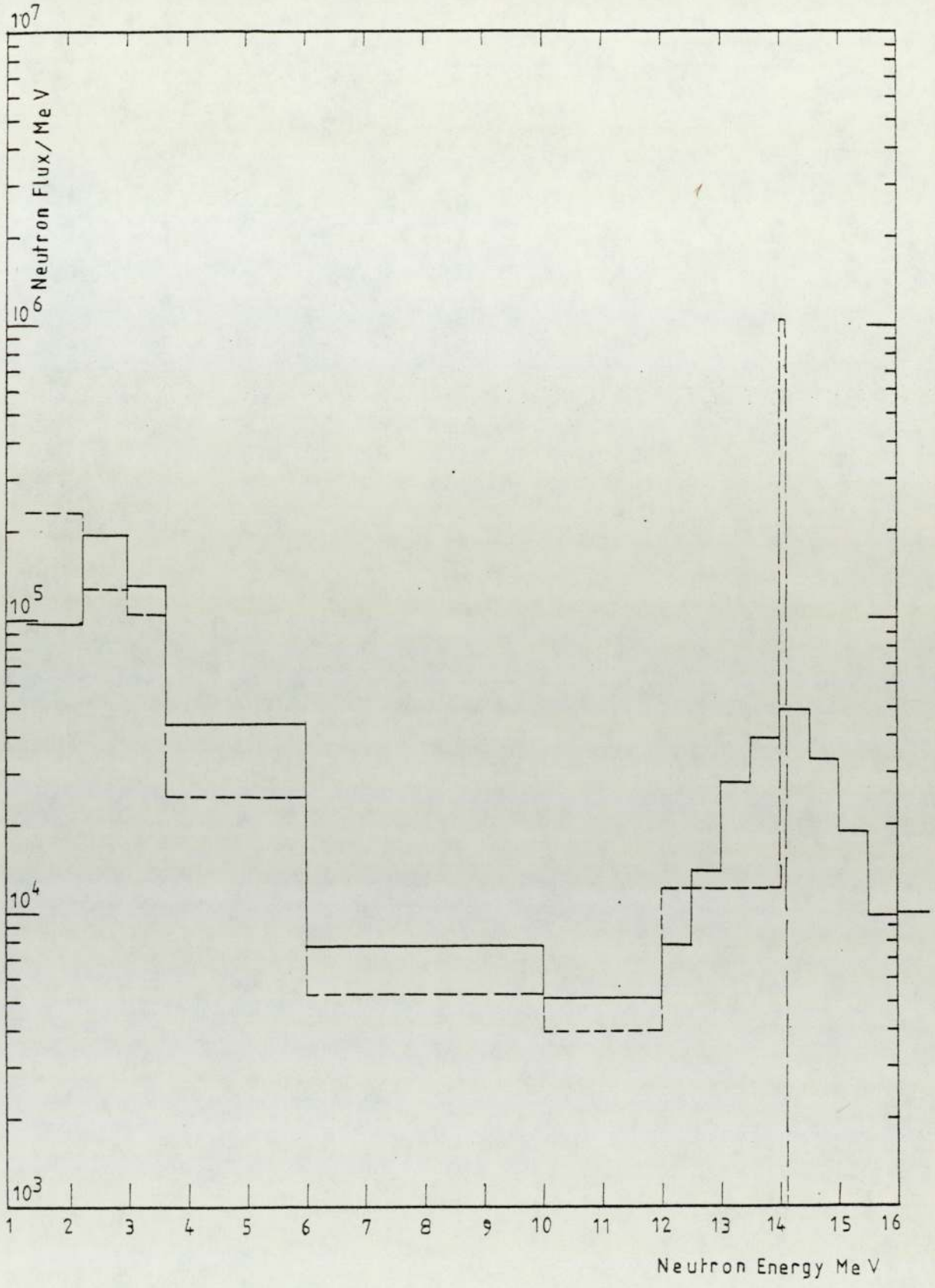

Fig[7-21] Fast Neutron Spectra inside a Mixture Shielding of LiF and U^{238} at 17.8 cm from the Centre.

-------- Calculated

_____ Measured

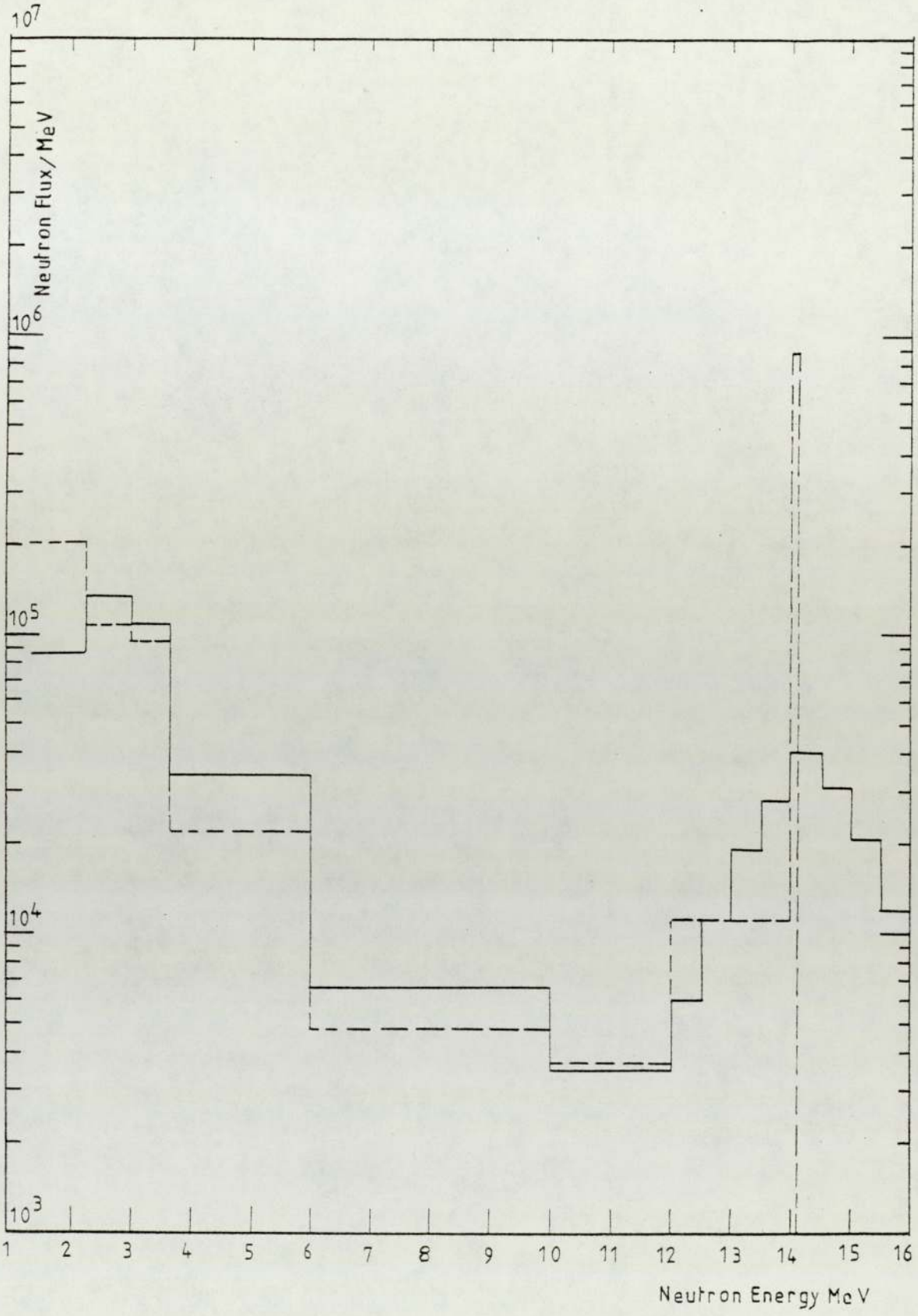

Fig[7-22] Fast Neutron Spectra inside a Mixture Shielding of LiF and U^{238} at 18.6 cm from the Centre.

-------- Calculated

_____ Measured

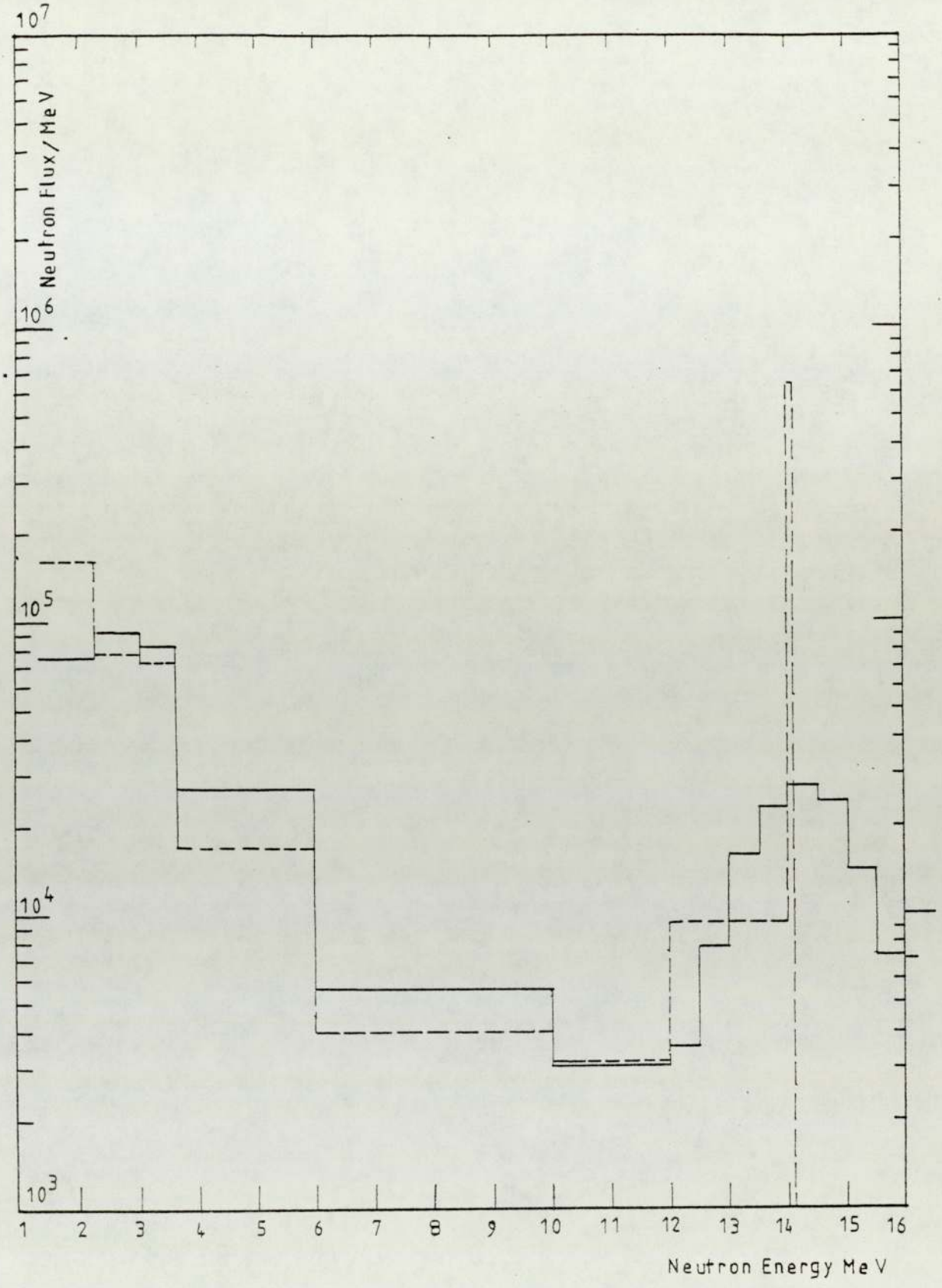

Fig [7-23] Fast Neutron Spectra inside a Mixture Shielding of LiF and U^{238} at 20.2 cm from the Centre.

-------- Calculated

_____ Measured

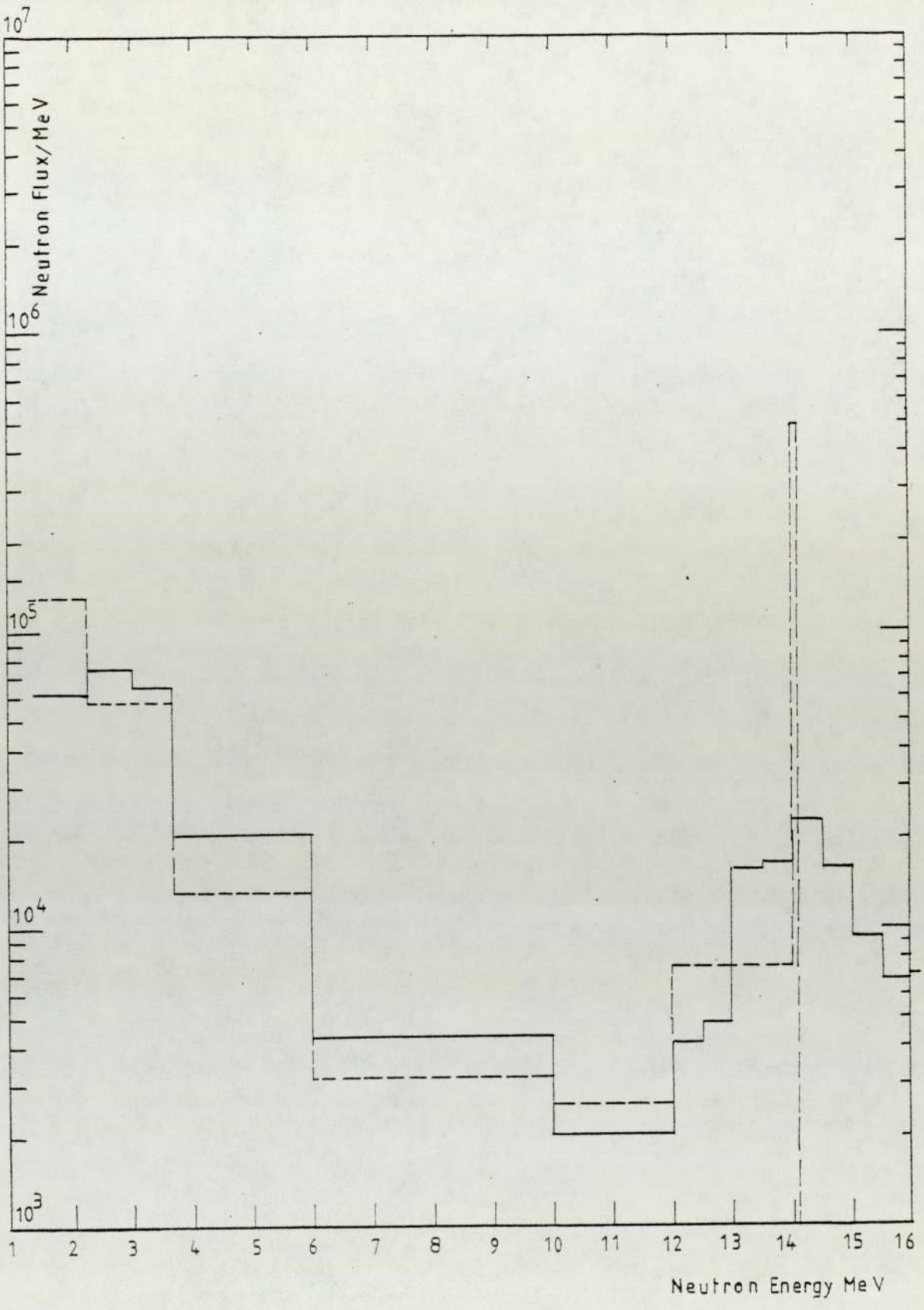

Fig[7-24] Fast Neutron Spectra inside a Mixture Shielding of LiF and U^{238} at 21.7 cm from the Centre.

-------- Calculated

_____ Measured

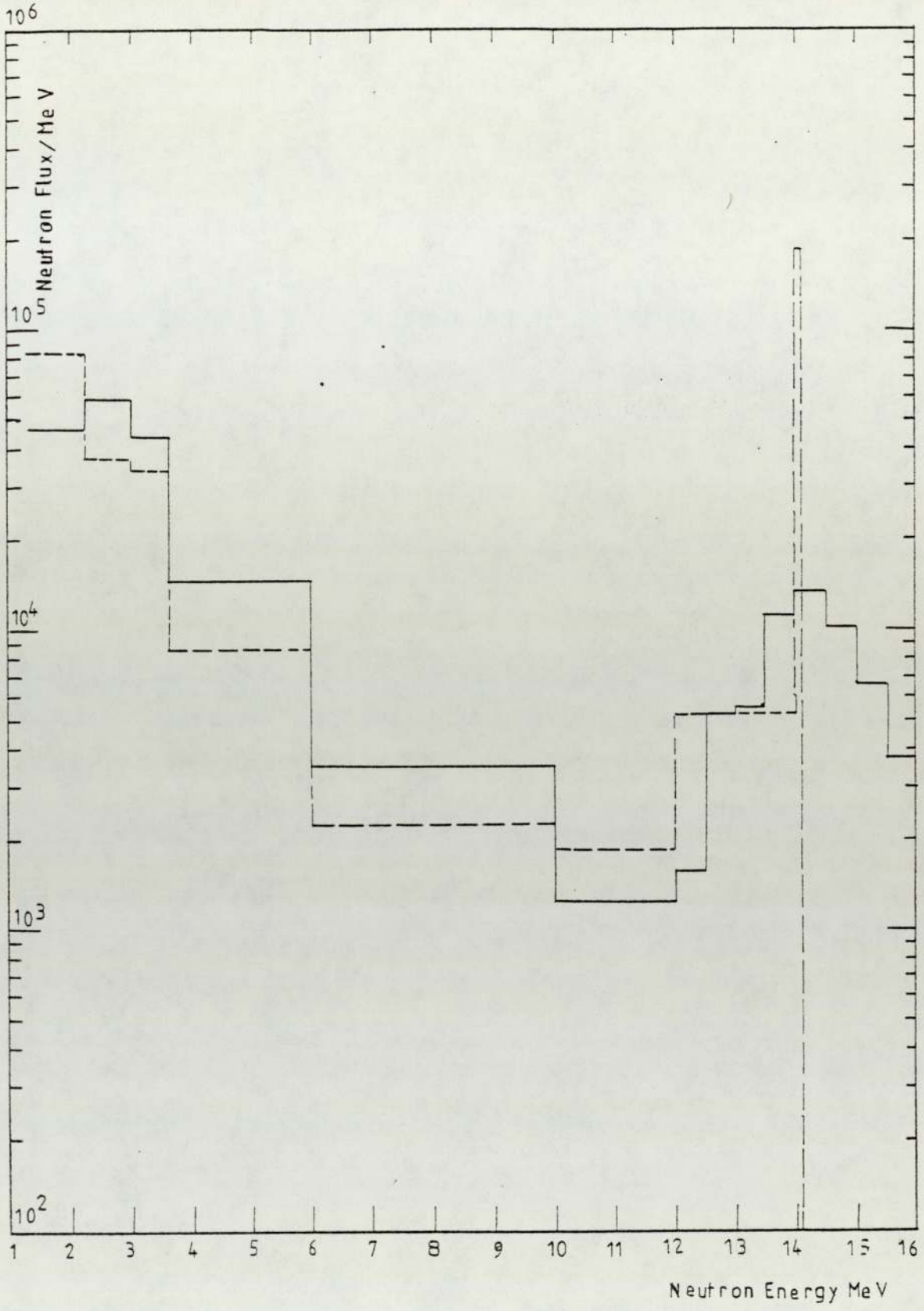

Fig[7-25] Fast Neutron Spectra inside a Mixture Shielding of LiF and U^{238} at 24.8 cm from the Centre.

-------- Calculated

_____ Measured

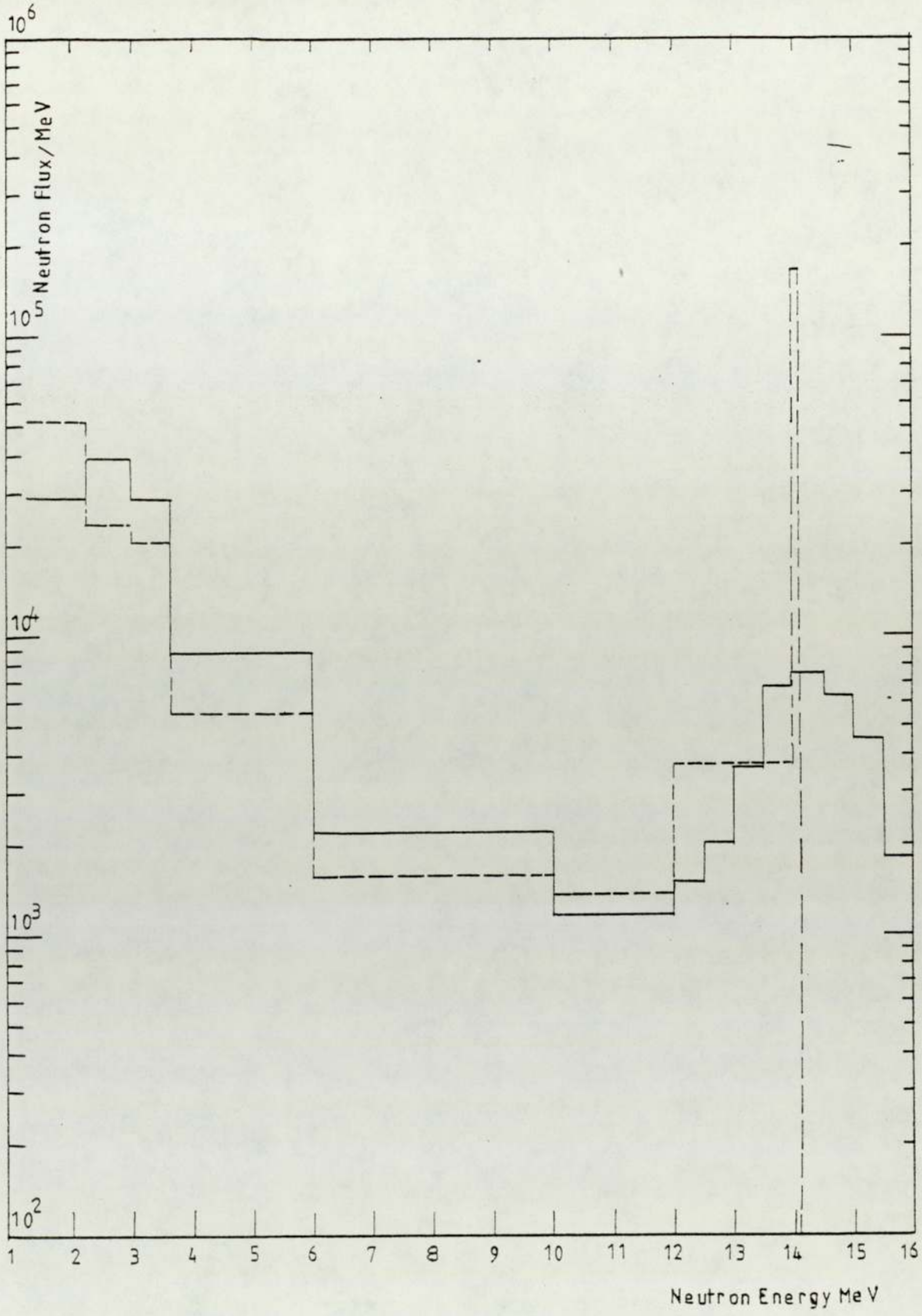

Fig[7-26] Fast Neutron Spectra inside a Mixture Shielding of LiF and U^{238} at 27.9 cm from the Centre.

-------- Calculated

_____ Measured

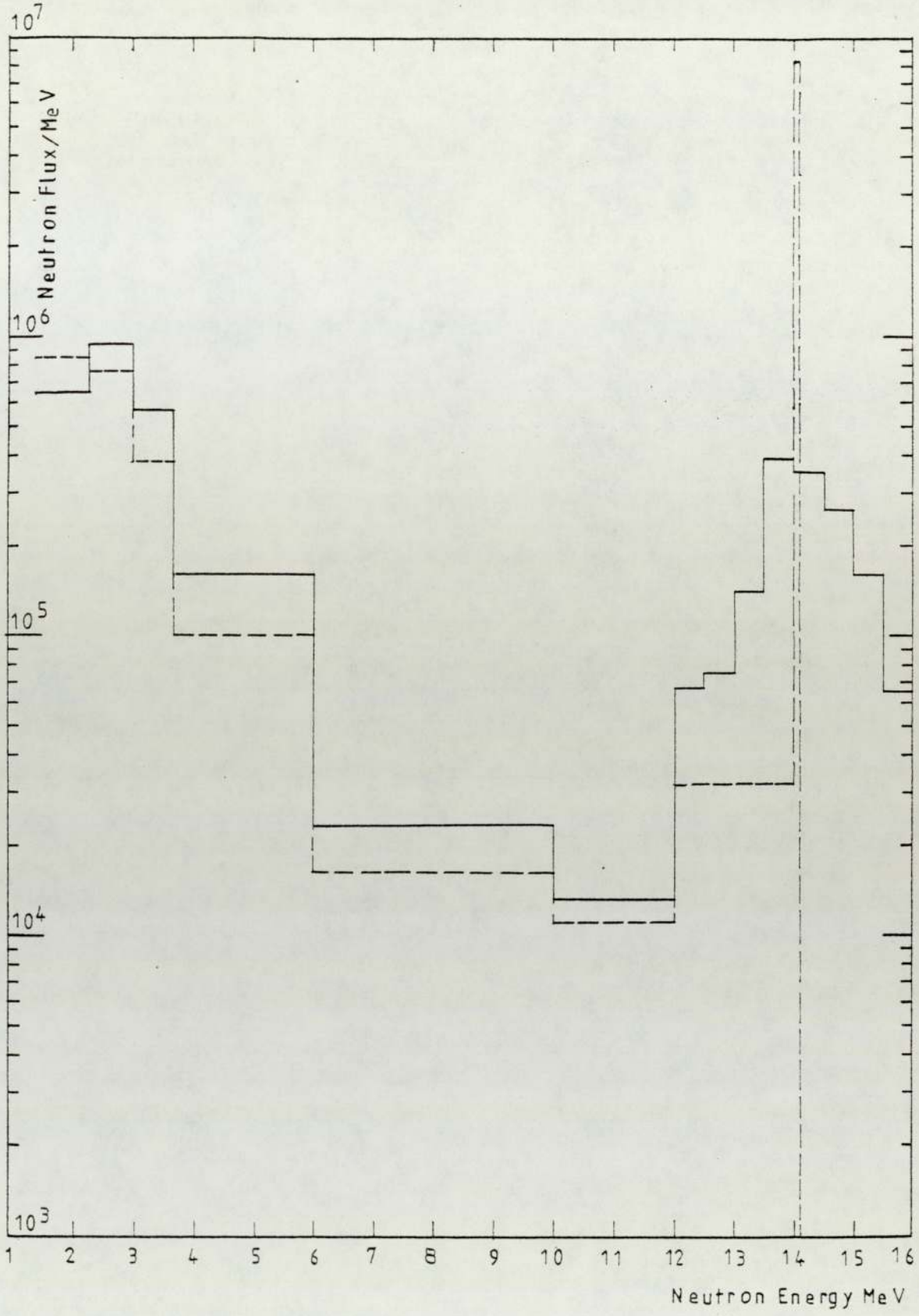

Fig[7-27] Fast Neutron Spectra inside a two Region of LiF and U^{238} Shielding at 9.3 cm from the Centre.

-------- Calculated

_____ Measured

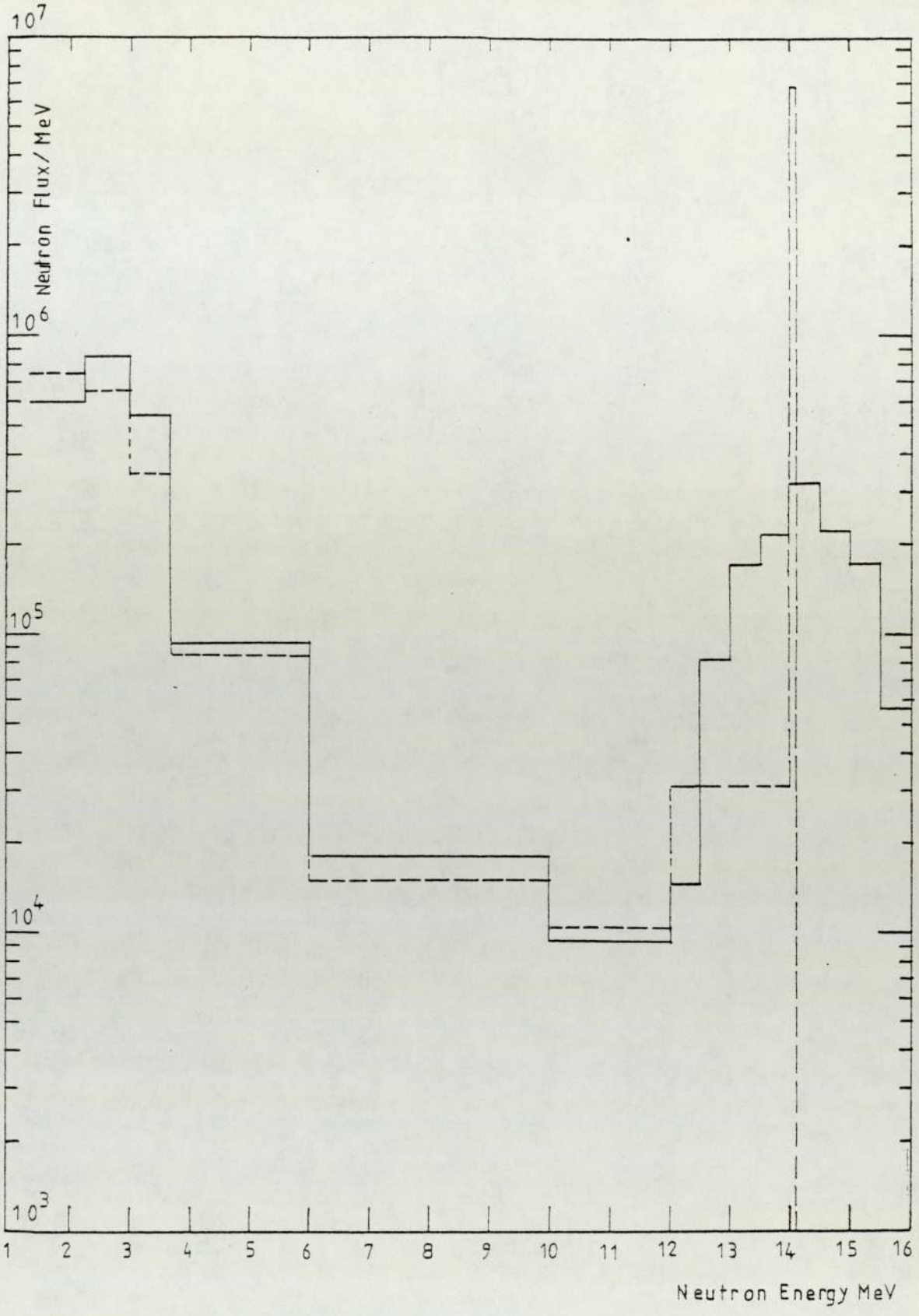

Fig[7-28] Fast Neutron Spectra inside a two Region of LiF and U^{238} Shielding at 10.1 cm from the Centre.

-------- Calculated

_____ Measured

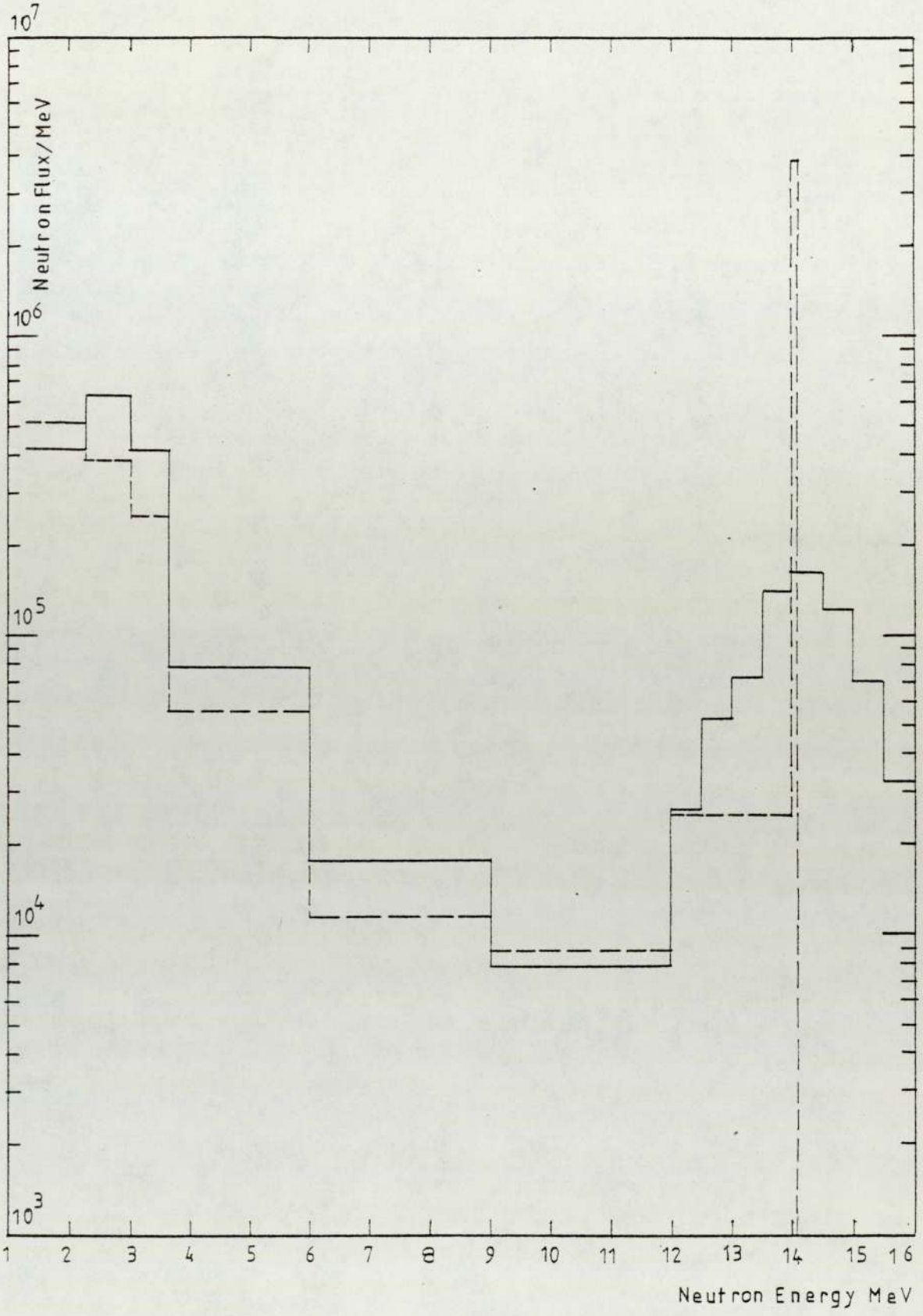

Fig[7-29] Fast Neutron Spectra inside a two Region of LiF and U^{238} Shielding at 12.4 cm from the Centre.

-------- Calculated

_____ Measured

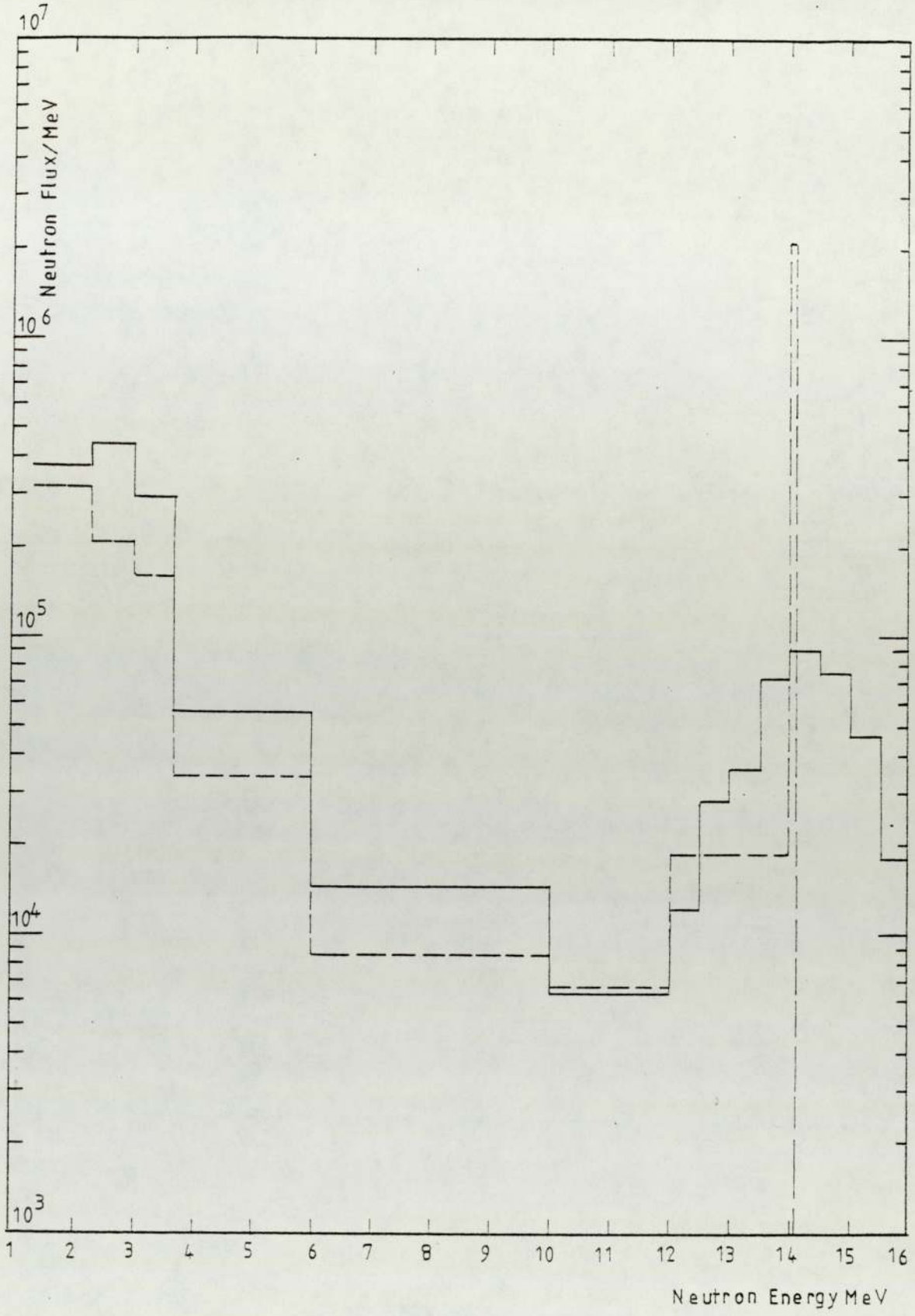

Fig[7-30] Fast Neutron Spectra inside a two Region of LiF and U^{238} Shielding at 15.5 cm from the Centre.

-------- Calculated

_____ Measured

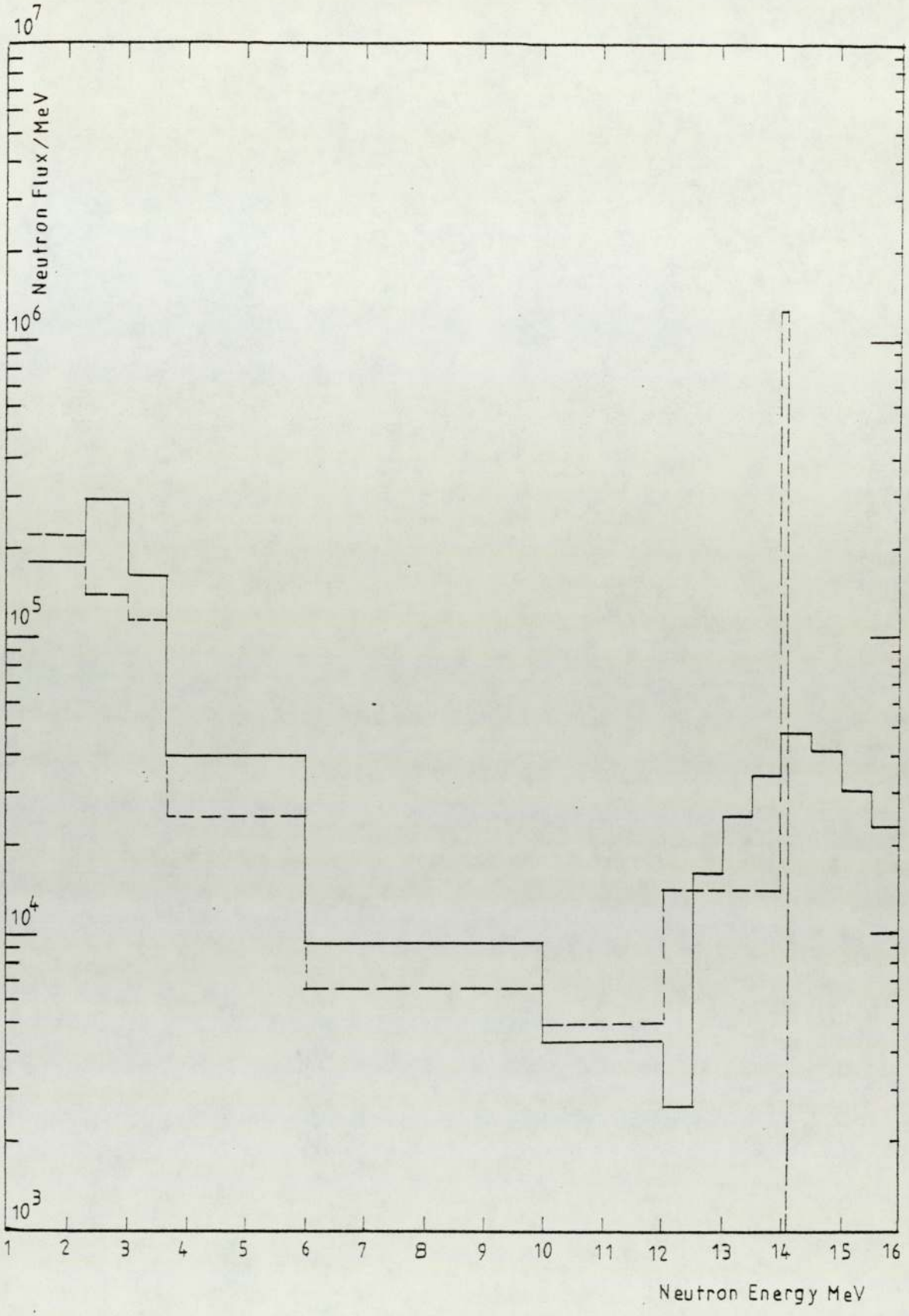

Fig[7-31] Fast Neutron Spectra inside a two Region of LiF and U^{238} Shielding at 17.8 cm from the Centre.

-------- Calculated

_____ Measured

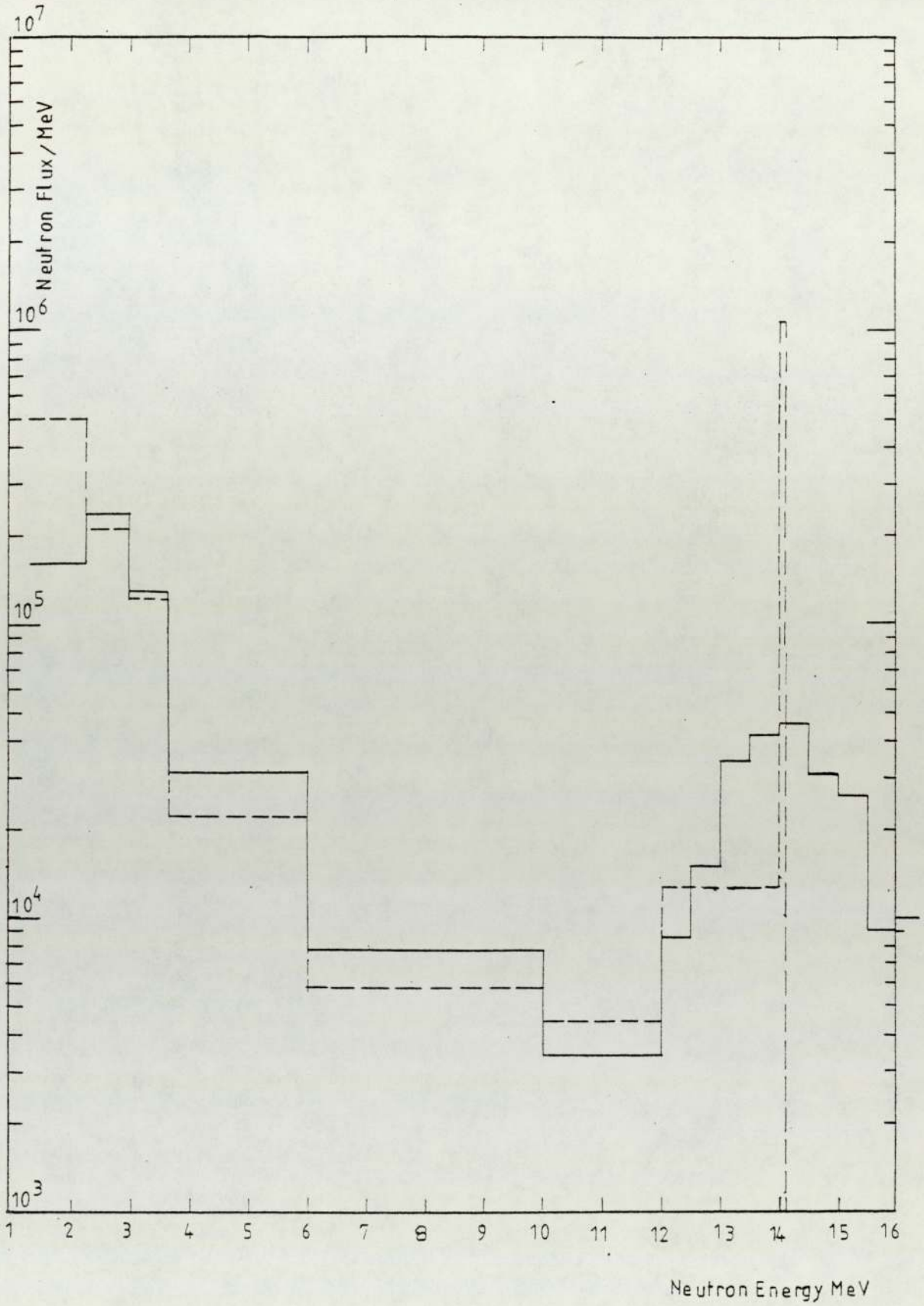

Fig[7-32] Fast Neutron Spectra inside a two Region of LiF and U^{238} Shielding at 18.6 cm from the Centre.

-------- Calculated

_____ Measured

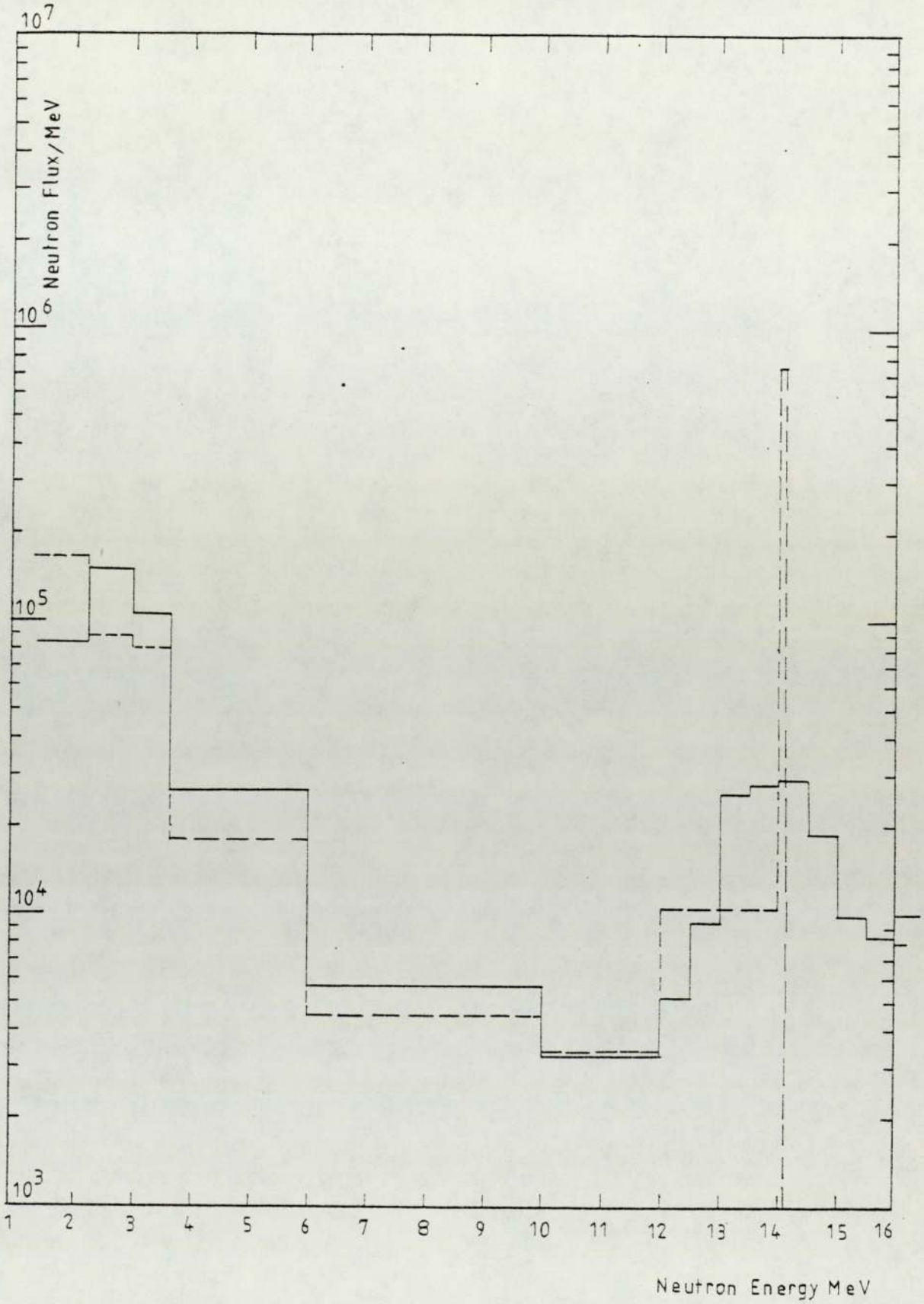

Fig[7-33] Fast Neutron Spectra inside a two Region of LiF and U^{238} Shielding at 20.2 cm from the Centre.

-------- Calculated

_____ Measured

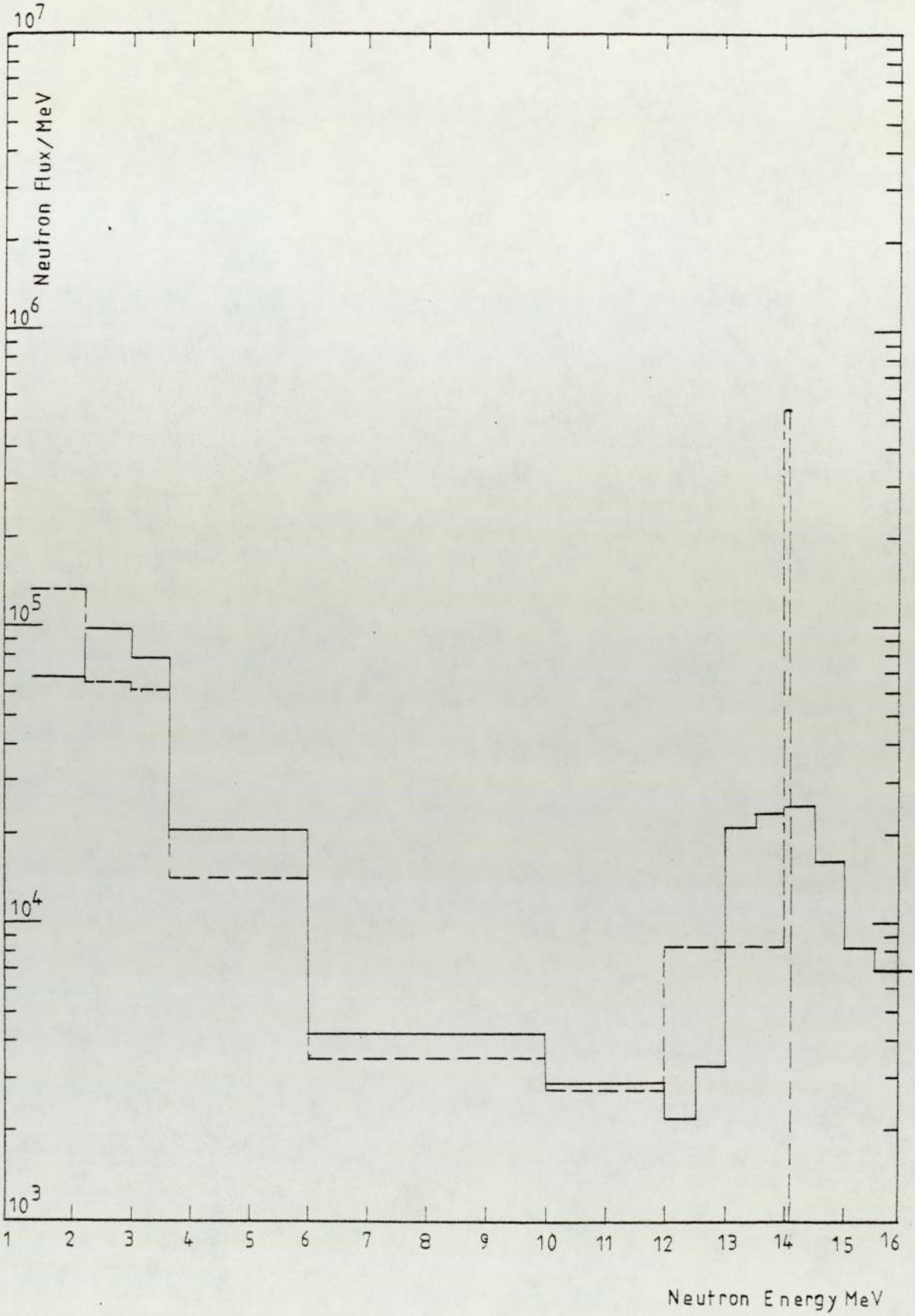

Fig[7-34] Fast Neutron Spectra inside a two Region of LiF and U^{238} Shielding at 21.7 cm from the Centre.

-------- Calculated

_____ Measured

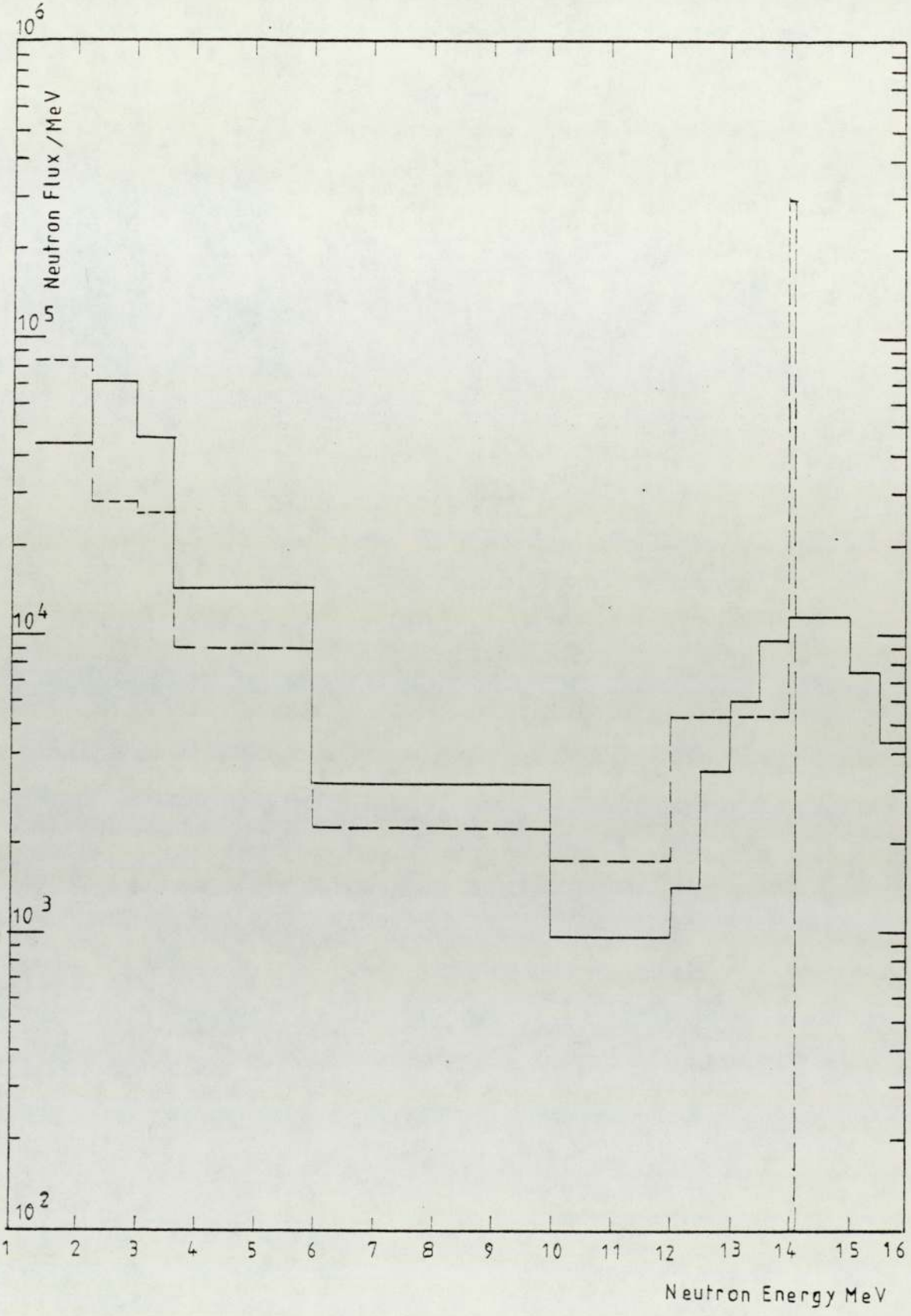

Fig[7-35] Fast Neutron Spectra inside a two Region of LiF and U^{238} Shielding at 24.8 cm from the Centre.

-------- Calculated

_____ Measured

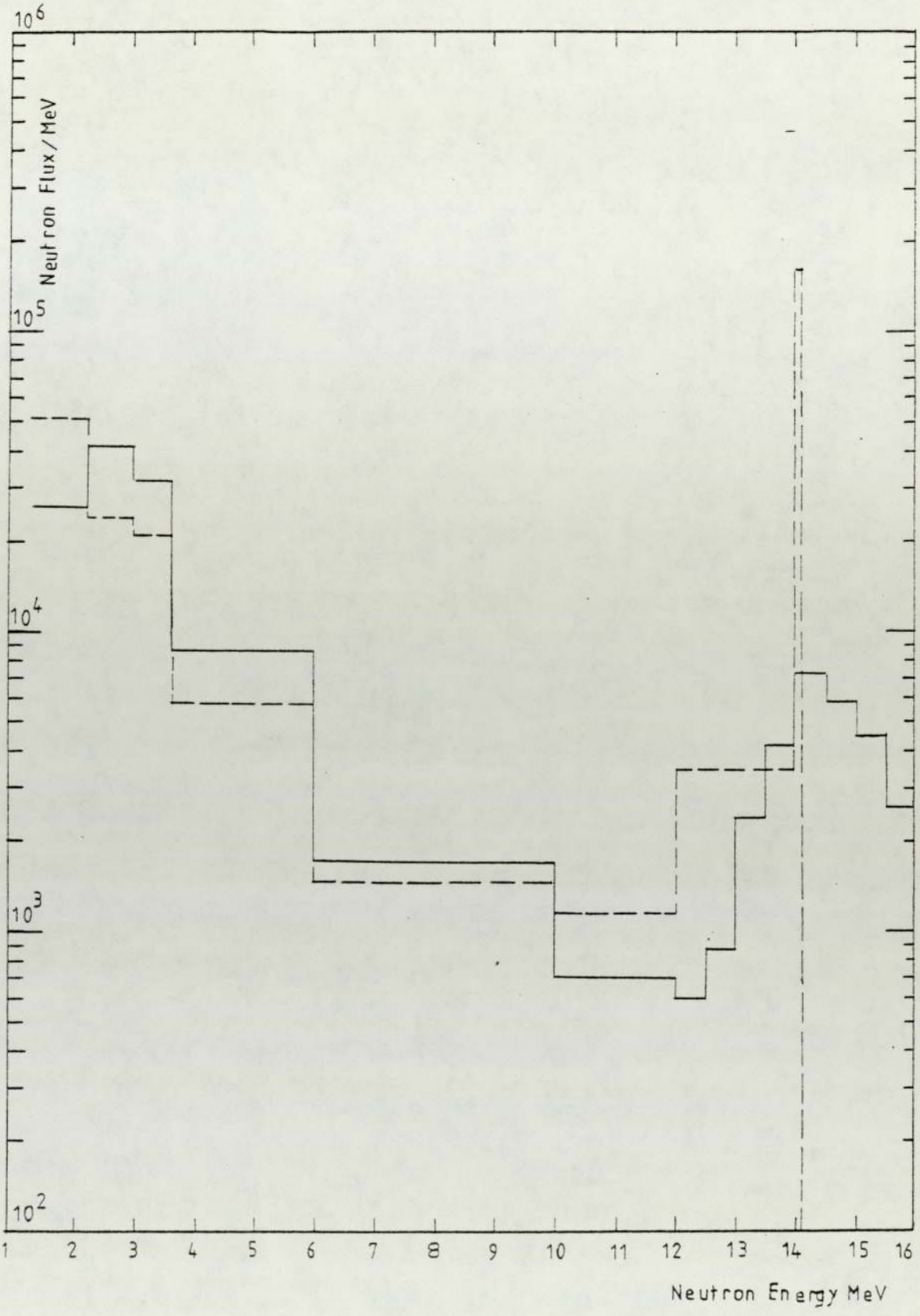

Fig [7-36] Fast Neutron Spectra inside a two region of LiF and U^{238} Shielding at 27.9 cm from the Centre.

-------- Calculated

_____ Measured

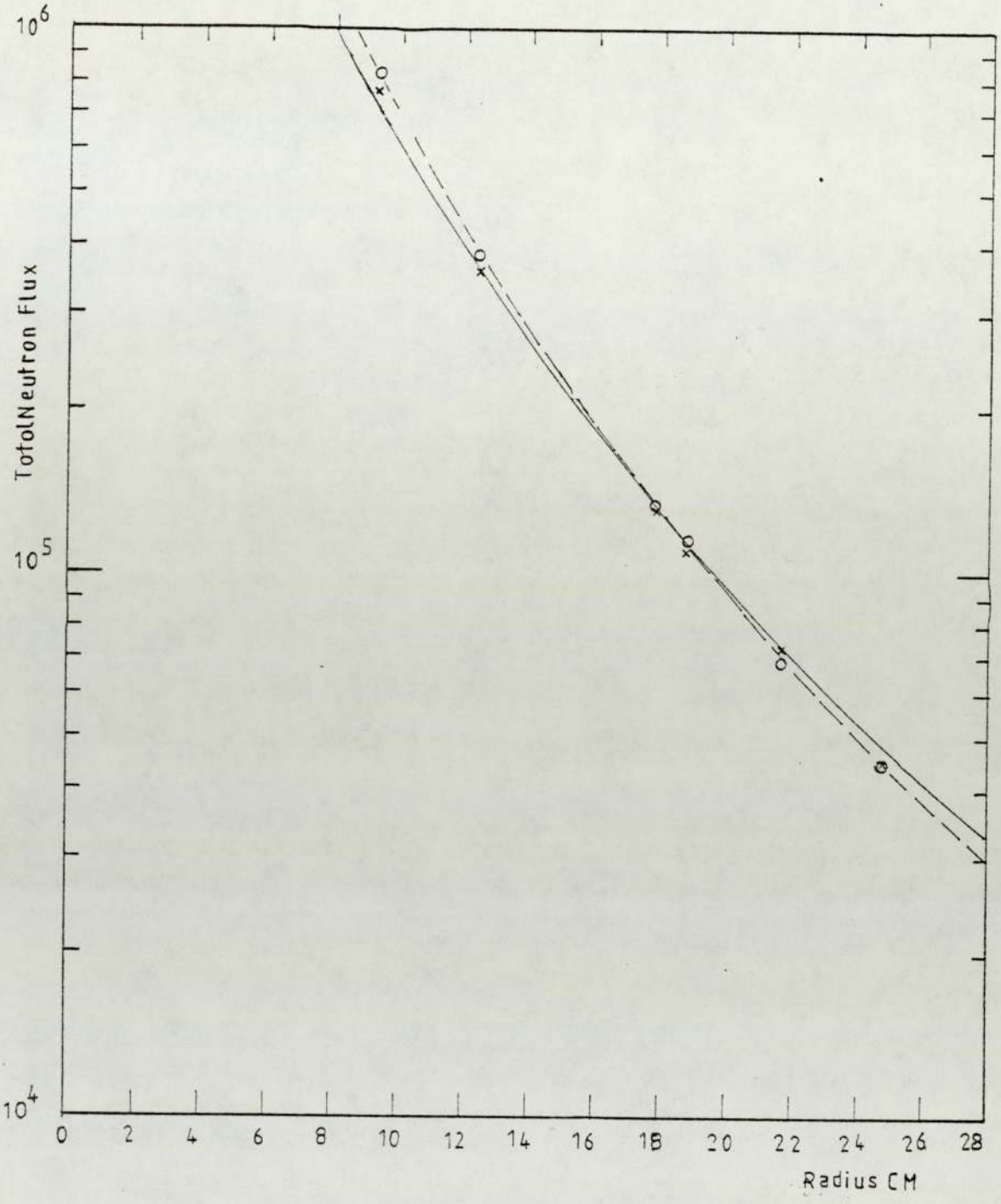

Fig[7-37] Neutron Flux Intensity inside a LiF Shielding for (14.0 - 14.1) MeV Energy Group.

-------- o Calculated

_____ x Measured

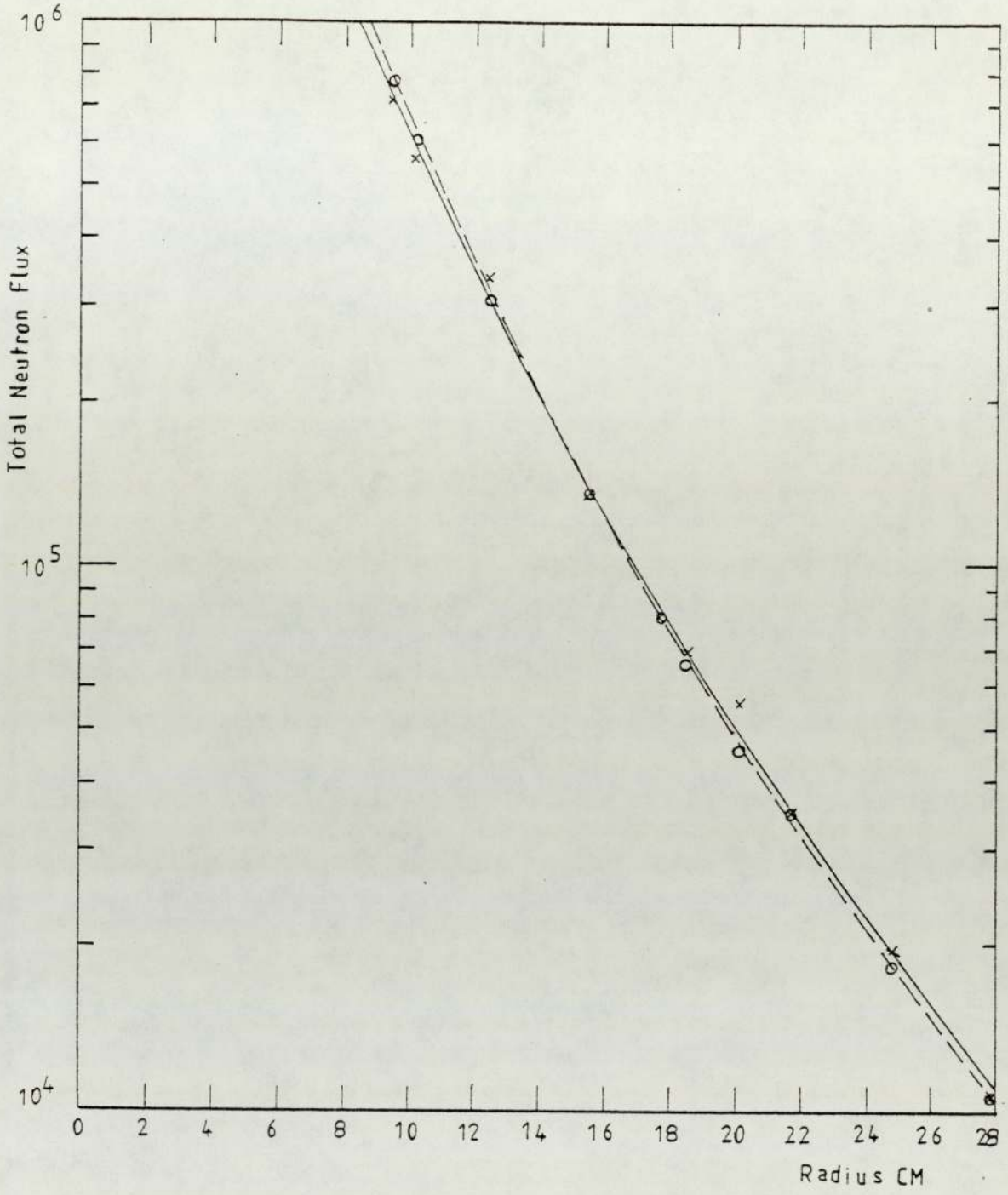

Fig[7-38] Neutron Flux Intensity inside a U^{238} Shielding for (14.0 - 14.1) MeV Energy Group

-------- o Calculated

_____ x Measured

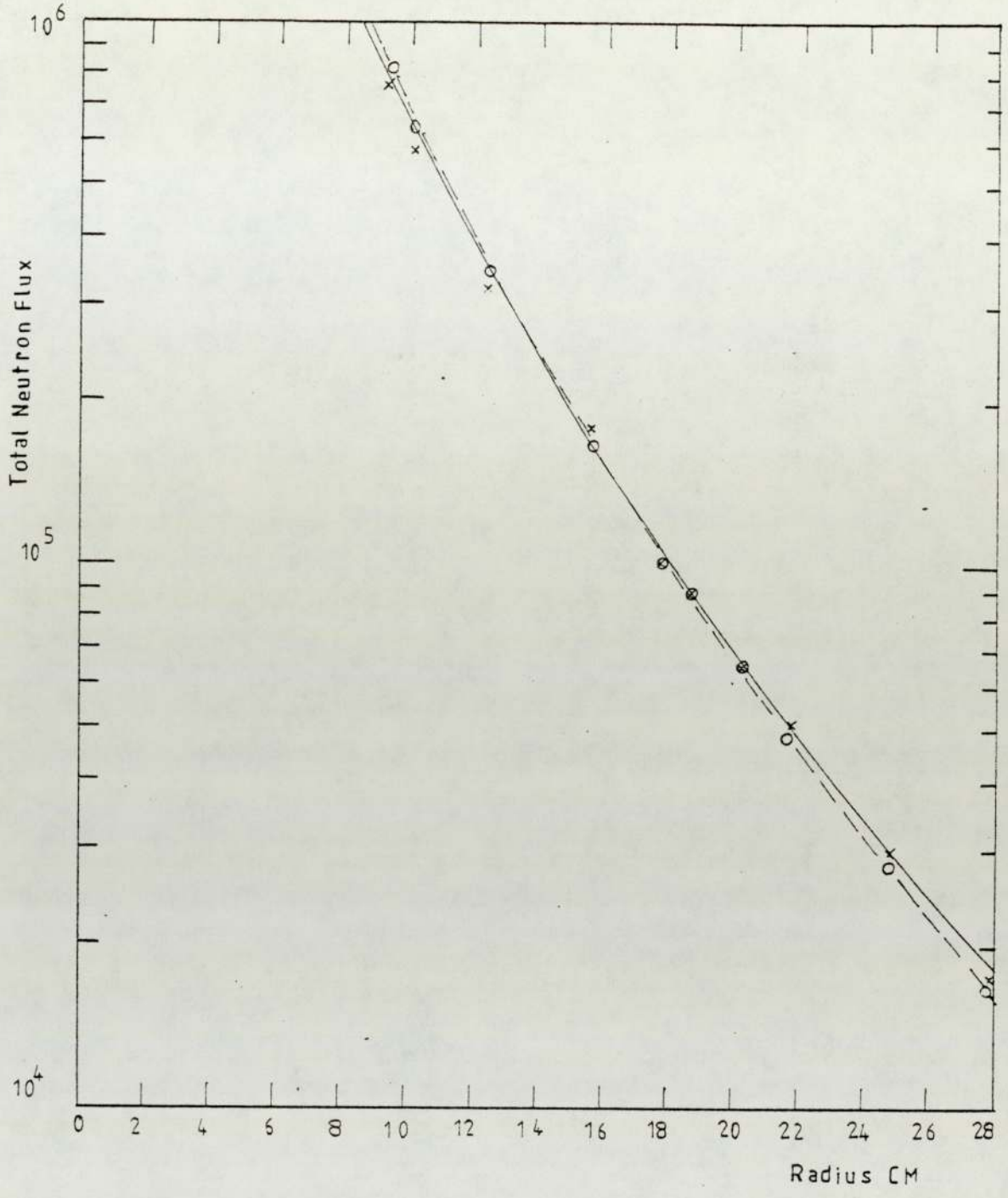

Fig[7-39] Neutron Flux Intensity inside a Mixture of LiF and U^{238} Shielding for (14.0 - 14.1) MeV Energy Group.

-------- o Calculated

_____ x Measured

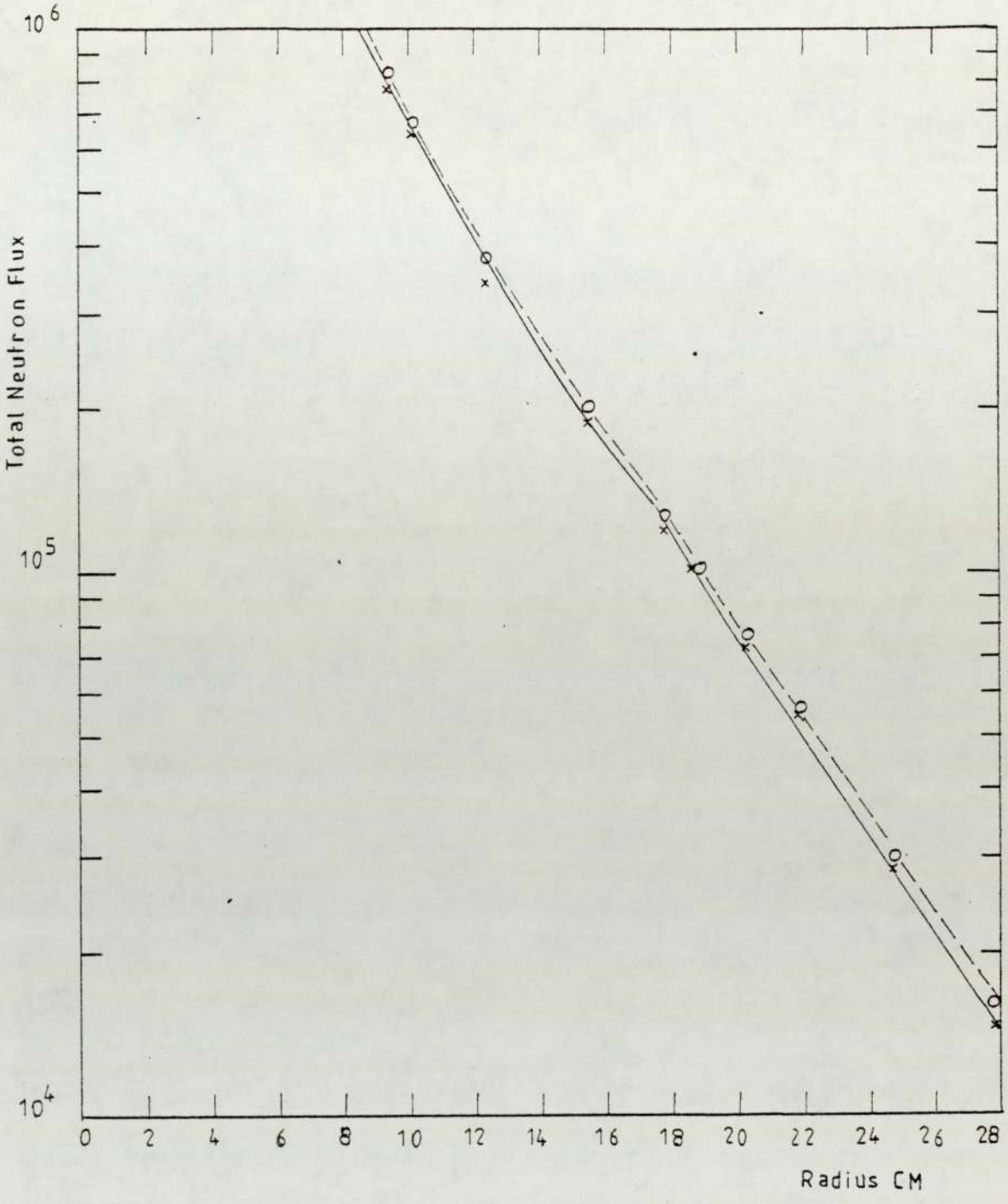

Fig[7-40] Neutron Flux Intensity inside a two Region of LiF and U^{238} Shielding (14.0 - 14.1) MeV Energy Group.

-------- o Calculated

_____ x Measured

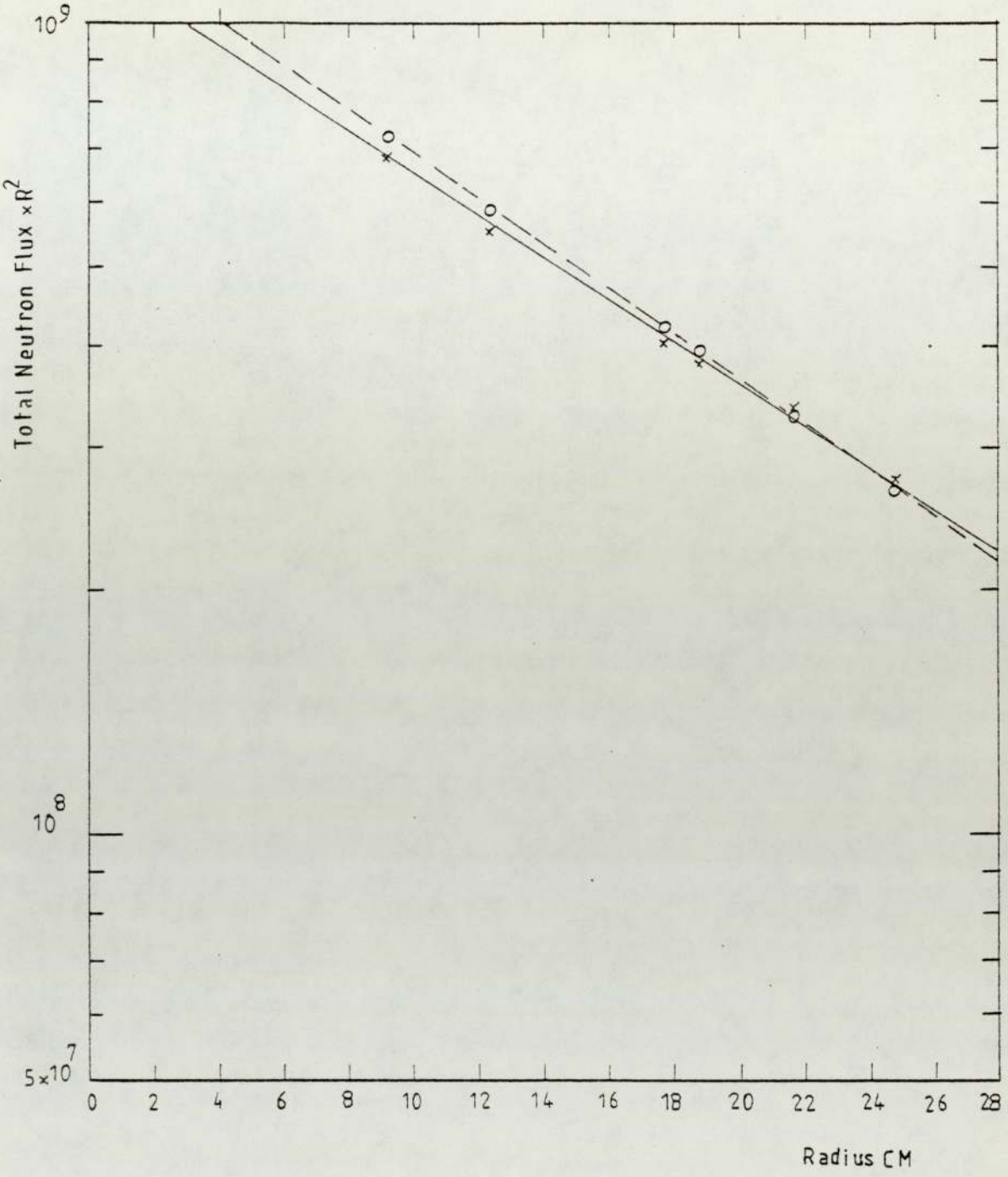

Fig[7-41] The Neutron Flux xR^2 for Energy Group (14.0 - 14.1) MeV inside a LiF Shielding.

-------- o Calculated

_____ x Measured

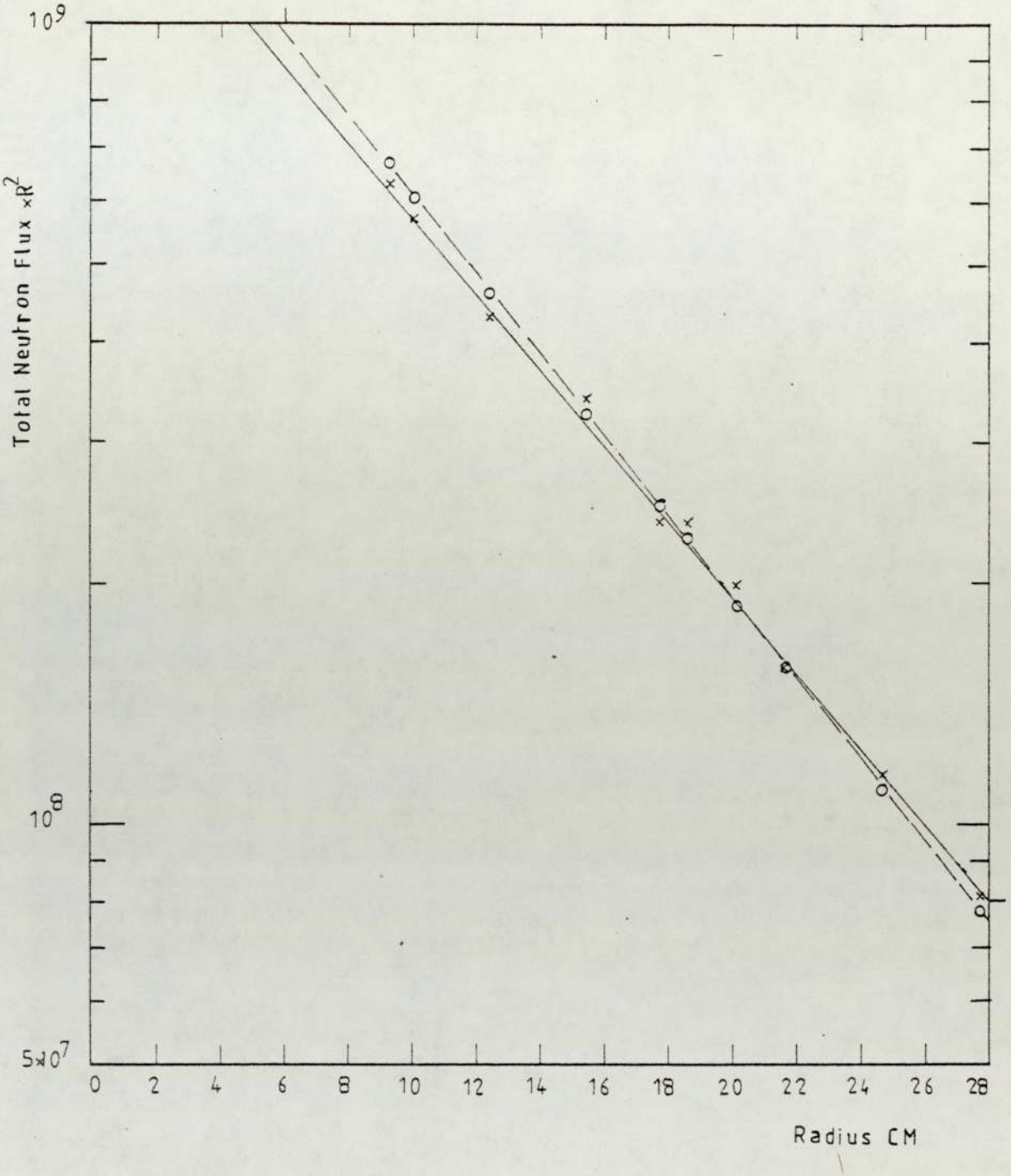

Fig[7-42] The Neutron Flux xR^2 for Energy Group (14.0 - 14.1) MeV inside a U^{238} Shielding.

-------- o Calculated

_____ x Measured

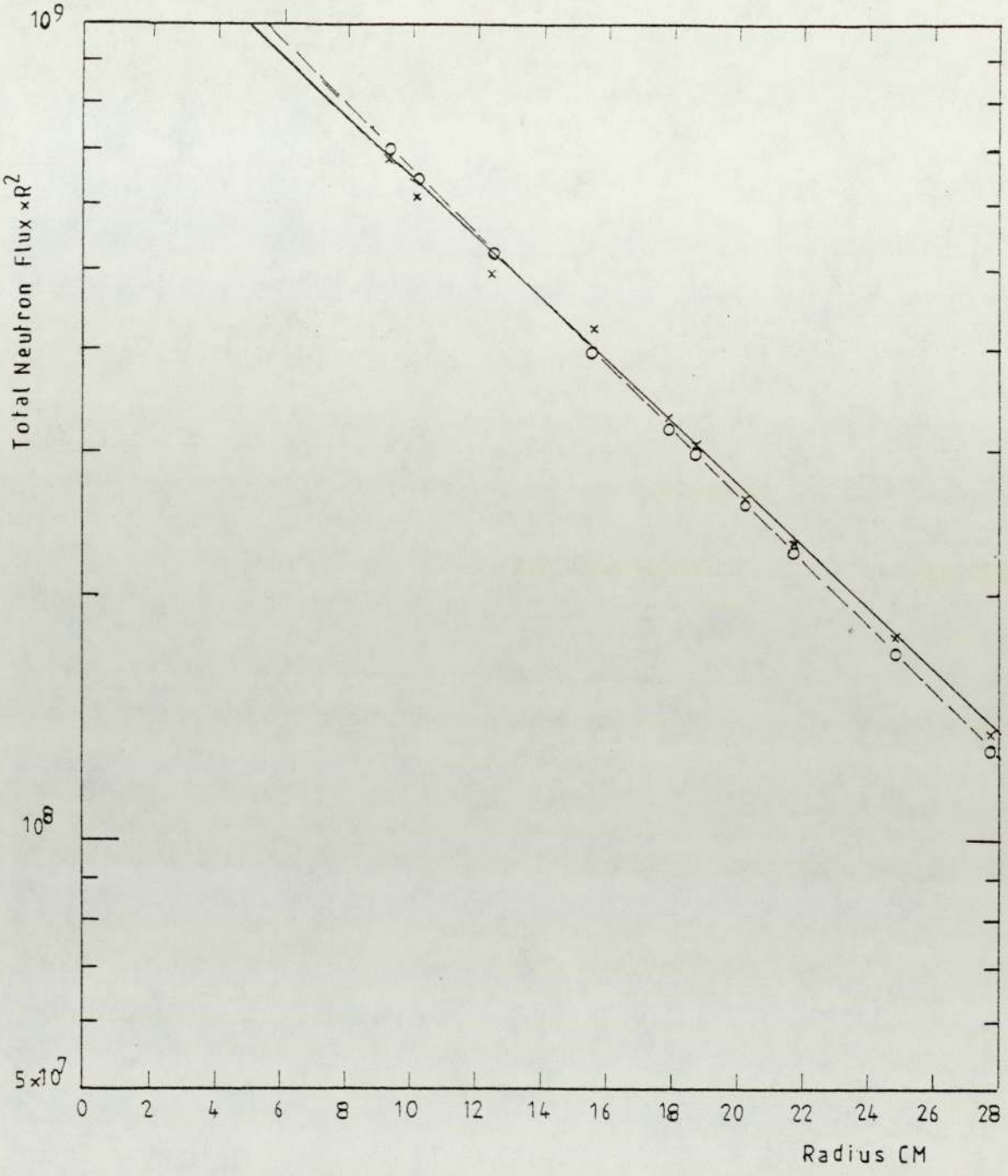

Fig[7-43] The Neutron Flux xR^2 for Energy Group (14.0 - 14.1) MeV inside a mixture of LiF and U^{238} Shielding.

-------- o Calculated

_____ x Measured

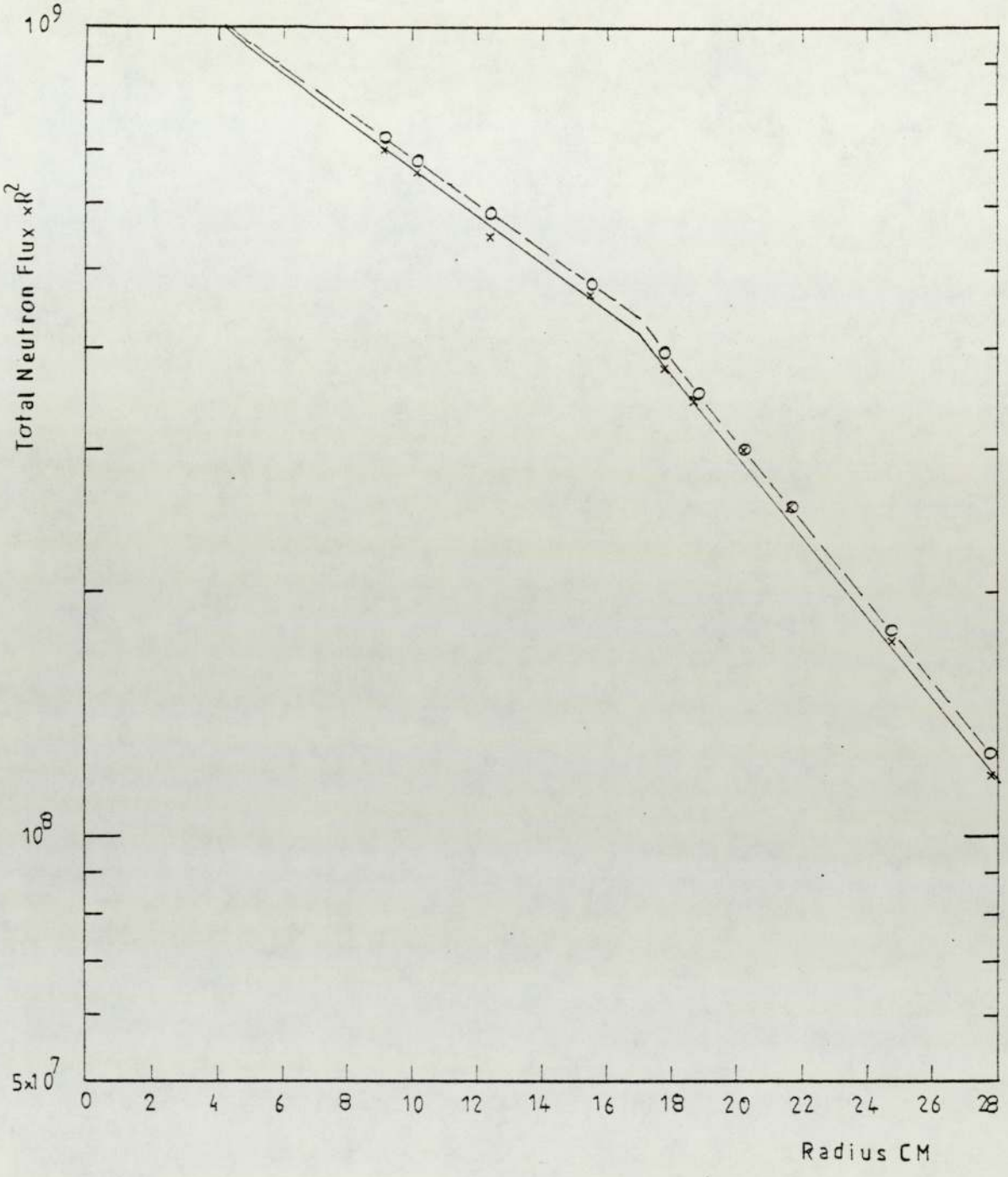

Fig[7-44] The Neutron Flux xR^2 for Energy Group (14.0 - 14.1) MeV inside a two Region of LiF and U^{238} Shielding.

-------- o Calculated

_____ Measured

CHAPTER 8

CONCLUSIONS AND DISCUSSION

The results of neutron spectrum measurements and calculations at various radii inside shields of LiF, U^{238}, a mixture of LiF and U^{238}, and a two region system of LiF and U^{238} have been presented in Chapter 7.

The following conclusions may be drawn:

1 - Cross-Sections Data-File

The agreement between the calculated and measured indicate the general validity of the cross-sections of the UKNDL file for ^{6}Li, ^{7}Li and ^{19}F and the modified YOM-20 data set for U^{238} and aluminium. It is not possible to look for detailed errors in the data because the flux is low apart from the 14.1 MeV flux and similarly it is not possible to carry out meaningful sensitivity calculations for the cross-section used for the shielding.

2 - The Calculation Method

The good agreement between the calculated and measured spectra, indicates that the calculation method used with its built in approximation of isotropic flux except for the 14.1 MeV neutron is valid for the experimental system used and the available data. The small computer time used during the calculation is especially an advantage.

For the overall spectrum shape the neutron flux per unit lethargy was plotted against the energy for both the calculated and the measured spectrum in the present work and compared with the result of B.Y. Underwood et al[119], who carried out similar measurements in

a 1.25 m diameter sphere of LiF, Fig. [8-1]. There is no direct correlation between the values along the vertical axis, since the measurements are at different radii, but spectra drawn in the figures show good agreement in general shape, especially for the calculated spectra.

This gives some confidence in the removal diffusion method, since the shape compares closely with transport calculations, although for a more precise check the removal diffusion calcuations would need to be performed for the large LiF sphere.

It will also be noticed that Underwood's experimental and theoretical spectra do not agree exactly, even though his results were analysed by the more precise response function matrix method. This may indicate some possible errors in cross-section.

The over-all spectral shape shows, for the shielding materials studied, that the lowest neutron intensity is in the energy group (12-10) MeV, and that is because the only neutron source at that region is from the 14.1 MeV inelastic scattered neutrons. The neutron intensity for lower energy groups increases. This is to be expected as the asymptotic slowing down flux tends to $\frac{1}{E}$ in the absence of absorption. In the uranium shielding the lower energy groups in shields containing uranium have a higher intensity than the lithium fluoride shields because of the fast fission neutrons produced in the shielding assembly.

3 - Comparison of the Shielding Assemblies Used

Measurements have been made for neutrons degraded in energy down to about 2 MeV. The LiF is more effective at lower energies because of the high elastic scatter cross-section, while for the uranium shielding it is noticed that the neutrons degraded from higher energy groups are more than for the LiF due to the fast fission neutrons

generated in the uranium and (n,n), (n,2n) and (n,3n) reactions.

The elastic scattering will be the best mechanism over the whole energy range for light materials such as LiF, but the inelastic reactions are very effective for the higher energy neutrons particularly for heavy atoms.

From the above it appears that no single shield material is ideal. The U^{238} is very effective in the energy range where the inelastic scattering process is predominant while one can find that LiF is best in the energy range where the elastic scattering is important. Fast fission of U^{238} increases the number of neutrons in the few MeV range and down to thermal energies and so would require additional shielding in this range.

Another form of the shielding assembly is the mixture of the LiF and U^{238} which is effectively better than that of either material separately over the whole energy range down to 2 MeV investigated. The two layers were arranged with the U^{238} on the outside in order to give better absorption of the gamma rays produced from inelastic scattering and neutron capture.

4 - The Removal Cross-Section

The removal cross-section was calculated for the different shielding assemblies for the first energy group (14.0 - 14.1) MeV, by assuming that it is equal to the transport cross-section which is a function of the elastic cross-section.

The removal cross-section measured for the U^{238}, a mixture of LiF and U^{238}, and for the two region of LiF and U^{238} are in agreement with those used in the calculations within the experimental error.

The microscopic removal cross-section for the U^{238} calculated from the measured removal cross-section is 2.96 barn, compared with σ_{tran} = 3.20 barn and σ_{non} = 2.86 barn used in the calculation. This indicates that the use of the transport cross-section for the removal cross-section is not right in the experimental measurement because of the poor resolving power of the detector used.

The source of the error mainly could be due to the detector efficiency in this energy range which might be due to uncertainties in hydrogen and carbon total cross-section used for the scintillator efficiency and shape correction. The other point which affects the comparison of the result is the different geometries used in the calculation (spherical) and those used in the experimental work (cylindrical with a point source).

For the LiF removal cross-section there is a material difference between that used in calculation and that measured experimentally, and that may be due to either of the following points.

a - From the measured removal cross-section a microscopic value for LiF of σ_{rem} = 1.60 barn is obtained. This compares with σ_{trans} = 1.967 barn, and $\sigma_{non\ el}$ = 1.311 barn obtained from the UKNDL data and is in between these two values. From Figure [8-2]$\bar{\mu}$, mean scattering cosine for ^{7}Li (^{6}Li is not so important due to its low isotropic abundance) from ENDF/B-IV files agrees reasonably with that used in the calculation (UKNDL-file) but from Figure [8-3] the UKNDL file has only one elastic scattering angular distribution for ^{19}F to cover the range 7-14 MeV, and consequently $\bar{\mu}$ at 14 MeV may really be higher leading to a lower value of σ_{rem}.

Figure [8-3] also shows $\bar{\mu}$ from the ENDF/B-IV file which has a value of 0.693 at 14 MeV. This reduces $(1-\bar{\mu})\sigma_{el}$ to 0.265 for ^{19}F and to 0.545 for LiF giving σ_{tran} = 1.864 barn which is closer to that calculated from the measured Σ_{rem} (1.60 barn).

b - With the broad peak for the 14.1 MeV measured the removal by elastic scattering could be even less than the $(1-\bar{\mu})\ \sigma_{el}$ and the total removal not much more than the $\sigma_{non\ el}$. This effect would be more important in LiF where $(1-\bar{\mu})\sigma_s$ is over 30% of the transport cross-section, whereas in U^{238} it is only 14%. So because of the poor resolution of the detector and the large range of the energy group the removal cross-section used should be less than the transport cross-section, but greater than the non-elastic cross-section.

5 - Suggestions for future work

For the future work the project could be improved from the experimental point of view as follows:

a - The pulse-shape discrimination fails to discriminate adequately between gamma rays and neutrons below about 2 MeV neutron energy and the neutron spectra were cut off below 1.35 MeV corresponding to a group boundary. So to study the neutron spectra removed from the 14.1 MeV neutron to below 0.5 MeV the pulse-shape discrimination method used by P. Speir et al[120], (which uses the zero crossing method with a specially designed amplifier in a single unit) or the pulse shape discriminator model 5010 manufactured by Link Systems Limited (which uses the charge comparison method) could be suitable. Both systems claim to have good discrimination between neutrons and gamma rays below 0.5 MeV, and can cover a dynamic pulse range of 400 : 1.

b - Because the LiF density inside the tubes is very low compared with molten LiF it is important to try to increase that density. This might be possible by compressing the powder into pellets in a hydraulic press.

c - The alpha-particle detector should be restored to backward direction at an angle 175^{o} to the deuteron beam, if the noise problem can be overcome, so it will simplify the construction of the shielding assembly. A change to a silicon surface barrier detector might have advantages due to its small size.

d - Remove as much scattering material as possible from the experimental area (not easy because of other uses equipment), so as to decrease as far as possible the back scattered neutrons.

e - Decrease the beam tube length and build it up from stainless steel so as to decrease the neutron production from D,D reaction (the results of a recent MSc project suggest that the yield of neutrons from a drive-in target is much less for stainless steel than for brass). Also decrease as far as possible the amount of metal near the target to reduce the number of degraded neutrons input to the system.

f - Build up a more nearly spherical shielding so it will be comparable with that used in the calculation. This could be done by using different lengths of tubes containing LiF.

g - From the point of view of shielding a three region shield could be tried. The first from a heavy material (U^{238}) for rapid energy degradation by inelastic scattering, and increase the neutron yield by fast fission and so aid tritium breeding, the second from a

lighter (LiF) material for slowing down by elastic scattered and produce more tritium, and the outer region from a heavy material to absorb the gamma rays produced in the previous layers.

h - If improved calculation methods could be adopted a single slab shield could be tried. The main advantage of this would be economy in materials and ease of construction.

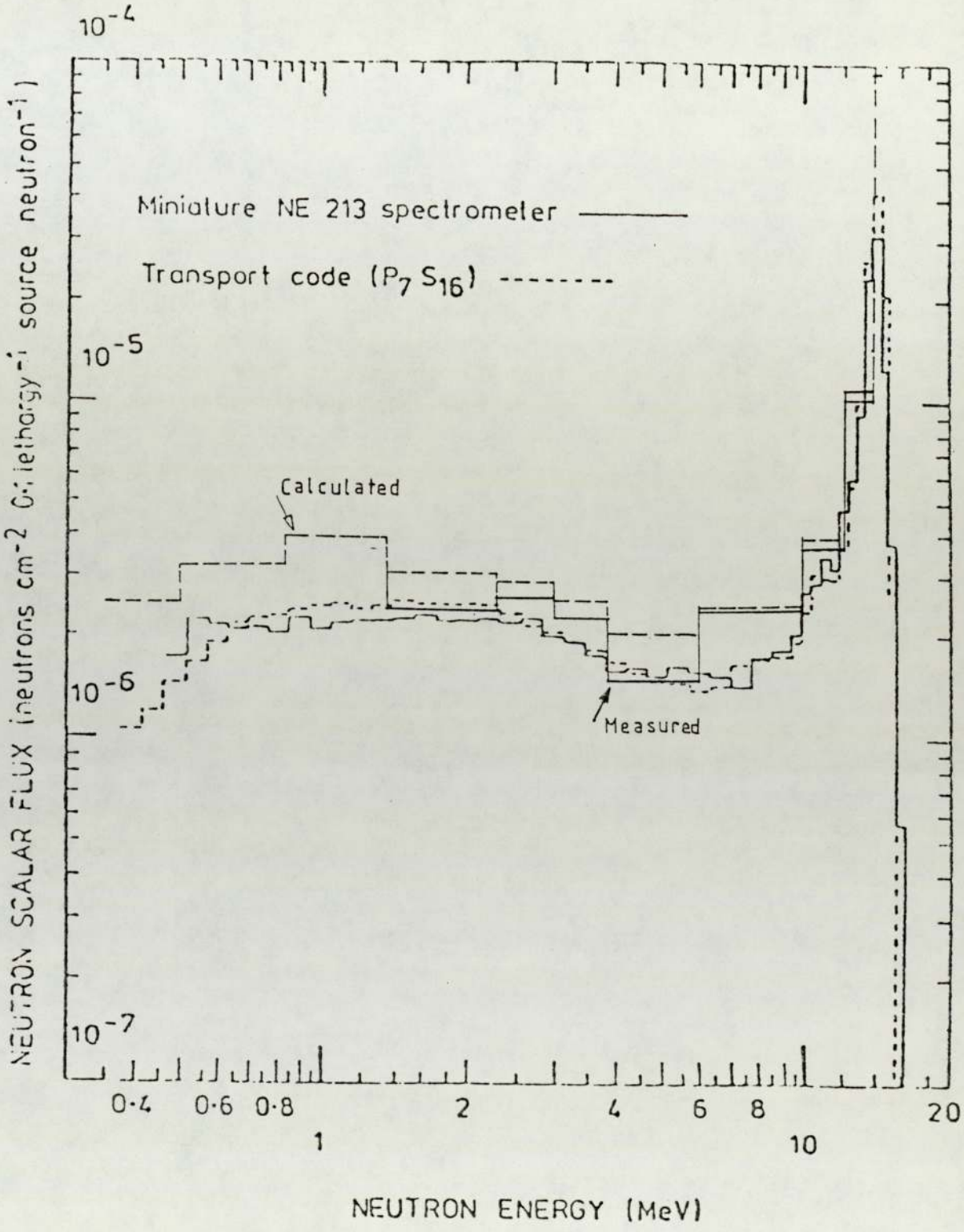

Fig. [8-1] Comparison between a Measured and Calculated Neutron Spectrum.

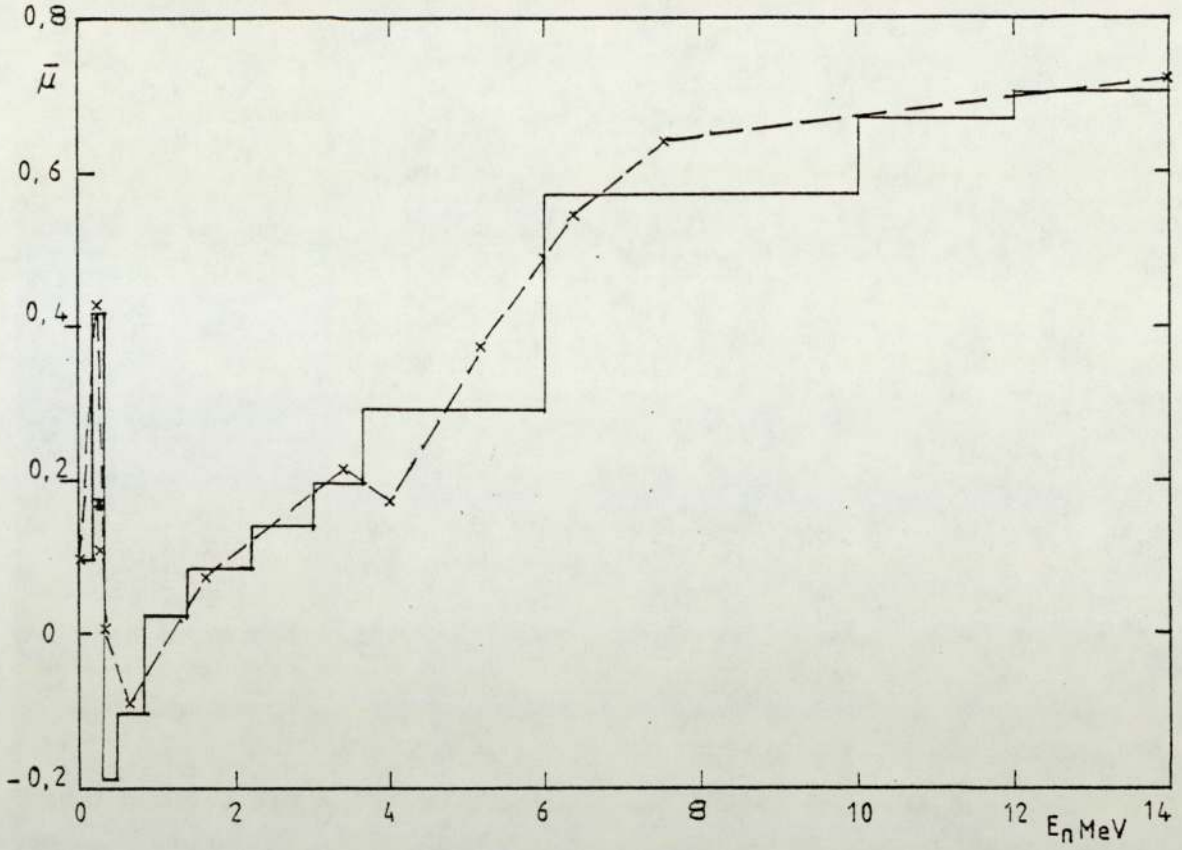

Fig. [8-2] The Mean Cosine of the Scattering Angle various the Neutron Energy for ^{7}Li.

-------- x ENDF/B - 1V file - UKNDL

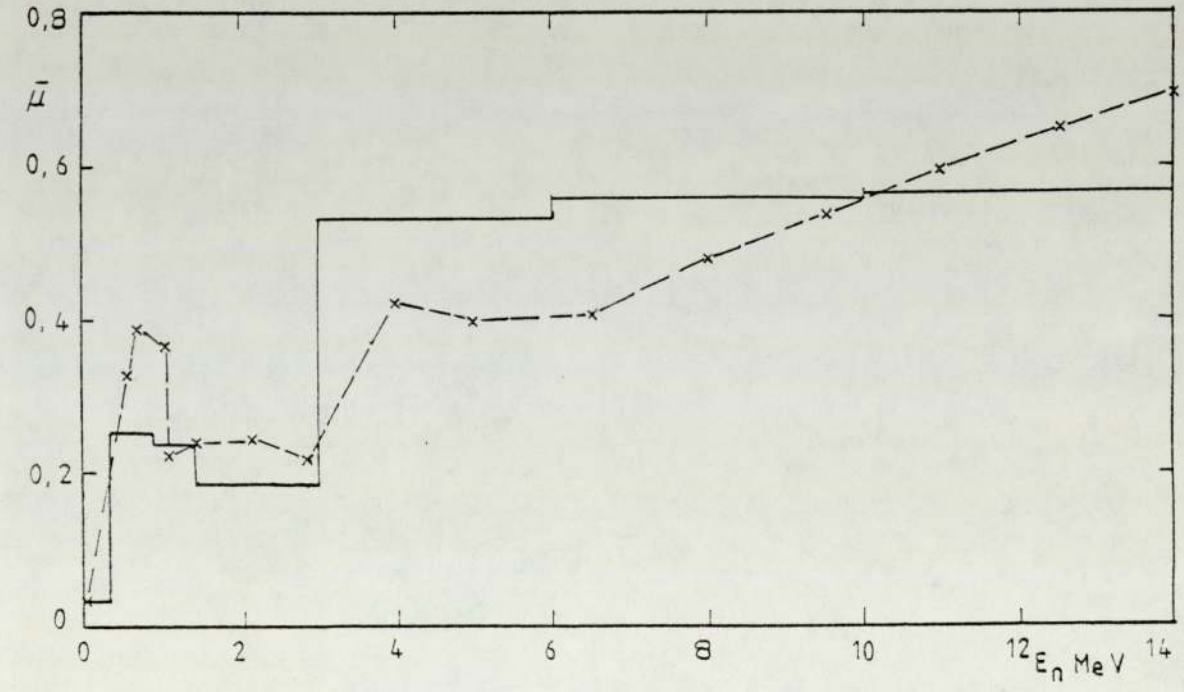

Fig. [8-3] The Mean Cosine of the Scattering Angle various the Neutron Energy for ^{19}F.

-------- x ENDF/B - 1V file - UKNDL

APPENDIX 1

PROGRAM NEUTRON: Transform of pulse amplitude distribution into neutron energy distribution by differential method.

```
'BEGIN'
'COMMENT' TRANSFORMATION OF PULSE
AMPLITUDE DISTRIBUTION INTO NEUTRON ENERGY DISTRIBUTION BY
DIFFERENTIAL METHOD;
'INTEGER' I,J,K,L,M,JJ,LL,MIN,MAX,LOG,J1,J2,IROW,L1,L2,K1,K2,LMAX,C12;
'REAL' G,SS,Q,F,CM,AR,FLOT,EMAX,DV,DL,DLL,FL,D,E;
'REAL' 'ARRAY' NEUL1:4],NL1:11,EPS[0:150],SCFL[:30],EB[2:20],CF[0:31];
'INTEGER' 'ARRAY' NJ[1:500];
Q:=1&9;
G:=1.1385;
AR:=1;
EPS[0]:=5.01359;EPS[1]:=2.76532;EPS[2]:=2.09901;EPS[3]:=1.76400;
EPS[4]:=1.54517;EPS[5]:=1.37350;EPS[6]:=1.21832;EPS[7]:=1.09308;
EPS[8]:=1.01182;EPS[9]:=0.95635;EPS[10]:=0.90356;EPS[11]:=0.85350;
EPS[12]:=0.79648;EPS[13]:=0.74712;EPS[14]:=0.72141;EPS[15]:=0.65517;
EPS[16]:=0.61543;EPS[17]:=0.60516;EPS[18]:=0.57310;EPS[19]:=0.54373;
EPS[20]:=0.52060;EPS[21]:=0.49617;EPS[22]:=0.47052;EPS[23]:=0.45214;
EPS[24]:=0.43352;EPS[25]:=0.41562;EPS[26]:=0.39918;EPS[27]:=0.38328;
EPS[28]:=0.36965;EPS[29]:=0.35656;EPS[30]:=0.34137;
EB[2]:=0.825;EB[3]:=1.35;EB[4]:=2.225;EB[5]:=3.66;
EB[6]:=3.668;EB[7]:=6.00;EB[8]:=10.00;EB[9]:=12.00;
EB[10]:=12.50;EB[11]:=13.00;EB[12]:=13.50;EB[13]:=14.00;
EB[14]:=14.50;EB[15]:=15.00;EB[16]:=15.50;EB[17]:=16.00;
EB[18]:=16.50;
NEXT:
FLOT :=READ; 'COMMENT' NUMBER OF EXPERIMENT;
'IF' FLOT <0 'THEN' 'GOTO' FINAL;
EMAX:=READ; 'COMMENT' COMPTON EDGE ENERGY FOR CALIBRATION;
K:=READ; 'COMMENT' CHANNEL NUMBER AT COMPTON EDGE;
I:=READ; 'COMMENT' INITIAL CHANNEL NUMBER OF INTEREST;
J:=READ; 'COMMENT' FINAL CHANNEL NUMBER OF INTEREST;
CM:=READ; 'COMMENT' ALPHA PARTICLE MONITOR COUNTS;
DV:=EMAX/K;
F:=G/(Q*CM*AR);
```

```
NEWLINE(4);
WRITETEXT ('(' EXPERIMENT%%NUMBER%=')');
PRINT(FLOT,3,0);
NEWLINE (2);
WRITETEXT('('EMAX%%=')');
PRINT(EMAX,2,3);
WRITETEXT('('MEV')');
SPACE (4);
WRITETEXT ('('K%%=')');
PRINT (K,3,0);
SPACE (4);
WRITETEXT('('CHANNEL%WIDTH%%=')');
PRINT(DV,1,3);
WRITETEXT('('MEV%P%CHANNEL')');
NEWLINE (2);
WRITETEXT ('('Q%%=')');
PRINT (Q,0,3);
SPACE (4);
WRITETEXT ('('GEOMETRY%%FACTOR%=')');
PRINT (G,0,4);
SPACE (4);
WRITETEXT ('('ALPHA%MONITOR%COUNTS%=')');
PRINT (CM,0,4);
SPACE (4);
WRITETEXT ('('CORRECTION%FACTOR%=')');
PRINT (F,2,4);
'BEGIN'
'REAL' 'ARRAY'COUNT,C,EE,EP,DPDE,A,EFF,DDVA,NF,NFC,NFA,CA,NFA2,
CB,EFFN,B,CMULT[I:J],CFC[I:J];
'FOR' M:=I 'STEP' 1 'UNTIL' J 'DO'
'BEGIN'
EE[M]:=M*DV;  'COMMENT' ELECTRON ENERGY IN CHANNEL M;
'IF' EE[M] 'LE'  1.85 'THEN'
EP[M]:=5.48*(EE[M]+0.667)
```

```
'ELSE'
EP[M]:=1.78*(EE[M]+1.1);  'COMMENT' PROTON ENERGY IN CHANNEL M;
'IF' EP[M] 'LE' 5.25 'THEN'
DPDE[M]:=0.245*EP[M]+0.5
'ELSE'
DPDE[M]:=0.564;
'END';
'FOR' M:=I 'STEP' 1 'UNTIL' J 'DO'
'BEGIN'
L:=ENTIER(EP[M]*2);
'IF' L 'GT' 29 'THEN' L:=29;
DL:=EP[M]*2-L;
EFFN[M]:=EPS[L]*(1-DL)+EPS[L+1]*DL;
'END';
'FOR' M:=I 'STEP' 1 'UNTIL' J 'DO'
'BEGIN'
COUNT[M]:=READ;
L:=ENTIER(COUNT[M]*16-6);
COUNT[M]:=COUNT[M]-L*16;
CA[M]:=COUNT[M];
'END';
JJ:=0;
AGAIN:
CB[I]:=(64*CA[I]+30*CA[I+1]+6*CA[I+2]-8*CA[I+3]-12*CA[I+4]-6*CA[I+5]
      +10*CA[I+6])/84;
CB[I+1]:=(30*CA[I]+24*CA[I+1]+18*CA[I+2]+12*CA[I+3]+6*CA[I+4]
      -6*CA[I+6])/84;
CB[I+2]:=(6*CA[I]+18*CA[I+1]+24*CA[I+2]+24*CA[I+3]+18*CA[I+4]+6*CA[I+5]
      -12*CA[I+6])/84;
'FOR' M:=I+3 'STEP' 1 'UNTIL' J-3 'DO'
CB[M]:=(-2*CA[M-3]+3*CA[M-2]+6*CA[M-1]+7*CA[M]+6*CA[M+1]+3*CA[M+2]
      -2*CA[M+3])/21;
CB[J-2]:=(-12*CA[J-6]+6*CA[J-5]+18*CA[J-4]+24*CA[J-3]+24*CA[J-2]
      +18*CA[J-1]+6*CA[J])/84;
```

```
CB[J-1]:=(-6*CA[J-6]+5*CA[J-4]+12*CA[J-3]+18*CA[J-2]+24*CA[J-1]
      +30*CA[J])/84;
CB[J]:=(10*CA[J-6]-6*CA[J-5]-12*CA[J-4]-3*CA[J-3]+6*CA[J-2]+30*CA[J-1]
      +64*CA[J])/84;
'FOR' M:=I 'STEP' 1 'UNTIL' J 'DO'
CA[M]:=CB[M];
JJ:=JJ+1;
'IF' JJ>4 'THEN' 'GOTO' PASS;
'GOTO' AGAIN;
PASS:
'FOR' M:=I 'STEP' 1 'UNTIL' J 'DO'
CB[M]:=CB[M]*DPDE[M];
DDVA[I]:=(-39*CB[I]-6*CB[I+1]+15*CB[I+2]+24*CB[I+3]+21*CB[I+4]+6*CB[I+5]
      -21*CB[I+6])/84;
DDVA[I+1]:=(-29*CB[I]-6*CB[I+1]+9*CB[I+2]+16*CB[I+3]+15*CB[I+4]
      +6*CB[I+5]-11*CB[I+6])/84;
DDVA[I+2]:=(-19*CB[I]-6*CB[I+1]+3*CB[I+2]+8*CB[I+3]+9*CB[I+4]+6*CB[I+5]
      -CB[I+6])/84;
'FOR' M:=I+3 'STEP' 1 'UNTIL' J-3 'DO'
DDVA[M]:=(-3*CB[M-3]-2*CB[M-2]-CB[M-1]+CB[M+1]+2*CB[M+2]+3*CB[M+3])/28;
DDVA[J-2]:=(CB[J-6]-6*CB[J-5]-9*CB[J-4]-8*CB[J-3]-3*CB[J-2]+6*CB[J-1]
      +19*CB[J])/84;
DDVA[J-1]:=(11*CB[J-6]-6*CB[J-5]-15*CB[J-4]-16*CB[J-3]-9*CB[J-2]
      +6*CB[J-1]+29*CB[J])/84;
DDVA[J]:=(21*CB[J-6]-6*CB[J-5]-21*CB[J-4]-24*CB[J-3]-15*CB[J-2]
      +6*CB[J-1]+39*CB[J])/84;
'FOR' M:=I 'STEP' 1 'UNTIL' J 'DO'
'BEGIN'
      B[M]:=1;
NFC[M]:=-EP[M]*DDVA[M]*DPDE[M]*F/(EFFN[M]*B[M]*DV*DV);
'END';
L:=2; M:=I;
S1:
'IF' EB[L] 'GT' EP[M] 'THEN' 'GOTO' S2 'ELSE'
```

```
'BEGIN'
L:=L+1;
'GOTO' S1;
'END';
S2:
L1:=L-1; NJ[L1]:=1;
S3:
'IF' EP[M] 'GT' EP[L] 'THEN' 'GOTO' S4 'ELSE'
M:=M+1;
'IF' M 'GT' J 'THEN' 'GOTO' S5 'ELSE' 'GOTO' S3;
S4:
NJ[L]:=M; L:=L+1;
'IF' L 'GT' LMAX 'THEN' 'GOTO' S5 'ELSE' 'GOTO' S3;
S5:
L2:=L; NJ[L2]:=J;
'FOR' L:=L1 'STEP' 1 'UNTIL' L2-1 'DO'
'BEGIN'
FL:=0;
K1:=NJ[L]; K2:=NJ[L+1];
'FOR' M:=NJ[L] 'STEP' 1 'UNTIL' NJ[L+1]-1 'DO'
FL:=FL+NFC[M]*(EP[M+1]-EP[M]);
NEWLINE(1);
PRINT(EP[K1],2,3);
PRINT(EP[K2],2,3);
PRINT(FL/(EP[K2]-EP[K1]),0,4);
'END';
'END';
'GOTO' NEXT;
FINAL:
'END';
****
```

APPENDIX 2

The solution of the diffusion equation by the finite difference method.

Equation 6-30, Chapter 6

$$a_{1n}\,\Phi_{n-1} + a_{2n}\,\Phi_n + a_{3n}\,\Phi_{n+1} = S_n \qquad \ldots\ldots\ldots\ldots \text{6-30}$$

For the inner radius when n = mh, we get for no neutrons current (i.e. no internal neutron source), at the inner radius

$$\Phi_{M-1} = \Phi_M$$

$$(a_{1M} + a_{2M})\,\Phi_M + a_{3M}\,\Phi_{M+1} = S_M \qquad \ldots\ldots\ldots\ldots \text{A2-1}$$

and for n = M + 1, and n = M + 2, we get

$$(a_{1M+1})\,\Phi_M + a_{2M+1}\,\Phi_{M+1} + a_{3M+1}\,\Phi_{M+2} = S_{M+1} \qquad \ldots\ldots\ldots\ldots \text{A2-2}$$

$$a_{1M+2}\,\Phi_{M+1} + a_{2M+2}\,\Phi_{M+2} + a_{3M+2}\,\Phi_{M+3} = S_{M+2} \qquad \ldots\ldots\ldots\ldots \text{A2-3}$$

and so on up to n = N

$$a_{1N}\,\Phi_{N-1} + a_{2N}\,\Phi_N + a_{3N}\,\Phi_{N+1} = S_N \qquad \ldots\ldots\ldots\ldots \text{A2-4}$$

for the outer boundary, the flux becomes zero at a distance λ (the linear extrapolation distance) given by a

λ = 2.13d beyond Nh

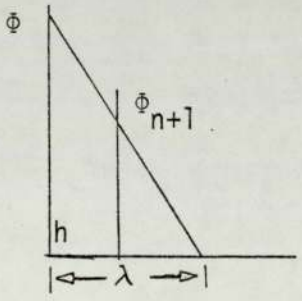

therefore

$$\Phi_{N+1} = \Phi_N \left(1 - \frac{h}{\lambda}\right)$$

$$\Phi_N \left(1 - \frac{h}{2.13d}\right) - \Phi_{N+1} = 0 \qquad \ldots\ldots\ldots\ldots \text{A2-5}$$

equation A2-1, A2-2, A2-3, A2-4, A2-5, build up in a matrix form as follows:

$$\begin{vmatrix} a_{1M}+a_2 & a_{3M} & 0 & 0 & 0 & 0 \\ a_{1M+1} & a_2 & a_{3M+1} & 0 & 0 & 0 \\ 0 & a_{1M+2} & a_2 & a_{3M+2} & 0 & 0 \\ 0 & 0 & a_{1M+3} & a_2 & a_{3M+3} & 0 \\ 0 & 0 & 0 & a_{1N} & a_2 & a_{3N} \\ 0 & 0 & 0 & 0 & 1-\frac{h}{2.13d} & -1 \end{vmatrix} \begin{vmatrix} \Phi_M \\ \Phi_{M+1} \\ \Phi_{M+2} \\ \Phi_{M+3} \\ \Phi_N \\ \Phi_{N+1} \end{vmatrix} = \begin{vmatrix} S_M \\ S_{M+1} \\ S_{M+2} \\ S_{M+3} \\ S_N \\ 0 \end{vmatrix}$$

1 - divided row 1 by $a_2 + a_{1M}$

$$\begin{vmatrix} 1 & \frac{a_{3M}}{a_2+a_{1M}} & 0 & 0 \\ a_{1M+1} & a_2 & a_{3M+1} & 0 \end{vmatrix} \begin{vmatrix} \Phi_M \\ \Phi_{M+1} \end{vmatrix} = \begin{vmatrix} \frac{S_M}{a_2+a_{1M}} \\ S_{M+1} \end{vmatrix}$$

let

$$A_M = \frac{a_{3M}}{a_2 + a_{1M}} \qquad \text{..... A2-6}$$

and

$$B_M = \frac{S_M}{a_2 + a_{1M}} \qquad \text{..... A2-7}$$

A_M is the negative of A_M used in the computer program Appendix 4 and Appendix 5.

2 - multiply first row by $-a_{1M+1}$ and added to the second row.

$$\begin{vmatrix} 1 & A_M & 0 & 0 \\ 0 & a_2-B_M\ a_{1M+1} & a_{3M+1} & 0 \end{vmatrix} \begin{vmatrix} \Phi_M \\ \Phi_{M+1} \end{vmatrix} = \begin{vmatrix} B_M \\ S_{M+1}-A_M\ a_{1M+1} \end{vmatrix}$$

3 - divided row two by diagonal element, and let

$$A_{M+1} = \frac{a_{3M+1}}{a_2 - A_M a_{1M+1}} \qquad \text{..... A2-8}$$

and

$$B_{M+1} = \frac{S_{M+1} - B_M a_{1M+1}}{a_2 - A_M a_{1M+1}} \qquad \text{..... A2-9}$$

$$\begin{vmatrix} 1 & A_M & 0 & 0 \\ 0 & 1 & A_{M+1} & 0 \\ 0 & a_{1M+2} & a_2 & a_{3M+2} \end{vmatrix} \quad \begin{vmatrix} \Phi_M \\ \Phi_{M+1} \\ \Phi_{M+2} \end{vmatrix} = \begin{vmatrix} B_M \\ B_{M+1} \\ B_{M+2} \end{vmatrix}$$

4 - by repeat steps 2, and 3 for each line in turn and in general but

$$A_n = \frac{a_{3n}}{a_2 - A_{n-1} a_{1n}} \qquad \text{..... A2-10}$$

$$B_n = \frac{S_n - B_{n-1} a_{1n}}{a_{2n} - A_{n-1} a_{1n}} \qquad \text{..... A2-11}$$

These recurrence relationships can be used from

n = M to N for A and

n = M to N+1 for B, by defining

$$A_{M-1} = -1$$

$$B_{M-1} = 0$$

This gives the anxiling matrix equation

$$\begin{vmatrix} 1 & A_M & 0 & 0 & 0 & 0 & 0 & 0 \\ 0 & 1 & A_{M+1} & 0 & 0 & 0 & 0 & 0 \\ 0 & 0 & 1 & A_{M+2} & 0 & 0 & 0 & 0 \\ 0 & 0 & 0 & 1 & A_{M+3} & 0 & 0 & 0 \\ 0 & 0 & 0 & 0 & 0 & 1 & A_{N-1} & 0 \\ 0 & 0 & 0 & 0 & 0 & 0 & 1 & A_N \\ 0 & 0 & 0 & 0 & 0 & 0 & 0 & 1 \end{vmatrix} \begin{vmatrix} \Phi_M \\ \Phi_{M+1} \\ \Phi_{M+2} \\ \Phi_{M+3} \\ \Phi_{N-1} \\ \Phi_N \\ \Phi_{N+1} \end{vmatrix} = \begin{vmatrix} B_M \\ B_{M+1} \\ B_{M+2} \\ B_{M+3} \\ B_{N-1} \\ B_N \\ B_{N+1} \end{vmatrix}$$

Hence

$$\Phi_{N+1} = B_{N+1}$$

but

$$B_{N+1} = \frac{B_N(1 - \frac{h}{2.13d})}{1 + A_N(1 - \frac{h}{2.13d})} \qquad \text{..... A2-12}$$

and

$$\Phi_N = \frac{\Phi_{N+1}}{(1 - h/2.13d)} \qquad \text{..... A2-13}$$

therefore

$$\Phi_N = \frac{B_N}{1 + A_N(1 - h/2.13d)} \qquad \text{..... A2-14}$$

and it is therefore not necessary to find Φ_{N+1} or B_{N+1}.

$$\Phi_{N-1} + A_{N-1}\,\Phi_N = B_{N-1}$$

$$\Phi_{N-1} = B_{N-1} - A_{N-1}\,\Phi_N$$

and the general relationship is

$$\Phi_n = B_n - A_n\,\Phi_{N+1} \qquad \text{..... A2-15}$$

If there is a source of neutron Φ at the centre of the sphere, the current at the inner boundary is $\frac{\Phi}{4\pi h^2 M^2}$, which is equal to

$- D \frac{d\Phi}{dr}$

$$- D \frac{d\Phi}{dr} = D \frac{(\Phi_{M-1} - \Phi_M)}{h} \qquad \text{..... A2-16}$$

The equation (6-29) for the inner boundary ($1- = Mh$) is now

$$[- \frac{D}{h^2} (1-\frac{1}{M}) - (\frac{2D}{h^2} + \Sigma)] \Phi_M - \frac{D}{h^2} (1+\frac{1}{M}) \Phi_{M+1}$$

$$= S_M + \frac{\Phi}{4\pi h^3 M^2} (1- \frac{1}{M}) \qquad \text{..... A2-17}$$

or

$$(a_{1M} + a_{2M}) \Phi_M + a_{3M} \Phi_{M+1} = S_M + \frac{\Phi}{4\pi h^3 M^2} (1 - \frac{1}{M}) \qquad \text{..... A2-18}$$

This leaves A_M unchanged and B_M can be calculated by putting

$$B_{M-1} = \frac{\Phi}{4\pi M^2 hD}$$

For the two region, the boundary between materials 1 and 2 at n = J, equation 6-31, 6-32 and 6-33 becomes

$$a_{1J} = - \frac{D1}{h^2} (1 - \frac{1}{J}) \qquad \text{..... A2-19}$$

$$a_{2J} = \left[(\frac{D_1+D_2}{h^2}) + \frac{\Sigma_1+\Sigma_2}{2} \right] \qquad \text{..... A2-20}$$

$$a_{3J} = - \frac{D^2}{h^2} (1 + \frac{1}{J}) \qquad \text{..... A2-21}$$

and

$$S_J = \frac{S_{J1} + S_{J2}}{2} \qquad \text{..... A2-22}$$

APPENDIX 3

Multigroup Fast neutron Data Preparation

```
UAALGOL
'BEGIN'  'COMMENT' MULTIGROUP FAST NEUTRON DATA PREPARATION;
'INTEGER' G,I,J,K,NMAT;
'REAL' ND,DR,Q,AA,BB,Z,Y,U,RX;
G:=READ; 'COMMENT'NUMBER OF ENERGY GROUPS;
NMAT:=READ; 'COMMENT' NUMBER OF MATERIALS;
'BEGIN'
'REAL''ARRAY'SFIS,SCAP,STR,SEL,SINT,MU,NU,FIS,NUF,CAP,TR,EL,REM,X,SC,
              MSC,D[1:G],P[1:G,1:G],
SCAT[1:G-1,2:G],P[1:G,1:G],SC[1:G+1];
RX:=0;
'FOR' I:=1 'STEP' 1 'UNTIL' G 'DO'
'BEGIN'
              SC[I]:=0;
              MSC[I]:=0;
              FIS[I]:=0;
              NUF[I]:=0;
      CAP[I]:=0;
      TR[I]:=0;
      EL[I]:=0;
      REM[I]:=0;
'END';
'FOR' I:=1 'STEP' 1 'UNTIL' G-1 'DO'
'FOR' J:=I+1 'STEP' 1 'UNTIL' G 'DO'
SCAT[I,J]:=0;
'FOR' K:=1 'STEP' 1 'UNTIL' NMAT 'DO'
'BEGIN'
      ND:=READ; 'COMMENT' NUMBER DENSITY;
      'FOR' I:=1 'STEP' 1 'UNTIL' G 'DO'
      'BEGIN'
            MU[I]:=READ; 'COMMENT' MEAN SCATTERING COSINE;
            NU[I]:=READ; 'COMMENT' NEUTRONS PER FISSION;
            SFIS[I]:=READ; 'COMMENT' MICROSCOPIC FISSION;
```

```
                STR[I]:=READ; 'COMMENT' MICROSCOPIC TRANSPORT;
                SEL[I]:=READ; 'COMMENT' MICROSCOPIC ELASTIC;
                SCAP[I]:=READ; 'COMMENT' MICROSCOPIC CAPTURE;
                SINT[I]:=READ; 'COMMENT' MICROSCOPIC INELASTIC TOTAL;
                'FOR' J:=1 'STEP' 1 'UNTIL' G 'DO'
                P[I,J]:=READ; 'COMMENT' INELASTIC PROBABILITIES;
        'FOR' J:=1 'STEP' 1 'UNTIL' G 'DO'
        PE[I,J]:=READ;  'COMMENT' ELASTIC PROBABILITIES;
        'END';
RX:=RX+STR[I]*ND;
        'FOR' I:=1 'STEP' 1 'UNTIL' G 'DO'
        'BEGIN'
                CAP[I]:=CAP[I]+SCAP[I]*ND;
AA:=(STR[I]-SINT[I]-SCAP[I]-SFIS[I])*ND;
                BB:=AA/(1-MU[I]);
                TR[I]:=TR[I]+AA;
                SC[I]:=SC[I]+BB;
                MSC[I]:=MSC[I]+BB*MU[I];
                AA:=SFIS[I]*ND;
                FIS[I]:=FIS[I]+AA;
               NUF[I]:=NUF[I]+AA*NU[I];
                EL[I]:=EL[I]+SEL[I]*ND;
                REM[I]:=REM[I]+SINT[I]*ND*(1-PE[I,I]);
        'END';
        'FOR' I:=1 'STEP' 1 'UNTIL' G-1 'DO'
        'FOR' J:=I+1 'STEP' 1 'UNTIL' G 'DO'
SCAT[I,J]:=SCAT[I,J]+ND*(SINT[I]*P[I,J]+SEL[I]*PE[I,J]);
'END';
'FOR' I:=1 'STEP' 1 'UNTIL' G 'DO'
'BEGIN'
        REM[I]:=REM[I]+EL[I]+CAP[I]+FIS[I];
        MU[I]:=MSC[I]/SC[I];
Y:=REM[I]/SC[I];
W:=0.21;
```

```
AA:=0.9;
'FOR' W:=W+0.05 'WHILE' AA 'LE' 1 'DO'
'BEGIN'
Z:=SQRT(Y/W);
AA:=EXP(2*Z*(1+5*W*MU[I])/(1+5*W*MU[I]*(1+Y)))*(1+Y-Z)/(1+Y+Z);
BB:=W-0.06;
'END';
W:=BB;
AA:=0.9;
'FOR' W:=W+0.01 'WHILE' AA 'LE' 1 'DO'
'BEGIN'
Z:=SQRT(Y/W);
AA:=EXP(2*Z*(1+5*W*MU[I])/(1+5*W*MU[I]*(1+Y)))*(1+Y-Z)/(1+Y+Z);
BB:=W-0.011;
'END';
W:=BB;
AA:=0.9;
'FOR' W:=W+0.001 'WHILE' AA 'LE' 1 'DO'
'BEGIN'
Z:=SQRT(Y/W);
AA:=EXP(2*Z*(1+5*W*MU[I])/(1+5*W*MU[I]*(1+Y)))*(1+Y-Z)/(1+Y+Z);
BB:=W-0.001;
'END';
D[I]:=BB/SC[I];
'END';
'FOR' I:=1 'STEP' 1 'UNTIL' 6 'DO'
'BEGIN'
NEWLINE(2);
PRINT(NUF[I],1,6);
PRINT(REM[I],1,6);
PRINT(D[I],1,6);
NEWLINE(1);
'FOR' J:=I+1 'STEP' 1 'UNTIL' 6 'DO'
'BEGIN'
```

```
NEWLINE(1);
PRINT(SCATT,JJ,1,6);
'END';
'END';
NEWLINE(2);
PRINT(KX,1,6);
'END';
'END';
***
```

APPENDIX 4

Multigroup diffusion by finite difference, spherical, one region

```
'BEGIN'
'COMMENT' MULTIGROUP DIFFUSION BY FINITE DIFFERENCE,
          SPHERICAL, ONE REGION, CENTRAL POINT SOURCE;
'INTEGER' G,I,J,K,L,M,N,NSTOP,ITN,N1,N2,N3,N4,N5,N6,N7,N8,N9,N10,N11,
          N12;
'REAL' DR,RX;
G:=READ;  'COMMENT' NUMBER OF ENERGY GROUPS;
'BEGIN'
'REAL' 'ARRAY' EB[1:G+1],X,SF,NUF,REM,D[1:G],SCAT[1:G-1,2:G],Q[1:11];
'FOR' I:=1 'STEP' 1 'UNTIL' G 'DO' SF[I]:=READ;
'FOR' I:=1 'STEP' 1 'UNTIL' G 'DO' X[I]:=READ;
'COMMENT' FRACTION OF FISSION NEUTRONS IN EACH GROUP;
'FOR' I:=1 'STEP' 1 'UNTIL' G+1 'DO' EB[I]:=READ;
'COMMENT' GROUP ENERGY BOUNDARIES IN MEV;
Q[1]:=READ;  'COMMENT' TOTAL NEUTRONS FROM POINT SOURCE;
'FOR' I:=2 'STEP' 1 'UNTIL' 11 'DO'
Q[I]:=READ;
NSTOP:=READ;  'COMMENT' NUMBER OF ITERATIONS, 1 IF NO FISSION;
'FOR' I:=1 'STEP' 1 'UNTIL' G 'DO'
'BEGIN'
NUF[I]:=READ;  REM[I]:=READ;  D[I]:=READ;
'FOR' J:=I+1 'STEP' 1 'UNTIL' G 'DO'
SCAT[I,J]:=READ;
'END';
RX:=READ;
NEXT:
M:=READ;  'IF' M<0 'THEN' 'GOTO' LAST;
N:=READ;  DR:=READ;
NEWLINE(1);
WRITETEXT('('INNER%%BOUNDARY=')');
PRINT(M*DR,3,2);  WRITETEXT('('CM')');
NEWLINE(1);
WRITETEXT('('OUTER%%BOUNDARY=')');
PRINT(N*DR,3,2);  WRITETEXT('('CM')');
```

```
N1:=READ;  N2:=READ;  N3:=READ;  N4:=READ;  N5:=READ;  N6:=READ;
N7:=READ;  N8:=READ;  N9:=READ;  N10:=READ;  N11:=READ;  N12:=READ;
'BEGIN'
'REAL' 'ARRAY' A,B[M-1:N],F[1:G,M:N],SCE[M:N];
'FOR' J:=M 'STEP' 1 'UNTIL' N 'DO'
F[1,J]:=Q[1]*EXP(-RX*DR*(J-M))/(12.568*DR*DR*J*J);
ITN:=1;
ITERATE:
I:=2;
AGAIN:
A[M-1]:=1;
B[M-1]:=Q[I]/(12.568*DR*DR*M*M*D[I]);
'FOR' J:=M 'STEP' 1 'UNTIL' N 'DO'
'BEGIN'
SCE[J]:=SF[I];
'FOR' K:=1 'STEP' 1 'UNTIL' I-1 'DO'
SCE[J]:=SCE[J]+SCAT[K,I]*F[K,J];
'IF'ITN>1 'THEN''FOR' K:=1 'STEP' 1 'UNTIL' G 'DO'
SCE[J]:=SCE[J]+X[I]*NUF[K]*F[K,J];
'END';
'FOR' J:=M 'STEP' 1 'UNTIL' N 'DO'
'BEGIN'
A[J]:=(J+1)/(J*(2+REM[I]*DR*DR/D[I])-(J-1)*A[J-1]);
B[J]:=A[J]*((J-1)*B[J-1]+J*SCE[J]*DR*DR/D[I])/(J+1);
'END';
F[I,N]:=B[N]/(1+A[N]*(DR/(2.75*D[I])-1));
'FOR' J:=N-1 'STEP' -1 'UNTIL' M 'DO'
F[I,J]:=A[J]*F[I,J+1]+B[J];
I:=I+1;
'IF' I 'LE' G 'THEN' 'GOTO' AGAIN;
ITN:=ITN+1;
'IF' ITN 'LE' NSTOP 'THEN' 'GOTO' ITERATE;
NEWLINE(2);
SPACE(25);
```

```
PRINT(N1*DR,2,1);
SPACE(5);
PRINT(N2*DR,2,1);
SPACE(5);
PRINT(N3*DR,2,1);
SPACE(5);
PRINT(N4*DR,2,1);
SPACE(5);
PRINT(N5*DR,2,1);
SPACE(5);
PRINT(N6*DR,2,1);
NEWLINE(1);
SPACE(25);
PRINT(N7*DR,2,1);
SPACE(5);
PRINT(N8*DR,2,1);
SPACE(5);
PRINT(N9*DR,2,1);
SPACE(5);
PRINT(N10*DR,2,1);
SPACE(5);
PRINT(N11*DR,2,1);
SPACE(5);
PRINT(N12*DR,2,1);
SPACE(5);
PRINT(N*DR,2,1);
NEWLINE(1);
'FOR' I:=1 'STEP' 1 'UNTIL' 6 'DO'
'BEGIN'
NEWLINE(1);
PRINT(I,2,0);
PRINT(EB[I],2,3);
PRINT(EB[I+1],2,3);
PRINT(F[I,N1]/(EB[I]-EB[I+1]),0,3);
```

```
PRINT(F[I,N2]/(EB[I]-EB[I+1]),0,3);
PRINT(F[I,N3]/(EB[I]-EB[I+1]),0,3);
PRINT(F[I,N4]/(EB[I]-EB[I+1]),0,3);
PRINT(F[I,N5]/(EB[I]-EB[I+1]),0,3);
PRINT(F[I,N6]/(EB[I]-EB[I+1]),0,3);
NEWLINE(1);
SPACE(23);
PRINT(F[I,N7]/(EB[I]-EB[I+1]),0,3);
PRINT(F[I,N8]/(EB[I]-EB[I+1]),0,3);
PRINT(F[I,N9]/(EB[I]-EB[I+1]),0,3);
PRINT(F[I,N10]/(EB[I]-EB[I+1]),0,3);
PRINT(F[I,N11]/(EB[I]-EB[I+1]),0,3);
PRINT(F[I,N12]/(EB[I]-EB[I+1]),0,3);
'IF' I=1 'THEN'
PRINT(F[1,N]/(EB[1]-EB[2]),0,3) 'ELSE'
PRINT(F[I,N]/(2.1*(EB[I]-EB[I+1])),0,3);
NEWLINE(1);
'END';
'END';
'GOTO' NEXT;
LAST:
'END';
'END';
****
```

APPENDIX 5

Multigroup diffusion by finite difference,

spherical, two region

```
'BEGIN'
'COMMENT' MULTIGROUP DIFFUSION BY FINITE DIFFERENCE,
          SPHERICAL, TWO REGION, CENTRAL POINT SOURCE;
'INTEGER' G,I,J,K,L,M,N,NSTOP,ITN,N1,N2,N3,N4,N5,N6,N7,N8,N9,N10,N11,
          N12;
'REAL' DR;
G:=READ;  'COMMENT' NUMBER OF ENERGY GROUPS;
'BEGIN'
'REAL' 'ARRAY' RX[1:2],X[1:G],EB[1:G+1],NUF,REM,D[1:G,1:2],
               SCAT[1:G-1,2:G,1:2],Q[1:11],SF[1:G];
'FOR' I:=1 'STEP' 1 'UNTIL' G 'DO' SF[I]:=READ;
'FOR' I:=1 'STEP' 1 'UNTIL' G 'DO' X[I]:=READ;
'COMMENT' FRACTION OF FISSION NEUTRONS IN EACH GROUP;
'FOR' I:=1 'STEP' 1 'UNTIL' G+1 'DO' EB[I]:=READ;
'COMMENT' GROUP ENERGY BOUNDARIES IN MEV;
Q[1]:=READ;  'COMMENT' TOTAL NEUTRONS FROM POINT SOURCE;
'FOR' I:=2 'STEP' 1 'UNTIL' 11 'DO'
Q[I]:=READ;
NSTOP:=READ;  'COMMENT' NUMBER OF ITERATIONS, 1 IF NO FISSION;
'FOR' K:=1,2 'DO'
'BEGIN'
'FOR' I:=1 'STEP' 1 'UNTIL' G 'DO'
'BEGIN'
NUF[I,K]:=READ;  REM[I,K]:=READ;  D[I,K]:=READ;
'FOR' J:=I+1 'STEP' 1 'UNTIL' G 'DO'
SCAT[I,J,K]:=READ;
'END';
RX[K]:=READ;
'END';
NEXT:
M:=READ;  'IF' M<11 'THEN' 'GOTO' LAST;
L:=READ;  N:=READ;  DR:=READ;
NEWLINE(1);
WRITETEXT('('INNER%%BOUNDARY=')');
```

```
PRINT(M*DR,3,2);  WRITETEXT('('CM')');
NEWLINE(1);
WRITETEXT('('MIDDLEXBOUNDARY=')');
PRINT(L*DR,3,2);  WRITETEXT('('CM')');
NEWLINE(1);
WRITETEXT('('OUTERXXBOUNDARY=')');
PRINT(N*DR,3,2);  WRITETEXT('('CM')');
N1:=READ;  N2:=READ;  N3:=READ;  N4:=READ;  N5:=READ;  N6:=READ;
N7:=READ;  N8:=READ;  N9:=READ;  N10:=READ;  N11:=READ;  N12:=READ;
'BEGIN'
'REAL' 'ARRAY' A,B[M-1:N],F[1:G,M:N],SCE1[M:L],SCE2[L:N];
'FOR' J:=M 'STEP' 1 'UNTIL' L-1 'DO'
F[1,J]:=Q[1]*EXP(-RX[1]*DR*(J-M))/(12.568*DR*DR*J*J);
'FOR' J:=L 'STEP' 1 'UNTIL' N 'DO'
F[1,J]:=Q[1]*EXP(-RX[1]*DR*(L-M)-RX[2]*DR*(J-L))/(12.568*DR*DR*J*J);
ITN:=1;
ITERATE:
I:=2;
AGAIN:
A[M-1]:=1;
B[M-1]:=Q[I]/(12.568*DR*DR*M*M*D[1,1]);
'FOR' J:=M 'STEP' 1 'UNTIL' L 'DO'
'BEGIN'
SCE1[J]:=0;
'FOR' K:=1 'STEP' 1 'UNTIL' I-1 'DO'
SCE1[J]:=SCE1[J]+SCAT[K,I,1]*F[K,J];
'IF' ITN>1 'THEN' 'FOR' K:=1 'STEP' 1 'UNTIL' G 'DO'
SCE1[J]:=SCE1[J]+X[I]*NUF[K,1]*F[K,J];
'END';
'FOR' J:=L 'STEP' 1 'UNTIL' N 'DO'
'BEGIN'
SCE2[J]:=SF[I];
'FOR' K:=1 'STEP' 1 'UNTIL' I-1 'DO'
SCE2[J]:=SCE2[J]+SCAT[K,I,2]*F[K,J];
```

```
'IF' ITN>1 'THEN' 'FOR' K:=1 'STEP' 1 'UNTIL' G 'DO'
SCE2[J]:=SCE2[J]+X[I]*NUF[K,J]*F[K,J];
'END';
'FOR' J:=M 'STEP' 1 'UNTIL' L-1 'DO'
'BEGIN'
A[J]:=(J+1)/(J*(2+REM[I,1]*DR*DR/D[I,1])-(J-1)*A[J-1]);
B[J]:=A[J]*((J-1)*B[J-1]+J*SCE1[J]*DR*DR/D[I,1])/(J+1);
'END';
A[L]:=(L+1)/(0.5*(L-1)*D[I,1]*(2+REM[I,1]*DR*DR/D[I,1])/D[I,2]
      +0.5*(L+1)*(2+REM[I,2]*DR*DR/D[I,2])-(L-1)*A[L-1]*D[I,1]/D[I,2]);
B[L]:=A[L]*(0.5*(L-1)*SCE1[L]*DR*D(+0.5*(L+1)*SCE2[L]*DR*DR
      +B[L-1]*D[I,1]*(L-1))/((L+1)*D[I,2]);
'FOR' J:=L+1 'STEP' 1 'UNTIL' N 'DO'
'BEGIN'
A[J]:=(J+1)/(J*(2+REM[I,2]*DR*DR/D[I,2])-(J-1)*A[J-1]);
B[J]:=A[J]*((J-1)*B[J-1]+J*SCE2[J]*DR*DR/D[I,2])/(J+1);
'END';
F[I,N]:=B[N]/(1+A[N]*(DF/(2.15*D[I,2])-1));
'FOR' J:=N-1 'STEP' -1 'UNTIL' M 'DO'
F[I,J]:=A[J]*F[I,J+1]+B[J];
I:=I+1;
'IF' I 'LE' G 'THEN' 'GOTO' AGAIN;
ITN:=ITN+1;
'IF' ITN 'LE' NSTOP 'THEN' 'GOTO' ITERATE;
NEWLINE(2);
SPACE(25);
PRINT(N1*DR,2,1);
SPACE(5);
PRINT(N2*DR,2,1);
SPACE(5);
PRINT(N3*DR,2,1);
SPACE(5);
PRINT(N4*DR,2,1);
SPACE(5);
```

```
PRINT(N5*DR,2,1);
SPACE(5);
PRINT(N6*DR,2,1);
NEWLINE(1);
SPACE(25);
PRINT(N7*DR,2,1);
SPACE(5);
PRINT(N8*DR,2,1);
SPACE(5);
PRINT(N9*DR,2,1);
SPACE(5);
PRINT(N10*DR,2,1);
SPACE(5);
PRINT(N11*DR,2,1);
SPACE(5);
PRINT(N12*DR,2,1);
SPACE(5);
PRINT(N*DR,2,1);
NEWLINE(1);
'FOR' I:=1 'STEP' 1 'UNTIL' 6 'DO'
'BEGIN'
NEWLINE(1);
PRINT(I,2,0);
PRINT(EB[I],2,3);
PRINT(EB[I+1],2,3);
PRINT(F[I,N1]/(EB[I]-EB[I+1]),0,3);
PRINT(F[I,N2]/(EB[I]-EB[I+1]),0,3);
PRINT(F[I,N3]/(EB[I]-EB[I+1]),0,3);
PRINT(F[I,N4]/(EB[I]-EB[I+1]),0,3);
PRINT(F[I,N5]/(EB[I]-EB[I+1]),0,3);
PRINT(F[I,N6]/(EB[I]-EB[I+1]),0,3);
NEWLINE(1);
SPACE(23);
PRINT(F[I,N7]/(EB[I]-EB[I+1]),0,3);
```

```
PRINT(FLI,N8]/(EBLI]-EBL[+1]),0,5);
PRINT(FLI,N9]/(EBLI]-EBL[+1]),0,5);
PRINT(FLI,N10]/(EB[1]-EB[+1]),0,5);
PRINT(FLI,N11]/(EBLI]-EBL[+1]),0,3);
PRINT(FLI,N12]/(EBLI]-EBL[+1]),0,5);
'IF' I=1 'THEN'
PRINT(FL1,N]/(EB[1]-EB[2]),0,5) 'ELSE'
PRINT(FLI,N]/(2.13*(EBLI]-EBL[+1])),0,3);
NEWLINE(1);
'END';
'END';
'GOTO' NEXT;
LAST:
'END';
'END';
****
```

APPENDIX 6

Least square fitting

```
      TRACE2
      MASTER ZAIN
      DIMENSION X(20),F(20),Z(20)
      READ(3,12)NUM
   12 FORMAT(I2)
      SUMZ=0.0
      SUMX=0.0
      SUMXZ=0.0
      SUMX2=0.0
      SUMD=0.0
      DO 14 I=1,NUM
      READ(3,18)F(I),X(I)
   18 FORMAT(F8.1,F6.1)
      Z(I)=ALOG(F(I)*X(I)**2)
      SUMZ=SUMZ+Z(I)
      SUMX=SUMX+X(I)
      SUMXZ=SUMXZ+X(I)*Z(I)
      SUMX2=SUMX2+X(I)*X(I)
   14 CONTINUE
      TERM=NUM*SUMX2-SUMX*SUMX
      A=(NUM*SUMXZ-SUMX*SUMZ)/TERM
      B=(SUMX2*SUMZ-SUMX*SUMXZ)/TERM
      DO 20 I=1,NUM
      D=(A*X(I)+(B-Z(I)))**2
      SUMD=SUMD+D
   20 CONTINUE
      DALTA=SQRT(NUM*SUMD/((NUM-2)*TERM))
      WRITE(6,11)A,B,DALTA
   11 FORMAT(1X,F6.4,2X,F10.3,2X,F6.4)
      DO 15 I=1,20
      READ(3,16)IR
   16 FORMAT(I2)
      FLUX=EXP(A*IR+B)/IR**2
      WRITE(6,13)IR,FLUX
   13 FORMAT(1X,I2,2X,E5.4)
   15 CONTINUE
      STOP
      END
****
```

REFERENCES

1. Sraker, E. A.
Nucl. Sci. and Eng. 34, 114, 1968

2. Yiftah, S. et al
Report IA 980, Nuclear Cross-section for fast reactors.
Israel Atomic Energy Commission 1964

3. UKNDL Cross-section data
obtained from OECD NEA Data Compilation Centre, 1975

4. Darvas, J.
EUR-4873e, report
Commission of the European Communities 1972

5. Tsoulfanides, N. et al
Nucl. Technology 21, 201, 1974

6. Hickman, R. G.
Nucl. Technology 26, 39, 1974

7. Leonard, B. R.
Nucl. Technology 20, 161, 1973

8. Selph, W.
Engineering Compendium on Radiation Shielding
Vol. 1, Chapter 5,
International Atomic Energy Agency, Vienna, 1968

9. Aronson, R. et al
Reactor handbook III, Part B, Chapter 9
Interscience publishers, 1962

10. Goldstein, H.
Principle of Reactor Shielding
Addison-Wesley Publishing Co. 1959

11. Price, B. T. et al
Radiation Shielding
Pergaman Press 1957

12. Glasstone, S. et al
Nuclear Reactor Engineering
D. Van Nostrand Company Inc. 1963

13. Bell, I. G.
LA-3385-Ms. Uc-20, Los Alamos Science
Laboratory, University of California,
U.S.A. 1965

14. Pimentel, C. A. et al
Nucl. Inst. and Method 148, 199, 1978

15. Menlove, H. O. et al
Nucl. Sci. and Eng. 33, 24, 1968

16. Lamarsh, R. J.
Introduction to Nuclear Reactor Theory
Addison-Wesley Publishing Company 1972

17. Brock, H. W. et al
Rev. Sci. Inst. 31, 1063, 1960

18. Brown, L. M.
Phys. Rev. 90, No. 1, 95, 1953

19. Johnson C. H. et al
Rev. Sci. Inst. 27, 468, 1956

20. Batchelor R. et al
Rev. Sci. Inst. 26, 1037, 1955

21. Garber, D. I. et al

Neutron Cross-section Vol. 11, Curves 1976

22. Thomas, A. R. et al

Nucl. Inst. and Methods 17, 97, 1962

23. Spowart, A. R.

Nucl. Inst. and Methods 75, 35, 1969

24. Dalten, A. W.

Nucl. Inst. and Methods 92, 221, 1971

25. Valail, G. S. et al

Nucl. Inst. and Methods 114, 429, 1974

26. Price, W. J.

Nuclear Radiation Detection

McGraw-Hill, Inc. 1964

27. Allen, W. D.

Neutron Detection

George Newnes Ltd., 1960

28. Marion, J. B. et al

Fast Neutron Physics, Part 1

Interscience Publishers Inc. 1960

29. Hill, N. W. et al

Nucl. Inst. and Methods 65, 8, 1968

30. Dorning, J. J. et al

Nucl. Inst. and Methods 145, 337, 1977

31. Toms, M. E.

I.E.E.E. Trans. Nucl. Science N5, 17, 3, 1970

32. Sasamoto, N. et al

Nucl. Inst. and Methods 148, 395, 1978

33. Hiebert, R. D. et al

Nucl. Inst. and Methods 142, 467, 1977

34. Brookes, F. D.

Nucl. Inst. and Methods 4, 151, 1959

35. Wright, G. T.

Proc. Phys. Soc. B49, 358, 1956

36. Verbinski, V. V. et al

Radiation Meas. in Nucl. Power

Inst. of Physics and Physical Society 1966

37. Love, T. A. et al

Rev. of Scien. Inst. 39, 4, 541, 1968

38. Masterson, T. G.

Nucl. Inst. and Method 88, 61, 1970

39. Abd-El-Raseki, M. M. et al

Nucl. Inst. and Method 141, 477, 1977

40. Cambiaghi, M. F. et al

Nucl. Inst. and Method 82, 106, 1970

41. Bonazzola, G. C. et al

Nucl. Inst. and Methods 87, 291, 1970

42. Onge, R. N. et al

Nucl. Inst. and Method 69, 25, 1969

43. Kellermann, H. J. et al

Nucl. Inst. and Method 94, 137, 1971

44. Mubarakmand S. et al

Nucl. Inst. and Method 93, 515, 1971

45. Chalupka, A. et al

Nucl. Inst. and Method 144, 167, 1977

46. Bertin, A. et al

Nucl. Inst. and Method 91, 649, 1971

47. Alexander, T. K. et al

Nucl. Inst. and Method 13, 244, 1961

48. Mathe, G. et al

Nucl. Inst. and Method 27, 10, 1964

49. McBeth et al

Nucl. Inst. and Methods 93, 99, 1971

50. Winyard, R. W. et al

Nucl. Inst. and Methods 95, 141, 1971

51. Tietsch, R. A. et al

I.E.E.E. Trans. on Nucl. Sci. NS-14,1, 131, 1967

52. Miller, T. G.

Nucl. Inst. and Methods 63, 121, 1968

53. Ahmad, M.

Nucl. Inst. and Methods 143, 255, 1977

54. Johnson, D. R. et al

Nucl. Inst. and Methods 75, 61, 1969

55. Maier, K. H. et al

Nucl. Inst. and Methods 59, 227, 1968

56. Savitzky, A. et al

Analyt. Chem. 36,8, 1627, 1964

57. Kazanzkii, Y. A. et al

Translated from Atomnoga Energaga (Soviet Atomic Energy)
20, 2, 143, 1966

58. Dulin, V. A. et al

Translated from Atomoga Energaga (Soviet Atomic Energy)
17, 6, 486, 1964

59. Lorch, E. A.

Inter. J. of Appl. Rad. and Isotop. 24, 585, 1973

60. Societe Anonyme de Machines Electrostiques

Grenoble Press, Paris

61. Al-Saji, A. R.

PhD Thesis, University of Aston in Birmingham, 1976

62. Catalogue of Radioactive Products

The Radio Chemical Centre, Amersham, England, 1965

63. Benvenist, J. et al

U.C.R.1. - 5619, 1959

64. Gunnerson, E. M. et al

Nucl. Inst. and Methods 8, 173, 1960

65. Hughes, D. E.

Pile Neutron Research Publishing Co. Inc. 1953

66. Bonner, T. W. et al

Phys. Rev. 88, 473, 1952

67. Fowler, J. L. et al

Rev. Mod. Phys. 28, 103, 1956

68. Argo M. V. et al

Phys. Rev. 87, 612, 1952

69. Arndid, W. R.

Phys. Rev. 93, 483, 1954

70. Hanson, A. O.

Rev. Mod. Phys. 21, 635, 1949

71. Benveniste, J. et al

UCRL - 4266, 1954

72. Kabir, S. M.

Nucl. Inst. and Methods 109, 533, 1973

73. Nuclear Enterprises Catalogue, 1973

74. Glasstone S. et al

The Elements of Nuclear Reactor Theory

D. Vannstrand Company Inc. 1966

75. Weinborg, A. W. et al

The Physical Theory of Neutron Chain Reactions

The University of Chicago, 1958

76. Glasstone, S.

Principles of Nuclear Reactor Engineering

Norwich MacMillan & Co. Ltd., 1956

77. Ornstein, L. S. et al

Physica, 4, 478, 1937

78. Fermi, E.

Riccra Scint. 7, 1, 1936

79. Roos, B. W. et al

Advances in Nuclear Science and Technology

Vol. 2, 1964

80. Magahid, R. M.

PhD Thesis, University of Aston in Birmingham, 1975

81. Case, K. M.

Ann. Phys. 9, 1, 1960

82. Mika, J.

Nucl. Sci. and Eng. 11, 415, 1961

83. Ferriger, J. H. et al

Ann. Phys. 22, 192, 1963

84. McInerney, J. J.

Nucl. Sci. and Eng. 22, 215, 1965

85. Mark, C.

CRT-340 Canadian Report,

Atomic Energy of Canada, 1944

86. Mark, C.

CRT-338 Canadian Report

Atomic Energy of Canada

87. Davison, B.

A.E.R.E. T/R-700 British Report

G.B. Atomic Energy Research Establishment

88. Carlson, B. G.

LA-1599, (revised version, LA-189) 1953

89. Barbucci, P. et al

Nucl. Sci. and Eng. 63, 179, 1977

90. Carlson, B. G. et al

Proc. of the Second U.N.C. on the peaceful uses of atomic energy, 1958

91. Miller, W. F. et al

Nucl. Sci. and Eng. 62, 391, 1977

92. Wallace, P. R. et al

Canadian Report M. T. 12, 1943

93. Marshak, R. E.

Rev. Mod. Phys. 19, 185, 1947

94. Goertzel, G. et al

Methods in Transport Problems, Progress in Nuclear Energy Series 1, Vol. 2, New York Pergamon Press, 1958

95. Spencer, L. V. et al

Phys. Rev. 81, 464, 1951

96. Coldstein, H. et al

NYO-3075, Report 1954

97. Kalos, M. H. et al

Necleoncies, 15, 64, 1957

98. Djomehri, M. J.

Nucl. Sci. and Eng. 60, 131, 1976

99. Arnecke, G. et al

KFK-2190 Kernforschungszentrum Karlsruhe 1976

100. Albert, R. D. et al

U.S.A.E.C. Report W.A.P.D.-15, 1950

101. Spinney, K. T.

A.E.R.E. T/R-2507, 1957

102. Chapman, R. D. et al

U.S.A.E.C. Report A.E.C.D. -3978, 1955

103. Broder, D. L. et al

Biological Shielding of Ships Reactors

Leningrad Sudpromgiz 1964

104. Avery, A. F. et al

A.E.R.E. R-3216 Report, 1960

105. Mandel, M. E.

A.E.R.E. T/R-1295 Report 1953

106. Tralli, N. et al

U.S.A.E.C. Report N40-3923, 1953

107. Rief H. et al

Nucl. Sci. and Eng. 30, 395, 1967

108. Spanier J. et al

Monte Carlo Principle and Neutron Transport

Problems, Wesley Publishing Company, 1969

109. Butler, J. et al

Engineering Compendium on Radiation Shielding, Vol 1

Int. Atomic Energy Agency - Vienna 1968

110. Beynon, T. D.

J. Phys. D. Appl. Phys. 8, 902, 1975

111. Avery, A. F.

AEEW-R-125

United Kingdom Atomic Energy Authority

Reactor Group

112. Fiebig, R.

U.K.A.E.A. Report AERE-R-5773, 1964

113. Bendall, D. E. et al

Proc. 4th Int. Conf. on Reactor Shielding,

Vol. 2, Paris 1972

114. Stacey, W. M.

Nucl. Sci. and Eng. 47, 449, 1972

115. Kaper, H. G. et al

Nucl. Sci. and Eng. 49, 27, 1972

116. Cooper, P. N.

Lecture Notes, University of Aston in Birmingham

117. Takeda, T. et al

J. of Nucl. Sci. and Tech. 9, 697, 1972

118. Kappler, F. W.

Nucl. Sci. and Eng. 67, 74, 1978

119. Underwood B. Y. et al

Birmingham Radiation Centre 1978

120. Speir P. et al

Nucl. Inst. and Methods 116, 53, 1974